PhD-FSTC-2016-32
The Faculty of Sciences, Technology and Communication

DISSERTATION

Defense held on 25/08/2016 in Belval

to obtain the degree of

DOCTEUR DE L'UNIVERSITÉ DU LUXEMBOURG

EN BIOLOGIE

by

Sean SAPCARIU
Born on 13 October 1983 in Silver Spring, (USA)

METABOLIC AND TRANSCRIPTIONAL CONTROL OF METABOLISM IN PRO-INFLAMMATORY MACROPHAGES

Dissertation defense committee

A-Prof Dr Karsten Hiller, dissertation supervisor
Associate Professor, Université du Luxembourg

A-Prof Dr Sarah-Maria Fendt
Associate Professor, VIB Vesalius Research Center, KU Leuven, Belgium

Dr Serge Haan, Chairman
Professor, Université du Luxembourg

Dr Joachim Kopka
Group Leader, Max-Planck-Institut für Molekulare Pflanzenphysiologie

Dr Nirmal Robinson
Group Leader, CECAD Institute, Universität zu Köln

Dr Alessandro Michelucci, Vice Chairman
Luxembourg Institute of Health

METABOLIC AND TRANSCRIPTIONAL CONTROL OF METABOLISM IN PRO-INFLAMMATORY MACROPHAGES

SEAN SAPCARIU

A thesis submitted in partial fulfillment of the
requirements for the degree of

Doctor of Biology

at the
Luxembourg Centre for Systems Biology
University of Luxembourg

August 2016

This presented Doctoral Thesis was performed at the:
Luxembourg Centre for Systems Biomedicine (LCSB), University of Luxembourg
under the supervision of:
Dr. Karsten Hiller, Metabolomics Group

Dissertation defense committee:

Prof. Dr. Serge Haan - Chairman
University of Luxembourg, Luxembourg

Dr. Alessandro Michelucci
Luxembourg Institute of Health, Luxembourg

Associate Professor Dr. Sarah-Maria Fendt
VIB Vesalius Research Center, KU Leuven, Belgium

Dr. Joachim Kopka
Max Planck Institute of Molecular Plant Physiology, Germany

Dr. Nirmal Robinson
CECAD Institute, University of Köln, Germany

Declaration of Authorship

I hereby confirm that the PhD thesis entitled "Metabolic and transcriptional control of metabolism in pro-inflammatory macrophages" has been written independently and without any other sources than those cited.

Luxembourg, _____

Name _____

ACKNOWLEDGMENTS

A gigantic list of names to say thank you to should appear here, as the work contained in this thesis was not the result of one person, but rather a collaborative effort of scientific work, moral and technical support, as well as countless other little things lead to a successful body of work.

A big thank you to my supervisor, Karsten Hiller, who has allowed me to hang out in his lab for a long time and generally be independent, so that I could find my own way through this crazy time. His support and aid when I needed it was invaluable throughout the past three years.

Thanks as well to my internal thesis committee, Alessandro Michelucci and Alex Skupin, for asking me lots of questions to push my ideas and work, and generally being there when I had questions of my own (which was often). Thank you to defense committee members, Serge Haan, Sarah-Maria Fendt, Joachim Kopka, and Nirmal Robinson, for taking the time to read my thesis and traveling to Luxembourg in order to help me finish.

A separate thank you to Serge Haan for letting me bother him as a Doctoral School representative, and to Nirmal Robinson for allowing such a fruitful collaboration between our two labs (and a huge thanks to Saray Gutiérrez for doing tons of work!)

The metabolomics group at the LCSB has been a fantastic place to work for the past few years, and there is not enough space for me to properly thank everyone for the great atmosphere, support both in and out of the lab, and everything else that made it fun to come into work every day. I owe you all much food and drink, and come see me individually if you want me to enumerate the reasons for my thanks.

Of course, thanks to my family in Luxembourg, Fabienne and Timo, for their love and support, as well as for keeping life interesting and making sure I had things to do aside from research. Thanks as well to my mother, who continues to support me with all the crazy things I do far away from where I grew up...

LIST OF PUBLICATIONS

Parts of this dissertation have been published as scientific articles during the process of my thesis, and are listed here. The full text, as well as my contributions, are provided in the results and appendix.

Publications in peer-reviewed journals

- **Sapcariu SC**, Kanashova T, Dilger M, Diabaté S, Oeder S, Passig J, Radischat C, Buters J, Sippula O, Streibel T, Paur HR, Schlager C, Mülhopt S, Stengel B, Rabe R, Harndorf H, Krebs T, Karg E, Gröger T, Weiss C, Dittmar G, Hiller K, Zimmermann R. Metabolic Profiling as well as Stable Isotope Assisted Metabolic and Proteomic Analysis of RAW 264.7 Macrophages Exposed to Ship Engine Aerosol Emissions: Different Effects of Heavy Fuel Oil and Refined Diesel Fuel. *PLoS One*, **2016**, 11(6), *10.1371/journal.pone.0157964*

- Cordes T, Wallace M, Michelucci A, Divakaruni AS, **Sapcariu SC**, Sousa C, Koseki H, Cabrales P, Murphy AN, Hiller K, Metallo CM. Immunoresponsive gene 1 and itaconate inhibit succinate dehydrogenase to modulate intracellular succinate levels. *Journal of Biological Chemistry*. **2016**, 291(27), 14274-14284. *doi:10.1074/jbc.M115.685792*

- Weindl D, Cordes T, Battello N, **Sapcariu SC**, Dong X, Wegner A, Hiller K. Bridging the gap between non-targeted stable isotope labeling and metabolic flux analysis. *Cancer & Metabolism*. **2016**, 4(1). *doi:10.1186/s40170-016-0150-z*

- Meiser J, Kraemer L, **Sapcariu SC**, Battello N, Ghelfi J, D'Herouel Aymeric F, Skupin A, Hiller K. Pro-inflammatory macrophages sustain pyruvate oxidation through pyruvate dehydrogenase for the synthesis of itaconate and to enable cytokine expression. *Journal of Biological Chemistry*. **2015**, 291(8), 3932-3946. *doi:10.1074/jbc.M115.676817*

- Oeder S[*], Kanashova T[*], Sippula O[*], **Sapcariu SC**[*], Streibel T, Arteaga-Salas, JM, Passig J, Dilger M, Paur HR, et-al. Particulate matter from both

heavy fuel oil and diesel fuel shipping emissions show strong biological effects on human lung cells at realistic and comparable in vitro exposure conditions. *PLoS One*. **2015**, 10(6). *doi:10.1371/journal.pone.0126536*

- **Sapcariu SC**, Kanashova T, Weindl D, Ghelfi J, Dittmar G, Hiller K. Simultaneous extraction of proteins and metabolites from cells in culture. *MethodsX*. **2014**, 1, 74-80. *doi:10.1016/j.mex.2014.07.002*

- Wegner A, Weindl D, JaÌger C, **Sapcariu SC**, Dong X, Stephanopoulos G, Hiller K. Fragment formula calculator (FFC): determination of chemical formulas for fragment ions in mass spectrometric data. *Analytical Chemistry*. **2014**, 86(4). *doi:10.1021/ac403879d*

- Wegner A, **Sapcariu SC**, Weindl D, Hiller K. Isotope cluster-based compound matching in gas chromatography/mass spectrometry for non-targeted metabolomics. *Analytical Chemistry*. **2013**, 85(8). *doi:10.1021/ac303774z*

Manuscripts planned to be submitted to peer-reviewed journals

- **Sapcariu SC**, Wolf C, Delcambre S, Krämer L, Dong X, Schneider J, Hiller K. Comparing and contrasting metabolism and cytokine expression during the early stages of inflammation in cell lines and primary macrophages. Manuscript in preparation.

- **Sapcariu SC***, Gutiérrez S*, Wolf C, Dong X, Delcambre S, Schneider J, Robinson N, Hiller K. SIRT3 decrease in pro inflammatory macrophages helps with polarization to a antimicrobial phenotype. Manuscript in preparation.

* These authors contributed equally to this work

CONTENTS

ABBREVIATIONS

α-KG alpha-ketoglutarate

ALI air-liquid interface

ATP adenosine 5′-triphosphate

BMDM bone marrow derived macrophage

CARKL carbohydrate kinase-like protein

DAMP damage-associated molecular pattern

DEP diesel exhaust particle

cDNA complementary deoxyribonucleic acid

EI electron ionization

ETC electron transport chain

GABA γ-Aminobutyric acid

GDH glutamate dehydrogenase

GC-MS gas chromatography coupled to mass spectrometry

HICE Helmholtz Virtual Institute of Complex Molecular Systems in Environmental Health

HIF-1α hypoxia-inducible factor-1 alpha

IDH1 isocitrate dehydrogenase isoform 1

IDH2 isocitrate dehydrogenase isoform 2

IFN-γ interferon-gamma

IL-1b interleukin-1 beta

IL-4 interleukin-4

Irg1 *immune-responsive gene 1*

LC-MS liquid chromatography coupled to mass spectrometry

LDH lactate dehydrogenase

LPS lipopolysaccharide

MAPK mitogen-activated protein kinase

MSTFA N-Methyl-N-trimethylsilylfluoroacetamide

MTBSTFA N-tert-butyldimethylsilyl- N-methyltrifluoroacetamide

MID mass isotopomer distribution

NF-κB nuclear factor NF-kappa-B

NLR nucleotide-binding oligomerization domain receptor

NMR nuclear magnetic resonance

PAMP pathogen-associated molecular pattern

PDH pyruvate dehydrogenase

PDK pyruvate dehydrogenase kinase

PM particulate matter

PPP pentose phosphate pathway

PRR pattern-recognition receptor

qPCR quantitative polymerase chain reaction

ROS reactive oxygen species

SDH succinate dehydrogenase

SIM selected ion monitoring

TBDMS tert-butyl dimethylsilyl

TCA cycle tricarboxylic acid cycle

TLR Toll-like receptor

TMS trimethylsilyl

TNF-α tumor necrosis factor alpha

SUMMARY

The metabolic activity of cells is crucial to their growth, survival, and quick response to shifts in the microenvironment. For macrophages, changes in metabolism have been shown to be implicated in their ability to shift phenotypes as a response to multiple cellular agonists, including bacteria and other pathogenic substances. Two specific metabolites from the TCA cycle in mitochondria have been found to be involved in pro-inflammatory macrophage activity, itaconic acid and succinic acid. Itaconic acid is a antimicrobial metabolite produced in macrophages as a side product in the TCA cycle, resulting from agonists such as LPS stimulation, while succinic acid is a metabolite in the TCA cycle which accumulates in pro-inflammatory macrophages for the purpose of increasing cytokine expression and glycolytic activity.

In this work, a combination of metabolomics analyses and other experimental techniques are used to investigate the regulation of these two metabolites, with the goal of understanding how metabolic changes are controlled both through cellular mechanisms and environmental cues. To do so, the metabolomics extraction method from our laboratory was published, with the goal of increasing standardization in the metabolomics research community. Extending the investigation of metabolomics studies in the lab, a comparison between primary macrophages and a common macrophage cell line was made, showing similarities in cytokine expression patterns with differences in scale, while the changes required to create an immortalized cell line make the metabolism under inflammation not comparable to primary cells.

Through multiple studies, itaconic acid is found to be increased in macrophages not only through LPS stimulation, but also in bacterial infection and anthropogenic aerosol exposure. Glucose flux into the mitochondria, thought to be inhibited in pro-inflammatory macrophages, is shown to be constitutively active in basal conditions and increased with LPS stimulation. In addition, succinic acid accumulation is shown to be regulated through an itaconic-acid dependent inhibition of a TCA cycle enzyme, controlled in part by the gene implicated in the production of itaconic acid, *Irg1*. Finally, the antimicrobial activity of macrophages through itaconic acid and pro-inflammatory cytokine secre-

tion is found to be linked to SIRT3, a mitochondrial deacetylase active in the regulation of multiple metabolic targets in the cell.

The combined results point to a tightly linked network of metabolic regulation in macrophages to promote antimicrobial activity and increased cytokines through the interplay of SIRT3, *Irg1*, succinic acid, and itaconic acid. In addition, the work in this thesis shows that the TCA cycle is extremely important for both metabolite production as well as regulation of cytokine expression in pro-inflammatory macrophages, showing a decoupling of central carbon metabolism under inflammatory conditions.

1

INTRODUCTION

1.1 THE ROLE OF INFLAMMATION IN INNATE IMMUNITY

The innate immune system is the first barrier in protecting its host from pathogens and tissue damage, serving as a non-specific defense mechanism that targets foreign and local sources of pathogens. Cells of the innate immune system recognize foreign pathogens using transmembrane protein receptors, called pattern-recognition receptors (PRRs), that bind to a wide variety of pathogen-associated molecular patterns (PAMPs). PAMPs are structurally-similar molecules, such as proteins, nucleic acids, or lipids, that are unique to microbial pathogens (Akira and Hemmi, 2003). The binding of PAMPs by PRRs initiates a signaling cascade that allows cells of the innate immune system to combat infection and induce tissue reparation after damage has been done. (Medzhitov, 2007). The biological pathway behind this process includes four stages: induction of the response through infection or tissue damage, sensing of the infection by innate immune cell based-receptor signaling, production of inflammatory mediators by the innate immune cells to help clear out the infection, and finally resolution plus termination of inflammation (Medzhitov, 2010).

In addition to inflammatory responses induced by foreign PAMPs, endogenous biomolecules, so-called damage-associated molecular patterns (DAMPs), can also initiate inflammation (Seong and Matzinger, 2004). These non-infectious stimuli are often result from tissue injury or cell death; they are generally sequestered from the immune system and only released as a result of cellular stress. Afterwards, they are incorrectly identified by the immune system as danger signals, and cause so-called "sterile inflammation" (Chen and Nuñez, 2010). DAMPs can be recognized by the same receptors as PAMPs, and have been seen to lead to similar inflammatory response pathways; for example, the TLR4 receptor can be stimulated by ligands from both pathogenic bacteria (such as lipopolysaccharide (LPS)) and products of cellular damage pathways (such as heat-shock protein 60), leading to the same cellular response (Seong

and Matzinger, 2004). Thus, there is some dispute as to whether PAMPs and DAMPs cause distinct mechanisms of action (Barton, 2008).

In the case of dysregulation of the acute inflammatory response, or improper removal of pathogens, the state of inflammation can persist, leading to chronic inflammation. Chronic inflammation has been associated with multiple diseases and disorders, including obesity and cardiovascular diseases (Hotamisligil, 2006), neurodegenerative diseases (McGeer and Mcgeer, 2004), and various cancers (Grivennikov *et al.*, 2010). Thus, the process and critical regulatory points of inflammation, as well as furthering the understanding of inflammatory dysregulation, are important fields of study for human health.

1.1.1 *Macrophage activation and polarization regulates the inflammatory response*

One of the main cell types implicated in the inflammatory response are macrophages, a phagocytic innate immune system cell. Macrophages are a form of differentiated monocyte which arise from hematopoietic stem cells in the bone marrow. Both circulating and tissue-resident macrophages are found in the body (Gordon and Taylor, 2005). Under certain conditions in damaged tissues, fully differentiated and mature macrophages have been seen to complement the tissue-resident cells in order to aid in tissue repair (Wang and Kubes, 2016).

The role of macrophages consists of the constant scanning for danger signals (PAMP and DAMP), while being primed for an immediate response if necessary, to return damaged tissue to homeostasis as quickly as possible (Murray and Wynn, 2011). Specialized receptors (PRRs, including Toll-like receptors (TLRs), nucleotide-binding oligomerization domain receptors (NLRs), and integrins) recognize these signals, and recognition stimulates signaling cascades which initiate the macrophage response (Taylor *et al.*, 2005). Macrophage activation can be hijacked by diseases or stopped from functioning correctly; dysregulation of macrophage activity has been associated with disorders such as metabolic disease (Chawla *et al.*, 2011) and tumorigenesis (Grivennikov *et al.*, 2010).

Macrophages can be stimulated into a variety of activated phenotypes, all with differing phenotypic differences and activities which are necessary for the different phases of an inflammatory response (Murray and Wynn, 2011). Typically, macrophages are classified into two phenotypes, "classical" activation

(also called M1 macrophages) and "alternative" activation (M2 macrophages) (Figure 1). Classically activated macrophages have a pro-inflammatory activity, while alternatively activated macrophages are involved in wound repair and have an anti-inflammatory phenotype (Murray and Wynn, 2011).

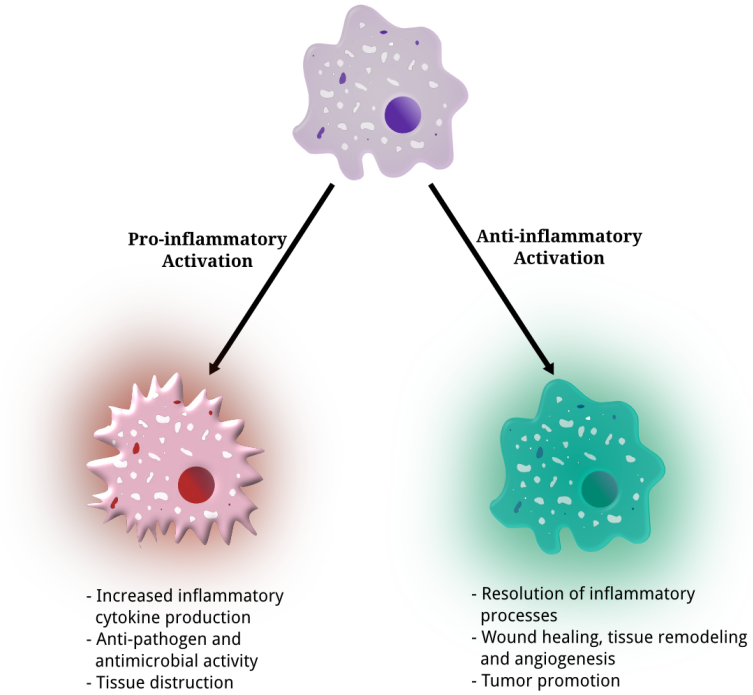

Figure 1: Macrophages are known to be activated either towards a pro-inflammatory or an anti-inflammatory phenotype. While there are different sub-activation phenotypes thought to exist for the two classifications, the activities of a macrophage polarized in either direction remain conserved.

While this dichotomy of macrophage phenotype naming is still in use today, there have been experts who deem that this classification is too limiting, and instead refer to a continuous spectrum of macrophage activation states which are able to adapt to specific situations required by the tissue at any specific time (Mosser and Edwards, 2008; Wynn *et al.*, 2013). In this thesis, I will use the term "pro-inflammatory macrophage" to refer to the activation state that I was most interested in studying.

Pro-inflammatory macrophages have a phagocytic activity, and are heavily involved in the active defense against pathogenic bacteria through phagocytosis as well as chemical means. These chemical effectors include nitric oxide and reactive oxygen species (ROS) production as well as the synthesis and

secretion of pro-inflammatory cytokines which coordinate the inflammatory response (Dale *et al.*, 2008). Inflammatory cytokines are small proteins which act as signaling molecules and support the coordination of the immune response (Duque and Descoteaux, 2015), or directly induce the destruction of pathogenic bacteria (Jayaraman *et al.*, 2013). The main cytokines induced in pro-inflammatory macrophages include interleukin-1 beta (IL-1b), tumor necrosis factor alpha (TNF-α), and IL-6, are induced by different signaling cascades, including nuclear factor NF-kappa-B (NF-κB) and mitogen-activated protein kinase (MAPK) (Barton, 2008; Shi *et al.*, 2009).

1.1.2 *Pro-inflammatory macrophage activation using lipopolysaccharide*

In vitro, LPS is the most commonly used to stimulate pro-inflammatory macrophage phenotypes (Mosser and Edwards, 2008). LPS is the main component of Gram-negative bacterial surface membranes and is recognized mainly by macrophage TLR4, but also TLR2 and CD14 surface receptors (Hirschfeld *et al.*, 2001). Binding of the ligand to the macrophage surface receptor induces a myeloid differentiation protein 88 (MyD88)-dependent signaling pathway leading to NF-κB activation and expression of the cytokines IL-1b, *Tnfa*, and IL-6 (Andreakos *et al.*, 2004). A parallel signaling pathway activated by LPS/MyD88 signaling is the MAPK pathway, which co-regulates NF-κB-dependent pro-inflammatory cytokine expression as well as regulates anti-inflammatory macrophage responses (such as IL-10 and STAT3) (Bode *et al.*, 2012).

1.1.3 *Anthropogenic aerosols as a source of inflammation in human health*

Air pollution from anthropogenic sources is consistently associated with negative health outcomes, such as asthma, cardiovascular problems, and cancer (Sydbom *et al.*, 2001; Wichmann, 2007). These aerosols consists of particulate matter (PM) suspended in a gas phase, which enters the environment and the air that we breathe. To link pro-inflammatory stimulation to human health and environmental factors, anthropogenic pollutants have also been used in macrophage exposure studies. Since the industrial revolution, there has been a steady increase in the amount of PM that are present in the air we breathe, and these particles have been in particular associated with higher levels of res-

piratory diseases (D'Amato *et al.*, 2005). A major source of PM from vehicles and certain industry, diesel exhaust particles (DEPs), have been heavily studied as an instigator for inflammation and immune system responses (Chaudhuri *et al.*, 2012; Provoost *et al.*, 2010; Reisetter *et al.*, 2011).

The Helmholtz Virtual Institute of Complex Molecular Systems in Environmental Health (HICE) project aims to investigate the mechanisms of human health effects influenced by anthropogenic aerosols in a comprehensive biological and chemical approach. To do so, a novel experimental setup was developed and applied to different aerosol sources. Experimental campaigns were carried out, each focusing on a single combustion aerosol, and a large team of researchers applied state of the art techniques to both characterize the aerosol as well as to profile the effects of the aerosol on biologically relevant cellular models. (Oeder *et al.*, 2015)

For the chemical analyses of the aerosol, a combination of online and offline measurement systems were applied, including gas chromatography coupled to mass spectrometry (GC-MS), high resolution mass spectrometry (ESI-FTICR-MS), energy-dispersive X-ray spectroscopy (EDX), on-line photo-ionization mass spectrometry, particle size distribution and number measurements, and others (Oeder *et al.*, 2015).

Parallel to the chemical analyses, multiple cell types were exposed to the combustion aerosol using a novel air-liquid interface (ALI) system (Mülhopt *et al.*, 2016), and the biological consequences were studied using "omics" techniques. A549 human epithelial lung cancer cells, Beas2b virus transformed lung epithelial cells and RAW 264.7 mouse macrophages were used, and analyzed using transcriptomics, proteomics, and metabolomics workflows.

While multiple studies have investigated the effects of PM emissions on lung cells (Chaudhuri *et al.*, 2012; Bhavaraju *et al.*, 2014; Shaw *et al.*, 2011), most experiments utilized submerged experiments, where particles are dissolved in the cell culture medium at specific concentrations, with no gas phase or combined aerosol exposure. While these studies have contributed valuable insights into particle effects on cell models, these exposure types do not accurately simulate inhalation of combustion emissions. Therefore, studies utilizing ALI exposure systems (such as those in the scope of the HICE project) represent a more biologically accurate exposure situation for lung epithelial cells.

ALI systems are a complex integration of technology allowing for simultaneous automated control of both aerosol conditions (such as heating, humidity, and flow), as well as cell exposure conditions (such as temperature, humidity, and accurate particle deposition). All materials must be compatible with biological exposure (and cause no confounding effects), and there must be enough exposure chambers for comprehensive experimental conditions. For this purpose, an 18-position fully automated ALI was built for the purpose of the HICE project, specifically designed with all of these features in mind (Mülhopt *et al.*, 2016)

Additionally, ALI studies are able to discern different effects due to the gas and particle components of aerosols through the use of in-line filters (Steiner *et al.*, 2013). ALI validation studies have been performed previously (Knebel *et al.*, 2002; Seagrave *et al.*, 2007), and multiple studies have used ALI technology to uncover novel chemical and biological insights, including more accurate particle deposition efficiencies modeling (Comouth *et al.*, 2013), the study of the response of co-cultures of epithelial cells and macrophages to waste incineration emission aerosol (Diabaté *et al.*, 2008), and discovery of specific aerosol constituents which contribute to toxicity of epithelial lung cells (Dilger *et al.*, 2016). In general, ALI systems are preferred compared to submerged experiments for cell exposure, as has been discussed previously (Paur *et al.*, 2011).

1.2 CENTRAL CARBON METABOLISM AND THE IMPORTANCE OF THE TCA CYCLE

Cellular metabolism is an extremely complex network of biochemical reactions, and looking at the whole system is beyond the scope of this work. Therefore, I focused mainly on the tricarboxylic acid cycle (TCA cycle) of central carbon metabolism in order to understand how macrophages utilize their fuel sources when challenged with a pro-inflammatory stimulus. Central carbon metabolism is a integral subset of cellular metabolism, and supports cellular processes required for cell survival, proliferation, and many more critical activities. These cellular functions define a large part of cellular homeostasis, and perturbations to these systems can lead to cellular dysregulation and disease (Metallo *et al.*, 2012; O'Neill and Hardie, 2013; Hiller and Metallo, 2013).

The two main carbon sources that the cell utilizes for metabolism are glucose and glutamine. Glucose is taken up into the cell through the glucose transporter GLUT1, a process which is conserved in all tissues and cells, including macrophages (Fukuzumi *et al.*, 1996). Glucose is then converted into pyruvate through glycolysis, a multi-step series of biochemical reactions taking place in the cytosol which serves the purpose of transforming glucose carbon into a form which can be efficiently converted into cellular energy sources. Once converted into pyruvate, glucose-derived carbon either enters the TCA cycle, where the carbon is used for energy production through oxidative phosphorylation via the electron transport chain (ETC), or is reduced to lactate and secreted from the cell.

1.2.1 *The TCA cycle and glutamine metabolism*

Glutamine uptake into cells feeds different cellular mechanisms, including amino acid synthesis, oxidative phosphorylation, and redox control. However, for central carbon metabolism, glutamine is converted into glutamate through glutaminase activity, and then funneled into the TCA cycle through glutamate dehydrogenase (GDH) (Newsholme *et al.*, 2003) or transanimation.

The series of reactions which compose the TCA cycle take place in the mitochondria of the cell, and serve as the main input of carbon for energy production through the ETC, located in the inner membrane of the mitochondria. Succinate dehydrogenase (SDH) directly links the ETC and the TCA cycle, through catalyzing the conversion of succinic acid to fumaric acid while simultaneously transporting electrons (Liu *et al.*, 2002). The TCA cycle operates mainly in the oxidative direction, using glucose- and glutamine-derived carbon as the main sources which feed a cycle involved in many integral cellular processes, including energy production (both ATP and NADH) (O'Neill and Hardie, 2013), biomass synthesis (including amino acids and fatty acids) (Fendt *et al.*, 2013), ROS production (Liu *et al.*, 2002), as well as production of cofactors important in the creation of bioprotective compounds (such as NADPH) (Yu *et al.*, 2012). However, flux through the TCA cycle can also move in a reductive direction, based upon factors such as mass action kinetics (Fendt *et al.*, 2013).

There is constant exchange of certain metabolites between the mitochondria and the cytosol, and many of the enzymes catalyzing the reactions in

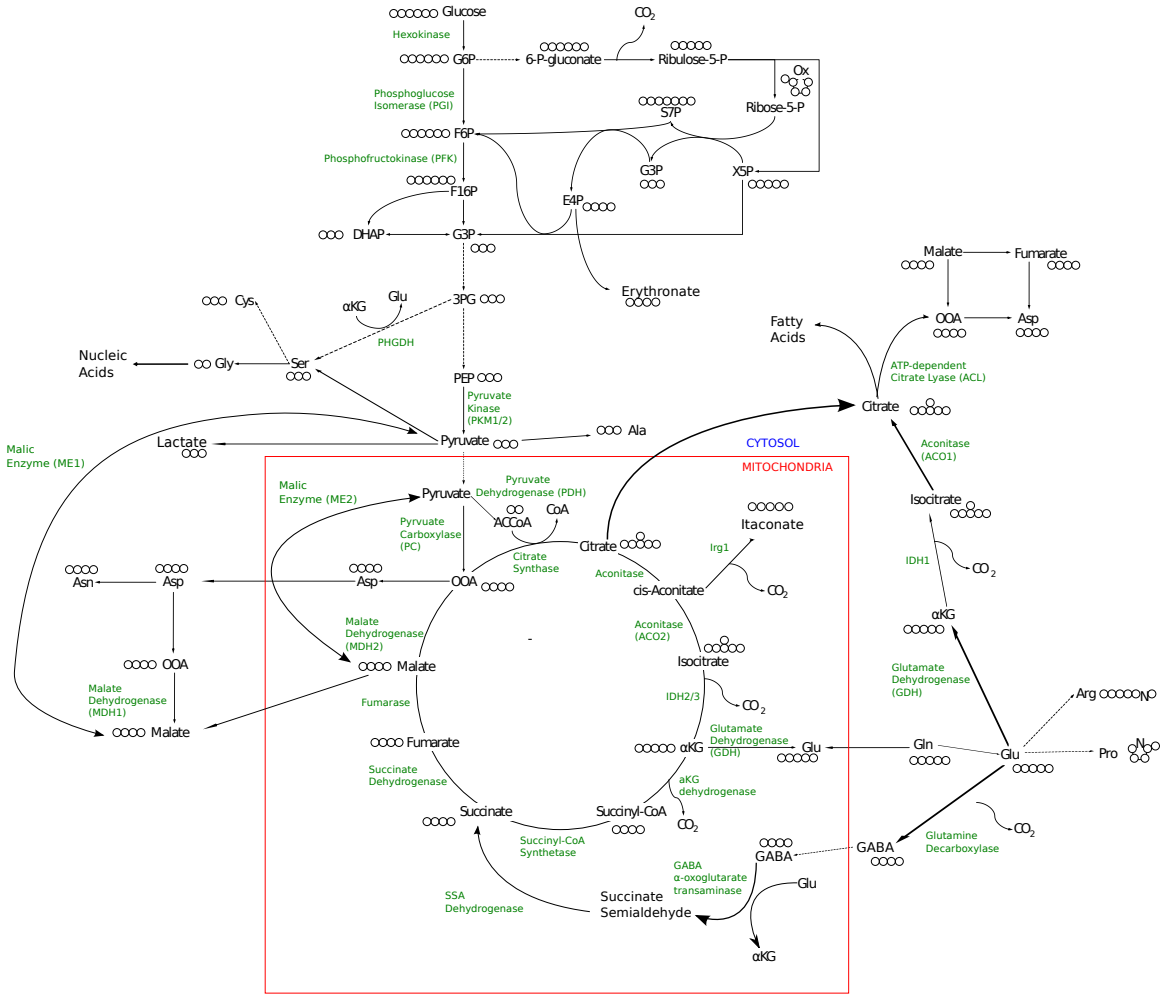

Figure 2: Central carbon metabolism. Metabolites are in black, and enzymes are in green. Circles next to each metabolite represent the number of carbons that each metabolite is comprised of.

the TCA cycle have complementary isoforms in both the mitochondria and the cytosol (Figure 2). Biochemical activity of these enzymes outside of the mitochondria can also affect cellular processes associated with the TCA cycle, such as acetyl-CoA production for lipogenesis (Metallo *et al.*, 2012).

The cyclical nature of the reactions in the TCA cycle create an extremely efficient carbon oxidation and energy production pathway, with many side pathways allowing for complete use of the carbon that enters the mitochondria. Glutamine-derived glutamate can be converted into signaling molecules (γ-Aminobutyric acid (GABA)), be used for nucleotide synthesis, create glucose through gluconeogenesis, or aid in the creation of nitric oxide (used for antimicrobial activity in macrophages) (Newsholme *et al.*, 2003).

1.2.2 *Regulation of metabolism through signaling pathways and metabolic changes*

Different utilization of glucose and glutamine in central carbon metabolism is regulated by thermodynamics of reactions under homeostasis, regulatory signals which monitor and react to the needs of the cell, as well as cellular perturbations which modify .

Cellular perturbations can activate signaling cascades which change the utilization of these carbon sources depending on the current needs of the cell, shifting carbon from "normal" activity to specific endpoints in order to react and adapt to environmental challenges. For example, cells under hypoxic conditions shift energy production from oxidative phosphorylation to glycolsis. This switch in cellular metabolism is mediated by the stabilization of hypoxia-inducible factor-1 alpha (HIF-1α), a transcription factor which upregulates pyruvate dehydrogenase kinase (PDK) (among many other enzymes), which in turn inhibits pyruvate dehydrogenase, leading to a reduction of glucose-derived carbon entry into the TCA cycle and increased lactate production through lactate dehydrogenase, also positively regulated by HIF-1α (Kim *et al.*, 2006).

Central carbon metabolism can also be hijacked by diseases, leading to a dysregulation of cellular processes that is used for the benefit of the diseased cell. While the above pathway is utilized by normal cells operating in hypoxic conditions, tumor cells have been observed to use the same pathway in normoxic conditions for increased glycolytic rates and production of large amounts of energy (Semenza, 2007), a phenomenon known as the Warburg effect (War-

burg *et al.*, 1927). The Warburg effect is associated with tumorigenesis, but has recently been seen in regulatory T cells (Shi and Pamer, 2011), and has been hypothesized to play a role in pro-inflammatory macrophages as well (Cramer *et al.*, 2003; Wen *et al.*, 2012).

Under certain cellular conditions, glutamine imported into the cell can be shunted in the reductive direction, leading to reductive carboxylation and production of citric acid, acetyl-CoA, and finally fatty acids. As with the pathway described above, this has been found to occur during hypoxia in cells, and is considered to be complementary to the reduced pyruvate oxidation into the TCA cycle (Metallo *et al.*, 2012). In addition, this chain of reactions has been shown to work independently of signaling pathways, depending instead on the ratio between α-ketoglutarate and citrate (Fendt *et al.*, 2013).

1.3 METABOLIC CHANGES OF MACROPHAGES UNDER INFLAMMATION

Inflammation-induced changes in macrophages are classically associated with cellular changes in cytokine production and signaling, phagocytosis, as well as differentiation processes (Murray and Wynn, 2011). Only recently has the influence of metabolism been studied with regards to macrophage polarization, and many insights have appeared which show the integral role of metabolism in the macrophage's response to inflammation. While new insights have been gained in both pro-inflammatory and anti-inflammatory macrophage metabolism, I have focuses on pro-inflammatory macrophages for this thesis Figure 3.

1.3.1 *Glycolytic changes differentiate macrophage activation*

Rodríguez-Prados *et al.* (2010) performed metabolic characterization of the glycolytic activity of macrophages stimulated to a variety of different pro-inflammatory and anti-inflammatory phenotypes. Using [1,2-$^{13}C_2$]-labeled glucose tracers, and sampling the medium of RAW 264.7 macrophages, they found that pro-inflammatory macrophages secreted more lactate compared to anti-inflammatory and unstimulated macrophages, but with no difference in the labeling patterns of these secreted glycolitic metabolites with different stimulations. In addition, the fructose-2,6-bisphosphate pool was found to be increased in pro-inflammatory macrophages, suggesting that the glycolytic activ-

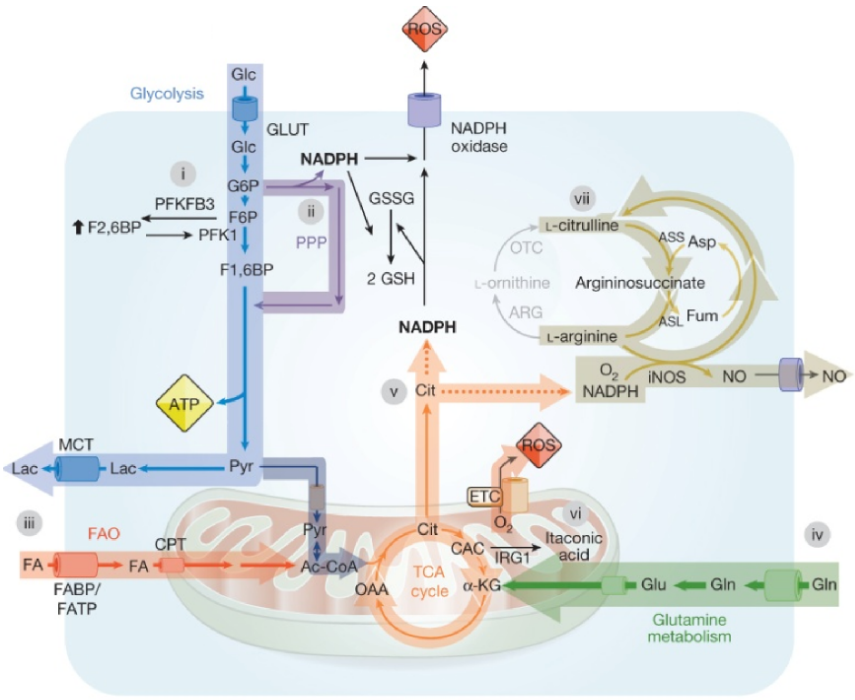

Figure 3: Metabolism of pro-inflammatory macrophages (Utilized from Ghesquière *et al.* (2014)). Pro-inflammatory macrophages have been found to have increased glycolysis for cellular energy production (with a reduced oxidative phosphorylation activity), while exhibiting a modified TCA cycle activity for the purpose of pro-inflammatory compound production. These compounds include ROS, nitric oxide, and itaconic acid. Glucose, glutamine, and fatty acids are utilized by the cell to fuel the various pathways necessary for pro-inflammatory macrophage metabolism. α-KG - α-ketoglutarate, Ac-CoA - acetyl-coenzyme A, ARG - arginase, ASL - argininosuccinate lyase, Asp - aspartate, ASS - argininosuccinate synthase, Cit - citrate, CPT - carnitine palmitoyltransferase, ETC, electron transport chain, F1,6BP - fructose 1,6-bisphosphate, F2,6BP - fructose 2,6 bisphosphate, F6P - fructose 6-phosphate, FA - fatty acid, FABP - fatty acid binding protein, FAO - fatty acid oxidation, FATP - fatty acid transfer protein, Fum - fumarate, G6P - glucose 6-phosphate, GAP - glyceraldehyde 3-phosphate, Glc - glucose, Gln - glutamine, Glu - glutamate, GLUT - glucose transporter, GSH - reduced glutathione, GSSG - oxidized glutathione, iNOS - inducible nitric oxide synthase, Lac - lactate, MCT - monocarboxylate transporter, NADPH - nicotinamide adenine dinucleotide phosphate, NO - nitric oxide, OAA - oxaloacetate, OTC - ornithine transcarbamylase, PFK1 - phosphofructokinase-1, PFKFB3, 6-phosphofructo-2-kinase/fructose-2,6-bisphosphatase-3, PPP - pentose phosphate pathway, Pyr - pyruvate, ROS - reactive oxygen species, TCA - tricarboxylic acid.

ity of macrophages stimulated to a pro-inflammatory phenotype is increased compared to anti-inflammatory macrophages or unstimulated cells. The TCA cycle was not studied, most likely as it was thought that HIF-1α mediated regulation strongly reduced oxidation of glucose towards oxidative phosphorylation, and that macrophages used mostly glycolsis for the production of energy. As a result, many studies simply dismissed metabolic flux through the TCA cycle in pro-inflammatory macrophages, since it could be shown that oxidative phosphorylation was significantly reduced; this is suggested even by O'Neill and Hardie (2013), on the forefront of macrophage metabolism.

Vats *et al.* (2006) found that anti-inflammatory macrophages have reduced glycolytic activity compared to their pro-inflammatory counterparts, and instead focus more on fatty acid oxidation and oxidative phosphorylation, due to induction of PPARγ-coactivator-1β (PGC-1β). In addition, inhibition of oxidative metabolism was shown to prevent polarization of macrophages to an anti-inflammatory phenotype, while having no effect on pro-inflammatory macrophage polarization. PGC-1β expression affected pro-inflammatory cytokine expression in addition to oxidative metabolism, reducing the secretion of IL-6 and IL-12 both *in vitro* and *in vivo*.

While transcriptional regulation is important for phenotypic changes in macrophages, direct regulation of metabolic pathways can also influence macrophage activation. Recently, Haschemi *et al.* (2012) screened RAW 264.7 mouse macrophages, finding an sedoheptulose kinase, carbohydrate kinase-like protein (CARKL), which is an important regulator of macrophage polarization through affecting glucose metabolism. *In vitro* and *in vivo*, decreased levels of CARKL were found with LPS stimulation, while IL-4 stimulation resulted in an increase of CARKL (Figure 4). In macrophages, this enzyme controls carbon flux from glucose through glycolsis and the pentose phosphate pathway (PPP), which affects glutathione and NADPH levels, pro-inflammatory cytokine expression and NF-κB activity, as well as oxygen consumption.

1.3.2 *Succinic acid links macrophage metabolism to cytokine secretion*

In 2013, the O'Neill lab discovered that the TCA cycle plays an important role in pro-inflammatory macrophages, and that LPS stimulation of primary mouse macrophages leads to increased intracellular succinic acid levels, and that this

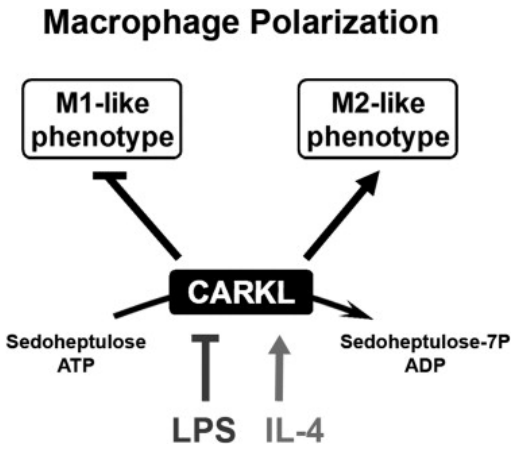

Figure 4: The role of CARKL in macrophage polarization. LPS stimulation inhibits CARKL activity, leading to a pro-inflammatory phenotype, while IL-4 stimulation promotes this enzyme, polarizing the macrophage to an anti-inflammatory phenotype. This polarization is regulated through CARKL's control of metabolic flow in the pentose phosphate pathway. From Haschemi *et al.* (2012)

succinic acid is metabolized from glutamine uptake into the cell (Tannahill *et al.*, 2013). Succinic acid was found to stabilize HIF-1α through inhibition of prolyl hydroxylase activity, leading to increased expression levels of IL-1b and increase of glycolytic activity through upregulation of GLUT1, lactate dehydrogenase (LDH), and other enzymes involved in glycolytic energy production.

Shortly after the role of succinate in pro-inflammatory macrophages was found, the mitochondrial metabolite was determined to have a key role in ROS production in ischemia reperfusion (Chouchani *et al.*, 2014). Using stable isotope labeled glucose and fatty acids to target TCA cycle intermediates under hypoxic ischemic conditions, reduced influx of normal carbon sources were found, and a reverse flow of SDH was observed, fed by aspartic acid. This was determined *in vivo* to cause ROS production upon reperfusion, showing that an accumulation of succinic acid is a main source of injury due to ischemia. Blockage of this accumulation reduced the damage in a rat stroke model, providing evidence for a role of succinic acid in ischemia reperfusion injury.

Other roles for succinic acid are beginning to emerge, both in macrophages and other cell types. Enzymes in metabolism have been shown to have lysine succinylation, including SDH, pyruvate dehydrogenase complex (Park *et al.*, 2013), and isocitrate dehydrogenase isoform 2 (IDH2) (Zhou *et al.*, 2016). Suc-

cinic acid signaling through succinate receptor 1 (SUCNR1), a G-protein coupled receptor, is also able to influence and enhance T cell immune response through synergy with TLR activation, affecting pro-inflammatory cytokine production (Rubic *et al.*, 2008).

1.3.3 *Itaconic acid - a mammalian antimicrobial metabolite*

In addition to the increase of succinic acid, an integral TCA cycle metabolite, a novel pathway branching off of the TCA cycle was linked to pro-inflammatory macrophage metabolism. Itaconic acid, a compound used for the synthesis of polymers, has been known to act as an antimicrobial, inhibiting the enzyme isocitrate lyase in multiple bacteria species McFadden and Purohit (1977); Patel and McFadden (1978). More recently, itaconic acid was found to be produced from cis-aconitate, and dramatically increased in LPS-stimulated mouse macrophages, the first time this metabolite was identified in a mammalian system (Strelko *et al.*, 2011).

A few years later, Michelucci *et al.* (2013) dug deeper into the production and regulation of itaconic acid in mammalian macrophages. Using stable-isotope labeling metabolomics techniques, production of itaconic acid from cis-aconitate was confirmed, and its presence in stimulated primary mouse and human macrophages was determined. In addition, the synthesis of itaconic acid production in mammalian cells was found to be catalyzed by the *immune-responsive gene 1* (*Irg1*) protein. Finally, the antimicrobial properties of itaconic acid were confirmed *in vitro*.

1.3.4 *Metabolic breakpoints highlight the TCA cycle in macrophage polarization*

Through an interpolated metabolomics and transcriptomics analysis combined with network integration, Jha *et al.* (2015) identified the rewiring of the TCA cycle during pro-inflammatory macrophage polarization. They found two "metabolic breakpoints" which contribute to the accumulation of itaconic and succinic acid. Using [U-$^{13}C_6$]-glucose and [U-$^{13}C_5$]-glutamine, carbon flux was seen to be blocked between citrate and alpha-ketoglutarate (α-KG), leading to an accumulation of citric acid. This flux blockage was linked to the downregulation of isocitrate dehydrogenase isoform 1 (IDH1) mRNA in pro-inflammatory

macrophages. While the diversion of carbon flux towards itaconic acid makes sense, the measurement of IDH1 is puzzling, as it is a cytosolic form of the enzyme, while the activity being described takes place in the mitochondria.

This increase in citrate can serve multiple roles in the TCA cycle. Infantino *et al.* (2011) determined that the mitochondrial citrate carrier is increased under LPS stimulation, leading to an increase of nitric oxide and ROS from citric acid metabolized to acetyl-CoA. The production of itaconic acid comes from a series of reactions directly downstream from citric acid production as well, and an increase of citric acid can serve an increase itaconic acid production. All three of these compounds are important mediators of pro-inflammatory macrophage activity, and highlight citric acid as an important pro-inflammatory metabolite.

In addition, Jha *et al.* (2015) pinpointed inefficient SDH activity, leading to a buildup of the succinic acid pool from glutamine uptake. At the same time, an increase in the metabolite malic acid was observed, hypothesized to arise from the aspartate-arginosuccinate shunt, which is an interface between the TCA cycle and the urea cycle in cells. The combination of increased citric acid (from glucose) and urea cycle activity (from glutamine) stresses the utilization of multiple cellular energy sources towards the same pro-inflammatory cellular function.

In the above studies, macrophages were found to modify their metabolism under pro-inflammatory conditions in order to produce multiple pro-inflammatory mediator molecules, including itaconic and succinic acid. These studies highlight the important role of these metabolites in pro-inflammatory macrophages, and solidify the TCA cycle as a vital player in macrophage metabolism during the inflammatory process.

1.4 SIRTUINS: LINKING METABOLISM AND THE IMMUNE RESPONSE

Sirtuins were discovered as a conserved family of class III histone lysine deacetylases which use NAD^+ as a cofactor in the post-translational modification of proteins (Michan and Sinclair, 2007). Current knowledge has elucidated many different properties of sirtuins that expands their scope of activity. They have been observed to act on other proteins than histones, to be able to perform additional post-translational modifications including demalonylation and desuccinylation (Du *et al.*, 2011; Peng *et al.*, 2011), and target proteins in different

cellular compartments, including in the mitochondria (He *et al.*, 2012). In recent years, sirtuins were increasingly studied because of their involvement in metabolism (reviewed in Houtkooper *et al.* (2012)), tied to aging related processes (Howitz *et al.*, 2003; Kanfi *et al.*, 2012), and associated with cancer (reviewed in Chalkiadaki and Guarente (2015)). The sirtuin family is composed of seven members, with different cellular localizations and activities (Figure 5). SIRT1 is the most well studied, located mainly in the nucleus with multiple integral transcription factors as targets, including HIF-1α, p53, and the FOXO family (Houtkooper *et al.*, 2012). The many links that are being discovered between sirtuins and diseases make these enzymes important areas of study for the future.

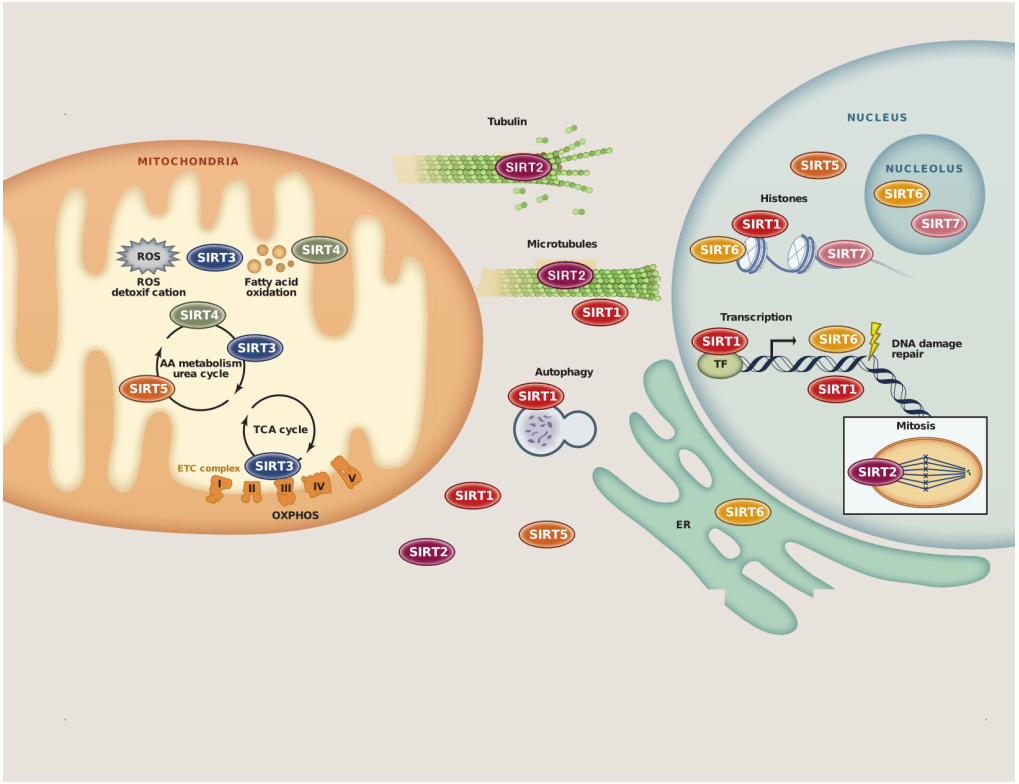

Figure 5: Sirtuin activity in the cell. The seven different sirtuin family members are known to be present and active in different parts of the cell, with regulatory effects on a wide variety of cellular functions. The most well studied sirtuin, SIRT1, is mainly present in the nucleus and is a known histone deacetylase, while SIRT3, SIRT4, and SIRT5 are present in the mitochondria and regulate cellular metabolism and reactive oxygen species production. Not much is known about the other sirtuins, and there is much current research in this direction. From Anderson *et al.* (2014)

1.4.1 *Connecting sirtuins and macrophage-mediated inflammation*

The effects of sirtuins on metabolism and other cellular processes has been seen to impact macrophages and their role in the inflammatory response. In 2004, SIRT1 was discovered to inhibit the transcription of NF-κB through targeting a lysine in one of the subunits crucial for transcriptional activity (Yeung *et al.*, 2004). Since then, SIRT1 deletion was shown to promote inflammation and metabolic dysfunction in models of adipose tissue (Chalkiadaki and Guarente, 2012) and metabolic disease in the liver (Purushotham *et al.*, 2009). Furthermore, the interplay between NF-κB and SIRT1 is thought to be an important part of the progression of the inflammatory state, through the control of the metabolic response to inflammation (Kauppinen *et al.*, 2013). By targeting AMP-activated protein kinase (AMPK) in macrophages, SIRT1 has also been found to have a role in bacterial infections, therefore mediating a metabolic switch between early-stage infection (with a Warburg effect-like phenotype) and late-stage infection (with more oxidative phosphorylation) (Moreira *et al.*, 2015).

Apart from SIRT1, other sirtuin family members play a role in inflammation. SIRT2 knockout bone marrow derived macrophages (BMDMs) show reduced expression of inflammatory cytokines, and diminished production ROS in response to LPS treatment (Lee *et al.*, 2014). In LPS-stimulated monocytes, SIRT1 and SIRT6 were shown to positively regulate both glucose as well as fatty acid uptake and oxidation (Liu *et al.*, 2012). While more links between different members of the sirtuin family and inflammatory macrophage activity are being hypothesized, these enzyme deacylases could be tightly involved in how macrophages behave under different stages of inflammation.

1.4.2 *Mitochondrial sirtuins target cellular metabolism*

Sirtuin activity affects many cellular activites, but most mitochondrial sirtuin targets are implicated in control of cellular metabolism. Within the mitochondria, three sirtuin family members are known to be active; SIRT3, SIRT4, and SIRT5 (Figure 5). Over 20 confirmed targets of mitochondrial sirtuins exist, including IDH2, GDH, and SDH. These enzymes affect important metabolic and

regulatory pathways (including the TCA cycle, urea cycle, fatty acid oxidation, ROS metabolism, and the ETC) critical for mitochondrial activity (He *et al.*, 2012).

While the study of sirtuins is an emerging field, knockouts, chemical activators, and chemical inhibitors have been used to artificially target activity through of mitochondrial sirtuins. These studies have identified sirtuins as implicated in mitochondrial dysregulation associated with metabolically-linked diseases. For example, SIRT5 has recently been discovered to be highly expressed in the heart, and knock out of *Sirt5* results in increased succinylation of proteins, decreased ATP production, and reduced long-chain fatty acid oxidation, all of which can lead to heart disease (Sadhukhan *et al.*, 2016). SIRT5-mediated lysine desuccinylation has been shown to decrease both pyruvate dehydrogenase complex (PDC) as well as SDH activity (Park *et al.*, 2013), as well as IDH2 (Zhou *et al.*, 2016).

In mouse liver, *Sirt4* knockdown was shown to increase the expression of *Sirt1* and *Sirt3*, while increasing fatty acid oxidation and oxygen consumption (Nasrin *et al.*, 2010). The role of SIRT4 in negatively affecting fatty acid metabolism was validated in fibroblasts, where SIRT4 repressed glutamine uptake (through GDH), cell proliferation, and tumor progression (Csibi *et al.*, 2013). SIRT4 regulation of GDH activity was also shown to affect TNF and doxorubicin toxicity through the opening of the mitochondrial permeability transition pore, with suppression of SIRT4 leading to decreased cytotoxicity (Verma *et al.*, 2013).

The most studied mitochondrial sirtuin, SIRT3, is an important regulator of mitochondrial metabolism, and is hypothesized to connect phenotypic aspects of pro-inflammatory macrophage response with the metabolic changes seen under these conditions. As I focus mainly on SIRT3 for this thesis, I will briefly summarize what is known about this mitochondrial regulator in the next section.

1.4.3 *SIRT3 - Current knowledge*

SIRT3 has been seen to affect multiple aspects of mitochondrial metabolism while being associated with different disease states. SIRT3 is a lysine deacetylase, modulating multiple metabolic pathways, including oxidative phospho-

rylation, fatty acid metabolism, and the TCA cycle, with over 933 possible acetylation sites affected in the mitochondria (Sol *et al.*, 2012).

SIRT3 has been shown in multiple studies to play a role in tumorigenesis through a series of interactions with important regulators of cell growth and metabolism. SIRT3 associates with Complex I of the ETC to modify its activity, thereby regulating levels of adenosine 5′-triphosphate (ATP) without affecting oxygen consumption (Ahn *et al.*, 2008). Deletion of *Sirt3* in fibroblasts leads to increased ROS production and genomic instability because of hyperacetylation on mitochondrial antioxidant manganese superoxide dismutase (mnSOD), a mitochondrial protein which detoxifies ROS (Tao *et al.*, 2010). SIRT3 inhibiting ROS has been validated by other studies, while at the same time inhibiting HIF-1α (Bell *et al.*, 2011). As HIF-1α is known to modulate glucose uptake and glycolysis, Finley *et al.* (2011a) discovered that SIRT3 destabilizes HIF-1α through ROS detoxification, inhibiting its activity and reducing tumor growth through suppressing rampant glucose metabolism (Warburg effect).

SIRT3 targets several enzymes in the TCA cycle, and can affect the way that glucose and glutamine are metabolized (Figure 6). SIRT3 was found to directly interact with two subunits of the SDH complex (both in the TCA cycle and in the ETC) (Cimen *et al.*, 2009; Finley *et al.*, 2011b), showing that deacetylation activity can target critical junctions within energy metabolism. In addition, SIRT3 can deacetylate IDH2 for the purpose of increasing levels of NADPH and glutathione, protecting against ROS-mediated damage (Yu *et al.*, 2012).

Most research on SIRT3 has been performed on tumor cells to elucidate its role on tumor progression, however, there have been studies linking SIRT3 to the inflammatory response in macrophages as well, mostly with regards to ROS regulation. Similar to the study above, IDH2 was shown to be a deacetylation target of SIRT3 in macrophages (Sheng *et al.*, 2015), which suggests a role for SIRT3 in macrophage-mediated ROS regulation. Palmieri *et al.* (2015) show that the mitochondrial citrate carrier is a SIRT3 target in pro-inflammatory macrophages, which is seen to have increased activity under glucose starvation conditions in order to increase both fatty acid production and NADPH synthesis.

SIRT3 knockdown also affects cytokine expression in macrophages, increasing levels of pro-inflammatory cytokines and mediators (such as iNOS and TNF-α) in RAW 264.7 cell line macrophages (Xu *et al.*, 2016). Conversely, in

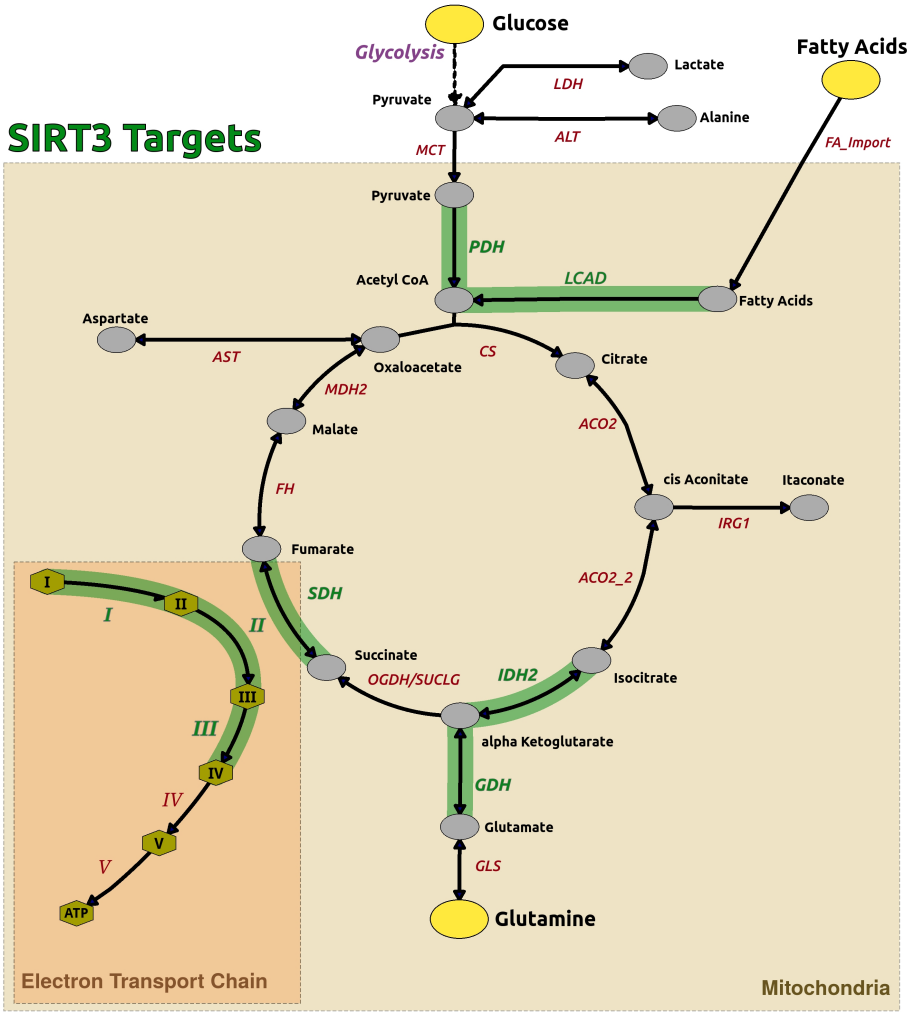

Figure 6: Selected SIRT3 targets in the mitochondria. SIRT3 has been shown to affect multiple enzymes in the mitochondria, impacting carbon import, oxidative phosphorylation through the electron transport chain, and important metabolic breakpoints in the TCA cycle. MCT - Monocarboxylate transporter, LDH - Lactate dehydrogenase, ALT - Alanine aminotransferase, PDH - Pyruvate dehydrogenase, FA_Import - Fatty acid import, LCAD - Long chain acyl-CoA dehydrogenase, AST - Aspartate aminotransferase, CS - Citrate synthase, ACO2/ACO2_2 - Aconitase 2, IRG1 - Cis-aconitate decarboxylase, IDH2 - Isocitrate dehydrogenase 2, GDH - Glutamate dehydrogenase, GLS - Glutaminase, OGDH/SUCLG - Oxoglutarate dehydrogenase, SDH - Succinate dehydrogenase, FH - Fumarate hydratase, MDH2 - Malate dehydrogenase 2, I-V - Complexes in the electron transport chain. Created using Omix (Droste *et al.*, 2011).

primary human macrophages treated with LPS, SIRT1 and SIRT3 mRNA and protein expression is decreased, lending more evidence to the hypothesis that sirtuin family members play a role in the macrophage inflammatory response Storka *et al.* (2013).

Interestingly, the "metabolic breakpoints" in pro-inflammatory macrophages put forth by Jha *et al.* (2015) correspond to two SIRT3 targets: IDH2 and SDH. While only *IDH2* activity has been confirmed to be affected by SIRT3 in macrophages, these findings were integral in motivating the studies described in this thesis. The current knowledge of SIRT3 and mitochondrial metabolic changes in pro-inflammatory macrophages point to an important role of mitochondrial deacetylation activity in the regulation of macrophage metabolism during the inflammatory process.

1.5 EXPERIMENTAL AND CELLULAR TOOLS FOR MACROPHAGE INFLAMMATION STUDIES

Since macrophages are an important aspect in understanding tissue homeostasis and disease progression, a large body of scientific studies focus on primary macrophages, cellular lines, and *in-vitro* experimental conditions established for this field. The majority of macrophage studies are done with RAW 264.7 cells, which are a Abelson Leukaemia Virus transformed macrophage-like cell line, widely used for *in vitro* studies of macrophage response under inflammatory conditions (e.g. Tannahill *et al.* (2013); Michelucci *et al.* (2013); Meiser *et al.* (2015); Cordes *et al.* (2016)). RAW 264.7 cells are easy to grow and handle in a laboratory setting, and are seen in the scientific community as consistent and comparable between experiments and laboratories. Much of the knowledge about macrophage activation and their role in inflammation has been generated using this cell line, and many of these findings have been shown to be directly parallel to *in vivo* activity (Berghaus *et al.*, 2010). It is important to note that RAW 264.7 cells have been transformed to be continuously proliferative, and this must be considered when drawing conclusions about *in vivo* cellular processes based upon results from these cells (Berghaus *et al.*, 2010).

As a step closer to *in vivo* systems, BMDMs are used in many studies to serve as primary cells that can be used in an *in vitro* laboratory setting. BMDMs are differentiated macrophages obtained through the culture of mammalian bone

marrow, typically from *Mus musculus*. Monocytes from bone marrow are differentiated into mature macrophages through continuous exposure to granulocyte macrophage colony-stimulating factor (GM-CSF). Differentiation is performed using either pure GM-CSF, or conditioned cell culture medium from L929 mouse fibroblasts, which produces GM-CSF and other factors which promote macrophage differentiation (Francke *et al.*, 2011; Boltz-Nitulescu *et al.*, 1987). As this cell model comes directly from individual animals, and is not transformed to be proliferative, it is considered to be a more applicable model for translating experimental results to *in vivo* cellular processes (Chamberlain *et al.*, 2009). However, BMDMs have a restricted life-span in laboratory settings, create inter-animal variability, and are much more costly to obtain and work with.

Since there are critical differences between RAW cells and BMDMs, it is important to understand the similarities and differences between the cell line and the primary cells, as well as where they can be comparable. Previous studies have compared RAW cells to BMDMs with regard to cytokine production, cell surface marker expression, and culture ability on different biomaterial surfaces. These studies revealed that RAW cells and BMDMs respond differently to LPS, with different cytokine response profiles and surface marker populations (Berghaus *et al.*, 2010; Chamberlain *et al.*, 2009).

A large variety of cytokines play a role in macrophage differentiation and their function *in vivo*; there is a strong polarization of important phenotype-inducing signals and secreted cellular signals between pro- and anti-inflammatory macrophages (Mantovani *et al.*, 2004). In *in-vitro* experiments, macrophages are stimulated into a pro-inflammatory phenotype by effectors such as LPS (a PAMP), and interferon-gamma (IFN-γ) (a signaling cytokine), and into an anti-inflammatory phenotype by compounds such as interleukin-4 (IL-4) and IL-13 (both signaling cytokines) (Gordon and Martinez, 2010).

In addition to the classical laboratory activation compounds of inflammation, some studies infect macrophages with live bacteria to provide a challenge which is more similar to an *in vivo* infection condition. Bacteria used for these studies can vary, but the most common are those of the genus *Salmonella*, and have been used to determine effects of infection on macrophages as well as to uncover novel regulatory factors in macrophage metabolism (Shi *et al.*, 2009; Michelucci *et al.*, 2013). *Salmonella* enterica serovar Typhimimurium (*S.*

Typhimuirum) is a gram-negative facultative anaerobic bacterium characterized by an induction of pro-inflammatory cytokine secretion in mouse models (Zhang *et al.*, 2003). Simultaneously, *S*. Typhimurium can modulate host cell metabolism and induce pro-inflammatory cell death through virulence effector proteins (Robinson *et al.*, 2012). There are multiple cellular defense mechanisms against *S*. Typhimurium infection, including phagolysosomal degradation, ROS production (West *et al.*, 2011) and itaconic acid production (Cordes *et al.*, 2015).

1.6 METABOLOMICS - MEASURING THE METABOLISM OF CELLS

Even today, metabolic activity is estimated based on the abundance and activity of enzymes (Moreira *et al.*, 2015). However, enzyme abundance can be affected by transcription and translation speeds, while activity can be modified through post-translational modifications, thermodynamic properties such as cellular pH, and other changes arising from normal and perturbed cellular processes. These changes can obscure the ability of protein studies to inform on actual metabolic changes, and while new knowledge has come through these studies, measuring precise changes in intracellular metabolite pools has been elusive.

Through breakthroughs in technology, high-throughput approaches targeting the different levels of cellular regulation are now possible. Transcriptomics and proteomics give valuable information on global changes in mRNA and proteins expression, while metabolomics complements these analyses through the measurement of intracellular metabolite pools. In this way, metabolomics provides a snapshot of biochemical reactions occurring in the cell, and provide a tool to study how these reactions are affected in response to different perturbations of the cellular environment. Metabolomics data can be applied in the use of metabolic profiling for different diseases (Hiller and Metallo, 2013), biomarker identification and diagnostic aids (Weiner 3rd *et al.*, 2012), as well as integration into mutli-omics networks for a deeper understanding of cellular systems (Bordbar *et al.*, 2012; Jha *et al.*, 2015).

Both targeted and non-targeted metabolomics approaches can be applied, depending on the scientific question that is asked. Non-targeted metabolomics is mostly used for biomarker determination, as well as global metabolome pro-

filing (Hiller *et al.*, 2011), while targeted metabolomics focuses on the analysis of specific compounds (Michelucci *et al.*, 2013; Tannahill *et al.*, 2013; Fendt *et al.*, 2013; Cordes *et al.*, 2016).

1.6.1 *Analytical pipeline - From quenching metabolism to measuring metabolites*

The metabolic profile of a cell can change on the order of seconds, so cellular metabolism must be quenched in order to both halt the function of biochemical pathways in the cell and to minimize the effects of experimental handling and sample preparation (Ewald *et al.*, 2009). Metabolic quenching must be a quick process, and a mixture of ice-cold water and methanol has been found to provide the highest extraction efficiency and minimal sample loss (Lin *et al.*, 2007; Sellick *et al.*, 2008). After quenching, cells are lysed, polar/non-polar metabolites are extracted, and analyzed. One advantage of metabolomics extractions is that proteins or mRNA can be extracted simultaneously, which minimizes the amount of experiments needed to obtain biological knowledge as well as minimizing the variation that comes with repeated experiments (Sapcariu *et al.*, 2014).

Commonly used techniques for measuring metabolites include GC-MS (Hiller *et al.*, 2009), liquid chromatography coupled to mass spectrometry (LC-MS) (Ewald *et al.*, 2009), and nuclear magnetic resonance (NMR) (Lin *et al.*, 2007), but for the purpose of this thesis I will focus on GC-MS. In short, for this technique, metabolite extracts are transfered into the gas phase, run through a capillary column with a stationary phase to aid with separation of different compounds, and finally ionized and measured on a detector. GC-MS analyses are highly reproducible, especially when using electron ionization (EI).

Metabolite extracts must be derivatized prior to gas phase transfer, in order to maximize volatility of compounds and therefore increase the amount that can be measured. For the work in this thesis, two types of compound derivatization was used, both of which replace the hydrogen in polar groups with non-polar derivatives. N-Methyl-N-trimethylsilylfluoroacetamide (MSTFA) was added to extracts to create trimethylsilyl (TMS) groups, and N-tert-butyldimethylsilyl-N-methyltrifluoroacetamide (MTBSTFA) was added to extracts to add tert-butyl dimethylsilyl (TBDMS) groups. The different derivatives are used depending on the compounds of interest in the analysis, as TBDMS groups are larger than TMS,

some compounds (e.g. glucose) become too large for the detector to measure, and therefore cannot be analyzed.

Finally, EI is a hard ionization technique, breaking the compound into multiple fragments before hitting the detector. This fragmentation pattern is reproducible for all EI measurements, and acts as a fingerprint that allows for the reproducible identification of metabolites based upon a library that can be created through the measurement of analytical standards.

1.6.2 *Stable isotope labeling and metabolic flux analysis*

Through the utilization of stable isotope labeling in cells, metabolomics analyses can be extended, allowing for the inference of the movement of metabolites through metabolic pathways. Labeled carbon from these tracers is integrated into metabolites through normal metabolic processes, and the labeling patterns of the various metabolites are measured and interpreted, in a technique called ^{13}C tracer analysis (Buescher *et al.*, 2015). The application of this technique is growing in metabolomics studies, and can be a very useful method of understanding how metabolic pathways change under different cellular conditions, such as inflammation in macrophages (Michelucci *et al.*, 2013; Jha *et al.*, 2015).

To perform these experiments, cells are cultured in medium with a stable isotope labeled tracer, targeted for the scientific question. ^{13}C-labeled tracers are commonly used in these analyses, and were used as well for the experiments performed in the scope of this thesis. Once the labeled carbon source is taken up, metabolism proceeds as normal under the experimental conditions, and the labeled carbon is metabolized throughout the pathways utilized by the cell. Depending on the differing metabolic pathways leading to target metabolites, labeling patterns of the compounds are different, forming a unique mass isotopomer distribution (MID). These MIDs can be measured by GC-MS, and changes in metabolic fluxes can be inferred based upon the result.

For the experiments in this study, I utilized two tracers: [U-$^{13}C_6$]glucose and [U-$^{13}C_5$]glutamine, allowing me to understand how carbons from these two main cellular inputs distributed to metabolites in central carbon metabolism under different experimental treatments.

GC-MS analysis, as described above, can differentiate between labeled and unlabeled compounds, as well as compounds with different amounts of iso-

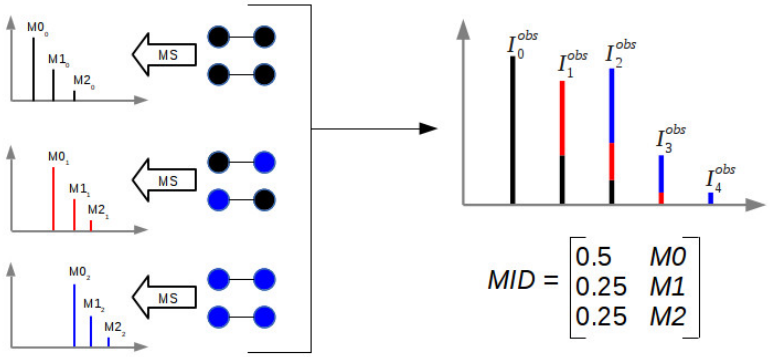

Figure 7: An example of a mass isotopomer distribution (Based on Hiller *et al.* (2011)). An differentially labeled example two atom compound is shown, as well as corresponding spectra which depend upon which atoms are unlabeled (black circle) or labeled (blue circle). Each labeled atom will shift the mass spectrum by one unit (left side). It should be noted that it is not possible to distinguish (in GC-MS analysis) between different isotopomers (i.e. compounds with the same number of labeled atoms, but on different positions). A mixture of the same compound with different amounts of labeled atoms will result in a complex spectrum with all labeling patterns mixed (right side). With this data, the MIDs of the compound can be algorithmically calculated.

topic enrichment. Once the mass spectra is measured, MIDs can be calculated for each metabolite (Figure 7). Each incorporated stable-isotope will shift the spectrum of the compound fragment by one mass unit; for example, labeled fragments of [U-$^{13}C_5$]glutamine will be shifted by five units (compared to non-labeled glutamine).

It must be noted that stable isotopes are also present in the environment (around 1% of carbon in nature are ^{13}C isotopes), and these natural abundances cause the formation of isotopic peaks in GC-MS spectra not containing artificial labeling. This natural isotopic enrichment must be corrected for in any calculation of MIDs.

1.7 OBJECTIVE OF THIS THESIS

The initiation of the pro-inflammatory phenotype in macrophages can be caused by a variety of factors, including environmental pollution and bacterial infection. Many aspects of pro-inflammatory macrophages are well characterized, such as cytokine expression, transcriptional changes, and phagocytic activity. Upregulation of cytokines such as IL-1b, and TNF-α through NF-κB and MAPK signaling pathways define the classical pro-inflammatory macrophage. However, the investigation of metabolic changes of macrophages in the inflammatory process remains an emerging field.

It is thought that macrophages can change their phenotype during the inflammatory process, leading to changes in metabolism which play a role in modifying macrophage energy use and antimicrobial activity. Previous metabolic studies have uncovered a glycolytic activity increase in pro-inflammatory macrophages (regulated by cytokines and their effectors), as well as the increase of two metabolites linked to inflammation: itaconic acid and succinic acid. While the regulation of itaconic acid as an antimicrobial compound was found to be controlled by *Irg1*/CAD activity, the buildup of succinic acid is due to a modification of TCA cycle activity.

The aim of this thesis is to follow up on the idea of the two metabolic breakpoints leading to the accumulation of itaconic and succinic acid suggested by Jha *et al.* (2015), in order to understand the connection between the important metabolic players in pro-inflammatory macrophages. To do this, the following questions guided this research:

- Does environmental pollution lead to the same metabolic changes in macrophages as classical bacterial infection?
- Is the pro-inflammatory macrophage phenotype comparable between primary cells and cell lines?
- How does the TCA cycle operate during inflammation, and how does it uncouple from its classical activity during the response to pro-inflammatory perturbations?
- Is there a connection between succinic acid and itaconic acid in pro-inflammatory macrophages?
- Are the metabolic changes in pro-inflammatory macrophages regulated in part by SIRT3?

Using classical and stable-isotope assisted metabolomics techniques, combined with the analysis of gene and protein regulation, the multiple studies in this work attempt to answer these questions as best as possible in order to probe further into the changes in the metabolism of macrophages under pro-inflammatory stimulation.

2

MATERIALS AND METHODS

2.1 CELL CULTURE AND REAGENTS

The mouse macrophage RAW 264.7 cell line was obtained from ATCC (ATCC TIB-71, Manassas, VA, USA). Cells were cultured in Dulbecco's Modified Eagle's Medium (DMEM) 5796 (Sigma Aldrich) with 10% Fetal Bovine Serum (PAA or Invitrogen) and 1% penicillin/streptamycine (Gibco, Invitrogen), and stored in an incubator at 37°C with 5% CO_2. Cells were grown and cultured in cell culture flasks (Thermo Fisher Scientific), and split through scraping three times a week.

For BMDM experiments, bone marrow (frozen in Fetal Bovine Serum with 15% DMSO) from C57Bl/6 mice was obtained, and cultured for 7 days in Roswell Park Memorial Institute medium (RPMI) 1640 VLE (Merck Millipore) supplemented with 10% Fetal Bovine Serum and 20% L929 cell culture supernatant (Dulbecco's Modified Eagle's Medium + 10% Fetal Bovine Serum) to differentiate cells into BMDMs. Medium was changed on day 2 and day 5 to promote differentiation, and cells were seeded on day 6, discarding any floating cells. Cells were detached by scraping, and all cell seeding and experiments were performed using RPMI without L929 supernatant.

The following inflammatory stimulants were used to induce pro-inflammatory macropahges: *Escherichia coli* purified LPS (Sigma Aldrich), recombinant mouse IFN-γ (R&D systems Europe). All concentrations for experiments are given in the text, and follow commonly used concentrations. Honokiol (Sigma Aldrich) was dissolved in ethanol and diluted in MilliQ water for stimulation. The maximum concentration of ethanol exposed to cells was 0.5%.

2.1.1 *Stable isotope labeling experiments*

For stable isotope labeling experiments, cells were cultured as above, but were seeded in a labeled medium 24 hours before treatment.

RAW cells were seeded in Dulbecco's Modified Eagle's Medium (D5030, Sigma Aldrich), supplemented with 3.7 g/L of sodium bicarbonate and 10% dialyzed fetal bovine serum. 25 mmol/L glucose and 5 mmol/L glutamine were also supplemented in the medium. For labeled glucose experiments, U-$^{13}C_6$-Glucose (Cambridge Isotope Laboratories) was substituted, and for labeled glutamine experiments, U-$^{13}C_5$-Glutamine (Campro Scientific) was substituted. The pH of the finished medium was adjusted to 7.4, sterile filtered through a 0.22 µm Steriflip filter unit (Merck Millipore), and stored at 4°C until use.

For BMDMs, RPMI 1640 was used, which contained either no glucose or no glutamine. For labeled glucose experiments, 11 mmol/L of U-$^{13}C_6$-Glucose (Cambridge Isotope Laboratories) was used, and for labeled glutamine experiments, 2 mmol/L of U-$^{13}C_5$-Glutamine (Campro Scientific) was used. The medium was pH adjusted and sterile filtered in the same manner as above.

2.2 STIMULATIONS AND EXPOSURE

2.2.1 *Inflammatory exposure in vitro*

Cells were stimulated for 6 hours at stated concentrations, except for the time-course experiments, where the time points are given. During stimulation, cells were incubated at 37°C with 5% CO_2. All experimental treatments were performed in biological triplicates.

2.2.2 *Air-Liquid Interface Experiments*

2.2.2.1 *Cell culture*

The mouse macrophage RAW 264.7 cell line was obtained from ATCC (ATCC© TIB-71™). Cells were cultured in RPMI-1640 medium supplemented with 10% (v/v) Fetal Bovine Serum and 100 U/ml penicillin, 100 mg/ml streptomycin (Life Technologies, Darmstadt), and cultivated in an incubator at 37°C with 5% CO_2. 24 hours before exposures, cells were seeded on PET Transwell© plates (3450, Corning), and placed in an ALI device (Vitrocell), which was connected to the engine. Cells were exposed to two treatments for each fuel type: unfiltered exhaust gas, and exhaust gas filtered for particulate matter. Control cells were placed in an incubator next to the ALI. For stable isotope labeling

experiments, cells were seeded 24 hours before the experiment in RPMI-1640 medium as above, with 12.5 mmol/L U-$^{13}C_6$-Glucose (Cambridge Isotope Laboratories, USA) substituted for unlabeled glucose.

2.2.2.2 *Engine and exposure*

A four-stroke single-cylinder direct-injected diesel engine test bed situated at the University of Rostock in the Chair of Piston Machines and Internal Combustion Engines was used to generate aerosol for the exposure study. Heavy fuel oil HFO 180 was used as a representative fuel for ship operation outside of sulfur emission control areas (SECAs). Distillate diesel fuel (DF) according to DIN EN 590 was used as a reference. The DF fuel represents a modern, sulfur-free distilled fuel as used in inland waterway transportation and SECAs. The engine ran at four different operating points: 100%, 75%, 50%, and 25% load at a nominal speed of 1,500 rev/min. A detailed characterization of the aerosol composition at the ALI exposure system was performed, (Reda *et al.*, 2015). The duration of each operation point was set in accordance to their weighting factors as described in ISO 8178-4 E2. The total cycle duration was 2 hours, and this cycle was run twice for a single exposure. To obtain comparable particle deposition doses for the experiments with the two fuel types, clean air dilution ratios of 1:40 and 1:100 were used for the exhaust aerosols of DF and HFO emissions, respectively. Based on a post-experiment gravimetric filter analysis of PM 2.5 and assuming a constant deposition probability of 1.5%, which was determined using previous measurements from ALI exposure systems (Comouth *et al.*, 2013), the particle mass deposited on the lung cell monolayer surface was calculated at 28 $\pm$ 1.5 ng/cm² (DF) and 56 $\pm$ 0.7 ng/cm² (HFO) for the 4 hour exposure (Oeder *et al.*, 2015).

2.2.2.3 *Air-liquid interface exposure*

An automated ALI exposure system station (VITROCELL Systems, GmbH, Waldkirch, Germany) with 18 exposure positions was used as the interface for cellular exposures of the diesel engine exhaust (Mülhopt *et al.*, 2008). ALI exposures were performed in a custom built mobile HICE S2 bio safety laboratory, placed next to the engine hall. Diluted DF or HFO aerosol was led through heated stainless steel lines from the engine test bed into the ALI sys-

tem. Exposures were performed as described for ALI exposures of BEAS2B and A549 epithelium cells (Oeder *et al.*, 2015).

Cells were seeded in fetal bovine serum supplemented RPMI-1640 on transferable 24 mm Transwell™ inserts with a 0.4 µm pore polyester membrane (Type #3450, Corning, NY, USA) 24h before exposure at a density of 1 x 10^6 cells/mL/insert (2.1 x 10^5 cells/cm² growth area) with 1.5 mL cell culture medium provided beneath the insert membrane. For cell exposure, the culture medium on the apical side was completely removed and cells were placed in the ALI exposure system with RPMI-1640 medium without FBS, supplemented with 10 mM HEPES, provided at the basolateral side. Cells were then exposed for 4h to the diluted and conditioned (85% r.h., 37°C, maintained by the ALI exposure system) aerosols with a controlled flow of 100 mL/min for each insert (Mülhopt *et al.*, 2016; Paur *et al.*, 2011). Cells were exposed to both the complete aerosol (with both particle phase and gas phase), and the gas phase only (with particles filtered out of the complete aerosol by a high efficiency particle membrane filter). All fuel-specific results represent both the filtered and unfiltered treatments, unless otherwise stated. Cells kept in an incubator at 37°C with 5% CO_2 were used as a control treatment. Metabolite extraction and GC-MS analysis took place as described for the other experiments.

2.2.2.4 *LDH release assay*

After exposure, medium from the compartment under the membrane was collected and frozen at -80°C for later analysis. An aliquot was used for quantification of released LDH, an indicator of plasma membrane integrity. An LDH detection kit was used in accordance with the manufacturers, instructions (Roche, Mannheim, Germany) with slight modifications: the dye solution was diluted 1:1 (v/v) with phosphate-buffered saline to slow down the reaction time caused by elevated LDH values due to the high cell densities used for ALI exposure experiments. After 20 minutes, before saturation was reached, the reaction was stopped and the absorbance of the reaction mix was measured at 490 nm with a microplate reader. Cells lysed with Triton X-100 (Sigma Aldrich) were used as a positive control for cellular toxicity. Absorbance read from the samples was normalized to the absorbance of blank medium. Statistical analysis was performed using an analysis of variance (ANOVA) test, followed by a post-hoc Tukey test for pairwise statistical analysis.

2.3 CELL COUNTING

All cell counting was performed on cells grown in 12-well culture plates. Cell culture medium was removed from the cells, and 1 mL of fresh medium was added to each well. Cells were detached using a cell scraper and then transfered into sample cups (Vi-Cell, Beckman Coulter). Cell count and viability was measured using a cell viability analyzer (Vi-Cell, Beckman Coulter).

2.4 METABOLITE AND MRNA EXTRACTION PROTOCOL

For all inflammatory stimulation experiments, cells were seeded on 12 well Nunclon coated plates (Thermo Scientific) two days before stimulation, to reduce variation and cellular stress due to handling.

The extraction protocol used in this thesis was published in 2014 Sapcariu *et al.* (2014). Cells were washed with 0.9% NaCl, and immediately quenched with 200 µL Chromasolv® Methanol (Sigma) at -20°C and 200 µL Millipore H_2O on ice. Cell extracts were scraped and added to eppendorf tubes containing 200 µL Chromasolv® chloroform at -20°C. Tubes with extract were then vortexed in a 4°C shaker at 1400 rpm for 20 minutes and centrifuged at 4°C for 5 minutes at 20,000 g. This results in a three-phase separation of the sample (Figure 8). 200 µL of the polar phase was transfered to a glass vial specific for GC-MS analysis (Chromatographie Zubehor Trott), dried in a rotary vacuum evaporator (Labconco) at -4°C overnight, and stored at -80°C until analysis. The interphase was washed with methanol and stored at -80°C until RNA extraction. As an internal standard for unlabeled experiments, ^{13}C-Ribitol was added to the extraction water at a concentration of 1 µg/mL. For labeled experiments, pentanedioic-d_6 acid was added to the extraction water at a concentration of 1 µg/mL.

2.5 GC-MS ANALYSIS

Derivitization was performed with an Gerstel autosampler directly before measurement on the GC-MS. Dried metabolites were dissolved in 15 µL of 2% methoxyamine hydrochloride in pyridine at a temperature of 40°C for 60 min-

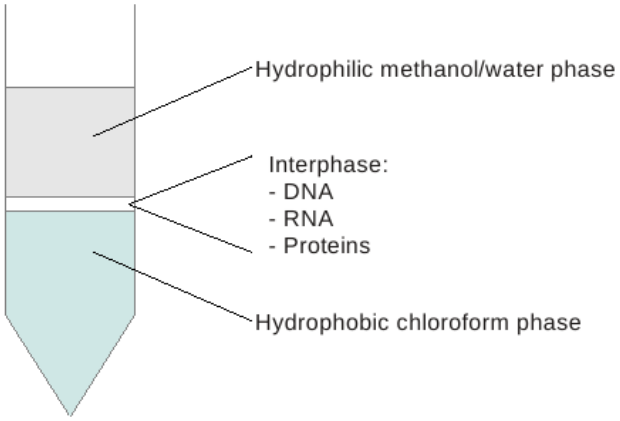

Figure 8: Three-phase methanol-chloroform extraction for biological samples. Hydrophilic phase was used for metabolite analysis using GC-MS, the interphase was used for qPCR analysis of extracted mRNA.

utes. Then, 15 µL of 2,2,2-trifluoro-N-methyl-N-trimethylsilyl-acetamide + 1% chloro-trimethyl-silane was added and incubated at 40°C for 30 minutes.

The metabolite extracts were measured on an Agilent 7890 GC containing with a 30 m DB-35MS capillary column. The GC was connected to an Agilent 5975C MS operating in electron ionization (EI) at 70 eV.

1 µL of derivatized sample was hot injected at 270°C in splitless mode. Helium was used as the carrier gas at a flow rate of 1 mL/min. The GC oven temperature was kept constant at 100°C for 2 minutes and then increased to 300°C at 10°C/min, where it was held for 4 minutes. The total GC-MS run time of one sample was 26 minutes. For relative quantification of metabolite levels, an alkane mix was run with the experimental sequence in order to provide retention index calibration for the experimental samples.

The MS source was kept at a constant temperature of 230°C and the quadrupole at 150°C. For relative quantification of metabolite levels, the detector was operated in scan mode with an m/z range of 70 to 800. For analysis of stable isotope labeling, the detector was operated in selected ion monitoring (SIM) mode.

2.6 MRNA EXTRACTION AND QUANTITATIVE REAL-TIME PCR

Washed interphases were dried in a rotary vacuum evaporator (Labconco) at 4°C until all liquid phase was evaporated, and then brought to room tem-

perature. RNA was extracted from the interphase of the samples using the Qiagen RNeasy minikit, and RNA purity was checked on a Thermo Scientific NanoDrop 2000C spectrophotometer. RNA was reverse transcribed into complementary deoxyribonucleic acid (cDNA) using Invitrogen SuperScript™ III reverse transcriptase, and stored at -20°C until qPCR analysis. All treatments were performed in technical triplicates on the 96-well plate for statistical robustness.

Analysis of cDNA was performed on a Roche LightCycler 480 II, with iq™ SYBR® green supermix including the fluorescent pigment and the polymerase required for the reactions. The program for the qPCR was as follows: activation of the polymerase for 3 minutes at 95°C, 40 amplification cycles (30 seconds denaturation at 95°C, 30 seconds annealing at 60°C, 30 seconds elongation at 72°C), melting curve analysis, and a cooling step at 40°C. Comparative quantification (using the ΔΔCt method) was performed using LibreOffice Calc. The primers used in qPCR analysis are shown in Table 1.

2.7 METABOLOMICS DATA ANALYSIS

Analysis of the raw peak data for both relative metabolite quantification and MID analysis was performed using MetaboliteDetector (Hiller *et al.*, 2009). This software provided chromatogram alignment, peak matching, and automated compound identification (using an in-house library). Raw data was exported from MetaboliteDetector and processed using either R statistical software (R Core Team, 2013) or LibreOffice Calc.

2.7.1 *Relative Metabolite Quantification*

All metabolites identified with MetaboliteDetector were verified through manual chromatogram analysis of characteristic fragment peaks.

Normalization of the metabolite raw data was performed using the following methods: First, all metabolites were normalized to the internal standard added to the extraction water in order to control for variations in extraction amount and GC-MS measurements. Where applicable, normalized metabolite signal intensity was further normalized to cell count as well as to the control

Il-1b forward	5′-GCTTCAGGCAGGCAGTATC-3′
Il-1b reverse	5′-AGGATGGGCTCTTCTTCAAAG-3′
Tnfα forward	5′-GGTTCTGTCCCTTTCACTCAC-3′
Tnfα reverse	5′-TGCCTCTTCTGCCAGTTCC-3′
Sirt1 forward	5′-GATGACAGAACGTCACACGC-3′
Sirt1 reverse	5′-ATTGTTCGAGGATCGGTGCC-3′
Sirt3 forward	5′-TCACAACCCCAAGCCCTTTT-3′
Sirt3 reverse	5′-GTGGGCTTCAACCAGCTTTG-3′
Sirt5 forward	5′-CCTGGATCCTGCCATTCTGG-3′
Sirt5 reverse	5′-GGGTCCGGGAAAATGAAACC-3′
Il6 forward	5′-CGGCCTTCCCTACTTCACAA-3′
Il6 reverse	5′-TCTGCAAGTGCATCATCGTT-3′
Il10 forward	5′-GCTGCCTGCTCTTACTGACT-3′
Il10 reverse	5′-CCTGGGGCATCACTTCTACC-3′
Irg1 forward	5′-GCAACATGATGCTCAAGTCTG-3′
Irg1 reverse	5′-TGCTCCTCCGAATGATACCA-3′
Hif-1 forward	5′-TGACGGCGACATGGTTTACA-3′
Hif-1 reverse	5′-AATATGGCCCGTGCAGTGAA-3′
Hif-2 forward	5′-AGGTCTGCAAAGGACTTCGG-3′
Hif-2 reverse	5′-CAAGTGTGAACTGCTGGTGC-3′
Casp3 forward	5′-TCATCTCGCTCTGGTACGGA-3′
Casp3 reverse	5′-ACACACACAAAGCTGCTCCT-3′
L27 forward	5′-ACATTGACGATGGCACCTC-3′
L27 reverse	5′-GCTTGGCGATCTTCTTCTTG-3′

Table 1: Primers used for qPCR Analysis

(or t=0) treatment, in order to provide a standard basis for comparison across experiments.

2.7.2 *Mass Isotopomer Distribution Analysis*

MIDs were determined from samples cultured with labeled tracers (as per Section 2.1.1) using SIM measurements. The data was corrected for natural isotope abundances using MetaboliteDetector software.

Weighted carbon contribution for labeled compounds was calculated using the following formula:

$\frac{1}{n} * \sum_{i=1}^{n} M_i * i$

where n is the number of carbons in the compound of interest, and M_i is the i^th mass isotopomer. Glucose and Glutamine contribution was calculated with samples from the same experimental replicate, and contribution from other sources was calculated by:

$1 - (C_{Glc} + C_{Gln})$

where C_{Glc} and C_{Gln} are the weighted carbon contributions from glucose and glutamine, respectively.

3

RESULTS AND PUBLICATIONS

SIMULTANEOUS EXTRACTION OF PROTEINS AND METABOLITES FROM CELLS IN CULTURE

Sapcariu SC, Kanashova T, Weindl D, Ghelfi J, Dittmar G, Hiller K. *MethodsX*. **2014**, 1, 74-80. *doi:10.1016/j.mex.2014.07.002*

This manuscript was written by me, based upon a laboratory protocol that is used in our lab as well as in the HICE project, in order to utilize the same experimental sample for multiple omics analysis techniques. I organized the preparation of the manuscript between all authors, and wrote the majority of it. The section on proteomics sample preparation and analysis was written by T. Kanashova, and the figure was created by D. Weindl.

MethodsX 1 (2014) 74–80

Contents lists available at ScienceDirect

MethodsX

journal homepage: www.elsevier.com/locate/mex

Simultaneous extraction of proteins and metabolites from cells in culture

Sean C. Sapcariu [a,c,*], Tamara Kanashova [b,c], Daniel Weindl [a], Jenny Ghelfi [a], Gunnar Dittmar [b,c,**], Karsten Hiller [a,c]

[a] Luxembourg Centre for Systems Biomedicine, University of Luxembourg, L-4362 Esch-Belval, Luxembourg
[b] Mass Spectrometry Core Unit, Max-Delbrück Center for Molecular Medicine, 13125 Berlin, Germany
[c] HICE – Helmholtz Virtual Institute of Complex Molecular Systems in Environmental Health – Aerosols and Health, Germany[1]

GRAPHICAL ABSTRACT

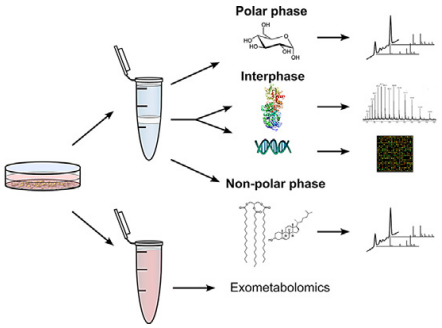

Three-phase methanol–water–chloroform extraction for biological samples. Examples of components available from each phase are shown. These different phases can be then used for a variety of different analysis methods on different levels of cellular regulation.

ABSTRACT

Proper sample preparation is an integral part of all omics approaches, and can drastically impact the results of a wide number of analyses. As metabolomics and proteomics research approaches often yield complementary information, it is desirable to have a sample preparation procedure which can yield information for both types of analyses from the same cell population. This protocol explains a method for the separation and isolation of metabolites and proteins from the same biological sample, in order for downstream use in metabolomics and

[1] www.hice-vi.eu.

* Corresponding author at: 7, avenue des Hauts-Fourneaux, L-4362 Esch-sur-Alzette, Luxembourg. Tel.: +352 46 66 44 6583.
** Corresponding author at: Robert-Rössle Strasse 10, 13125 Berlin, Germany. Tel.: +49 30 94062642.
E-mail addresses: sean.sapcariu@uni.lu (S.C. Sapcariu), gdittmar@mdc-berlin.de (G. Dittmar).

http://dx.doi.org/10.1016/j.mex.2014.07.002

proteomics analyses simultaneously. In this way, two different levels of biological regulation can be studied in a single sample, minimizing the variance that would result from multiple experiments. This protocol can be used with both adherent and suspension cell cultures, and the extraction of metabolites from cellular medium is also detailed, so that cellular uptake and secretion of metabolites can be quantified.

Advantages of this technique includes:

1. Inexpensive and quick to perform; this method does not require any kits.
2. Can be used on any cells in culture, including cell lines and primary cells extracted from living organisms.
3. A wide variety of different analysis techniques can be used, adding additional value to metabolomics data analyzed from a sample; this is of high value in experimental systems biology.

ARTICLE INFO
Method name: Combined metabolomics and proteomics extraction
Keywords: Sample preparation, Metabolomics, Proteomics, Biomolecule extraction, Isolation, GC/MS, LC/MS
Article history: Received 3 June 2014; Accepted 9 July 2014; Available online 18 July 2014

Method details

Washing cells, quenching metabolism, extraction and separation of phases

Materials

- Living cells, cultured on petri dishes or multi-well plates. Cells can be incubated with a labeled tracer (for example: ^{13}C or ^{15}N) for downstream flux analysis
  - Cells should be confluent in the wells, with a consistent cell number between samples. The amount of cells will vary depending on cell type used, but we have found using around 1 million cells in each well of a 6-well multiwell plate gives good results for both techniques.
- 0.9% NaCl at room temperature
- High purity (MS grade) methanol at −20 °C
- High purity (MS grade) chloroform at −20 °C
- Millipore or equivalently pure water on ice
- Cell scrapers
- Eppendorf tube shaker at 4 °C
- Centrifuge at 4 °C
- *Note*: This list does not include generic laboratory equipment, which are assumed to be available.

The metabolic profile of a cell can change in as little as a few seconds. Therefore, the most important step in metabolite extraction is the quenching of metabolism; this ensures that the metabolic pathways in the cells do not continue to function, and that the cellular state at the point of extraction is as close as possible to the desired analysis time point [1]. This quenching must be performed quickly. There has been much discussion as to which extraction fluids are best for quenching and measuring metabolites [2,3]; however, it is generally agreed that a mixture of water and methanol provides the best extraction efficiency with minimal loss. Both fluids are added directly to the cells, and should be kept as cold as possible (methanol at −20 °C and water on ice).

Once the metabolic processes have been quenched, the next step is to lyse the cells, separating both the polar and non-polar metabolites from the other cellular substances at the same time. While methanol and water will extract the polar metabolites from a sample, non-polar metabolites must be separated with a non-polar solvent. Therefore, we use chloroform [4] with the methanol/water mixture to separate the polar and non-polar metabolites efficiently. Adherent cells quenched with methanol and water are scraped from the multi-well plates and added to cold chloroform to allow for separation of polar and non-polar phases. These extracts are agitated to complete cell lysis and centrifuged to fully separate the layers.

This is a crucial step for experimental consistency; different amounts of cells in different samples will lead to incorrect comparisons of metabolite levels (which can also occur with cell seeding). Therefore, care should be taken to adequately scrape all wells and transfer as much cellular material as possible from the wells to the chloroform.

After these steps, the cells are shaken to completely lyse the membranes allowing for a more efficient extraction of all possible biomolecules. After shaking, there should be a clear separation between the polar and non-polar phase for the metabolites, with a well-defined interphase containing proteins and nucleic acids.

Procedure – adherent cells

The following procedure is for adherent cells cultured on a 6-well multiplate. For cells cultured on a 12-well multiplate, divide the amount of extraction fluids by two. Amounts for other cell culture vessels should be adjusted accordingly.

1. Retain medium for quantification of cellular consumption and secretion of metabolites.
2. Wash cells with 1 mL 0.9% NaCl. Phosphate buffer solution is avoided because it would create a large phosphate peak during mass spectrometric analysis, masking lower intensity metabolites.
3. Quench cells by adding 400 μL methanol at −20 °C followed by 400 μL Millipore H_2O on ice. As soon as the methanol has been added, place the multiwell plate on ice for the next steps.
4. Scrape wells with a cell scraper. Make sure that as few cells as possible remain attached to the plate through careful and thorough scraping.
5. Transfer cell extract into an Eppendorf tube containing 400 μL chloroform at −20 °C.
6. Agitate cells in a tube shaker (pre-cooled to 4 °C) for 20 min at 1400 rpm, followed by 5 min of centrifugation at a minimum of 16,100 × *g* at 4 °C.

Procedure – suspension cells

The following procedure is for suspension cells cultured on a 6-well multiplate. For cells cultured on a 12-well multiplate, divide the amount of extraction fluids by two. Amounts for other cell culture vessels should be adjusted accordingly.

1. Centrifuge cells in medium at 250 × *g* for 5 min to pellet the cells, collect medium and retain for quantification of cellular consumption and secretion of metabolites.
2. Wash cells with 1 mL 0.9% NaCl, centrifuge at 250 × *g* for 5 min to pellet the cells, then discard NaCl.
3. Quench cells by adding 400 μL methanol at −20 °C and 400 μL Millipore H_2O on ice.
4. Add 400 μL chloroform at −20 °C to the cells, transfer to Eppendorf tubes.
5. Agitate cells in a tube shaker (pre-cooled to 4 °C) for 20 min at 1400 rpm, followed by 5 min of centrifugation at a minimum of 16,100 × *g* at 4 °C.

Procedure – cell types with both adherent and suspension fractions

For cell types which are both suspended and adherent in culture, the procedure must be modified somewhat to avoid over-dilution of the metabolites. The following procedure is for cells cultured on a 6-well multiplate. Amounts for other cell culture vessels should be adjusted accordingly.

1. Collect the medium from the plate, centrifuge cells in medium at 250 × *g* for 5 min to pellet the cells, collect medium and retain for quantification of cellular consumption and secretion of metabolites.
2. Wash the adherent fraction and suspension fraction of cells each with 1 mL 0.9% NaCl, centrifuge at 250 × *g* for 5 min to pellet the cells, then discard NaCl.
3. Quench cells by adding 200 μL methanol at −20 °C and 200 μL Millipore H_2O on ice to both the suspension cell pellet and the adherent cell pellet. As soon as the methanol has been added, place the multiwell plate on ice for the next steps.
4. Scrape wells containing adherent cell fraction with a cell scraper. Make sure that, as few cells as possible remain attached to the plate through careful and thorough scraping. Transfer the quenched cells to the corresponding non-adherent cell fraction.

5. Add 400 μL chloroform at −20 °C to the cells, transfer to Eppendorf tubes.
6. Agitate cells in a tube shaker (pre-cooled to 4 °C) for 20 min at 1400 rpm, followed by 5 min of centrifugation at a minimum of 16,100 × *g* at 4 °C.

Separation of phases and polar metabolite extraction

Materials

- Glass vials for GC analysis
- Rotary vacuum evaporator
- High purity (MS grade) methanol at −20 °C

After centrifugation, the different phases are now separated, and each one can be sampled for further analysis with multiple techniques. For gas chromatography coupled to mass spectrometry (GC/MS) analysis, samples need to be transfered to a glass vial and dried at a low temperature under vacuum to avoid metabolite degradation. No liquid should remain in the glass vials after drying, and vials should be brought to room temperature under vacuum to avoid condensation. If liquid is still present in the vial, simply dry further in the rotary evaporator. For liquid chromatography coupled to mass spectrometry (LC/MS) analysis, the polar phase can be used directly for injection after transferring to a glass vial.

Procedure

The following procedure is for adherent cells cultured on a 6-well multiplate. For cells cultured on a 12-well multiplate, divide the amount of polar phase extracted by half.

1. Carefully transfer 300 μL of the polar (upper) phase to a glass vial without touching the interphase.
2. Evaporate polar phase in a rotary vacuum evaporator at −4 °C until dry (or overnight). When vials are dry, raise temperature on the rotary vacuum evaporator to room temperature for 30 min before removing the vials to avoid condensation. After capping vials, store at −80 °C until analysis.
3. Remove unused polar phase while avoiding the removal of any interphase. After polar phase is almost completely removed, tilt the Eppendorf tube at a 45°, so that the interphase moves out of the way and the non-polar phase is more easily accessible. If analysis of non-polar phase is to be performed, transfer 300 μL into a glass vial and dry the same way as the polar phase. Otherwise, discard the non-polar phase, being careful not to remove the interphase.
4. Wash the interphase with 300 μL methanol at −20 °C, and centrifuge for 10 min at a minimum of 16,100 × *g* at 4 °C.
5. Remove methanol, process interphase to extract proteins or mRNA for further analysis. Alternatively, add 50 μL methanol at −20 °C, and store interphase at −80 °C until further extraction of nucleic acids or proteins.
6. *Optional: For metabolomics analysis of amino acids in the protein fraction, hydrolyze the interphase as follows:* Remove methanol from interphase. Heat interphase overnight in 400 μL of 6M HCl in a tightly sealed tube at 100 °C. Transfer 100 μL to a glass vial and dry in a rotary vacuum evaporator at −4 °C until dry. Store at −80 °C until analysis.

Protein extraction from interphase and sample preparation for LC/MS proteomics analysis

Materials

- Denaturation buffer (6 mol/L urea, 2 mol/L thiourea, 20 mmol/L HEPES, adjusted to pH 8.0)
- 10 μmol/L TCEP (tris(2-carboxyethyl)phosphine), dissolved in ABC-buffer (50 mmol/L ammonium bicarbonate, adjusted to pH 8.5)
- 55 mmol/L chloroacetamide, dissolved in ABC-buffer (as above)

- 0.5 μg/μL Endopeptidase LysC dissolved in ABC-buffer (as above) – trypsin or other proteases can also be used (at the same concentration)
- 10% trifluoroacetic acid (TFA)
- Rotary vacuum evaporator
- Sonicator
- Stage tips, used for desalting

For proteomics analyses, it is necessary to further process the interphase so that the proteins contained within can be analyzed on an LC-MS/MS instrument. For the proteomics analysis the proteins have to be chemically modified and digested to peptides. The proteins are first unfolded and the disulfide bonds are reduced, removing their tertiary and secondary structure, leaving only a chain of amino acids. The second step is the alkylation of the cysteines in order to prevent the spontaneous formation of disulfide bonds. The last step is the digest with a specific protease to generate peptides for the LC-MS/MS analysis. In case the LC system is not equipped with a pre-column the peptides can be concentrated and desalted using stage-tip purification [5].

Procedure

1. Dry the washed interphases (containing the protein fraction) for 15 min in a rotary vacuum evaporator at 35 °C.
2. Resuspend the proteins in 60 μL of denaturation buffer, and sonicate for 1 min to break up protein aggregates.
3. Quantify proteins using a Bradford assay, and isolate a total amount of 100 μg of protein.
4. Mix 2 μL of the TCEP solution with the 100 μg of the sample protein (in solution) in a new Eppendorf tube, and incubate for 30 min at room temperature to reduce the disulfide bonds in the proteins.
5. Add 1 μL of chloroacetamide solution to 10 μL of the sample protein, and incubate for 20 min at room temperature, alkylating the cysteine residues.
6. Add 4 μL of LysC to the solution, and incubate for 3 h at room temperature to digest the proteins. At this point, the samples can be acidified to pH <2.5 by adding 10 μL of 10% TFA solution to stop the digestion, fractionated, desalted using stage tips, and analyzed using LC-MS/MS.

   As an alternative to the LysC digestion in step 6, the proteins can be digested using trypsin using the following steps:
   - In this case, dilute the sample with 4× ABC (Make sure the end concentration of urea in the sample does not exceed 2 mol/L).
   - Next, add 2 μL trypsin and incubate overnight at room temperature. Stop the digestion by adding 10 μL of 10% TFA solution, acidifying the sample to pH <2.5. At this point, the samples can be fractionated, desalted using stage tips, and analyzed using LC-MS/MS.

Extraction of metabolites from cell culture medium

Materials

- An 8:1 mixture of methanol:H_2O at −20 °C
- Glass vials for GC analysis
- Centrifuge at 4 °C
- Refrigerated rotary vacuum evaporator

An important part of characterizing the metabolic state of cells is understanding the uptake and secretion of biomolecules. This can be measured through metabolomic analysis of cell culture medium used in an experiment. This information can be used to understand the energetic needs of a cell in different conditions, and is complementary to the amounts of metabolites inside cellular compartments. For analysis methods such as ^{13}C-metabolic flux analysis, quantification of cellular uptake and secretion rates are a vital part of the information needed to infer metabolic fluxes [6].

Procedure

The following procedure is for high glucose medium (25 mmol/L). For media with less glucose, the dilutions can be reduced.

1. Prepare Eppendorf tubes with 450 μL 8:1 methanol:H_2O at −20 °C.
2. Mix medium well; transfer 50 μL to the extraction fluid. Mix by shortly vortexing.
3. Centrifuge tubes for 5 min at a minimum of 16,100 × *g* at 4 °C.
4. Transfer 100 μL of supernatant to a glass vial and dry in a rotary vacuum evaporator at −4 °C. Cap and store vials at −80 °C until analysis.

Optional: extension of this technique

If desired, alternate extraction techniques can be applied to the interphase after metabolic extraction. As the interphase contains both nucleic acids and proteins, these biomolecules can be isolated for alternate forms of analysis simultaneously with metabolomics. A hydrolysis of the interphase would break down the biomolecules, allowing analysis of individual nucleobases or amino acids using GC/MS and LC/MS. Nucleic acids, such as mRNA or DNA, can be extracted and used for transcriptomics and genomics analyses (microarrays, qPCRs, and others).

Additional information

Integration of biological data across multiple levels of regulation increases the robustness of any experimental result. In many cases, separate experiments are performed (either sequentially or in parallel) using the same conditions, in order to target proteins, metabolites, RNA, or DNA through the individual experiments. Even though care is taken to minimize variation, differences between experiments can sometimes occur due to forces outside of the experimentalist's control. Methods which enable extraction of multiple types of biological material from single experiments allow direct comparison of different cellular activities.

Sample preparation determines the overall sensitivity, accuracy, and robustness of a biological analysis, and is therefore a very important step in experimental design. Thus, it is also the ideal place to modify a protocol for the extraction of multiple type of biological materials. Since Bligh and Dyer published their protocol on extraction of lipids [4], there has been a consistent effort to improve upon extraction methods for metabolomics analyses. Particularly in recent times, as the methods and techniques of metabolomics have increased in use, there has been a concurrent increase of comparisons of different improvements on metabolite extraction protocols.

Complementary to metabolomics analysis, mass spectrometry-based proteomics can be used to investigate the protein composition of a cell, to determine the members of protein complexes, their structure, the protein composition of organelles, and the dynamics of these processes. Protocols for the extraction of proteins have also been steadily improving over the last few decades [7,8], and it is possible to take advantage of the similarities between these techniques and metabolomics extraction techniques to extend current methods.

As it has been often stated that the chloroform/methanol/water extraction is optimal over a large range of compound classes [2,3,9], we intend to broaden the scope of this protocol, including a method for quantification of cellular metabolic uptake and secretion as well as adding the ability for simultaneous proteomics analysis (or analyses of other "omics" levels) in the same sample. This will allow for more robust systems biology approaches for the integration of different cellular regulatory levels, where metabolomics can be used as a base for the understanding of different cellular phenotypes.

It should be noted that this extraction technique could be applied for a wide variety of different approaches. Modern techniques, such as ^{13}C-flux analysis, stable isotope labeling by amino acids in cell culture (SILAC) proteomics, or the analysis of the posttranslational modification state of proteins and their dynamics [8] can be used along with this protocol.

Roume et al. [10] have previously described a comprehensive method for extraction from microbial communities; while this method is comprehensive, it requires multiple kits and a large time

commitment. The protocol described here is inexpensive and relatively quick to perform. In addition, our protocol is designed for and tested on mammalian as opposed to microbial cells. Weckwerth et al. [11] also have an existing protocol for extraction of multiple types of biomolecules from a single sample, but their protocol is designed primarily for plant cells. More steps are necessary to break down the plant cell walls, which increases the time and complexity compared to the technique described here.

Conflicts of interest

The authors declare no conflicts of interest.

Acknowledgements

This authors acknowledge financial support from the HICE Virtual Institute. S.C.S., K.H., D.W., and J.G. also acknowledge financial support from the Fonds National de la Recherche (FNR). Specifically, K.H. and D.W. are funded by the ATTRACT program Metabolomics Junior Group. *MethodsX* thanks the (anonymous) reviewers of this article for taking the time to provide valuable feedback.

References

[1] J.C. Ewald, S. Heux, N. Zamboni, High throughput quantitative metabolomics: workflow for cultivation, quenching, and analysis of yeast in a multiwell format, Anal. Chem. 81 (May (9)) (2009) 3623–3629. , http://dx.doi.org/10.1021/ac900002u.
[2] C.Y. Lin, H. Wu, R.S. Tjeerdema, M.R. Viant, Evaluation of metabolite extraction strategies from tissue samples using NMR metabolomics, Metabolomics 3 (January (1)) (2007) 55–67. , http://dx.doi.org/10.1007/s11306-006-0043-1.
[3] C.A. Sellick, D. Knight, A.S. Croxford, A.R. Maqsood, G.M. Stephens, R. Goodacre, A.J. Dickson, Evaluation of extraction processes for intracellular metabolite profiling of mammalian cells: matching extraction approaches to cell type and metabolite targets, Metabolomics 6 (May (3)) (2010) 427–438. , http://dx.doi.org/10.1007/s11306-010-0216-9.
[4] E.G. Bligh, W.J. Dyer, A rapid method of total lipid extraction and purification, Can. J. Biochem. Physiol. 37 (8) (1959) 911–917. , http://dx.doi.org/10.1139/o59-099.
[5] J. Rappsilber, Y. Ishihama, M. Mann, Stop and go extraction tips for matrix-assisted laser desorption/ionization, nanoelectrospray, and LC/MS sample pretreatment in proteomics, Anal. Chem. 75 (3) (2003) 663–670. , http://dx.doi.org/10.1021/ac026117i.
[6] K. Maier, U. Hofmann, M. Reuss, K. Mauch, Identification of metabolic fluxes in hepatic cells from transient ^{13}C-labeling experiments. Part II: Flux estimation, Biotechnol. Bioeng. 100 (June (2)) (2008) 355–370. , http://dx.doi.org/10.1002/bit.21746.
[7] D. Wessel, F. Ulf-Ingo, A method for the quantitative recovery of protein in dilute solution in the presence of detergents and lipids, Anal. Biochem. 138 (1) (1984) 141–143. , http://dx.doi.org/10.1016/0003-2697(84)90782-6.
[8] T.C. Walther, M. Mann, Mass spectrometry-based proteomics in cell biology, J. Cell Biol. 190 (4) (2010) 491–500. , http://dx.doi.org/10.1083/jcb.201004052.
[9] K. Dettmer, N. Nürnberger, H. Kaspar, M.A. Gruber, M.F. Almstetter, P.J. Oefner, Metabolite extraction from adherently growing mammalian cells for metabolomics studies: optimization of harvesting and extraction protocols, Anal. Bioanal. Chem. 399 (January (3)) (2011) 1127–1139. , http://dx.doi.org/10.1007/s00216-010-4425-x.
[10] H. Roume, E.E.L. Muller, T. Cordes, J. Renaut, K. Hiller, P. Wilmes, A biomolecular isolation framework for eco-systems biology, ISME J. 7 (January (1)) (2013) 110–121. , http://dx.doi.org/10.1038/ismej.2012.72.
[11] W. Weckwerth, K. Wenzel, O. Fiehn, Process for the integrated extraction, identification and quantification of metabolites, proteins and RNA to reveal their co-regulation in biochemical networks, Proteomics 4 (1) (2004) 78–83. , http://dx.doi.org/10.1002/pmic.200200500.

PARTICULATE MATTER FROM BOTH HEAVY FUEL OIL AND DIESEL FUEL SHIPPING EMISSIONS SHOW STRONG BIOLOGICAL EFFECTS ON HUMAN LUNG CELLS AT REALISTIC AND COMPARABLE IN VITRO EXPOSURE CONDITIONS

Oeder S*, Kanashova T*, Sippula O*, Sapcariu SC*, Streibel T, Arteaga-Salas, JM, Passig J, Dilger M, Paur HR, Schlager C, et-al. *PLoS One*. **2015**, 10(6). *doi:10.1371/journal.pone.0126536*

* These authors contributed equally to this work

This article was a collaborative effort from the HICE consortium, based upon an experimental campaign combining analytical chemistry and multiple omics analyses techniques to characterize ship diesel aerosol and its effects on epithelial lung cells. I aided in the design and organization of the experiments performed during the campaign, and was as well responsible for the extraction procedure of the cells for metabolomics and proteomics analyses (based upon the technique detailed in the previous manuscript). For the preparation of the manuscript, I performed all measurement and data analysis for the metabolomics samples, and the initial creation of the figures relating to this data, including figure 3c,g,h, figure S6, and figure S9 (the figures were finalized by another author). In addition, I wrote the section on metabolomics methods, results, and discussion, and was involved in editing the manuscript for English proofreading.

PLOS ONE

RESEARCH ARTICLE

Particulate Matter from Both Heavy Fuel Oil and Diesel Fuel Shipping Emissions Show Strong Biological Effects on Human Lung Cells at Realistic and Comparable *In Vitro* Exposure Conditions

Sebastian Oeder[1,2,3☯], Tamara Kanashova[1,4☯], Olli Sippula[1,5☯], Sean C. Sapcariu[1,6☯], Thorsten Streibel[1,7,8☯], Jose Manuel Arteaga-Salas[1,8☯], Johannes Passig[1,7☯], Marco Dilger[1,9,10], Hanns-Rudolf Paur[1,9], Christoph Schlager[1,9], Sonja Mülhopt[1,9], Silvia Diabaté[1,10], Carsten Weiss[1,10], Benjamin Stengel[1,11], Rom Rabe[1,11], Horst Harndorf[1,11], Tiina Torvela[5], Jorma K. Jokiniemi[1,5,12], Maija-Riitta Hirvonen[1,5,13], Carsten Schmidt-Weber[2], Claudia Traidl-Hoffmann[3,14], Kelly A. BéruBé[1,15], Anna J. Wlodarczyk[1,15], Zoë Prytherch[1,15], Bernhard Michalke[16], Tobias Krebs[1,17], André S. H. Prévôt[18], Michael Kelbg[1,19], Josef Tiggesbäumker[1,19], Erwin Karg[8], Gert Jakobi[8], Sorana Scholtes[1,8], Jürgen Schnelle-Kreis[8], Jutta Lintelmann[8], Georg Matuschek[8], Martin Sklorz[7], Sophie Klingbeil[1,7], Jürgen Orasche[8], Patrick Richthammer[1,8], Laarnie Müller[8], Michael Elsasser[8], Ahmed Reda[8], Thomas Gröger[8], Benedikt Weggler[1,8], Theo Schwemer[7], Hendryk Czech[7], Christopher P. Rüger[7], Gülcin Abbaszade[8], Christian Radischat[1,7], Karsten Hiller[1,6], Jeroen T. M. Buters[1,2,3‡], Gunnar Dittmar[1,4‡], Ralf Zimmermann[1,7,8‡*]

1 HICE—Helmholtz Virtual Institute of Complex Molecular Systems in Environmental Health—Aerosols and Health, www.hice-vi.eu, Neuherberg, Rostock, Munich, Karlsruhe, Berlin, Waldkirch, Germany, Kuopio, Finland, Cardiff, UK, Esch-Belval, Luxembourg, **2** Center of Allergy and Environment (ZAUM), Helmholtz Zentrum München and Technische Universität München, Member of the German Center for Lung Research (DZL), Munich, Germany, **3** CK-CARE, Christine Kühne Center for Allergy Research and Education, Davos, Switzerland, **4** Mass Spectrometry Core Unit, Max Delbrück Center for Molecular Medicine Berlin-Buch, Germany, **5** University of Eastern Finland, Department of Environmental Science, P.O. Box 1627, FI-70211 Kuopio, Finland, **6** Luxembourg Centre for Systems Biomedicine, University of Luxembourg, L-4362 Esch-Belval, Luxembourg, **7** Joint Mass Spectrometry Centre, Chair of Analytical Chemistry, Institute of Chemistry, University Rostock, Rostock, Germany, **8** Joint Mass Spectrometry Centre, CMA—Comprehensive Molecular Analytics, Helmholtz Zentrum München, Neuherberg, Germany, **9** Institute for Technical Chemistry (ITC), Karlsruhe Institute of Technology, Campus North, Karlsruhe, Germany, **10** Institute of Toxicology and Genetics (ITG), Karlsruhe Institute of Technology, Campus North, Karlsruhe, Germany, **11** Chair of Piston Machines and Internal Combustion Engines, University Rostock, Rostock, Germany, **12** VTT Technical Research Centre of Finland, P.O. Box 1000, FI-02044 VTT, Espoo, Finland, **13** National Institute for Health and Welfare, Department of Environmental Health, P.O. Box 95, FI-70701, Kuopio, Finland, **14** Institute of environmental medicine, UNIKA-T, Technische Universität, Munich, Germany, **15** Lung and Particle Research Group, School of Biosciences, Cardiff University, Cardiff, Wales, United Kingdom, **16** Research Unit Analytical BioGeoChemistry, Helmholtz Zentrum München—German Research Center for Environmental Health GmbH, Neuherberg, Germany, **17** Vitrocell GmbH, Waldkirch, Germany, **18** Laboratory of Atmospheric Chemistry, Paul Scherrer Institute (PSI), Villigen, Switzerland, **19** Institute of Physics, University Rostock, Rostock, Germany

☯ These authors contributed equally to this work.
‡ These authors also contributed equally to the manuscript.
* ralf.zimmermann@helmholtz-muenchen.de

OPEN ACCESS

Citation: Oeder S, Kanashova T, Sippula O, Sapcariu SC, Streibel T, Arteaga-Salas JM, et al. (2015) Particulate Matter from Both Heavy Fuel Oil and Diesel Fuel Shipping Emissions Show Strong Biological Effects on Human Lung Cells at Realistic and Comparable *In Vitro* Exposure Conditions. PLoS ONE 10(6): e0126536. doi:10.1371/journal.pone.0126536

Academic Editor: Shama Ahmad, University of Alabama at Birmingham, UNITED STATES

Received: October 14, 2014

Accepted: April 2, 2015

Published: June 3, 2015

Data Availability Statement: All relevant data are within the paper and its Supporting Information files. Additionally, transcriptomics data are available from Gene Expression Omnibus (accession number GSE63962). Proteomics data are available from ProteomicsDB (ID: PRDB004215).

Funding: HICE partners received funding from the Impulse and Networking Funds (INF) of the Helmholtz Association (HGF), Berlin, Germany. The support of HICE by the Helmholtz Zentrum München

and University of Rostock is gratefully acknowledged. Sebastian Oeder also received funding from CK-CARE Teilbereich A. Sean Sapcariu and Karsten Hiller acknowledge financial support from the Fonds National de la Recherche (FNR), specifically the ATTRACT program Metabolomics Junior Group. Funding from the Academy of Finland (Grant No: 258315 & 259946), Saastamoinen foundation and the strategic funding of the University of Eastern Finland for project "sustainable bioenergy, climate change and health" is acknowledged. Funding from the German Science Foundation (DFG ZI 764/5-1, ZI 764/3-1, INST 264/56-1 and 264/77-1) helped to achieve the presented results. We also thank SNSF and DFG for funding for the DACH project WOOSHI. Vitrocell GmbH provided support in the form of a salary for author T. Krebs, but did not have any additional role in the study design, data collection and analysis, decision to publish, or preparation of the manuscript. The specific roles of the authors are articulated in the 'author contributions' section.

Competing Interests: Tobias Krebs is an employee of Vitrocell GmbH, Tübingen, Germany. This does not alter the authors' adherence to PLOS ONE policies on sharing data and materials.

Abstract

Background

Ship engine emissions are important with regard to lung and cardiovascular diseases especially in coastal regions worldwide. Known cellular responses to combustion particles include oxidative stress and inflammatory signalling.

Objectives

To provide a molecular link between the chemical and physical characteristics of ship emission particles and the cellular responses they elicit and to identify potentially harmful fractions in shipping emission aerosols.

Methods

Through an air-liquid interface exposure system, we exposed human lung cells under realistic *in vitro* conditions to exhaust fumes from a ship engine running on either common heavy fuel oil (HFO) or cleaner-burning diesel fuel (DF). Advanced chemical analyses of the exhaust aerosols were combined with transcriptional, proteomic and metabolomic profiling including isotope labelling methods to characterise the lung cell responses.

Results

The HFO emissions contained high concentrations of toxic compounds such as metals and polycyclic aromatic hydrocarbon, and were higher in particle mass. These compounds were lower in DF emissions, which in turn had higher concentrations of elemental carbon ("soot"). Common cellular reactions included cellular stress responses and endocytosis. Reactions to HFO emissions were dominated by oxidative stress and inflammatory responses, whereas DF emissions induced generally a broader biological response than HFO emissions and affected essential cellular pathways such as energy metabolism, protein synthesis, and chromatin modification.

Conclusions

Despite a lower content of known toxic compounds, combustion particles from the clean shipping fuel DF influenced several essential pathways of lung cell metabolism more strongly than particles from the unrefined fuel HFO. This might be attributable to a higher soot content in DF. Thus the role of diesel soot, which is a known carcinogen in acute air pollution-induced health effects should be further investigated. For the use of HFO and DF we recommend a reduction of carbonaceous soot in the ship emissions by implementation of filtration devices.

Introduction

Epidemiological studies provide compelling evidence that pollution by airborne particulate matter (PM) derived from fossil fuel combustion is an important cause of morbidity and

premature death [1, 2]. Chronic PM exposure can induce short-term (e.g., cardiovascular diseases or asthma) and long-term health effects, most notably cancer. Diesel automobile emissions were recently classified as human carcinogens by the International Agency for Research on Cancer [3].

Diesel ship emissions substantially contribute to worldwide anthropogenic PM levels, which account for up to 50% of the PM-related air pollution in certain coastal areas, rivers and ports [4–7]. Epidemiological studies attribute up to 60,000 annual deaths from lung and cardiovascular disease [8] to ship engine PM. A variety of new regulations will soon be implemented to ensure cleaner ship emissions [9–11]. Low-grade heavy fuel oils (HFOs) contain high levels of sulphur, toxic polycyclic aromatic hydrocarbons (PAHs) and transition metals. Current regulations target HFO use by limiting their sulphur content. In this context, the maximum sulphur content in shipping fuel is internationally regulated by the International Maritime Organisation (IMO) at 3.5%; in most European and US coastal areas, the maximum allowed sulphur content is 1% (Sulphur Emission Control Areas, SECA) [12, 13]. Furthermore, in 2015, a 0.1% sulphur fuel limit will be implemented in the Baltic and North Sea SECAs [14]. To comply with these new sulphur limits, highly refined distillate fuels are necessary (diesel fuel, DF, or marine gas oil, MGO). Currently, MGO is the most used distillate fuel for marine shipping and contains up to 1% sulphur. In 2011, 170 million tons of HFO and 43 million tons of MGO and DF were consumed by ship diesel engines worldwide [15, 16]. This volume corresponds to approximately 21% of global fuel consumption [17].

The biological and health effects of land-based diesel engine emissions have been extensively studied using submersed cell cultures subjected to collected diesel exhaust particles [18, 19]. This submersed cell culture approach neglects the effect of airborne particle exposure, which can result in low sensitivity in measuring biological effects [20]. An alternative is the air-liquid interface (ALI) cell exposure technology. Current systems are technically mature enough to enable reproducible, direct, on-site exposure of lung cell culture to emission aerosols under realistic dilution, flow and humidity conditions [21]. Multiple ALI-exposure studies using car diesel engines [22–25] highlight the improved sensitivity of ALI systems compared with submerged toxicological test systems that use collected diesel exhaust particles (DEP) [20].

Up to now three main causes for PM-induced health effects have been identified: genotoxicity, inflammation and oxidative stress; other mechanisms have also been described [19]. Thus far, all information on diesel PM has been inferred from research on car emissions. However, diesel emissions from ships differ greatly from car or truck diesel emissions due to the fuel composition (HFO) and combustion characteristics of ship engines [26]. Thus, the practice currently used to estimate the health impacts of ship diesel emissions based on analogous car or truck emissions [8, 12, 27] is problematic. The high levels of toxic compounds [6, 28] suggest that HFO emissions produce more detrimental acute and chronic toxic effects than car or truck diesel emissions.

This study targets the biological effects of airborne PM from both diesel and HFO ship emissions based on their chemical compositions. The joint analysis of the biological multi-omics data with the comprehensive aerosol analysis results provides an extensive overview of affected biological mechanisms and pathways and further identifies potentially harmful fractions of the shipping aerosols.

Results and Discussion

Experimental setup

The experimental setup is illustrated in Fig 1 (details in S1 and S2 Figs and in S1 Text). Briefly, we operated a four-stroke, one-cylinder common rail research ship diesel engine (80 kW)

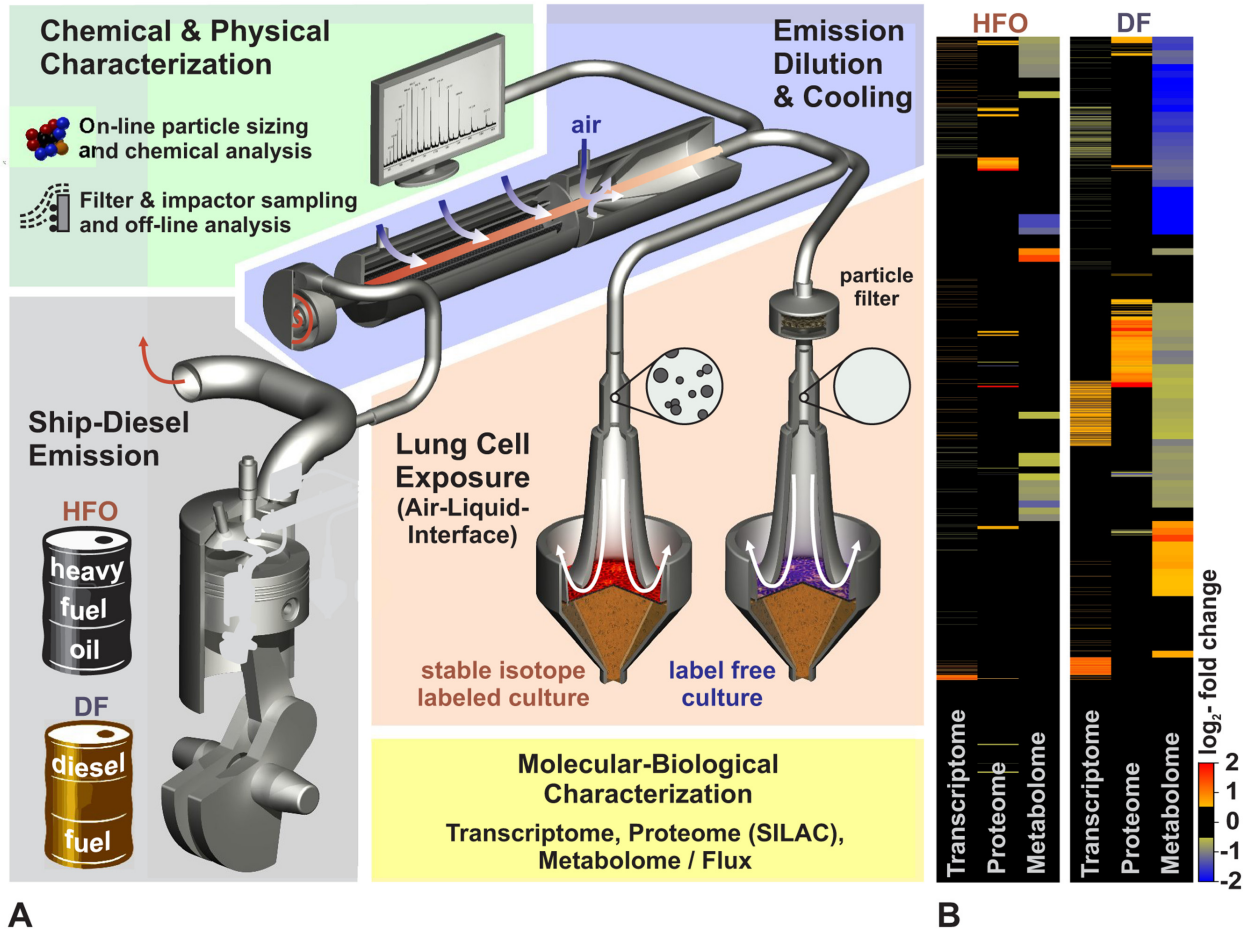

Fig 1. Experimental set-up and global omics analyses. (A) An 80 KW common-rail-ship diesel engine was operated with heavy fuel oil (HFO) or refined diesel fuel (DF). The exhaust aerosols were diluted and cooled with clean air. On-line real-time mass spectrometry, particle-sizing, sensor IR-spectrometry and other techniques were used to characterise the chemical composition and physical properties of the particles and gas phase. Filter sampling of the particulate matter (PM) was performed to further characterise the PM composition. Lung cells were synchronously exposed at the air-liquid-interface (ALI) to aerosol or particle-filtered aerosol as a reference. The cellular responses were characterised in triplicate at the transcriptome (BEAS-2B), proteome and metabolome (A549) levels with stable isotope labelling (SILAC and $^{13}C_6$-glucose). (B) Heatmap showing the global regulation of the transcriptome, proteome and metabolome.

doi:10.1371/journal.pone.0126536.g001

using either HFO (HFO 180) containing 1.6% sulphur or DF containing less than 0.001% sulphur and 3.2% plant oil methyl ester in compliance with the 2014 IMO-SECA-legislation (DIN EN590, see S1 Fig for the engine and fuel properties), which represents the common dual-fuel use in commercial shipping [10, 29]. The engine was operated according to the test cycle ISO 8178–4 E2 for ship diesel engines with a balance between harbour-manoeuvring and cruising engine-loads (Fig 2). The combustion aerosol was cooled and diluted with sterile air. Chemical and physical properties of the HFO and DF aerosol were comprehensively characterised using state-of-the-art, on-line and real-time techniques as well as off-line filter sample analyses. Results are summarised in Fig 2 (for details, see SI). In parallel with aerosol characterisation, confluent layers of two human epithelial lung cell lines (the human lung alveolar cancer cell line A549, purchased from the American Type Culture Collection, ATCC CCL-185; http://www.lgcstandards-atcc.org/Products/All/CCL-185.aspx, and human SV40-immortalised bronchial epithelial cells BEAS-2B, purchased from ATCC, CRL-9609; http://www.lgcstandards-atcc.org/

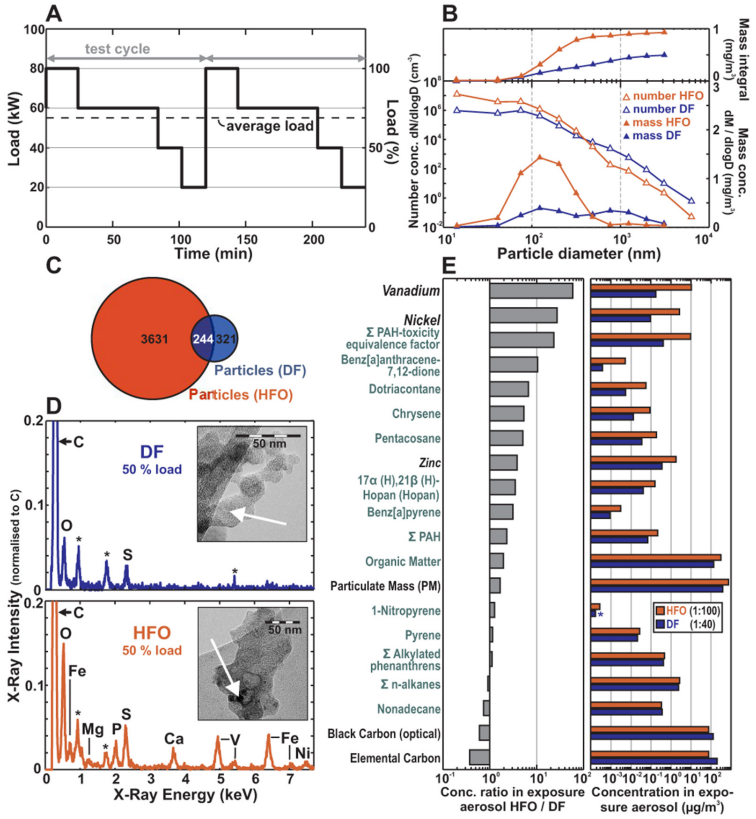

Fig 2. Chemical and physical aerosol characterisation. (A) The ship diesel engine was operated for 4 h in accordance with the IMO-test cycle. (B) Approximately 28 ng/cm^2 and 56 ng/cm^2 were delivered to the cells from DF and HFO, respectively, with different size distributions. The HFO predominantly contained particles <50 nm, and the DF predominantly contained particles >200 nm, both in mass and number. (C) Number of chemical species in the EA particles. (D) Transmission electron microscope (TEM) images and energy-dispersive X-ray (EDX) spectra of DF-EA and HFO-EA; heavy elements (black speckles, arrow); and contributions of the elements V, P, Fe and Ni in the HFO particles using EDX (* = grid-material). (E) Exemplary EA concentrations (right) and concentration ratios (left) for particulate matter-bound species. For all experiments, n = 3.

doi:10.1371/journal.pone.0126536.g002

Products/All/CRL-9609.aspx)) [30] were exposed to the diluted engine exhaust for 4 h at the ALI (Fig 1). Epithelial lung cells have direct contact to inhaled aerosol particles and gases and were therefore used as a model of aerosol inhalation. The cell lines A549 and BEAS-2B have been widely used for testing particles and gases at the air-liquid-interface [31–36]. The BEAS-2B cells are considered to better resemble the situation in human lung tissue while requirements for the cultivation of the cancer derived cell line A549 are better suited for labeling with the L-D_4-Lysine isotope maker for the quantitative proteomics. The transcriptomics methodology is not based on metabolic labelling and thus well suited for the analysis of BEAS-2B cells. The quantitative comparative proteomics approach requires the labelling of the cells with D4-Lysine. However the BEAS-2B cells require specialized media and coating of the plates, which is currently incompatible with the metabolic labelling. Therefore simultaneuos SILAC-based proteomic and metabolic analysis was performed with the established A549 cell model. In summary the cells were analysed using transcriptome (BEAS-B), SILAC-proteome (A549), metabolome and metabolic flux measurements (A549) as well as cytotoxicity tests (A549). The omics data are stored in Gene Expression Omnibus (GSE63962) and Proteomics DB

(PRDB004215), respectively. All experiments were performed in triplicate (3 independent exposures) and referenced to filtered aerosol (for normalising the effects induced by the gas phase) because particles and particle-related chemicals play an important role in the health relevance of diesel exhaust [37] and are therefor in the focus of this study.

The first phase of the experiment was used to find the optimal dose for the large-scale analysis. Cells in the setup were exposed to different concentrations of aerosols. The reaction of the cells was monitored using the Alamar Blue viability test. Due to the higher particle concentration in HFO-exhaust (see below) a dilution of 1:100 was required to achieve a non-impaired cell status while for DF-exhaust a lower dilution of 1:40 was possible without any viability impairment (i.e., a no acute toxicity exhaust dilution; S3A Fig). By applying the different dilution ratios of 1:40 (DF) and 1:100 (HFO) for the exhaust gases for no acute toxicity at 4 h exposure, a similar deposition dose (deposited particle mass per confluent cell culture surface area, see below) was achieved. Based on a gravimetric filter analysis of PM 2.5 and assuming a size-independent, constant deposition probability of 1,5% after Comouth et al. [38], the accumulated particle mass deposited on the lung cell monolayer surface area was roughly estimated as 28 ± 1.5 (DF) and 56 ± 0.7 ng/cm^2 (HFO) per 4 h exposure duration (see S3C Fig) with the variance of the mass measurement expressed by the standard deviation of the filter samples. A more elaborated model taking into account the particle size distribution from an electric low pressure impactor (ELPI) and a size dependent deposition probability after Comouth et al. [38], which was determined using previous measurements from ALI exposure systems, predicts 15.7 (DF) and 41.5 ng/cm^2 (HFO) per 4 h exposure. Even for improved deposition approximation model, the estimated uncertainties, however, are rather high (about a factor of 2). Therefore the deposition dose in both cases can be considered being approximately equal for DF and HFO. We decided to perform the exposure for omics measurements at these dilutions, in order to compare the specific molecular biological effect strength at an about equal deposition dose. Note that in the following all aerosol parameters are reported considering the specific emission-aerosol dilution factors (i.e. the exposure aerosol, EA, as delivered to the cells).

Chemical and physical analysis

Consistent with previous studies [29], only small concentration differences of gaseous compounds were found in the emissions of the ship engine using the two fuels. An exception was SO_2 (4 mg/m^3), which was below toxicity threshold after dilution in the HFO-EA. In addition, the EA concentrations of the further potentially toxic gases NO, NO_2 and CO were below 16.3, 0.4 and 7 ppm, respectively. These values are below the reported toxicity thresholds for the air-liquid interface [39, 40] and even below the general NIOHS lifetime workplace 8-hr exposure limit values of 25, 1 and 35 ppm, respectively [41].

The concentration of particles with an aerodynamic diameter larger than 200 nm was higher for the DF-EA (particle number and mass concentration), whereas nanoparticles smaller than 50 nm were approximately 100-fold more abundant for the HFO-EA (see the size distributions in Fig 2). However, note that the mass contribution of these nanoparticles is very small. TEM images of the particles show that the smaller HFO particles (Fig 2) contained high levels of amorphous organic material around carbonaceous fractal cores with metal inclusions. The DF-EA particle analysis reveals a different picture (Fig 2), in which the particles appear larger and are mostly composed of pure carbonaceous aggregates with spherical soot cores (Ø ~ 20–30 nm). A layered graphite-like carbon structure became visible at a higher TEM magnification (S3 Fig). Based on the size-dependent deposition function described by Comouth *et al.* [38] (S3 Fig) and the low specific density of the observed fractal soot aggregates in DF-EA (Fig 2), the deposited mass for the DF-EA cell exposure experiments is slightly lower than the above

estimates. The particles deposited from the HFO-EA were of a higher dose in mass and number compared to the DF-EA exposure.

Energy-dispersive X-ray spectroscopy (EDX, Fig 2) on TEM showed large differences between HFO-EA and DF-EA particles with regard to the abundance of heavy elements. High intensities of elements such as vanadium, nickel, sulphur and iron were detected in the HFO particles, whereas the DF particles primarily contained carbon and oxygen in the EDX spectrum. Fig 2 shows an overview of the differences in the inorganic and organic chemical composition (Fig 2) as well as the absolute concentrations of the respective substances in the DF- and HFO-exposure aerosol particles (Fig 2 and S4 Fig). Almost all of the measured components, except elemental carbon and black carbon, were more abundant in HFO-EA compared with DF-EA, despite a 2.5-fold higher dilution for HFO-EA.

On-line aerosol mass spectrometry and off-line analyses showed considerably higher mass concentrations of particle-bound organic material and much more complex organic material in the HFO-EA (S1 Table). High-resolution mass spectrometry (ESI-FTICR-MS) revealed 3631 different polar organic compounds in the HFO particles compared with only 321 in the DF particles (Fig 2); 244 compounds were common to both fuel types. The quantification of aromatic and aliphatic compounds (S4 Fig) revealed that higher molecular weight components were more abundant in the HFO particles (green text in Fig 2), such as the higher molecular weight carcinogenic PAH benzo[a]pyrene (Fig 2 and S4 Fig). The sum of PAH toxicity equivalency factors (Fig 2), which ranks different toxic PAHs weighted by their concentration and relative toxicity, was more than 10-fold higher in HFO-PM compared with DF-PM (Fig 2). The only component over-represented in the DF-PM was the elemental carbon fraction (EC) and the corresponding optically measured "black carbon" factor (BC; Fig 2).

Summarising the chemical and physical characterisations, particles emitted from ship engines differ in concentration, size distribution, morphological appearance and chemical composition depending on whether DF or HFO is used. The DF particles in the inhalable size region were dominated by elemental carbon-rich soot-aggregate particles [29], whereas the HFO particles were smaller (nanoparticles) and rich in organic material, including known organic air toxicants (PAHs and their derivatives) and reactive transition metals such as V, Ni, Fe and Zn (S4 Fig). However, it shall be noted that also DF-PM contains organic compounds in relatively high concentrations. The HFO-PM just contains much higher concentrations (Fig 2).

Exposure and deposition dose

We exposed human lung cells for 4 h to concentrations which are corresponding to occupational exposure scenarios or 10 times the concentration of an ambient high concentration scenario (EA ~ 390 μg DF PM2.5/m^2 and ~760 μg HFO PM2.5/m^2). This concentration corresponds to an ALI mass deposition dose of about 28 and 56 ng PM/cm^2 for DF and HFO respectively.

These doses can be related to the human respiratory tract using the specific deposition efficiency for different lung regions. From the measured size distribution and an estimated effective particle density based on the mass-mobility-relation for aggregated diesel particles (between 1.1 and about 0.1 g cm^{-3}, derived from [42, 43]), a deposition simulation was performed using a recently updated model [44, 45] for the tracheobronchial lung region. A 4 h exposure of a human being to the EA concentrations used in our experiments would result to a tracheobronchial deposition of about 1.5 and 5 ng PM/cm^2 for DF and HFO, respectively. Thus the deposited mass in an ALI experiment corresponds to about 3 days (DF) or 2 days (HFO) exposure time for an exposed person (note that for an equal dilution of 1:100 in both EAs the actual deposited tracheobronchial dose for DF would correspond to a 7.5 days exposure of a person). However, one should keep in mind that the size distribution may change quickly in the ambient atmosphere

and in the airways, e.g. by coagulation or water condensation, causing additional uncertainty thereby. The similarity between the size dependent deposition curve [38] for the ALI-system and for the lung deposition curve [44] suggests a good transferability of the results, in particular for the tracheobronchial region. In conclusion, the deposited mass concentration of at an equal dilution of DF PM mass would be about ¼ of the deposited HFO PM. This however, only holds true for directly emitted aerosols. In the atmosphere the more polar, sulphate containing HFO emission particle will quickly grow considerably by water condensation, while the hydrophobic DF particles size distribution will remain stable for longer time [46, 47]. Therefore, emission size distributions might, to some extent, equalise soon.

Biological analysis

To relate the extensive chemical and physical characterisation of the exhaust aerosols to biological effects, the HFO and DF emission particles were directly deposited on human lung cells using ALI exposure technology. Transcriptome, proteome, metabolome and metabolic flux analyses were performed, which yielded parallel and relative quantification of 42205 different transcripts, 6192 proteins and 400 metabolic molecules. To reduce variability, the proteins and metabolites were extracted from the same cell material (A549) that was previously metabolically labelled using D_4-lysine (SILAC proteomics) and $^{13}C_6$-glucose (metabolic flux analysis). Ribonucleic acid (RNA) was isolated from BEAS-2B cells exposed through the same ALI exposure system and was used for the transcriptome analyses [20].

The transcriptome, proteome and metabolome analyses revealed widespread changes in the cellular system upon exposure to both HFO and DF aerosol particles. Surprisingly, more gene expression levels were regulated in the DF-particle-exposed cells (i.e., the response was more widespread compared with the HFO-particle-treated cells on all "omic"-levels; $p<0.001$, Figs 1 and 3 and S5 Fig). The most significantly regulated genes, proteins and metabolites also differed between the DF and HFO (S6 Fig), which shows that the response to emissions of each type of fuel differed quantitatively and qualitatively in both human lung cell lines. A higher regulation alone only proofs a stronger biological reaction onto the deposited PM at the given exposure conditions (i.e. 4 h exposure at a deposition dose below measurable cytotoxicity) and does not necessarily indicate a higher toxicity or risk of disease.

Further conclusions can be drawn from a specific biological pathway analysis. Pro-inflammatory signaling, chemical response (such as xenobiotic metabolism) and oxidative stress pathways were indicated by the regulated genes (Fig 3 and S6 Fig)[19]. The HFO particles specifically induced the transcription of primary and secondary inflammation markers (IL-8, IL-6 and IL-1), and both fuel types affected the cytokines CSF3, CXCL1, and CXCL2. Considering xenobiotic metabolism, CYP1A1 (PAH metabolism) was induced by exposure to HFO particles (which corresponds to the higher PAH concentrations in HFO PM), whereas the DF particles affected other cytochromes (CYP3A4 and CYP17A1) and the carbosulphotransferase CHST6 (Fig 3).

In addition to these, in the context of aerosol exposure well-known pathways [19, 48], we searched for other cellular responses undergoing modulation. A meta-analysis combining the proteome and transcriptome data was performed to examine the significant enrichment of gene ontology (GO) terms. The results indicate that the HFO and DF particle effects were distinct (Fig 3 and, in more detail, S7 Fig). Particles from both fuels induced effects on cell motility, the cellular stress response, the response to organic chemicals, proliferation and cell death (Fig 3 and S7 Fig). Genes and proteins associated with vesicle transport pathways were enriched, which might be connected to the endocytosis of diesel particulate matter.

The pathways specifically regulated by DF particle exposure included the general translation pathway (Fig 3, S7 Fig and S2 Table). The translational elongation, RNA-processing and

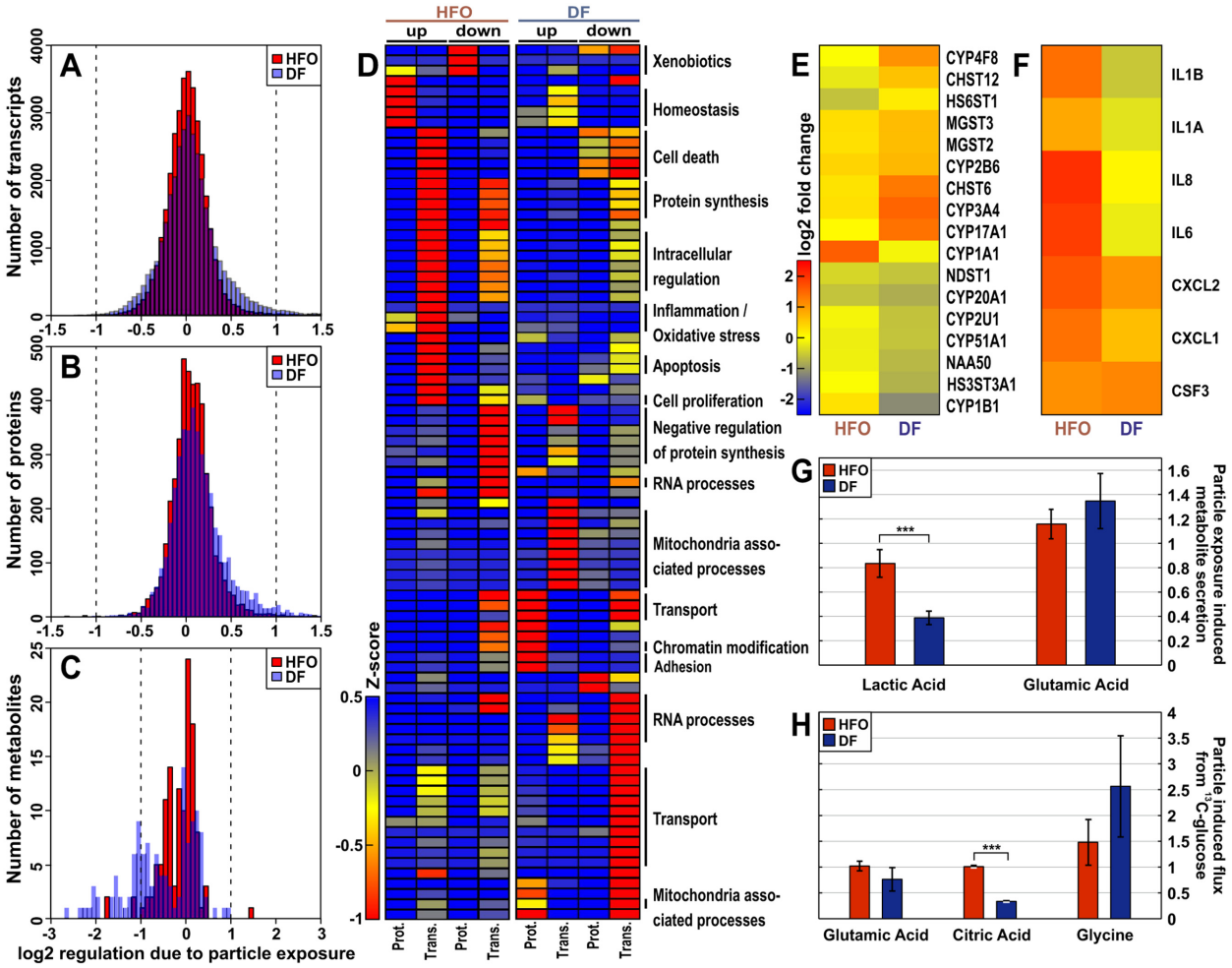

Fig 3. Effects of shipping particles on lung cells. The net effects from the particles were referenced against the gaseous phase of the emissions. (A) Number of the regulated components in the transcriptome shows more genes regulated by the DF than the HFO particles (in BEAS-2B cells). Similar results were observed for the proteome (B) and metabolome (C) (in A549 cells). (D) Meta-analyses for the transcriptome and proteome using the combined Gene Ontology (GO) term analysis of the 10% most regulated transcripts and proteins. Individual GO terms are listed in S2 Table; the hierarchical pathways are indicated on the right. (E) Gene regulation of Wiki-pathway bioactivation; (F) gene regulation of Wiki-pathway inflammation; g, secreted metabolites; and h, metabolic flux measurements using ^{13}C-labelled glucose. For all experiments, n = 3.

doi:10.1371/journal.pone.0126536.g003

ribosome translation pathways were down-regulated, whereas the pathways that affect chromatin organisation and modification were up-regulated. The down-regulated pathways included histone acetylation, which may result in DF particle-induced epigenetic changes. Other pathways modulated by DF particles were involved in processes such as cell junction organisation and cell adhesion. Pathways such as the energy metabolism, cell junction and cell adhesion were clearly affected in both cell lines when assessed using transcriptomics and proteomics but differed in the direction of regulation (Table 1, S2 Table and Fig 3), which indicates a time-delayed reaction in the cell. Exposure to DF particles induced mitochondria-associated genes and proteins, which indicates that mitochondrial stress was induced, whereas the HFO particles did not yield this response.

Pathways specifically regulated by the HFO particles include the homeostasis, oxidative stress and inflammatory response pathways, whereas the metabolic and biosynthetic processes were slightly down-regulated (Fig 3 and S2 Table).

Table 1. Summary of the main HFO- and DF-particle exposure effects.

Effect	HFO	DF
Pro-inflammatory signaling	↑	-
Oxidative stress	↑	-
Cell homeostasis	↑	-
Response to chemicals	↑	↓↑
Cellular stress response	↑	↑
Motility	↑	↑
Endocytosis	↑	↑
Cellular signalling	MAPK, TGF beta, PDGF, EGF, GPCR	ID, kinase cascade
Energy metabolism	-	↓↑[x]
Protein synthesis	-	↓
Protein degradation	-	↑
RNA metabolism	-	↓
Chromatin modifications	-	↑
Cell junction and adhesion	-	↓↑*

The arrows indicate the direction of regulation for cellular functions derived from the most statistically significant enriched Gene Ontology terms from the transcriptome, proteome, and metabolome (details in S2 Table).

[x] BEAS-2B up, A549 down

* BEAS-2B down, A549 up

doi:10.1371/journal.pone.0126536.t001

Interestingly, the proteomics data reveal a direct induction of cell-cell interaction remodelling, whereas the transcriptomics data show a down-regulation of similar GO terms. This finding can be explained by assuming an immediate response of the proteome e.g. by stabilizing the already synthesized proteins, while the transcriptome shows the shut-down of the system in a time-delayed response. Although 40% of the observed protein regulation can be explained by the changes in mRNA abundance, most of the changes indicate other modes of regulation. Protein can be degraded in direct response to PM exposure, and translation or transcription may be too slow to change the protein concentrations after 4 h of exposure [49].

The metabolome analyses supported the finding that biosynthetic and protein synthesis processes were down-regulated in the DF particle-treated cells. ATP-binding cassette transporters, which are involved in actively transporting biomolecules across membranes, were also affected (S2 Table). Further information supporting the inhibition of biosynthetic activities includes the negatively affected metabolites secreted by the cells (Fig 3). The pathways affected by HFO particle exposure include glycolysis and pyrimidine metabolism. Glycolysis is a pathway that is typically altered during inflammation and is generally increased in cells under inflammatory conditions [50].

Glucose flux into lactic acid through glycolysis was significantly reduced ($p<0.05$) in cells treated with DF particles (Fig 3 and S9 Fig). Mammalian cells oxidise glucose and glutamine in the TCA cycle to produce $NADH/H^+$, which is re-oxidised in the respiratory chain to produce ATP. DF exposure strongly decreases the levels of relative glucose oxidation in the TCA cycle compared with HFO, as reflected by the significantly lower levels of labelled citric acid ($p<0.001$; ratio data: Fig 3). Simultaneously, we observed an increase in glucose-derived carbon flux into glycine (Fig 3); enhanced glycine metabolism has previously been associated with tumourigenesis in lung cancer [51]. These observations suggest a lower ATP production and, hence, lower available energy compared with HFO. Increased carbon flux into glycine is

directly linked to the increased transformation of hydroxymethyl groups through one-carbon metabolism. The latter is essential for DNA synthesis and repair.

Conclusions

We assessed human lung cell responses to ship exhaust particles. A unique combination of extensive chemical and physical aerosol characterization and multiple omics analysis was used to generate a broad overview on cellular mechanisms affected by shipping particles and to identify possibly harmful constituents of two types of ship exhaust aerosols. While not providing a classical toxicological risk assessment, which would require the testing of multiple doses and timepoints, this study rather gives a comprehensive picture on the cellular responses to ship exhaust particles after short-term exposure, which should be used as starting point for more mechanistic studies. Although the HFO particles deposited in the ALI system were about equal in mass, higher in number and contained a large excess of toxic compounds, DF particle exposure induced a broader biological reaction in the human lung cells (BEAS-2B and A549) on all investigated "omic" levels. As discussed, a stronger affected cell metabolism is not an adverse effect *per se*, but it holds a higher risk of disturbance of normal cell functions. Within known pathways, such as pro-inflammatory signaling, oxidative stress and xenobiotic metabolism, the levels of certain well-known indicators (e.g., IL-1/6/8 and CYP1A1) surged following HFO particle exposure. In contrast, DF particles strongly affected basic cellular functions (energy and protein metabolism) and mechanisms little yet known to be affected by aerosol treatment, such as mRNA processing and chromatin modification.

The obtained results also suggest formulating specific hypotheses and are motivating further experiments to proof or disproof those. In this context the role of freshly formed “elemental carbon, EC” fractions and the influence of organic compounds on the biological activity should be investigated. The relatively large EC fraction in DF exhaust is one of the prominent differences between the two particle types. The chemical and physical surface properties of freshly formed EC fractions might be of relevance here. Laboratory experiments using e.g. combustion aerosol standard generator (CAST,[52]), which allows to generate fresh combustion particles with adjustable EC/OC ratios, are currently under preparation.

There is no doubt that the carcinogenic emissions from HFO-operated vessels need to be minimized and HFOs should be replaced by refined modern DF (at least if no flue gas cleaning systems are installed). HFO emissions contain among other constituents high concentrations of toxic metals (V, Ni etc.) and polycyclic aromatic hydrocarbons. However, also emission of diesel engines operated with refined DF, are known to be toxic and carcinogenic, although the toxicant concentrations are much lower [8] than in HFO emissions. Consequently the implementation of emission reduction measures for land-based diesel engines started decades ago (e.g. with sulfur-reduced fuels) [18] and current efforts are directed towards the reduction of particle emissions from diesel automobiles. Due to the substantial contribution of ship emissions to global pollution, ship emissions are the next logical target for improving air quality worldwide, particularly in coastal regions and harbour cities. In this context our findings on the biological effects of HFO and DF ship diesel emissions can contribute to the current debate about the reduction measures to be implemented for shipping. The results from this study provide the information that at comparable lung deposition doses the acute biological activity of particles of ship emissions from DF fuelled ships is not less relevant than the activity of HFO emission particles. This supports the suggestion that a general reduction of the PM emissions (not the SO_2 emission) from shipping in harbours and the vicinity of the coast should be implemented for both, HFO- and DF-operated ships. Efficient particle filter technology (e.g., electrostatic precipitation or bag-filtration) is available. From a regulatory perspective, the next step

should be the introduction of legal emissions limits for respirable PM (e.g. PM 2.5, in [mg/m^3]) from ship emissions [29].

Supporting Information

S1 Fig. Sampling setup. (A) Simplified scheme of the sampling and measurement setup. DR = dilution ratio, TC = temperature control, T = temperature measurement, P = pressure meter. (B) Detailed setup of the used sampling train with porous tube and ejector diluter units. (C) Properties of the used diesel fuel (DF) and heavy fuel oil (HFO). Most noticeable are the high viscosity and high sulfur content of HFO compared with distillate fuels like EN 590 diesel. (D) Experimental engine parameters. The engine is a single cylinder engine with common rail injection system representing state of the art medium speed marine diesel engines. The dual fuel system allows operation with both distillate and residual fuels.
(EPS)

S2 Fig. Air-Liquid-Interface (ALI) exposure. HICE exposure system: the left part shows the data acquisition and control unit for the mass flow controllers, humidity and temperature. The exposure unit in the right part contains three Vitrocell modules and is thermostated to 37°C. Each module has six positions for cell exposure to either complete or filtered aerosol for gas phase referencing. The flow through each of the exposure positions is individually controlled by a mass flow controller (lower left) Cell exposure: the aerosol passes through the aerosol inlet and is streaming directly over the cell cultures.
(EPS)

S3 Fig. Particle dosing and morphology. (A) Cell viability at DF and HFO aerosol particle dose. A549 cells were exposed for 4h to 1:40 diluted DF or 1:100 diluted HFO. Directly after exposure, cell viability was measured by reduction of Alamar Blue and compared to cells exposed to the filtered aerosols. Reported are the means relative to filtered aerosol ± SD from 3 (HFO) or 2 (DF) independent experiments. As requested for the further 'omics study, the viability is not impaired by the DF or HFO particle exposure. (B) Size dependent deposited dose of DF and HFO particles (left ordinate) as well as deposition probability (W, right ordinate) calculated according to Comouth et al. (1) for a size dependent density profile. (C) Mass dose of DF and HFO particles deposited per cell area. Data are estimated from gravimetric filter samples (case 1, 2) and from electrical low pressure impactor (ELPI) size distributions (case 3, 4). Calculations are performed assuming a constant deposition probability of W = 1.5% for all particle diameters (case 1, 2). For comparison, calculations are performed additionally using the size dependent probability Wρ(D) based on Comouth et al. (*31*) and a particle density based on a mass-mobility relationship for DF and HFO (case 3, 4). In all cases the deposited PM dose is about a factor 2 higher for the HFO case. d-g, TEM images of diesel fuel exposure aerosol particles. The typical soot agglomerate structure (D,E) and the layered graphitic structure (F,G) is typical for rather pure, elemental carbon containing soot. (H-L), TEM images of heavy fuel oil exposure aerosol particles. The often much smaller particles consist of heavier elements (black speckles) and tarry substance (crusted appearance). The HFO-EA soot particles have a more amorphous structure than the diesel fuel soot (J).
(EPS)

S4 Fig. Compounds in particulate matter. (A) Exemplary sum-parameters and compound-class data for exposure aerosol (EA) particulate matter for HFO-EA and DF-EA. Particular abundance and statistic parameters' ratios (a), absolute concentrations (b) and statistic parameters on the sample complexity (c) reveal a substantial complexity of the organic-chemical composition of the particulate matter. [1]EC/OC coupled to SPI, [2]EC/OC coupled to REMPI,

[3]EC/OC-analysis (thermal-optical method), [4]AMS, [5]Filter weighing. [6]Aethalometer, [7]Comprehensive two-dimensional gas chromatography/Time-of-flight mass spectrometry, [8]Fourier-Transform Ion Cyclotron Resonance Mass Spectrometry with atmospheric chemical ionization, [9]Fourier-Transform Ion Cyclotron Resonance Mass Spectrometry with electrospray ionization, [10]Thermal desorption/direct derivatization gas chromatography/Mass spectrometry, [11]GC/MS. (B) Elemental analysis of the particulate matter. Exemplary concentrations-ratios (HFO-EA- over DF-EA-particles) of elements (left). Absolute concentrations of the species in the HFO-EA- (red bars) and DF-EA-particles (blue bars) are also shown (right). Method: ICP-AES. (C) Exemplary concentration-ratios (HFO-EA- over DF-EA-particles) of polycyclic aromatic hydrocarbons (PAH) (left). Absolute concentrations of the species in the HFO-EA- (red bars) and DF-EA-particles (blue bars) are also shown (right). The larger the PAH-structure, the stronger is the prevalence of the compound in the HFO-EA-particles. Methods: [1]Thermal desorption/derivatization gas chromatography/Mass spectrometry, [2]Gas chromatography/mass spectrometry, [3]Liquid chromatography/Tandem mass spectrometry. (D) Exemplary concentration-ratios (HFO-EA- over DF-EA-particles) of aliphatic hydrocarbons (left). Absolute concentrations of the species in the HFO-EA- (red bars) and DF-EA-particles (blue bars) are also shown (right). The same behaviour as in the PAH compound class is observed: The larger the aliphatic-structure, the stronger is the prevalence of the compound in the HFO-EA-particles.
(EPS)

S5 Fig. DF regulates more transcripts, proteins and metabolites than HFO. (A-C) Comparison of regulation magnitude and regulation significance (obtained with a two-tailed t-Student's t-test on the replicate measurements). Mean of log2 fold change aerosol/filtered is plotted vs. -log10 p-value of complete datasets of transcriptome in BEAS-2B cells (A), proteome (B) and metabolome (C) in A549 cells for DF and HFO. (D-F), Comparison of regulation magnitude and abundance of regulated transcripts, proteins or metabolites. Mean of $\log_2$ fold change aerosol/filtered is plotted vs. mean of $\log_{10}$ fold intensity of complete datasets of transcriptome (D), proteome (E) and metabolome (F) for DF and HFO.
(EPS)

S6 Fig. Cellular responses to DF and HFO differ qualitatively. (A-C) Distinct patterns of regulation of DF and HFO. Hierarchical clustering of highest regulated entities of each omic approach: transcriptomics (A) (BEAS-2B), proteomics (B) and metabolomics (C) (A549). (D,E) Pathways known to be affected by diesel particle exposure. Transcriptome pathway analysis was performed using 1.5-fold regulated genes. Typical PM-influenced pathways were selected and according gene regulation were clustered hierarchically. Apoptosis (D, pro- and anti-apoptotic genes), Oxidative stress (E).
(EPS)

S7 Fig. Meta-analysis of gene ontology-terms in the proteomic and transcriptomic measurement of DF and HFO particle-treated samples. Significantly regulated proteins in A549 cells were determined using 10% of lowest and 10% of highest log2 fold change in the ratio Aerosol/Gas and a cut-off of—log10(p-value) >1 for 3 replicates. According to the high identification number, significantly regulated transcripts in BEAS-2B cells were determined using 5% of lowest and 5% of highest log2 fold change of Aerosol/Gas and a cut-off of—log10(p-value) >1 for 3 replicates. GO term analysis was performed using David Tool. The p-values of GO-terms were z-transformed, hierarchically clustered, and plotted as a heat map.
(EPS)

S8 Fig. DF- and HFO-particles disrupt lung epithelial integrity. (A) Histopathology of HFO-/DF-particle treated NHBE cells. Light microscopy histological analysis of sections of the NHBE cultures treated with PBS (control), and (B) HFO, (C) DF and (D) CB120 at a dose 150 μg/cm^2 for 24 h. Hematoxylin and eosin staining, scale bar = 50 μm. (E) TEM micrographs of HFO- and (F) DF-particle treated NHBE cells. Ribosome agglomeration in cells of the NHBE cultures after 24 h incubation at a dose 150 μg/cm^2; n = 5. Scale bar = 2 μm.
(EPS)

S9 Fig. Secreted metabolites and metabolomic flux analysis. Metabolism of U-^{13}C-Glucose through central carbon metabolism in A549 cells. Reduced model of central carbon metabolism, with labeled atom transition marked for selected metabolites. Red circles = ^{13}C labeled carbon; Blue circles = ^{13}C labeled carbon from Malic Enzyme activity; White circles = ^{12}C unlabeled carbon. Selected Secreted Metabolite Ratios. Selected metabolites were measured through GC/MS analysis of cellular medium post exposure. Values shown are the ratios of unfiltered treatments to filtered treatments for each fuel type during three replicates. Metabolic flux measurements based on ^{13}C-labeled glucose. Filtered and unfiltered aerosol samples were analyzed separately.
(EPS)

S10 Fig. Exemplary light microscopic image of a confluent A459 cell layer. 4x10^5 A549 cells were seeded into a 24mm trans-well insert. After 24h and just before ALI-exposure, confluence was checked by light microscopy.
(TIF)

S1 Table. Chemical Analytics of Ship Exhaust Particles.
(XLSX)

S2 Table. Biological Responses to Ship Exhaust Particles.
(XLSX)

S1 Text. Materials and Methods.
(DOCX)

Acknowledgments

The technical efforts of Anita Wüst, Evelyn Hübner, Renate Effner, Jenny Ghelfi, Thekla Cordes, and Christian Jäger are greatly appreciated. We thank Patrick Beaudette for carefully reading the manuscript.

Author Contributions

Conceived and designed the experiments: SO T. Kanashova OS SCS T. Streibel JP MD HRP SM SD CW HH JKJ MRH KAB MK EK GJ MS JO LM ME AR TG CR KH JB GD RZ. Performed the experiments: SO T. Kanashova OS SCS JP MD CS BS RR TT AJW ZP BM AP MK EK GJ JL GM MS JO PR LM ME AR BW T. Schwemer HC CPR GA CR. Analyzed the data: SO T. Kanashova OS SCS T. Streibel JMAS JP MD SD CW BS RR TT AJW ZP BM AP MK JT EK GJ JSK JL GM MS SK JO PR LM ME AR TG BW T. Schwemer HC CPR GA CR KH JB GD RZ. Contributed reagents/materials/analysis tools: SO T. Kanashova OS SCS T. Streibel JMAS JP MD HRP CS SM SD CW BS RR HH TT JKJ MRH CSW CTH KAB AJW ZP BM T. Krebs AP MK JT EK GJ SS JSK JL GM MS SK JO PR LM ME AR TG BW T. Schwemer HC CPR GA CR KH JB GD RZ. Wrote the paper: SO T. Kanashova OS SCS T. Streibel JMAS JP MD SM BS KAB AJW ZP JT EK GJ SS JSK JL GM MS SK JO LM ME AR TG BW T. Schwemer HC CPR

GA CR KH JB GD RZ. Initially conceived and designed the study: T. Streibel HRP CW HH JKJ MRH KAB T. Krebs JT EK JSK JL KM MS TG KH JB GD RZ.

References

1. Pope CA 3rd, Dockery DW. Air pollution and life expectancy in China and beyond. Proc Natl Acad Sci USA. 2013; 110(32):12861–2. doi: 10.1073/pnas.1310925110 PMID: 23847200
2. Chen Y, Ebenstein A, Greenstone M, Li H. Evidence on the impact of sustained exposure to air pollution on life expectancy from China's Huai River policy. Proc Natl Acad Sci USA. 2013; 110(32):12936–41. doi: 10.1073/pnas.1300018110 PMID: 23836630
3. Benbrahim-Tallaa L, Baan RA, Grosse Y, Lauby-Secretan B, El Ghissassi F, Bouvard V, et al. Carcinogenicity of diesel-engine and gasoline-engine exhausts and some nitroarenes. Lancet oncol. 2012; 13 (7):663–4. PMID: 22946126
4. Dalsoren SB, Eide MS, Endresen O, Mjelde A, Gravir G, Isaksen ISA. Update on emissions and environmental impacts from the international fleet of ships: the contribution from major ship types and ports. Atmos Chem Phys. 2009; 9:2171–94.
5. Matthias V, Bewersdorff I, Aulinger A, Quante M. The contribution of ship emissions to air pollution in the North Sea regions. Environ pollut. 2010; 158(6):2241–50. doi: 10.1016/j.envpol.2010.02.013 PMID: 20226578
6. Ault AP, Moore MJ, Furutani H, Prather KA. Impact of emissions from the Los Angeles port region on San Diego air quality during regional transport events. Environ Sci Technol. 2009; 43(10):3500–6. PMID: 19544846
7. Poplawski K, Setton E, McEwen B, Hrebenyk D, Graham M, Keller P. Estimation and assesment of cruise ship emissions in Victoria, BC, Canada. Atmos Environ. 2011; 45:824–33.
8. Corbett JJ, Winebrake JJ, Green EH, Kasibhatla P, Eyring V, Lauer A. Mortality from ship emissions: a global assessment. Environ Sci Technol. 2007; 41(24):8512–8. PMID: 18200887
9. EPA. Diesel Boats and Ships. Available: http://www.epa.gov/otaq/marine.htm. Accessed March 2014) 2014.
10. Lack DA, Cappa CD, Langridge J, Bahreini R, Buffaloe G, Brock C, et al. Impact of fuel quality regulation and speed reductions on shipping emissions: implications for climate and air quality. Environ Sci Technol. 2011; 45(20):9052–60. doi: 10.1021/es2013424 PMID: 21910443
11. Blatcher DJ, Eames I. Compliance of Royal Naval ships with nitrogen oxide emissions legislation. Marine pollution bulletin. 2013; 74:10–8. doi: 10.1016/j.marpolbul.2013.07.010 PMID: 23906471
12. Winebrake JJ, Corbett JJ, Green EH, Lauer A, Eyring V. Mitigating the health impacts of pollution from oceangoing shipping: an assessment of low-sulfur fuel mandates. Environ Sci Technol. 2009; 43 (13):4776–82. PMID: 19673264
13. Borrell Fontelles J, Straw J. Directive 2005/33/EC of the Europen Parliament and the council. OJEU. 2005; L191/59(22.7.2005).
14. Khan MY, Giordano M, Gutierrez J, Welch WA, Asa-Awuku A, Miller JW, et al. Benefits of two mitigation strategies for container vessels: cleaner engines and cleaner fuels. Environ Sci Technol. 2012; 46 (9):5049–56. doi: 10.1021/es2043646 PMID: 22468877
15. Gaetjens. http://smm-hamburg.com/fileadmin/img/content/programme/downloads/programmpunkte_de/491_7351_gaetjens.pdf 2012.
16. Eyring V, Isaksen ISA, Berntsen T, Collins WJ, Corbett JJ, Endresen O, et al. Transport impacts on atmosphere and climate: Shipping. Atmospheric Environment. 2010; 44(37):4735–71. doi: 10.1016/j.atmosenv.2009.04.059
17. Eyring V, Köhler HW, van Aardenne J, Lauer A. Emissions from international shipping. J Geophys Tes. 2005; 110:D17305.
18. Lloyd AC, Cackette TA. Diesel engines: environmental impact and control. J Air & Waste Manag Assoc. 2001; 51(6):809–47.
19. Schwarze PE, Totlandsdal AI, Lag M, Refsnes M, Holme JA, Ovrevik J. Inflammation-related effects of diesel engine exhaust particles: studies on lung cells in vitro. BioMed research international. 2013; (685142:):1–13. doi: 10.1155/2013/685142 PMID: 23509760
20. Holder AL, Lucas D, Goth-Goldstein R, Koshland CP. Cellular response to diesel exhaust particles strongly depends on the exposure method. Toxicol Sci: an official journal of the Society of Toxicology. 2008; 103(1):108–15. doi: 10.1093/toxsci/kfn014

21. Paur H-R, Cassee F, Teeguarden J, Fissan H, Diabate S, Aufderheide M, et al. In-vitro cell exposure studies for the assessment of nanoparticle toxicity in the lung—A dialog between aerosol science and biology. J Aerosol Sci. 2011; 42(10):668–92. doi: 10.1016/j.jaerosci.2011.06.005

22. Tsukue N, Okumura H, Ito T, Sugiyama G, Nakajima T. Toxicological evaluation of diesel emissions on A549 cells. Toxicol in vitro. 2010; 24(2):363–9. doi: 10.1016/j.tiv.2009.11.004 PMID: 19900534

23. Cooney DJ, Hickey AJ. Cellular response to the deposition of diesel exhaust particle aerosols onto human lung cells grown at the air-liquid interface by inertial impaction. Toxicol in vitro. 2011; 25 (8):1953–65. doi: 10.1016/j.tiv.2011.06.019 PMID: 21756993

24. Oostingh GJ, Papaioannou E, Chasapidis L, Akritidis T, Konstandopoulos AG, Duschl A. Development of an on-line exposure system to determine freshly produced diesel engine emission-induced cellular effects. Toxicol in vitro. 2013; 27(6):1746–52. doi: 10.1016/j.tiv.2013.04.016 PMID: 23684770

25. Kooter IM, Alblas MJ, Jedynska AD, Steenhof M, Houtzager MM, Ras M. Alveolar epithelial cells (A549) exposed at the air-liquid interface to diesel exhaust: First study in TNO's powertrain test center. Toxicol in vitro. 2013; 27(8):2342–9. doi: 10.1016/j.tiv.2013.10.007 PMID: 24161370

26. Adam TW, Chirico R, Clairotte M, Elsasser M, Manfredi U, Martini G, et al. Application of modern online instrumentation for chemical analysis of gas and particulate phases of exhaust at the European Commission heavy-duty vehicle emission laboratory. Anal Chem. 2011; 83(1):67–76. Epub 2010/12/04. doi: 10.1021/ac101859u PMID: 21126058

27. Mueller D, Uibel S, Takemura M, Klingelhoefer D, Groneberg DA. Ships, ports and particulate air pollution—an analysis of recent studies. J Occup Med Toxicol. 2011; 6:31. doi: 10.1186/1745-6673-6-31 PMID: 22141925

28. Cooper J. Exhaust emissions from ships at berth. Atmos Environ. 2003; 37:3817–30.

29. Winnes H, Fridell E. Particle emissions from ships: dependence on fuel type. J Air & Waste Manag Assoc. 2009; 59(12):1391–8.

30. Reddel RR, Ke Y, Gerwin BI, McMenamin MG, Lechner JF, Su RT, et al. Transformation of human bronchial epithelial cells by infection with SV40 or adenovirus-12 SV40 hybrid virus, or transfection via strontium phosphate coprecipitation with a plasmid containing SV40 early region genes. Cancer Res. 1988; 48(7):1904–9. PMID: 2450641

31. Kooter IM, Alblas MJ, Jedynska AD, Steenhof M, Houtzager MM, van Ras M. Alveolar epithelial cells (A549) exposed at the air-liquid interface to diesel exhaust: First study in TNO's powertrain test center. Toxicol in vitro. 2013; 27(8):2342–9. doi: 10.1016/j.tiv.2013.10.007 PMID: 24161370

32. Steinritz D, Mohle N, Pohl C, Papritz M, Stenger B, Schmidt A, et al. Use of the Cultex(R) Radial Flow System as an in vitro exposure method to assess acute pulmonary toxicity of fine dusts and nanoparticles with special focus on the intra- and inter-laboratory reproducibility. Chemico-biol Int. 2013; 206 (3):479–90. doi: 10.1016/j.cbi.2013.05.001 PMID: 23669118

33. Herzog F, Clift MJ, Piccapietra F, Behra R, Schmid O, Petri-Fink A, et al. Exposure of silver-nanoparticles and silver-ions to lung cells in vitro at the air-liquid interface. Part Fibre Toxicol. 2013; 10:11. doi: 10.1186/1743-8977-10-11 PMID: 23557437

34. Persoz C, Achard S, Momas I, Seta N. Inflammatory response modulation of airway epithelial cells exposed to formaldehyde. Toxicol Lett. 2012; 211(2):159–63. doi: 10.1016/j.toxlet.2012.03.799 PMID: 22484645

35. Baber O, Jang M, Barber D, Powers K. Amorphous silica coatings on magnetic nanoparticles enhance stability and reduce toxicity to in vitro BEAS-2B cells. Inhal Toxicol 2011; 23(9):532–43. doi: 10.3109/08958378.2011.592869 PMID: 21819260

36. Diabate S, Mulhopt S, Paur HR, Krug HF. The response of a co-culture lung model to fine and ultrafine particles of incinerator fly ash at the air-liquid interface. Atla-Altern Lab Anim. 2008; 36(3):285–98. PMID: 18662093

37. Patel MM, Chillrud SN, Deepti KC, Ross JM, Kinney PL. Traffic-related air pollutants and exhaled markers of airway inflammation and oxidative stress in New York City adolescents. Environ Res. 2013; 121:71–8. doi: 10.1016/j.envres.2012.10.012 PMID: 23177171

38. Comouth A, Saathoff H, Naumann K-H, Muelhopt S, Paur H-R, Leisner T. Modelling and measurement of particle deposition for cell exposure at the air—liquid interface. J Aerosol Sci. 2013; 63(0):103–14. doi: 10.1016/j.jaerosci.2013.04.009

39. Karthikeyan S, Thomson EM, Kumarathasan P, Guenette J, Rosenblatt D, Chan T, et al. Nitrogen dioxide and ultrafine particles dominate the biological effects of inhaled diesel exhaust treated by a catalyzed diesel particulate filter. Toxicol Sci. 2013; 135(2):437–50. doi: 10.1093/toxsci/kft162 PMID: 23897985

40. Ghio AJ, Dailey LA, Soukup JM, Stonehuerner J, Richards JH, Devlin RB. Growth of human bronchial epithelial cells at an air-liquid interface alters the response to particle exposure. Part Fibre Toxicol. 2013; 10(1):25. doi: 10.1186/1743-8977-10-25

41. Dept. of Health and Human Services. NIOHS pocket guide to chemical hazards. Barsan M, editor. Cincinnati Ohio: NIOHS publications; 2007.

42. Pagels J, Khalizov AF, McMurry PH, Zhang RY. Processing of Soot by Controlled Sulphuric Acid and Water Condensation: Mass and Mobility Relationship. Aerosol Sci Technol. 2009; 43(7):629–40. doi: 10.1080/02786820902810685

43. Park K, Cao F, Kittelson DB, McMurry PH. Relationship between particle mass and mobility for diesel exhaust particles. Environ Sci Technol. 2003; 37(3):577–83. doi: 10.1021/es025960v PMID: 12630475

44. Ferron GA, Upadhyay S, Zimmermann R, Karg E. Model of the Deposition of Aerosol Particles in the Respiratory Tract of the Rat. II. Hygroscopic Particle Deposition. J Aerosol Med Pulm Drug Deliv. 2013; 26(2):101–19. doi: 10.1089/jamp.2011.0965 PMID: 23550602

45. Karg E, Ferron GA. The hygroscopic particle lung deposition model Neuherberg / Munich: Helmholtz Zentrum München; 2014 [cited 2014]. Available: http://www.helmholtz-muenchen.de/en/neu-cma/research/facilities/lung-deposition-model/index.html.

46. Wehner B, Birmili W, Gnauk T, Wiedensohler A. Particle number size distributions in a street canyon and their transformation into the urban-air background: measurements and a simple model study. Atmos Environ. 2002; 36(13):2215–23.

47. Vignati E, Berkowicz R, Palmgren F, Lyck E, Hummelshoj P. Transformation of size distributions of emitted particles in streets. Sci Total Environ. 1999; 235(1–3):37–49. PMID: 10535125

48. Oeder S, Jorres RA, Weichenmeier I, Pusch G, Schober W, Pfab F, et al. Airborne indoor particles from schools are more toxic than outdoor particles. Am J Respir Cell Mol Biol. 2012; 47(5):575–82. doi: 10.1165/rcmb.2012-0139OC PMID: 22904196

49. Schwanhausser B, Busse D, Li N, Dittmar G, Schuchhardt J, Wolf J, et al. Global quantification of mammalian gene expression control. Nature. 2011; 473(7347):337–42. doi: 10.1038/nature10098 PMID: 21593866

50. Palsson-McDermott EM, O'Neill LA. The Warburg effect then and now: from cancer to inflammatory diseases. BioEssays. 2013; 35(11):965–73. doi: 10.1002/bies.201300084 PMID: 24115022

51. Zhang WC, Shyh-Chang N, Yang H, Rai A, Umashankar S, Ma S, et al. Glycine decarboxylase activity drives non-small cell lung cancer tumor-initiating cells and tumorigenesis. Cell. 2012; 148(1–2):259–72. doi: 10.1016/j.cell.2011.11.050 PMID: 22424234

52. Mueller L, Jakobi G, Orasche J, Karg E, Sklorz M, Abbaszade G, et al. Online determination of polycyclic aromatic hydrocarbon formation from a flame soot generator. Anal Bioanal Chem. 2015. doi: 10.1007/s00216-015-8549-x

METABOLIC PROFILING AS WELL AS STABLE ISOTOPE ASSISTED METABOLIC AND PROTEOMIC ANALYSIS OF RAW 264.7 MACROPHAGES EXPOSED TO SHIP ENGINE AEROSOL EMISSIONS: DIFFERENT EFFECTS OF HEAVY FUEL OIL AND REFINED DIESEL FUEL

Sean C. Sapcariu, Tamara Kanashova, Marco Dilger, Silvia Diabaté, Sebastian Oeder, Johannes Passig, Christian Radischat, Jeroen Buters, Olli Sippula, Thorsten Streibel, Hanns-Rudolf Paur, Christoph Schlager, Sonja Mülhopt, Benjamin Stengel, Rom Rabe, Horst Harndorf, Tobias Krebs, Erwin Karg, Thomas Gröger, Carsten Weiss, Gunnar Dittmar, Karsten Hiller, Ralf Zimmermann *PLoS One*. **2016**, 11(6). *doi:10.1371/journal.pone.0157964*

This article is a follow-up and extension of Oeder *et al.* (2015), focusing on metabolic and proteomic changes in macrophages, to study the effects of ship engine aerosol on cells directly involved in inflammation. Similar to the previous paper, I helped organize and execute the experiments during the campaign, and was responsible for all measurement and analysis of the metabolomics data. In addition, I conceived the idea for the paper, wrote and submitted the manuscript, as well as made all figures except for figures 1 and 6.

PLOS ONE

RESEARCH ARTICLE

Metabolic Profiling as Well as Stable Isotope Assisted Metabolic and Proteomic Analysis of RAW 264.7 Macrophages Exposed to Ship Engine Aerosol Emissions: Different Effects of Heavy Fuel Oil and Refined Diesel Fuel

Sean C. Sapcariu[1,12]*, Tamara Kanashova[2,12], Marco Dilger[3,4,12], Silvia Diabaté[3,12], Sebastian Oeder[5,6,12,13], Johannes Passig[7,12], Christian Radischat[7,12], Jeroen Buters[5,6,12,13], Olli Sippula[8,12], Thorsten Streibel[7,9,12], Hanns-Rudolf Paur[4,12], Christoph Schlager[4,12], Sonja Mülhopt[4,12], Benjamin Stengel[10,12], Rom Rabe[10,12], Horst Harndorf[10,12], Tobias Krebs[11,12], Erwin Karg[9], Thomas Gröger[9], Carsten Weiss[3,12], Gunnar Dittmar[2,12], Karsten Hiller[1,12], Ralf Zimmermann[7,9,12]*

1 Luxembourg Centre for Systems Biomedicine 6, avenue du Swing, L-4362 Esch-sur-Alzette, Luxembourg, **2** Mass Spectrometry Core Unit, Max Delbrück Center for Molecular Medicine Berlin-Buch, Berlin, Germany, **3** Institute of Toxicology and Genetics (ITG), Karlsruhe Institute of Technology, Campus North, Karlsruhe, Germany, **4** Institute for Technical Chemistry (ITC), Karlsruhe Institute of Technology, Campus North, Karlsruhe, Germany, **5** Center of Allergy and Environment (ZAUM), Helmholtz Zentrum München and Technische Universität München, Munich, Germany, **6** CK-CARE, Christine Kühne Center for Allergy Research and Education, Davos, Switzerland, **7** Joint Mass Spectrometry Centre, Division of Analytical and Technical Chemistry, Institute of Chemistry, University Rostock, Rostock, Germany, **8** University of Eastern Finland, Department of Environmental Science, P.O. Box 1627, FI-70211 Kuopio, Finland, **9** Joint Mass Spectrometry Centre, CMA – Comprehensive Molecular Analytics, Helmholtz Zentrum München, Neuherberg, Germany, **10** Chair of Piston Machines and Internal Combustion Engines, University Rostock, Rostock, Germany, **11** Vitrocell GmbH, Tübingen, Germany, **12** HICE – Helmholtz Virtual Institute of Complex Molecular Systems in Environmental Health – Aerosols and Health, Neuherberg, Rostock, Munich, Karlsruhe, Berlin, Waldkirch, Germany; Kuopio, Finland; Cardiff, United Kingdom; Esch-Belval, Luxembourg, **13** German Center for Lung Research (DZL), Munich, Germany

* sean.sapcariu@uni.lu (SCS); ralf.zimmermann@helmholtz-muenchen.de (RZ)

OPEN ACCESS

Citation: Sapcariu SC, Kanashova T, Dilger M, Diabaté S, Oeder S, Passig J, et al. (2016) Metabolic Profiling as Well as Stable Isotope Assisted Metabolic and Proteomic Analysis of RAW 264.7 Macrophages Exposed to Ship Engine Aerosol Emissions: Different Effects of Heavy Fuel Oil and Refined Diesel Fuel. PLoS ONE 11(6): e0157964. doi:10.1371/journal.pone.0157964

Editor: Josué Sznitman, Technion - Israel Institute of Technology, ISRAEL

Received: January 20, 2016

Accepted: June 8, 2016

Published: June 27, 2016

Data Availability Statement: The metabolomics and LDH data from this study are contained in the supporting information. The proteomics data is uploaded onto Proteomics DB: https://www.proteomicsdb.org/#projects/4242, with the ID: PRDB004242.

Funding: HICE partners received funding from the Impulse and Networking Funds (INF) of the Helmholtz Association (HGF), Berlin, Germany. The support of HICE by the Helmholtz Zentrum München

Abstract

Exposure to air pollution resulting from fossil fuel combustion has been linked to multiple short-term and long term health effects. In a previous study, exposure of lung epithelial cells to engine exhaust from heavy fuel oil (HFO) and diesel fuel (DF), two of the main fuels used in marine engines, led to an increased regulation of several pathways associated with adverse cellular effects, including pro-inflammatory pathways. In addition, DF exhaust exposure was shown to have a wider response on multiple cellular regulatory levels compared to HFO emissions, suggesting a potentially higher toxicity of DF emissions over HFO. In order to further understand these effects, as well as to validate these findings in another cell line, we investigated macrophages under the same conditions as a more inflammation-relevant model. An air-liquid interface aerosol exposure system was used to provide a more biologically relevant exposure system compared to submerged experiments, with cells exposed to either the complete aerosol (particle and gas phase), or the gas phase only

and University of Rostock is gratefully acknowledged. Sebastian Oeder also received funding from CK-CARE Teilbereich A. Sean Sapcariu and Karsten Hiller acknowledge financial support from the Fonds National de la Recherche (FNR), specifically the ATTRACT program Metabolomics Junior Group. Funding from the Academy of Finland (Grant No: 258315 & 259946), Saastamoinen foundation and the strategic funding of the University of Eastern Finland for project "sustainable bioenergy, climate change and health" is acknowledged. Funding from the German Science Foundation (DFG ZI 764/5-1, ZI 764/3-1, INST 264/56-1 and 264/77-1) helped to achieve the presented results. The authors also thank SNSF and DFG for funding for the DACH project WOOSHI. Vitrocell GmbH provided support in the form of a salary for author T. Krebs, but did not have any additional role in the study design, data collection and analysis, decision to publish, or preparation of the manuscript. The other funders had no role in study design, data collection and analysis, decision to publish, or preparation of the manuscript.

Competing Interests: The authors of this manuscript have read the journal's policy and have the following competing interests: Tobias Krebs is an employee of Vitrocell GmbH, Tübingen, Germany. This does not alter the authors' adherence to PLOS ONE policies on sharing data and materials.

(with particles filtered out). Data from cytotoxicity assays were integrated with metabolomics and proteomics analyses, including stable isotope-assisted metabolomics, in order to uncover pathways affected by combustion aerosol exposure in macrophages. Through this approach, we determined differing phenotypic effects associated with the different components of aerosol. The particle phase of diluted combustion aerosols was found to induce increased cell death in macrophages, while the gas phase was found more to affect the metabolic profile. In particular, a higher cytotoxicity of DF aerosol emission was observed in relation to the HFO aerosol. Furthermore, macrophage exposure to the gas phase of HFO leads to an induction of a pro-inflammatory metabolic and proteomic phenotype. These results validate the effects found in lung epithelial cells, confirming the role of inflammation and cellular stress in the response to combustion aerosols.

Introduction

Air pollution from anthropogenic sources are consistently associated with adverse health effects, such as asthma, cardiovascular problems, and cancer [1, 2]. Near harbors and other water-based industrial areas, there is a large amount of exhaust from ship engines, which run on different fuel types with very different chemical compositions. Marine gas oil, or diesel fuel (DF), is similar to the standard fuel used in diesel automobiles, while heavy fuel oil (HFO) has very different chemical properties, including much higher levels of toxic chemicals, such as polycyclic aromatic hydrocarbons, carbonylic compounds, and also different transition metals. Epidemiological studies have associated the combustion of these fuels with an increased incidence of lung and cardiovascular diseases [3], and it is important to study the mechanisms of these effects so that through technology, measures can be taken which focus on minimizing the health problems caused by ship emissions.

A prominent effect of combustion aerosols on human health is an increase of inflammatory responses in affected tissues. As inhalation is the main route of aerosol exposure, the lungs are primarily affected. Many studies have investigated the effects of particulate matter (PM) emissions on lung cells (both *in vitro* and *in vivo* [4–7]), but most of these studies have focused on the use of submerged experiments. While useful for studying the effects of particles present in aerosols, these exposures are less representative of real-world inhalation of combustion emissions. For this reason, exposure at an air-liquid interface (ALI) can be used to represent a more biologically accurate exposure to lung epithelial cells, as well as other cells present in lung tissue. In addition to being a more realistic *in vitro* model system, these experiments are able to elucidate differences between the gas and particle components of aerosols through the use of in-line filters [8]. Validation studies for the ALI system have been performed previously [9, 10], and there have also been multiple studies that have used ALI technology to uncover novel chemical and biological insights, including more accurate modeling of particle deposition efficiencies [11], as well as the investigation of epithelial cell-macrophage co-culture responses to waste incineration emission aerosol [12]. In addition, and not only for the reasons outlined above, ALI systems are preferred compared to submerged experiments for cell exposure, as has been discussed previously [13].

In the framework of the international project HICE (Helmholtz Virtual Institute of Complex Molecular Systems in Environmental Health, www.hice-vi.eu) a novel ALI exposure technology for cell exposure in the field has been established in conjunction with multi-omics cellular response studies. This concept has been applied to study emissions from a ship engine

and their effects on a lung epithelial cell line [14]. To summarize the previous study, biological effects triggered by PM from ship diesel engines in a lung epithelial cell line pointed out that particles originated from the use of refined, sulfur-free DF induce a similar or even stronger acute activation of many adverse pathways than the use of HFO [14]. This was a surprising result, as PM from HFO contains much higher concentrations of known toxic compounds, including polycyclic aromatic hydrocarbons (PAH), oxygenated compounds and transition metals, such as vanadium and nickel [14, 15]. In addition, one of the main pathways affected was the inflammatory response, promoting increased transcription of pro-inflammatory markers, including IL-8, IL-1, and CXCL2, particularly for HFO exposure. It was also hypothesized that endocytosis of particulate matter was regulated in response to both fuel types. Transcriptomic and proteomic effects highlighted that energy metabolism was affected as well, suggesting a focus on metabolism would be interesting for this study. In order to extend the results of the previous study to a more inflammatory-focused and phagocytotic model, as well as to compare the effects of DF and HFO exposure in another cell type to validate the previous findings, we used the same experimental setup to simultaneously investigate a macrophage cell line using a primarily metabolism-focused approach, supported by quantitative proteomics (SILAC) and cytotoxicological measurements.

Macrophages are a type of differentiated phagocytotic monocyte that have important roles in both innate and adaptive immunity, and particularly in the inflammatory response [16]. There is a large heterogeneity in macrophage phenotypes (largely related to their activation states) [17], and these cells play an important role in maintaining tissue homeostasis, mediating pro- and anti-inflammatory reactions, as well as a variety of other well-characterized functions [18]. In lung tissue, macrophages are present in much higher amounts than other immune cells [19], and populations can increase under inflammatory conditions (along with the associated pro-inflammatory phenotypic changes) [20].

The effect of combustion aerosols on the induction of inflammation in macrophage populations has been studied both in ALI experiments and in animal studies [12, 21–23]. While much of the research has focused on cytokine production, transcriptional expression, and physiological effects (such as changes in immune cell populations) involved in aerosol-induced acute lung inflammation, metabolic changes due to these conditions have been largely unexplored. Where metabolism has been mentioned, it has been tied to enzymatic activity or transcriptional regulation of metabolic genes and proteins. Metabolomics studies focus on the metabolic profile in the cell, looking at changes in the effector molecules in the various biochemical pathways that control cell function [24]. Non-targeted metabolomics analyses provide a comprehensive view of metabolites present in a biological system, while stable isotope-assisted metabolomics makes use of labeled tracer molecules to elucidate the flux of biomolecules through central carbon metabolism [25]. In addition, metabolomics data can be integrated with other data to uncover a more complete picture of biological function [26].

In this study, we expose a murine macrophage cell line to diluted emission aerosols from a ship diesel engine operated with two types of marine fuel: DF and HFO, and study the cytotoxic, metabolic, and proteomic effects. DF is commonly used in inland waterway transportation, while HFO and DF are both used in sea-based transportation. The study mimics a real-life engine load scenario, with both a full aerosol exposure and a particle-filtered aerosol exposure (with only the gas phase exposed to the cells), in order to look at the net effect of the particles. The gas phase of these aerosols is characterized, and cellular effects are presented from a metabolomics point of view, with integration of complementary data from toxicological and proteomic studies. Using this approach, we were able to highlight the metabolic changes and some proteomic effects associated with the inflammatory response of macrophages to aerosol exposure. Furthermore, the current work aims to verify the findings of the previous study on lung epithelial cells, in order to

add support to their conclusion that DF PM exposure may have similar or possibly stronger biological effects than HFO exposure at comparable deposition doses.

Materials and Methods

Engine and exposure

A four-stroke single-cylinder direct-injected diesel engine test bed situated at the University of Rostock in the Chair of Piston Machines and Internal Combustion Engines was used to generate aerosol for the exposure study. Heavy fuel oil HFO 180 was used as a representative fuel for ship operation outside of sulfur emission control areas (SECAs). Distillate diesel fuel (DF) according to DIN EN 590 was used as a reference. The DF fuel represents a modern, sulfur-free distilled fuel as used in inland waterway transportation and SECAs. The engine ran at four different operating points: 100%, 75%, 50%, and 25% load at a nominal speed of 1,500 rev/min. A detailed characterization of the aerosol composition at the ALI exposure system was performed, [27]. The duration of each operation point was set in accordance to their weighting factors as described in ISO 8178-4 E2. The total cycle duration was 2 hours, and this cycle was run twice for a single exposure. To obtain comparable particle deposition doses for the experiments with the two fuel types, clean air dilution ratios of 1:40 and 1:100 were used for the exhaust aerosols of DF and HFO emissions, respectively. The diluted concentrations of PM 2.5 in the aerosols were 340 $\mu g/cm^3$ and 760 $\mu g/cm^3$ for DF and HFO, respectively. Based on these values, and a post-experiment gravimetric filter analysis of PM 2.5 and assuming a constant deposition probability of 1.5%, which was determined using previous measurements from ALI exposure systems [11], the particle mass deposited on the lung cell monolayer surface was calculated at 28 ± 1.5 ng/cm^2 (DF) and 56 ± 0.7 ng/cm^2 (HFO) for the 4 hour exposure [14].

Physical and chemical profiling of aerosols

Profiling of the particulate matter from the exposure aersosols from both fuel types was performed as in the previous study [14, 15]. To summarize, on-line and off-line analysis techniques, including gas chromatography mass spectrometry, high resolution mass spectrometry (ESI-FTICR-MS), energy-dispersive X-ray spectroscopy (EDX), on-line aerosol mass spectrometry, well as others have been used. Detailed information on the particulate matter analysis has been reported previously [14], and a summary is shown in S1 Fig. On-line analyses were performed in parallel with cellular exposures, and off-line techniques were performed using particulate matter collected on filters during cellular exposures.

Data on gas phase aerosol compounds were derived from on-line photo-ionization mass spectrometry [28]. Aromatic species were measured by resonance enhanced multi-photon ionization (REMPI) mass spcectrometry, which utilizes intense short laser pulses of 266 nm generated by a Nd:YAG laser. Ionization occurs by subsequent ionization of two photons, providing selectivity and enhanced sensitivity for aromatic species. Benzene and butadiene were analyzed by on-line single photon ionization (SPI) mass spectrometry using 126 nm Vacuum-UV radiation generated by an electron beam pumped rare gas excimer lamp [29]. Ionization occurs by absorption of a single photon. Carbonyl compounds were sampled by derivatisation with 2,4-dinitrophenylhydrazine (DNPH) using commercially available cartridges 'ORBO/555' (Sigma Aldrich, USA) and subsequently analyzed by GC-MS [27]

Cell culture conditions

The mouse macrophage RAW 264.7 cell line was obtained from ATCC (ATCC© TIB-71™). Cells were cultured in RPMI-1640 medium supplemented with 10% (v/v) Fetal Bovine Serum

and 100 U/ml penicillin, 100 mg/ml streptomycin (Life Technologies, Darmstadt), and cultivated in an incubator at 37°C with 5% CO_2. For stable isotope labeling experiments, cells were seeded 24 hours before the experiment in RPMI-1640 medium as above, with 12.5 mmol/L U-$^{13}C_6$-Glucose (Cambridge Isotope Laboratories, USA) substituted for unlabeled glucose.

Air-liquid interface exposure

An automated ALI exposure system station (VITROCELL Systems, GmbH, Waldkirch, Germany) with 18 exposure positions was used as the interface for cellular exposures of the diesel engine exhaust [30]. ALI exposures were performed in a custom built mobile HICE S2 bio safety laboratory, placed next to the engine hall. Diluted DF or HFO aerosol was led through heated stainless steel lines from the engine test bed into the ALI system. The combustion aerosols coming from the engine's exhaust pipe were cooled and diluted with sterile air, and then transferred directly to the ALI for cellular exposure. A PM 2.5 impactor removed large particles before the exhaust entered the ALI system. Cells exposed to complete aerosols used the humidified exhaust from the engine, while cells exposed to only the gas phase had particles removed directly above the cell chamber using a Whatman HEPA polydisc filter (GE Healthcare). Exposures were performed as described for ALI exposures of BEAS2B and A549 epithelium cells [14].

Cells were seeded in FCS supplemented RPMI-1640 on transferrable 24 mm Transwell® inserts with a 0.4 μm pore polyester membrane (Type #3450, Corning, NY, USA) 24h before exposure at a density of 1 x 10^6 cells/mL/insert (2.1 x 10^5 cells/cm^2 growth area) with 1.5 mL cell culture medium provided beneath the insert membrane. For cell exposure, the culture medium on the apical side was completely removed and cells were placed in the ALI exposure system with RPMI-1640 medium without FBS, supplemented with 10 mM HEPES, provided at the basolateral side. Cells were then exposed for 4h to the diluted and conditioned (85% r.h., 37°C, maintained by a software controlled humidifier in the ALI exposure system) aerosols with a controlled flow of 100 mL/min for each insert [13, 30]. Cells were exposed to both the complete aerosol (with both particle phase and gas phase), and the gas phase only (with particles filtered out of the complete aerosol by a high efficiency particle membrane filter). All fuel-specific results represent both the filtered and unfiltered treatments, unless otherwise stated.

LDH release assay

After exposure, medium from the compartment under the membrane was collected and frozen at -80°C for later analysis. An aliquot was used for quantification of released lactate dehydrogenase (LDH), an indicator of plasma membrane integrity. An LDH detection kit was used in accordance with the manufacturers' instructions (Roche, Mannheim, Germany) with slight modifications: the dye solution was diluted 1:1 (v/v) with PBS to slow down the reaction time caused by elevated LDH values due to the high cell densities used for ALI exposure experiments. After 20 minutes, before saturation was reached, the reaction was stopped and the absorbance of the reaction mix was measured at 490 nm with a microplate reader. Absorbance read from the samples was normalized to the absorbance of blank medium. Statistical analysis was performed using an analysis of variance (ANOVA) test, followed by a post-hoc Tukey test for pairwise statistical analysis. Cells exposed with HEPA-filtered ambient air humidified to 85% r.h. at 37°C used as a control treatment. Cells used for a positive control for cellular toxicity were kept under control conditions and lysed with Triton X-100 (Sigma Aldrich) for 30 minutes prior to the end of the exposure period.

Metabolite extraction and GC-MS processing

For metabolomics experiments, cells kept in an incubator at 37°C with 5% CO_2 were used as a control treatment. Metabolite extraction was performed as previously described [31]. Briefly, after washing cells with 0.9% NaCl, a 1:1:1 extraction using methanol, water, and chloroform was used to quench metabolism and create a three-phase separation. Cells were agitated for 20 minutes and then centrifuged to enforce phase separation. 200 μL of the polar phase was used for gas chromatography coupled to mass spectometry (GC-MS) analysis. The interphase was then used for proteomics analysis.

Compound derivatization was performed with a Gerstel autosampler directly before measurement on the GC-MS. Dried metabolites were dissolved in 15 μL of 2% methoxyamine hydrochloride in pyridine at a temperature of 40°C for 30 minutes. Then, 15 μL of 2,2,2-trifluoro-N-methyl-N-trimethylsilyl-acetamide + 1% chloro-trimethyl-silane was added and incubated at 40°C for 30 minutes. Methoxyamine hydrochloride derivatization breaks apart cyclic forms of some metabolites, reducing confusing of metabolites with different forms (such as glucose) eluting at different times based upon their structure. 2,2,2-trifluoro-N-methyl-N-trimethylsilyl-acetamide + 1% chloro-trimethyl-silane is used to block polar groups and allow for efficient transition of the metabolites into the gas phase.

The metabolite extracts were measured on an Agilent 7890 GC with a 30 m DB-35MS capillary column (Agilent Technologies) with an internal diameter of 0.25 mm and a film of 0.25 μm. The GC was connected to an Agilent 5975C MS operating in electron ionization (EI) at 70 eV. The MS source was kept at a constant temperature of 230°C and the quadrupole at 150°C. The detector was operated in scan mode with an m/z range of 70 to 800.

1 μL of derivatized sample was injected at 270°C in splitless mode. Helium was used as the carrier gas at a flow rate of 1 mL/min. The GC temperature program started at 80°C with a hold for 6 minutes, followed by a gradient of 6°C/min to 300°C, a hold for 10 minutes, and an additional gradient of 10°C/min to 325°C. The total splitless GC-MS run time of one sample was 59 minutes. An alkane mix was run with the experimental sequence in order to provide retention index calibration for the experimental samples. The above program was used for the measurement of polar intracellular metabolic extracts from samples. In order to determine secretion of lactic acid, both control and experimental cellular medium was analyzed with the above parameters in a 25 minute method.

All chromatograms were normalized to a standard alkane mix (Sigma 68281) to standardize retention times (RT) to retention indicies (RI) across sample runs. To identify metabolites found in experimental chromatograms, an in-house developed metabolite library was used, and mass spectra as well as normalized RI values were compared. This library was created by running analytical standards run on the same instruments using the same parameters as our experimental samples. All identified metabolites were verified using the NIST 11 spectral database [32]. Metabolic analysis and mass isotopomer distribution (MID) calculation, including correction for naturally occuring stable isotopes, was performed with the MetaboliteDetector software [33, 34].

Metabolic data were factor-normalized based on standardized pool samples run with each GC-MS sequence. The pool samples were a standardized extract of intracellular metabolites from control conditions, to provide a baseline and control for GC-MS drift and buildup on the GC column. Changes in the pool samples were calculated, and this factor was applied to normalize the experimental samples. In order to reduce noise and to focus on metabolites changing between conditions, a further filtering was applied, removing all compounds present in less than 80% of all treatments. All metabolic statistical significance measurements were performed using an unpaired, two-tailed student's t-test unless otherwise noted.

Stable isotope labeling by amino acids in cell culture (SILAC)

RAW 264.7 mouse macrophages were cultured for six passages as above, with either 48.67 μg/mL H4-lysine (lysine 0, Sigma-Aldrich) or D4-lysine (lysine 4, Sigma-Aldrich) to achieve complete labeling of the proteome [35]. In order to detect unlabeled contaminants for each sample the reverse experiment was performed by exchanging lysine 0 and lysine 4.

Proteome extraction and LC-MS/MS analysis of peptides

Proteome extraction was performed as previously described [31]. In brief, after metabolite extraction as above, the proteins were present in the interphase of the sample. The tertiary and secondary structure of the proteins were broken down with TCEP and chloroacetamide, and LysC protease was added to digest the proteins. After this, the samples were used for liquid chromatography coupled to two-dimensional mass spectrometry (LC-MS/MS).

The protein extracts were digested using an automated sample-preparation workflow [36]. The purified peptides were lyophilized and resuspended in 0.06% FA/3% ACN buffer and separated on an in-house packed reversed-phase chromatography column (20 cm length, 75 μm ID, 3 μm—Dr. Maisch C18). A 155 min gradient (solvent A: 5% acetonitrile, 0.1% formic acid; solvent B: 80% acetonitrile, 0.1% formic acid) was applied for the samples. A volume of 5 μL sample was injected and the peptides eluted with gradients of 4 to 76% ACN and 0.1% formic acid in water at flow rates of 0.25 μL/m. The samples were injected into a Q-Exactive Orbital-trap mass spectrometer (Thermo-Fisher GmbH, Germany) using electrospray ionization at spray voltage of 2.2 kV and measured twice in a data-dependent acquisition mode, selecting the top 10 peaks for HCD fragmentation. MS acquisition was performed at a resolution of 70,000 in the scan range from 300 to 1700 m/z. Dynamic exclusion was set to 30 s and the normalized collision energy to 26eV. The mass window for precursor ion selection was set to 2.0 m/z.

Proteomics Data Analysis and Bioinformatics

The recorded MS-files were analyzed using the MaxQuant software package (version 1.2.2.5) with the IPI-mouse database (version 3.84) complemented with frequently observed contaminants using oxidation and acetylation as variable modifications and carbamidomethylation of cysteins as fixed modification with a maximum of 2 missed cleavages.

Data obtained from the mass spectrometric data was log-transformed for the Aerosol/Gas replicates. Means for the four replicates were calculated and used for the determination of significantly regulated proteins. The cut-off for the experiments was set to 10% for the up- and downregulated proteins. The regulated proteins were used for the Gene Ontology analysis using the DAVID online tool [37].

Results

Chemical and physical properties of the ship engine exposure aerosol

In order to understand the composition of the aerosols that the cells were exposed to, analysis of the chemicals in both the particulate matter (PM) (see ref. [14] and S1 Fig for a summary) and the gas phase (new data presented in this work in Fig 1) of ship engine emission from both fuels was performed. Note that the data presented in S1 Fig and Fig 1 are representing the exposure concentrations as subjected to the cells in the ALI systems (thus including the different dilution ratios that were applied to generally equalize the PM concentrations). The physical characterization (PM size distribution and mass) has been reported in detail previously [14]. This information, along with the new data on the gas phase composition (Fig 1), has been used to obtain as well as estimate and validate the estimated exposure dose for HFO and DF PM (see

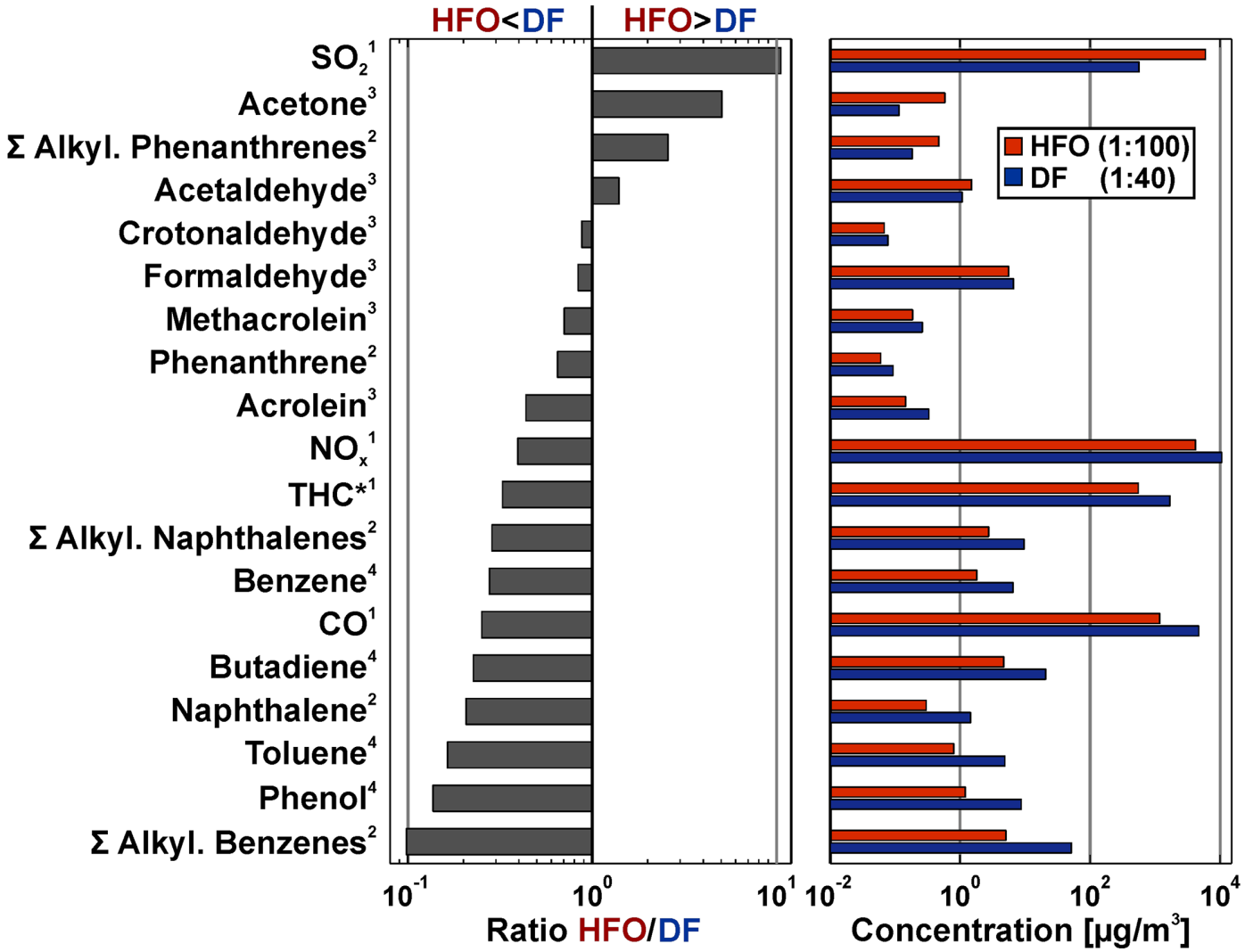

Fig 1. Characterization of gas phase from HFO and DF aerosol (cell exposure concentrations including dilution). The concentrations of each component measured in the aerosol are shown on the right, while the concentration ratios are shown on the left. Exponents refer to method used: (1) Gas monitor, (2) On-line photo ionisation mass spectrometry (REMPI-MS), (3) Gas chromatography mass spectromery, (4) On-line photo ionisation mass spectrometry (SPI-MS).

doi:10.1371/journal.pone.0157964.g001

above). In the following, the previously reported chemical composition of the particulate matter is summarized and the here newly reported gas phase composition results of the exposure aerosol are discussed.

The PM of the HFO exposure aerosols exhibits much higher concentrations of organic compounds compared to the DF PM. This includes the carcinogenic polycyclic aromatic hydrocarbons as well as aliphatic compounds, such as alkanes (S1 Fig). Investigations with modern high-resolution analytical methods, such as comprehensive two-dimensional gas chromatography with ultra-high resolution mass spectrometry, depict that HFO PM also exhibits a largely increased chemical complexity, as well as considerably higher amounts of toxic transition metals, such as vanadium, nickel and iron [14]. Conversely, the PM of DF aerosols contains more "carbonaceous soot," measured either thermo-optically as elemental carbon (EC) or optically

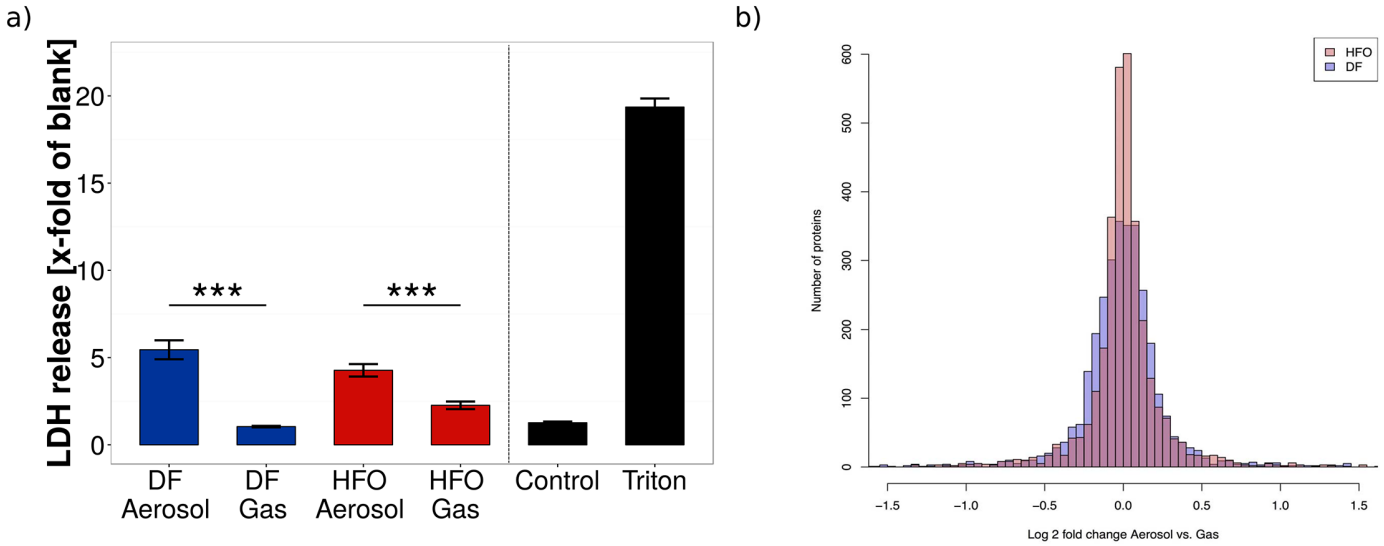

Fig 2. Toxicity of aerosol exposure on macrophages occurs with exposure to both fuel types. (a) Lactate dehydrogenase (LDH) assays were performed on cellular medium after exposure to complete aerosol and filtered aerosols (without particles). DF dilution was 1:40, while HFO dilution was 1:100 in order to obtain comparable particle levels. Blank represents cell free medium, used as a negative control. Triton represents cells lysed with Triton, used as a positive control. Levels represent the mean of three biological replicates (*** = $p < 0.001$. Error bars represent s.e.m.) (b) Density plot of Log2 fold change distribution of regulated proteins of RAW 264.7 cells in response to DF and HFO particles. RAW 264.7 cells show broadening of the protein regulation in response to DF particles (blue) in comparison to HFO particles (red), which indicates higher amount of regulated proteins in DF treated samples.

doi:10.1371/journal.pone.0157964.g002

as black carbon (BC) [15]. The reduced EC and BC values ("soot") in HFO exhaust is likely due to the high sulfur content of the HFO fuels, which quenches the formation of the larger aromatics and therefore also of soot in the combustion process [38]. In the previous study, the relatively higher content of rather pure carbonaceous soot in the DF PM was associated with the surprisingly high biological activity of DF PM. The results of the comprehensive gas characterization of the exposure aerosol are depicted in Fig 1. With the applied dilution differences, many gas phase compounds (including the bulk pollutants CO and NO) are 2 to 3 times more abundant in the DF exposure aerosol compared to HFO. One of the main differences is that the sum of the alkylated benzenes are found at higher concentrations in DF aerosol while the alkylated phenanthrenes (three-ring PAHs) are considerably more abundant in the HFO aerosol (Fig 1). These compounds are partially unburnt fuel residues and the differences are due to the different boiling point cuts in DF and HFO generation [15]. Smaller alkylated PAHs are currently suspected to be biologically active and potentially health relevant [39–41]. Carboxylic compounds in sum are about equally abundant in HFO and DF aerosol, with acetaldehyde and acetone being more concentrated in the HFO aerosol, while formaldehyde and other low abundant aldehydes are more abundant in the DF aerosol. Furthermore, the content of SO_2 is very high in the HFO aerosol compared to DF. The SO_2 concentration, however, is below the concentration where adverse effects are expected, which was determined in the previous study to be 2 ppm for transcriptomics, and 3.3 ppm for LDH release [14].

Toxicity of aerosol exposure to macrophage cells

DF and HFO aerosol (1:40 and 1:100 diluted, respectively) exposure both led to a detectable loss of membrane integrity due to cell death after 4 hours, with a slightly higher toxicity for the DF aerosol (Fig 2). When the particulate phase was removed from the aerosol through filtering,

resulting in an exposure of the cells to the combustion gases only, the toxicity clearly decreased and no significant difference to either the controls or the cell-free "blank" medium could be observed.

The clear reduction of released LDH after particle removal indicates a predominantly particle mediated toxicity for DF aerosol exposure. For HFO aerosol exposure, the gas phase (filtered aerosol) shows some toxicity, although a 2.5 times larger dilution was set for the HFO emissions in order to establish comparable particle deposition doses. This suggests that the HFO gas phase shows more acute cytotoxicity than the DF gas phase, which might be attributed to the higher concentration of gaseous toxic compounds, such as gaseous aldehydes and ketones [27] or alkylated polyaromatic species in the HFO exhaust [39–41]. Thus, with the tested dilution ratios, the gases formed by the DF are not, or in the case of HFO combustion to a part, responsible for the observed aerosol toxicity. The main toxicity, however, is governed by the particle exposure, and it is likely that DF particles show even a stronger cytotoxic impact compared to the HFO particles. These results are in line with our previous study on lung epithelial cells, in which DF particle exposure was shown to produce larger biological effects than HFO particle exposure at comparable deposition doses [14]. These findings are surprising, as the concentration of known toxic compounds (such as PAH, oxygenated species, or heavy metals) is much higher in HFO particles than DF particles. Note that LDH release is a rather strong cytotoxicity endpoint, reflecting irreversible cell death by membrane damage. A lower LDH-based toxicity, therefore, does not exclude the presence of strong adverse cellular effects.

Results from the proteomics analysis show that particles from DF ship diesel combustion aerosols cause broader proteomic response in RAW 264.7 cells than particles from HFO ship diesel combustion. Fig 2 shows a larger distribution of proteins that are differentially regulated in response to DF in comparison to HFO, which indicates higher amount of up and down regulated proteins in DF combustion treated samples. This result is very similar to the previous observations in lung epithelial cells [14], and reinforces this finding in a further lung-relevant cell type. The broadening of protein regulation does not itself prove increased toxicity, but instead shows a wide biological reaction to the given aerosol exposure conditions. In conjunction with the cytotoxicity data, the proteomics results support for the conclusion that DF particle exposure leads to a higher cytotoxic effect in macrophages compared to the HFO particle exposure, likely due to the relatively high soot content of the DF aerosol.

Differential metabolic profiles of aerosol-treated macrophages

Non-targeted metabolomics analysis uncovered 230 compounds present in the four different conditions. After normalization and filtering out compounds present in less than 80% of each treatment, 203 compounds were subjected to principal component analysis (PCA) and ANOVA analysis. PCA analysis shows groupings based upon fuel type (70.8% of explained variance), with minimal separation due to particle phase (7% of explained variance) (Fig 3). This result is the opposite of the toxicity profile, suggesting that metabolic effects are due to the gas phase of the aerosol more than the PM.

After ANOVA analysis, 167 compounds were found to be significantly differing between HFO and DF exposure at a cutoff of $p < 0.01$. Of the compounds discovered, 34 were able to be identified with our in-house metabolite library, and are listed in S1 Table. Clustering of significantly changed metabolite groupings show almost no separation between complete aerosol and gas phase exposure (Fig 3). This suggests that the effect of the particulate matter on the metabolic profile of macrophages is negligible, compared to the gas phase. Most compounds were found at increased levels with HFO exposure, while relatively fewer compounds (including Tyrosine and glycerol) are increased under DF treatment.

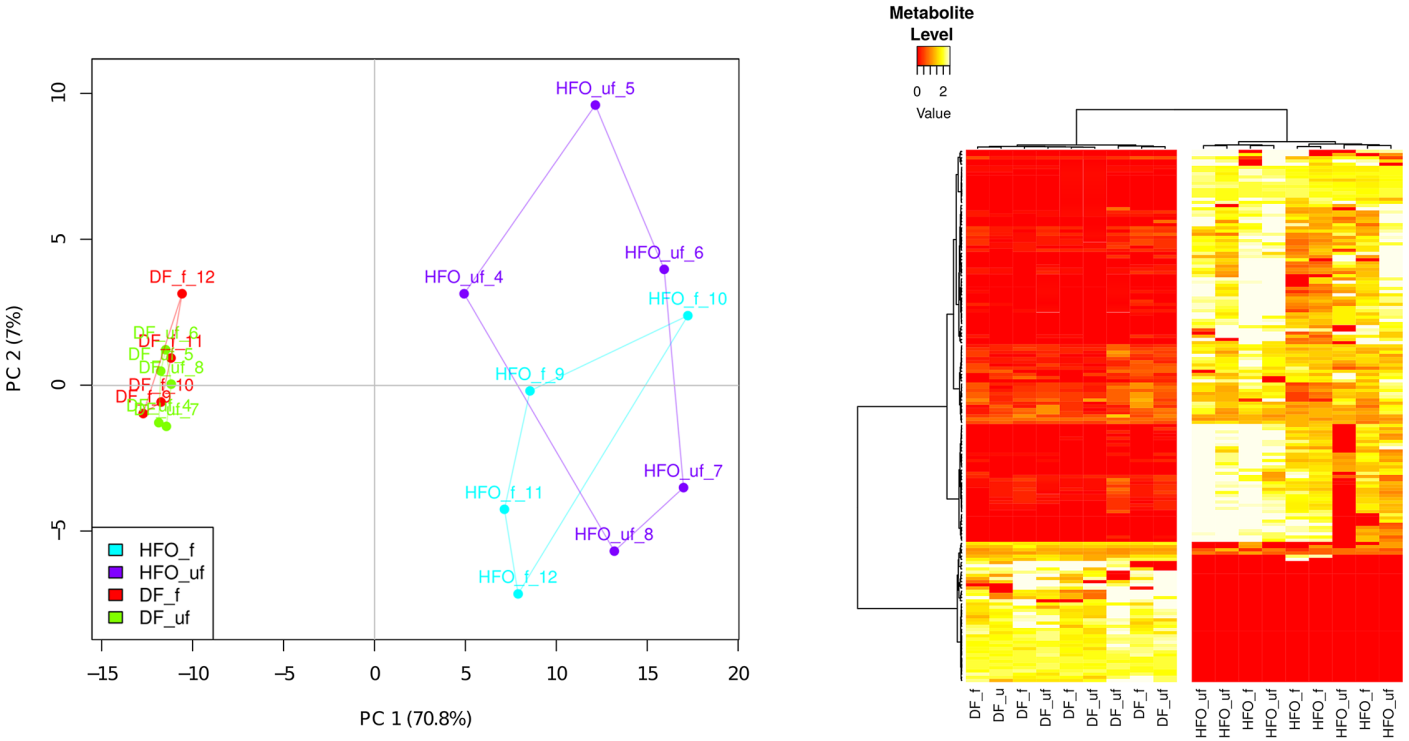

Fig 3. Metabolic profile of macrophages exposed to combustion aerosols. (a) Principal Component Analysis shows separation of fuel types, but no separation by presence of particles. (b) Heatmap represents metabolites with significantly differing abundances between treatments (ANOVA test, $p < 0.01$). Data was batch normalized, and metabolites found in less than 80% of all treatments were removed. DF: Diesel Fuel, HFO: Heavy Fuel Oil, f: filtered aerosol exposure (n = 4), uf: unfiltered (complete) aerosol exposure (n = 5).

doi:10.1371/journal.pone.0157964.g003

Certain metabolites found increased in HFO-exposed macrophages suggest a pro-inflammatory metabolic phenotype, specifically succinic acid and lactic acid (Fig 4). Succinic acid levels have been found to be increased in pro-inflammatory macrophages to aid increased inflammatory cytokine production [26]; this has been shown to lead to an increased glycolytic flux with reduced pyruvate intake into the TCA cycle [42]. Increased glycolysis with decreased pyruvate flux into the TCA cycle would shunt the flux towards lactic acid. This cellular metabolism profile is common in certain cellular conditions, and is often called the Warburg effect [43]. The Warburg effect is mostly associated with tumor cells, however has been recently found to be present in pro-inflammatory macrophages. [44]

Another metabolite, itaconic acid, has been associated with antimicrobial activity of pro-inflammatory macrophages [45]. Itaconic acid has only been found in certain immune cells (including macrophages), and only when these cells were in a pro-inflammatory state. Therefore, it is a good marker for inflammatory macrophages. To identify this metabolite, experimental spectra were compared to an itaconic acid standard measured previously and integrated into our metabolite identification library (S2 Fig). Itaconic acid was found in all macrophages exposed to HFO aerosols, but was not present in DF-treated macrophages (Fig 4), a result independent of the presence of PM therefore an effect of gas phase exposure. Some itaconic acid was also found in the control cells, at higher levels than DF treatment. The DF treated cells have a much more complicated chromatogram, and this would increase the noise baseline for the analysis. The itaconic acid signal might fall below the baseline, and would

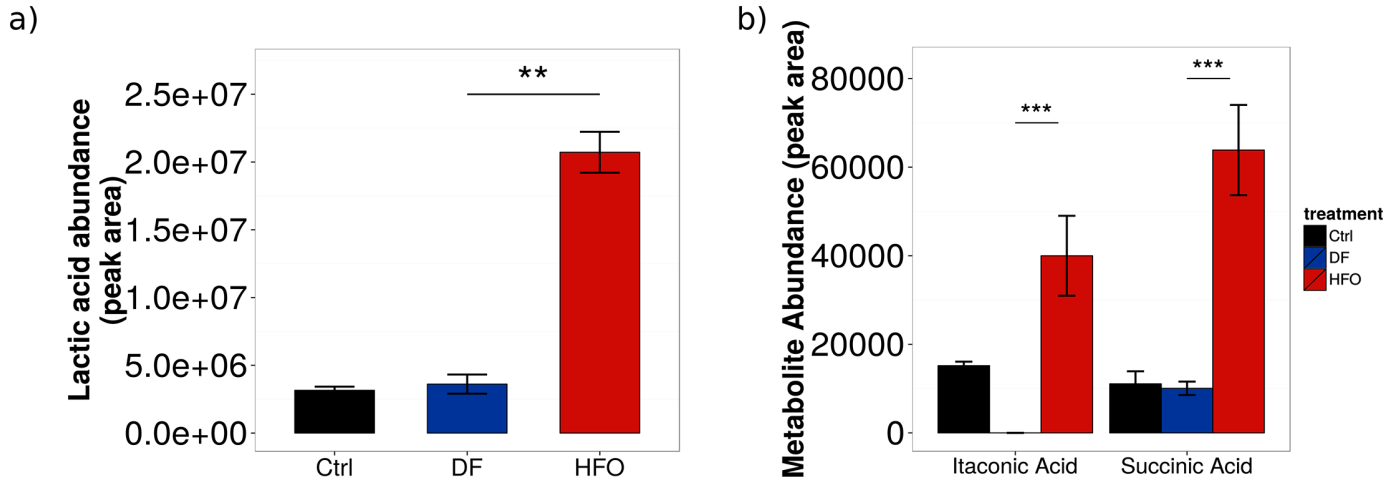

Fig 4. Levels of intracellular metabolite pools in aerosol-exposed macrophages. Pools of (a) lactic acid, (b) succinic acid, and itaconic acid were measured. Levels represent the mean of 9 biological replicates. *** = $p < 0.001$. Error bars represent s.e.m.

doi:10.1371/journal.pone.0157964.g004

therefore be not measured even if it is present in low amounts. However, its presence in macrophages stimulated with aerosols could point to a novel role for this metabolite in inflammation-governed environmental health effects.

The metabolic profile of HFO-exposed macrophages also shows increased levels of other compounds compared to DF-exposure. The increase of adenine and uracil, two bases involved in nucleic acid synthesis, suggests increased cellular DNA and RNA production, a process known to be increased in activated macrophages [46]. Adenine is also an important molecule for energy metabolism, present in both ATP and NAD^+; its increase could be tied to an increased cellular energy production from increased glycolytic flux to lactic acid (which produces ATP, and aids in NAD+/NADH balancing), necessary for macrophages dealing with inflammatory stimuli.

Effects of aerosol treatment on metabolic dynamics: Carbon flux from glucose to intracellular metabolites

Stable-isotope labeling provides a complementary source of information on how glycolytic flux is impacted by combustion aerosol exposure. By looking at the labeling pattern of certain metabolites in cells cultured with uniformly ^{13}C-labeled glucose, we were able to gain insight into how the glucose is metabolized in the cell through central carbon metabolism, and the rates of glycolysis and glucose oxidation can be compared between different conditions. We measured the labeling in lactic acid, giving more information into glycolytic flux, as well as two metabolites from the TCA cycle (fumaric acid and glutamic acid), which allows the tracing of how glucose is differentially oxidized through the TCA cycle with exposure to the different combustion aerosols.

While both aerosol types lead to a similar amount of lactic acid labeling derived from glucose (Fig 5), labeling of TCA cycle intermediates derived from glucose were significantly reduced in DF exposure compared to HFO exposure (Fig 5). These results suggest that DF-exposed macrophages have a decreased amount of relative glucose oxidation into the TCA cycle compared to macrophages with HFO-exposure. As HFO stimulates a pro-inflammatory phenotype in the macrophages, this decrease in glucose oxidation is presumably tied to an

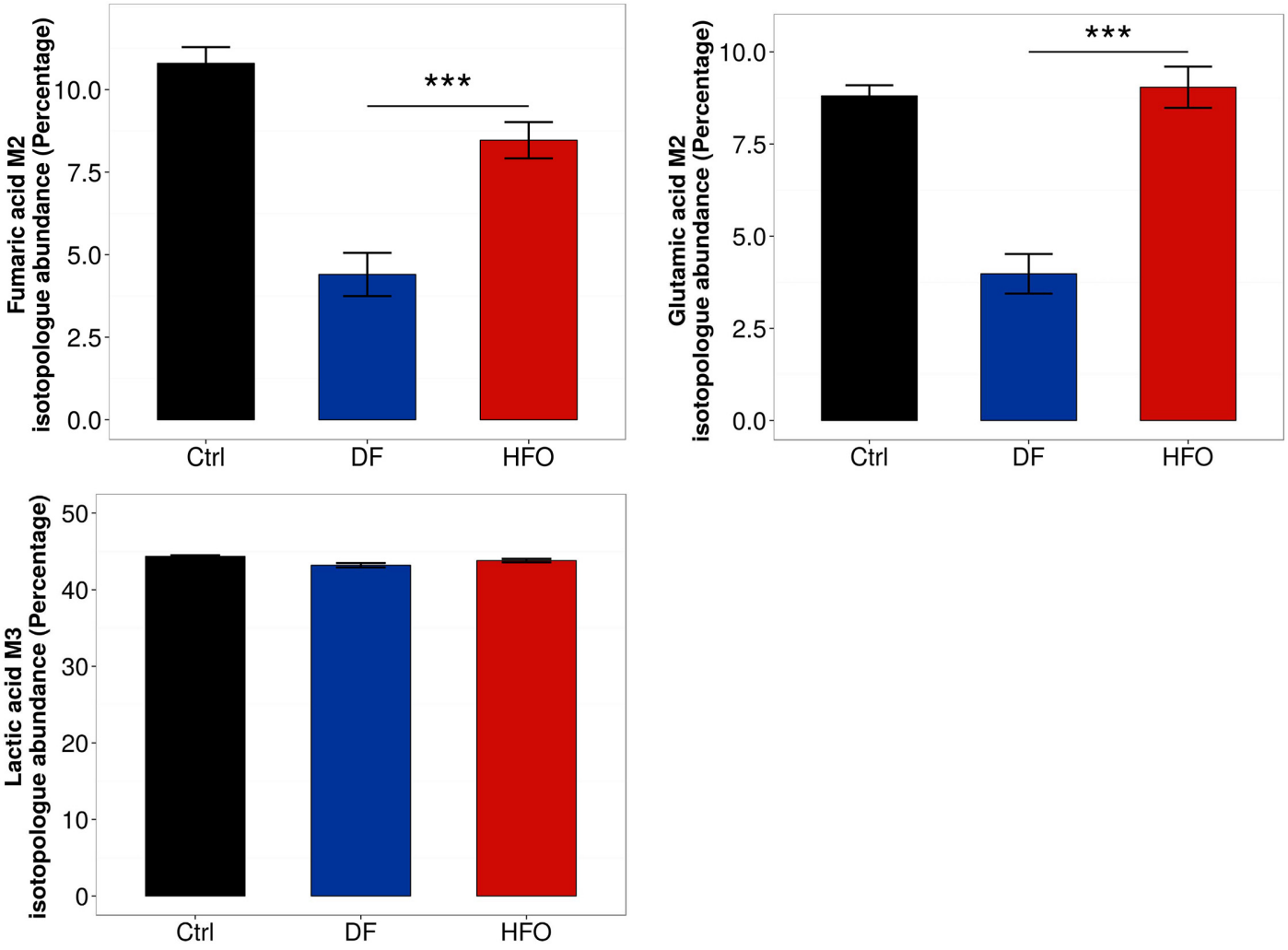

Fig 5. Relative oxidation of glucose in the TCA cycle for aerosol-exposed macrophages. Metabolism of U-$^{13}C_6$-Glucose was measured in macrophages after exposure. (a) M2 fumaric acid isotopologue levels, (b) M2 glutamic acid isotopologue levels, and (c) M3 lactic acid isotopologue levels. Levels represent the mean of 4–6 biological replicates. *** = $p < 0.001$. Error bars represent s.e.m.

doi:10.1371/journal.pone.0157964.g005

alternative metabolic phenotype. As it is known that macrophages exhibit a wide variety of phenotypic states depending on the stimulant [47], the metabolic changes seen here suggest a macrophage state slightly different from canonical activation states.

Effects of combustion aerosol treatment on the proteome in RAW 264.7 macrophages

Analysis of the changes to the proteome of exposed RAW 264.7 cells support the findings of the metabolomics analysis, with differing regulation of proteins by HFO particles compared to DF particles (Fig 2 and S3 Fig). An analysis for gene set enrichment of the regulated proteins using the DAVID online pathway analysis tool [37] showed that different pathways and

biological processes are induced in response to DF and HFO particles. Two of the main pathways seen to be affected by PM exposure are endocytosis and the activation of the immune response.

Proteins relating to the GO term endocytosis (GO:0006897) were found to be upregulated in both HFO and DF treated samples, while the different fuel types induced activation of different groups of proteins involved in endocytosis (S8 Fig). Proteins involved in the immune response pathway (GO:0006955) were found to be upregulated only in HFO treated macrophages ($p = 0.059$), while DF stimulation shows no significant upregulation of the pathway (Fig 6). This data supports the metabolic analysis in so far that enrichment of the immune response pathway GO term indicates an activation of inflammatory pathways on a larger scale, mainly through the NF-kappa-B (NF-kB) signaling pathway (Fig 6).

Stimulation of the toll-like receptor (TLR2) leads to activation of NF-kB, which plays a key role in regulating the immune response. Tumor necrosis factor alpha-induced protein 8-like protein 2 (TNFAIP8L2) acts as a negative regulator of innate and adaptive immunity by maintaining immune homeostasis. TNFAIP8L2 prevents hyperresponsiveness of the immune system by negative regulation of TLR2, and inhibition of NF-kappa-B activation [48]. Peroxiredoxin 2 (Pdrx2) reduces hydrogen peroxide and is involved in redox regulation of the cell. Prdx2 inhibits NF-kB activation, which is induced by H_2O_2, and regulates immune response [49].

These findings in macrophages are in line with the previous study on lung epithelial cells [14]: the endocytosis pathway was found to be upregulated after aerosol exposure from both fuel types, while the immune response was only upregulated after HFO exposure.

Discussion

Results from this study point to a differential effect between the gas and particle phases of combustion aerosols from ship engines on RAW 264.7 macrophages. For both of the fuel types studied, the emitted particle phase has a strong impact on cytotoxicity, while the gas phase of the aerosol alone has a stronger effect on the internal metabolism of the cells. The stronger gas phase effects seen with HFO aerosol suggest that the source of these effects could be from the compound class of smaller alkylated polycyclic aromatic hydrocarbons, such as alkylated phenanthrenes. These compounds are the only more abundant compound class detected in the HFO aerosol gas phase, if the (at the applied dilution) toxicologically noncritical sulfur dioxide is neglected. While this cannot be directly proven by this study, the results here motivate further experiments with semi-volatile compounds, such as smaller alkylated aromatics, to determine what, if any, gas phase effects are caused by their presence.

As different cellular effects can be seen due to gas exposure compared to combined gas and particle exposure, currently used submerged cell culture particle exposure experiments only partially highlight aerosol-induced changes in cellular metabolism; there should be more of a focus on research done with complete aerosol exposure in order to elucidate biological effects which are closer to those found *in vivo*.

The findings from this study validate and confirm the rather surprising results of the previously reported lung epithelial cell based multi-omics experiments on the effect of shipping engines emissions on lung epithelial cells [14], and extend the findings to a completely different cell type. This includes the observation that, according to the chemical analysis, the supposedly much less toxic particles from high quality, refined diesel fuel (DF) induce a broader biological reaction in lung cells than heavy fuel oil (HFO) particles at comparable exposure doses, although the toxicant concentration in particles from the latter is extremely high. As the overall particle mass deposited on the cells from DF exposure was lower than that from HFO, and the

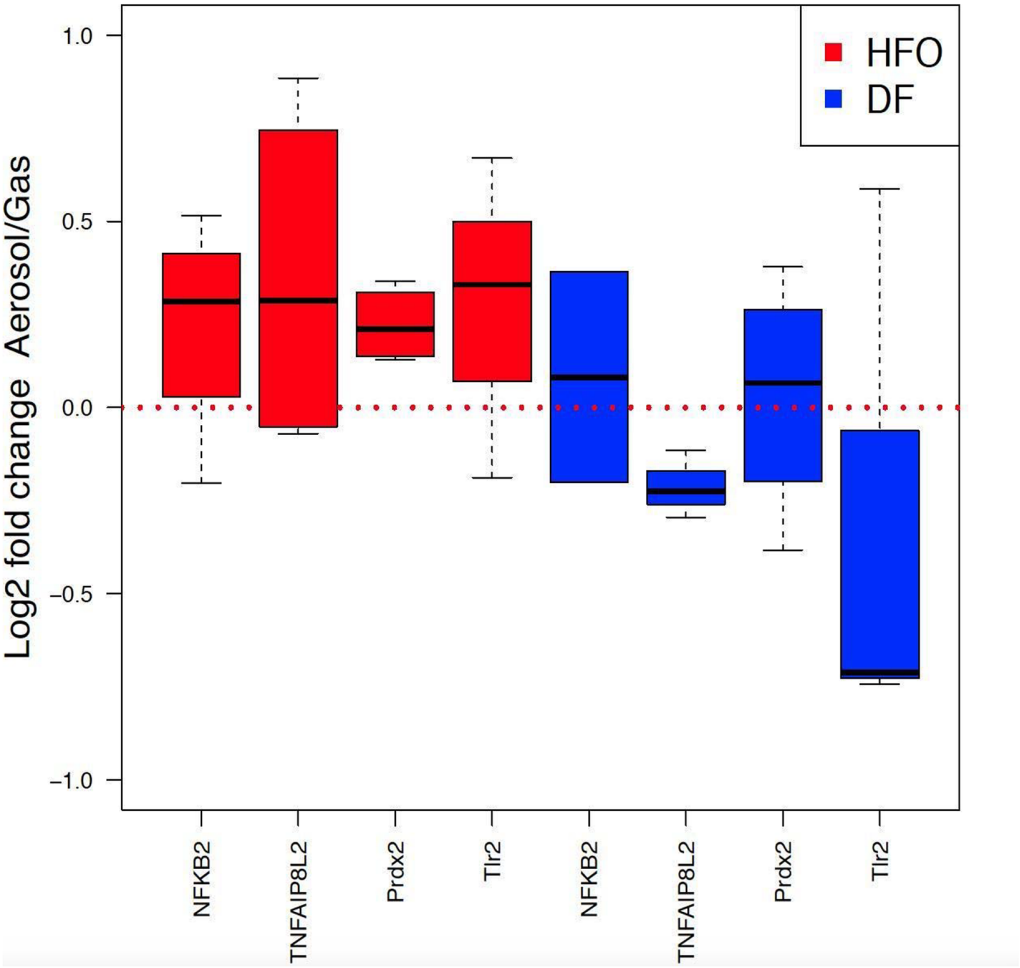
HFO
DF
Log2 fold change Aerosol/Gas
1.0
0.5
0.0
−0.5
−1.0
NFKB2
TNFAIP8L2
Prdx2
Tlr2
NFKB2
TNFAIP8L2
Prdx2
Tlr2

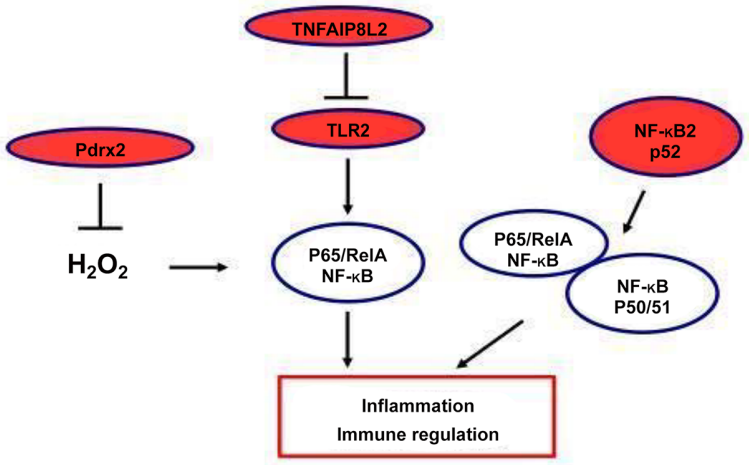
TNFAIP8L2
TLR2
Pdrx2
H_2O_2
P65/RelA
NF-κB
NF-κB2
p52
P65/RelA
NF-κB
NF-κB
P50/51
Inflammation
Immune regulation

Fig 6. HFO particles induce activation of immune response in RAW 264.7 macrophages. (a) The Gene Ontology term GO:0006955, corresponding to activation of immune response, was found to be significantly up-regulated in HFO-treated samples (p = 0.059) and not regulated in the DF-treated samples. (b) Model of how the regulated proteins found in this study affect the NF-kB immune response pathway in the cell. Stimulation of the toll-like receptor (TLR2) leads to activation of NF-kB. Tumor necrosis factor alpha-induced protein 8-like protein 2 (TNFAIP8L2) acts as a negative regulator of TLR2, preventing hyperresponsiveness of the immune system, and inhibiting NF-kappa-B activation. Peroxiredoxin 2 (Pdrx2) reduces hydrogen peroxide, inhibiting NF-kappa-B activation.

doi:10.1371/journal.pone.0157964.g006

toxicity was around the same for both fuel types, it follows that DF exhaust is more toxic than was previously thought, and possibly on par with HFO. It was concluded that the high concentration of soot-like, elemental carbon in DF likely is responsible for this surprising effect [14]. As in the previous study with epithelial cells, a broader proteomic response after DF aerosol exposure was also seen in the macrophages, whereas HFO aerosol exposure was found to be an important inflammatory instigator, both on a metabolite and protein level. Endocytosis, which was identified as a regulated pathway in the epithelial cells, is also upregulated with exposure from both fuel types in macrophages, which is likely associated with particle uptake (S8 Fig).

Furthermore, it was observed in the previous study [14] that DF and HFO particles induce different biological pathways, assuming a different mode of action for the fairly different particle types (i.e. DF particles consist of carbon rich soot-like particle agglomerates while HFO particles are smaller, with mixed carbon/metal oxide cores and a surface covered with organic compounds and sulfates). The applied exposure concentrations (which are the same as in this study) were too low to induce direct cytotoxic effects in the epithelial cells. The macrophages, however, represent the first line of defense against particles and other pathogens in the lung. They can readily engulf the deposited particles through phagocytosis and thus are more vulnerable to PM exposure than lung epithelial cells. The cytotoxicity results summarized in Fig 2 suggest that the DF particles exhibit a stronger cytotoxicity than the particles from the HFO aerosol. This lends further evidence to the unexpected result from the previous study, that cleaner fuels (i.e. fuels that reduce the emission of toxic chemicals) do not automatically implicate a lower acute cytotoxicity of the formed particles.

Previous studies using submerged culture exposure of collected particles show induction of cytotoxicity and inflammatory signals in epithelial cells as well as macrophages [4, 6]. Our results, determined using the more realistic air-liquid interface cell exposure, support these findings by adding metabolic inflammatory signals found under aerosol exposure. However, it becomes clear from our data that the strength of inflammatory signals depend on the specific properties and source of the aerosol, and that this effect is not only dependent on particle exposure alone. HFO aerosols stimulate a pro-inflammatory response in the macrophages, leading to an increase in metabolites and protein regulatory pathways known to be associated with antimicrobial activity and a pro-inflammatory phenotype. This is especially highlighted by the induction of a metabolite indicating inflammation, itaconic acid, by HFO exposure. Proteomics data supports this finding by showing an upregulation of inflammatory-associated proteins in the NF-kB signaling pathway. This phenotypic effect is solely induced by the gas phase of the combustion aerosol. The increase of succinic acid levels in macrophages suggest a role for HIF-1a in this process, and these signaling pathways would be promising for continued research into aerosol-based inflammation in macrophages.

While air-liquid interface exposures already represent a step towards a more realistic model of airway exposure, an important further improvement would be taking into account the pulmonary surfactant system, integrating it into an improved air-liquid interface exposure system. It has been shown that proteins from this system have an impact on how pathogen-associated

molecular pattern recognizing proteins and cytokines are expressed in stimulated macrophgaes [50], and addition of this system into the experimental setup used in this study would thus increase it's applicability even further.

As metabolism is becoming more and more implicated in the inflammatory response of many cells (including macrophages), as well as the progression of many diseases (including cardiovascular diseases and cancer), studies integrating metabolomics with other techniques (such as proteomics), probing the effect of anthropogenic aerosols on metabolism, are vital to increase our understanding of cellular mechanisms underlying the negative health effects. Furthermore, a focus should be put on studies that characterize the complete aerosols found in the environment, with in-depth research as well on the possible effects of gaseous components on human health. In this way, the complex composition of aerosols can be broken down, and simpler models of aerosol can be studied to understand the most important components of aerosol relative to human health effects. Finally, it can be seen that fuel changes alone are not sufficient for the mitigation of health effects from aerosol combustion, and means of reducing particles should be integrated into the reduction of shipping-related health effects.

Finally, this work support the conclusion of the previous work [14], that legislation enforcing fuel changes (i.e. establishment of sulphur emissions control areas, SECA [51] alone are not sufficient for a safe mitigation of health effects from shipping aerosol emissions. Moreover, measures reducing particles and toxic gases from shipping emissions (exhaust gas scrubbers, particle filters, precipitators, or others) need to be further developed and legally prescribed for the reduction of shipping-related health effects.

Supporting Information

S1 File. Previous Supporting Work. The manuscript Oeder *et al* 2015, which is referenced by this work.
(PDF)

S1 Table. Metabolite List. List of final 34 metabolites identified in experimental intracellular samples. All compounds were identified with an in-house library.
(EPS)

S2 Table. Metabolomcs Dataset. Non-targeted metabolomics dataset containing the 230 compounds found in each of the four different experimental conditions.
(CSV)

S3 Table. LDH Dataset. Raw data from the lactate dehydrogenase (LDH) assay.
(CSV)

S1 Fig. Chemical Characterization of Particulate Matter In Aerosol. Concentrations (right) and concentration ratios (left) of particulate matter-bound species in HFO and DF aerosols. Modified from Oeder et al, 2015. Exponents refer to methods used to obtain data: (5) ICP-AES, (6) Thermal desorption/direct derivatization gas chromatography/Mass spectrometry, (7) AMS, (8) Filter weighing, (9) EC/OC-analysis (thermal-optical method), (10) Aethalometer.
(EPS)

S2 Fig. Itaconic Acid Identification. Mass spectrum of experimentally discovered itaconic acid (top) compared with the in-house library spectrum (bottom). Retention index of experimental compound was 1417.21, while retention index of library compound is 1409.20. Using the ICBM algorithm for matching, experimental itaconic acid was identified with a score of 0.97.
(EPS)

S3 Fig. Proteome Christmas Tree Plot. Comparison of regulation magnitude and abundance of regulated proteins. Mean of log2 fold change Aerosol vs. Gas is plotted vs. mean of log10 fold sum of intensities of complete dataset of proteins in response to DF (blue) and HFO (red) particles. RAW 264.7 cells show broadening of the protein regulation in response to DF particles (blue) in comparison to HFO particles (red), corresponding to higher amount of up and down regulated proteins in DF particles treated samples.
(EPS)

S4 Fig. Proteome Volcano Plot. Comparison of regulation magnitude and regulation significance. Mean of log2 fold change Aerosol vs. Gas is plotted vs. -log10 p-value of complete dataset of proteome in response to DF (blue) and HFO (red) particles. RAW 264.7 cells show broadening of the significant protein regulation in response to DF particles (blue) in comparison to HFO particles (red), corresponding to higher amount of significantly up and down regulated proteins in DF particles treated samples.
(EPS)

S5 Fig. Proteome Correlation Plot. Correlation of log2 fold changes Aerosol vs. Gas between HFO and DF. Log2 fold changes Aerosol vs. Gas of protein regulation in response to HFO and DF show no correlation (Cor2 = 00357), which indicates that HFO and DF particles cause different regulation of different proteins in RAW 264.7 cells.
(EPS)

S6 Fig. Proteome QQ Plot—DF. The Q–Q plot for proteomic response of RAW 264.7 cells to DF Aerosol vs. DF Gas. The line is a parametric curve with the parameter, which is the interval for the quantile. The points with linearly related distributions lie on the line, which suggests that they are normally distributed. On the left and right sides of the plot the points are not linearly related and show no normal distribution, which corresponds to populations of up and down regulated proteins in response to DF particles.
(EPS)

S7 Fig. Proteome QQ Plot—HFO. The Q–Q plot for proteomic response of RAW 264.7 cells to HFO Aerosol vs. HFO Gas. The line is a parametric curve with the parameter, which is the interval for the quantile. The points with linearly related distributions lie on the line, which suggests that they are normally distributed. On the left and right sides of the plot the points are not linearly related and show no normal distribution, which corresponds to populations of up and down regulated proteins in response to HFO particles.
(EPS)

S8 Fig. Regulation of Endocytosis Related Proteins. DF and HFO particles induce activation of different proteins involved in endocytosis in RAW 264.7 macrophages. The Gene Ontology term Endocytosis was found up regulated in HFO and DF Aerosol vs. Gas treated samples. This data suggests that particles play a role in the regulation of endocytosis in macrophages. Necap1, Necap2 and Lrp1 (red) are up regulated in HFO treated samples, while Lrp1, Vamp7, Tfrc and Ube3a (blue) are up regulated in DF treated samples.
(EPS)

Acknowledgments

This work was funded by the Helmholtz Virtual Institute of Complex Molecular Systems in Environmental Health: Aerosol and Health (www.hice-vi.eu). We would like to thank the entire HICE consortium for their aid an assistance for these experiments. SCS and KH are

supported by the Fonds National de la Recherche, Luxembourg (ATTRACT A10/03).

Author Contributions

Conceived and designed the experiments: SCS T. Kanashova MD SO JP CR JB OS TS HRP CS SM HH EK TG CW GD KH RZ. Performed the experiments: SCS T. Kanashova MD JP CR OS CS BS RR EK. Analyzed the data: SCS T. Kanashova MD SD SO JP CR JB OS TS BS RR EK TG CW GD KH RZ. Contributed reagents/materials/analysis tools: SCS T. Kanashova MD SD SO JP CR JB OS TS HRP CS SM BS RR HH T. Krebs EK TG CW GD KH RZ. Wrote the paper: SCS T. Kanashova MD CW GD KH RZ.

References

1. Sydbom A, Blomberg A, Parnia S, Stenfors N, Sandström T, Dahlén SE. Health effects of diesel exhaust emissions. The European respiratory journal. 2001 Apr; 17(4):733–46. Available from: http://www.ncbi.nlm.nih.gov/pubmed/11401072 doi: 10.1183/09031936.01.17407330 PMID: 11401072
2. Wichmann HE. Diesel exhaust particles. Inhalation Toxicology. 2007; 19(S1):241–244. Available from: <Go to ISI>://000249434300031. doi: 10.1080/08958370701498075 PMID: 17886072
3. Corbett JJ, Winebrake JJ, Green EH, Kasibhatla P, Eyring V, Lauer A. Mortality from Ship Emissions: A Global Assessment. Environmental Science & Technology. 2007; 41(24):8512–8518. Available from: http://pubs.acs.org/doi/abs/10.1021/es071686z doi: 10.1021/es071686z
4. Bhavaraju L, Shannahan J, William A, McCormick R, McGee J, Kodavanti U, et al. Diesel and biodiesel exhaust particle effects on rat alveolar macrophages with in vitro exposure. Chemosphere. 2014 Jun; 104:126–133. Available from: http://linkinghub.elsevier.com/retrieve/pii/S0045653513015403 doi: 10.1016/j.chemosphere.2013.10.080 PMID: 24268344
5. Shaw CA, Robertson S, Miller MR, Duffin R, Tabor CM, Donaldson K, et al. Diesel exhaust particulate-exposed macrophages cause marked endothelial cell activation. American Journal of Respiratory Cell and Molecular Biology. 2011 Jun; 44(6):840–851. Available from: http://www.ncbi.nlm.nih.gov/pubmed/20693402 doi: 10.1165/rcmb.2010-0011OC PMID: 20693402
6. Li N, Wang M, Oberley TD, Sempf JM, Nel AE. Comparison of the Pro-Oxidative and Proinflammatory Effects of Organic Diesel Exhaust Particle Chemicals in Bronchial Epithelial Cells and Macrophages. The Journal of Immunology. 2002; 169(8):4531–4541. Available from: http://jimmunol.org/content/169/8/4531.abstract doi: 10.4049/jimmunol.169.8.4531 PMID: 12370390
7. Fritsch-Decker S, Both T, Mulhopt S, Paur HR, Weiss C, Diabaté S. Regulation of the arachidonic acid mobilization in macrophages by combustion-derived particles. Particle and fibre toxicology. 2011; 8 (1):1–18. doi: 10.1186/1743-8977-8-23
8. Steiner S, Czerwinski J, Comte P, Müller LL, Heeb NV, Mayer A, et al. Reduction in (pro-)inflammatory responses of lung cells exposed in vitro to diesel exhaust treated with a non-catalyzed diesel particle filter. Atmospheric Environment. 2013; 81(C):117–124. Available from: http://dx.doi.org/10.1016/j.atmosenv.2013.08.029\npapers2://publication/doi/10.1016/j.atmosenv.2013.08.029 doi: 10.1016/j.atmosenv.2013.08.029
9. Knebel JW, Ritter D, Aufderheide M. Exposure of human lung cells to native diesel motor exhaust–development of an optimized in vitro test strategy. Toxicology in vitro: an international journal published in association with BIBRA. 2002; 16(2):185–192. doi: 10.1016/S0887-2333(01)00110-2
10. Seagrave J, Dunaway S, McDonald JD, Mauderly JL, Hayden P, Stidley C. Responses of differentiated primary human lung epithelial cells to exposure to diesel exhaust at an air-liquid interface. Experimental lung research. 2007; 33(1):27–51. Available from: http://www.ncbi.nlm.nih.gov/pubmed/17364910 doi: 10.1080/01902140601113088 PMID: 17364910
11. Comouth A, Saathoff H, Naumann KH, Muelhopt S, Paur HR, Leisner T. Modelling and measurement of particle deposition for cell exposure at the air–liquid interface. Journal of Aerosol Science. 2013; 63:103–114. Available from: http://linkinghub.elsevier.com/retrieve/pii/S0021850213001171 doi: 10.1016/j.jaerosci.2013.04.009
12. Diabaté S, Mülhopt S, Paur HR, Krug HF. The response of a co-culture lung model to fine and ultrafine particles of incinerator fly ash at the air-liquid interface. Alternatives to laboratory animals: ATLA. 2008 Jul; 36(3):285–98. Available from: http://www.ncbi.nlm.nih.gov/pubmed/18662093 PMID: 18662093
13. Paur HR, Cassee FR, Teeguarden J, Fissan H, Diabate S, Aufderheide M, et al. In-vitro cell exposure studies for the assessment of nanoparticle toxicity in the lung-A dialog between aerosol science and biology. Journal of Aerosol Science. 2011; 42(10):668–692. doi: 10.1016/j.jaerosci.2011.06.005
14. Oeder S, Kanashova T, Sippula O, Sapcariu SC, Streibel T, Arteaga-Salas JM, et al. Particulate Matter from Both Heavy Fuel Oil and Diesel Fuel Shipping Emissions Show Strong Biological Effects on

Human Lung Cells at Realistic and Comparable In Vitro Exposure Conditions. Plos One. 2015; 10(6): e0126536. Available from: http://dx.plos.org/10.1371/journal.pone.0126536 doi: 10.1371/journal.pone.0126536 PMID: 26039251

15. Sippula O, Stengel B, Sklorz M, Streibel T, Rabe R, Orasche J, et al. Particle Emissions from a Marine Engine: Chemical Composition and Aromatic Emission Profiles under Various Operating Conditions. Environmental Science & Technology. 2014 Oct; 48(19):11721–11729. Available from: http://pubs.acs.org/doi/abs/10.1021/es502484z doi: 10.1021/es502484z

16. Barton GM. A calculated response: control of inflammation by the innate immune system. Journal of Clinical Investigation. 2008 Feb; 118(2):413–420. Available from: http://www.jci.org/articles/view/34431 doi: 10.1172/JCI34431 PMID: 18246191

17. Gordon S, Taylor PR. Monocyte and macrophage heterogeneity. Nature Reviews Immunology. 2005 Dec; 5(12):953–964. Available from: http://www.nature.com/doifinder/10.1038/nri1733 doi: 10.1038/nri1733 PMID: 16322748

18. Murray PJ, Wynn TA. Protective and pathogenic functions of macrophage subsets. Nature reviews Immunology. 2011 Nov; 11(11):723–37. Available from: http://www.pubmedcentral.nih.gov/articlerender.fcgi?artid=3422549&tool = pmcentrez&rendertype = abstract doi: 10.1038/nri3073 PMID: 21997792

19. Olsen HH, Grunewald J, Tornling G, Sköld CM, Eklund A. Bronchoalveolar Lavage Results Are Independent of Season, Age, Gender and Collection Site. PLoS ONE. 2012 Aug; 7(8):e43644. Available from: http://dx.plos.org/10.1371/journal.pone.0043644 doi: 10.1371/journal.pone.0043644 PMID: 22952729

20. Wynn TA, Chawla A, Pollard JW. Macrophage biology in development, homeostasis and disease. Nature. 2013 Apr; 496(7446):445–55. Available from: http://www.ncbi.nlm.nih.gov/pubmed/23619691 doi: 10.1038/nature12034 PMID: 23619691

21. Castranova V, Bowman L, Reasor MJ, Lewis T, Tucker J, Miles PR. The response of rat alveolar macrophages to chronic inhalation of coal dust and/or diesel exhaust. Environmental Research. 1985 Apr; 36(2):405–419. Available from: http://linkinghub.elsevier.com/retrieve/pii/0013935185900349 doi: 10.1016/0013-9351(85)90034-9 PMID: 2579806

22. Salvi S, Blomberg A, Rudell B, Kelly F, Sandström T, Holgate S, et al. Acute Inflammatory Responses in the Airways and Peripheral Blood After Short-Term Exposure to Diesel Exhaust in Healthy Human Volunteers. American Journal of Respiratory and Critical Care Medicine. 1999 Mar; 159(3):702–709. Available from: http://www.atsjournals.org/doi/abs/10.1164/ajrccm.159.3.9709083 doi: 10.1164/ajrccm.159.3.9709083 PMID: 10051240

23. Schwarze PE, Totlandsdal AI, Låg M, Refsnes M, Holme JA, Ø vrevik J. Inflammation-Related Effects of Diesel Engine Exhaust Particles: Studies on Lung Cells In Vitro. BioMed Research International. 2013 Jan; 2013:1–13. Available from: http://www.hindawi.com/journals/bmri/2013/685142/ doi: 10.1155/2013/685142

24. Ewald JC, Heux S, Zamboni N. High-Throughput Quantitative Metabolomics: Workflow for Cultivation, Quenching, and Analysis of Yeast in a Multiwell Format. Analytical Chemistry. 2009 May; 81(9):3623–3629. Available from: http://pubs.acs.org/doi/abs/10.1021/ac900002u doi: 10.1021/ac900002u PMID: 19320491

25. Hiller K, Metallo C, Stephanopoulos G. Elucidation of Cellular Metabolism Via Metabolomics and Stable-Isotope Assisted Metabolomics. Current Pharmaceutical Biotechnology. 2011 Jul; 12(7):1075–1086. Available from: http://www.eurekaselect.com/openurl/content.php?genre = article&issn=1389-2010&volume=12&issue=7&spage=1075 doi: 10.2174/138920111795909096 PMID: 21466455

26. Tannahill GM, Curtis AM, Adamik J, Palsson-McDermott EM, McGettrick aF, Goel G, et al. Succinate is an inflammatory signal that induces IL-1β through HIF-1α. Nature. 2013 Apr; 496(7444):238–242. Available from: http://www.nature.com/doifinder/10.1038/nature11986 doi: 10.1038/nature11986 PMID: 23535595

27. Reda AA, Schnelle-Kreis J, Orasche J, Abbaszade G, Lintelmann J, Arteaga-Salas JM, et al. Gas phase carbonyl compounds in ship emissions: Differences between diesel fuel and heavy fuel oil operation. Atmospheric Environment. 2014; 94:467–478. Available from: http://dx.doi.org/10.1016/j.atmosenv.2015.03.057 doi: 10.1016/j.atmosenv.2014.05.053

28. Radischat C, Sippula O, Stengel B, Klingbeil S, Sklorz M, Rabe R, et al. Real-time analysis of organic compounds in ship engine aerosol emissions using resonance-enhanced multiphoton ionisation and proton transfer mass spectrometry. Analytical and bioanalytical chemistry. 2015;p. 1–13.

29. Eschner MS, Zimmermann R. Determination of photoionization cross-sections of different organic molecules using gas chromatography coupled to single-photon ionization (SPI) time-of-flight mass spectrometry (TOF-MS) with an electron-beam-pumped rare gas excimer light source (EBEL): influence of molecular structure and analytical implications. Applied spectroscopy. 2011; 65(7):806–816. PMID: 21740643

30. Mülhopt S, Dilger M, Diabaté S, Schlager C, Krebs T, Zimmermann R, Buters J, Oeder S, Wäscher T, Weiss Carsten, et al. Toxicity testing of combustion aerosols at the air–liquid interface with a self-contained and easy-to-use exposure system. Journal of Aerosol Science. 2016; 96:38–55. doi: 10.1016/j.jaerosci.2016.02.005

31. Sapcariu SC, Kanashova T, Weindl D, Ghelfi J, Dittmar G, Hiller K. Simultaneous extraction of proteins and metabolites from cells in culture. MethodsX. 2014 Jul; 1(1):74–80. Available from: http://dx.doi.org/10.1016/j.mex.2014.07.002 doi: 10.1016/j.mex.2014.07.002 PMID: 26150938

32. Wegner A, Sapcariu SC, Weindl D, Hiller K. Isotope Cluster-Based Compound Matching in Gas Chromatography/Mass Spectrometry for Non-Targeted Metabolomics. Analytical Chemistry. 2013 Apr; 85 (8):4030–4037. Available from: http://pubs.acs.org/doi/abs/10.1021/ac303774z doi: 10.1021/ac303774z PMID: 23514283

33. Hiller K, Hangebrauk J, Jäger C, Spura J, Schreiber K, Schomburg D. MetaboliteDetector: Comprehensive Analysis Tool for Targeted and Nontargeted GC/MS Based Metabolome Analysis. Analytical Chemistry. 2009 May; 81(9):3429–3439. Available from: http://pubs.acs.org/doi/abs/10.1021/ac802689c doi: 10.1021/ac802689c PMID: 19358599

34. Wegner A, Weindl D, Jäger C, Sapcariu SC, Dong X, Stephanopoulos G, et al. Fragment Formula Calculator (FFC): Determination of Chemical Formulas for Fragment Ions in Mass Spectrometric Data. Analytical Chemistry. 2014 Feb; 86(4):2221–2228. Available from: http://pubs.acs.org/doi/abs/10.1021/ac403879d doi: 10.1021/ac403879d PMID: 24498896

35. Ong Se, Mann M. A practical recipe for stable isotope labeling by amino acids in cell culture (SILAC). Nature protocols. 2006; 1(6):2650–60. Available from: http://www.ncbi.nlm.nih.gov/pubmed/17406521 doi: 10.1038/nprot.2006.427 PMID: 17406521

36. Kanashova T, Popp O, Orasche J, Karg E, Harndorf H, Stengel B, et al. Differential proteomic analysis of mouse macrophages exposed to adsorbate-loaded heavy fuel oil derived combustion particles using an automated sample-preparation workflow. Analytical and Bioanalytical Chemistry. 2015; 407 (20):5965–5976. Available from: http://link.springer.com/10.1007/s00216-015-8595-4 doi: 10.1007/s00216-015-8595-4 PMID: 25772565

37. Huang DW, Lempicki RA, Sherman BT. Systematic and integrative analysis of large gene lists using DAVID bioinformatics resources. Nature Protocols. 2009; 4(1):44–57. doi: 10.1038/nprot.2008.211

38. Streibel T, Mühlberger F, Geißler R, Saraji-Bozorgzad M, Adam T, Zimmermann R. Influence of sulphur addition on emissions of polycyclic aromatic hydrocarbons during biomass combustion. Proceedings of the Combustion Institute. 2015; 35(2):1771–1777. doi: 10.1016/j.proci.2014.07.046

39. Andersson JT, Achten C. Time to Say Goodbye to the 16 EPA PAHs? Toward an Up-to-Date Use of PACs for Environmental Purposes. Polycyclic Aromatic Compounds. 2015; 35(2-4):330–354. doi: 10.1080/10406638.2014.991042 PMID: 26823645

40. Vondráček J, Švihálková-Šindlerová L, Pěnčíková K, Marvanová S, Krčmář P, Ciganek M, et al. Concentrations of methylated naphthalenes, anthracenes, and phenanthrenes occurring in Czech river sediments and their effects on toxic events associated with carcinogenesis in rat liver cell lines. Environmental Toxicology and Chemistry. 2007; 26(11):2308–2316. doi: 10.1897/07-161R.1 PMID: 17941746

41. Kang HJ, Lee SY, Roh JY, Yim UH, Shim WJ, Kwon JH. Prediction of Ecotoxicity of Heavy Crude Oil: Contribution of Measured Components. Environmental science & technology. 2014; 48(5):2962–2970. doi: 10.1021/es404342k

42. Kim Jw, Tchernyshyov I, Semenza GL, Dang CV. HIF-1-mediated expression of pyruvate dehydrogenase kinase: A metabolic switch required for cellular adaptation to hypoxia. Cell Metabolism. 2006 Mar; 3(3):177–185. Available from: http://linkinghub.elsevier.com/retrieve/pii/S1550413106000623 doi: 10.1016/j.cmet.2006.02.002 PMID: 16517405

43. Warburg O. Injuring of Respiration the Origin of Cancer Cells. Science. 1956; 123(3191):309–14. Available from: http://www.ncbi.nlm.nih.gov/pubmed/13298683 doi: 10.1126/science.123.3191.309 PMID: 13298683

44. Palsson-McDermott EM, Curtis AM, Goel G, Lauterbach MA, Sheedy FJ, Gleeson LE, et al. Pyruvate kinase M2 regulates Hif-1α activity and IL-1β induction and is a critical determinant of the warburg effect in LPS-activated macrophages. Cell Metabolism. 2015; 21(1):65–80. doi: 10.1016/j.cmet.2014.12.005 PMID: 25565206

45. Michelucci A, Cordes T, Ghelfi J, Pailot A, Reiling N, Goldmann O, et al. Immune-responsive gene 1 protein links metabolism to immunity by catalyzing itaconic acid production. Proceedings of the National Academy of Sciences. 2013 May; 110(19):7820–7825. Available from: http://www.pnas.org/cgi/doi/10.1073/pnas.1218599110 doi: 10.1073/pnas.1218599110

46. Bitterman PB, Saltzman LE, Adelberg S, Ferrans VJ, Crystal RG. Alveolar macrophage replication. One mechanism for the expansion of the mononuclear phagocyte population in the chronically inflamed

lung. Journal of Clinical Investigation. 1984 Aug; 74(2):460–469. Available from: http://www.jci.org/articles/view/111443 doi: 10.1172/JCI111443 PMID: 6746904

47. Mosser DM, Edwards JP. Exploring the full spectrum of macrophage activation. Nature Reviews Immunology. 2008 Dec; 8(12):958–969. Available from: http://www.nature.com/doifinder/10.1038/nri2448 doi: 10.1038/nri2448 PMID: 19029990

48. Sun H, Gong S, Carmody RJ, Hilliard A, Li L, Sun J, et al. TIPE2, a negative regulator of innate and adaptive immunity that maintains immune homeostasis. Cell. 2008; 133(3):415–426. doi: 10.1016/j.cell.2008.03.026 PMID: 18455983

49. Kang SW, Chae HZ, Seo MS, Kim K, Baines IC, Rhee SG. Mammalian peroxiredoxin isoforms can reduce hydrogen peroxide generated in response to growth factors and tumor necrosis factor-α. Journal of Biological Chemistry. 1998; 273(11):6297–6302. PMID: 9497357

50. Henning LN, Azad AK, Parsa KVL, Crowther JE, Tridandapani S, Schlesinger LS. Pulmonary surfactant protein A regulates TLR expression and activity in human macrophages. The Journal of Immunology. 2008; 180(12):7847–7858. doi: 10.4049/jimmunol.180.12.7847 PMID: 18523248

51. Borrell FJ, Straw J. Directive 2005/33/EC of the Europen Parliament and the council OJEU, 2015

PRO-INFLAMMATORY MACROPHAGES SUSTAIN PYRUVATE OXIDATION THROUGH PYRUVATE DEHYDROGENASE FOR THE SYNTHESIS OF ITACONATE AND TO ENABLE CYTOKINE EXPRESSION

Meiser J, Kraemer L, Sapcariu SC, Battello N, Ghelfi J, D'Herouel Aymeric F, Skupin A, Hiller K. *Journal of Biological Chemistry*. **2015**, 291(8), 3932-3946.
doi:10.1074/jbc.M115.676817

This study shows that pyruvate oxidation into the TCA cycle in pro-inflammatory macrophages, previously thought to be blocked in a HIF-1α and PDK dependent manner, actually occurs for the purpose of producing itaconic acid. For this article, I aided in the design and execution of experiments which resulted in various metabolomics and qPCR results used throughout the initial study and revisions requested by the reviewers (including figures 2, 3, and 6). In addition, I analyzed most of the qPCR and metabolomics data that I created, and created preliminary figures which were then finalized by J. Meiser. During the writing and submission process, I helped revise the manuscript for scientific clarity and correct English, as well as aiding in the writing of other documents required for submitting the paper (including the cover letter and response to reviewer comments).

⌘ *Author's Choice*

THE JOURNAL OF BIOLOGICAL CHEMISTRY VOL. 291, NO. 8, pp. 3932–3946, February 19, 2016

Pro-inflammatory Macrophages Sustain Pyruvate Oxidation through Pyruvate Dehydrogenase for the Synthesis of Itaconate and to Enable Cytokine Expression*

Received for publication, July 22, 2015, and in revised form, December 11, 2015 Published, JBC Papers in Press, December 17, 2015, DOI 10.1074/jbc.M115.676817

Johannes Meiser, Lisa Krämer, Sean C. Sapcariu[1], Nadia Battello, Jenny Ghelfi, Aymeric Fouquier D'Herouel, Alexander Skupin, and Karsten Hiller[2]

From the Luxembourg Centre for Systems Biomedicine, University of Luxembourg, 6 Avenue de Swing, L-4367 Belvaux, Luxembourg

Upon stimulation with Th1 cytokines or bacterial lipopolysaccharides, resting macrophages shift their phenotype toward a pro-inflammatory state as part of the innate immune response. LPS-activated macrophages undergo profound metabolic changes to adapt to these new physiological requirements. One key step to mediate this metabolic adaptation is the stabilization of HIF1α, which leads to increased glycolysis and lactate release, as well as decreased oxygen consumption. HIF1 abundance can result in the induction of the gene encoding pyruvate dehydrogenase kinase 1 (PDK1), which inhibits pyruvate dehydrogenase (PDH) via phosphorylation. Therefore, it has been speculated that pyruvate oxidation through PDH is decreased in pro-inflammatory macrophages. However, to answer this open question, an in-depth analysis of this metabolic branching point was so far lacking. In this work, we applied stable isotope-assisted metabolomics techniques and demonstrate that pyruvate oxidation is maintained in mature pro-inflammatory macrophages. Glucose-derived pyruvate is oxidized via PDH to generate citrate in the mitochondria. Citrate is used for the synthesis of the antimicrobial metabolite itaconate and for lipogenesis. An increased demand for these metabolites decreases citrate oxidation through the tricarboxylic acid cycle, whereas increased glutamine uptake serves to replenish the TCA cycle. Furthermore, we found that the PDH flux is maintained by unchanged PDK1 abundance, despite the presence of HIF1. By pharmacological intervention, we demonstrate that the PDH flux is an important node for M(LPS) macrophage activation. Therefore, PDH represents a metabolic intervention point that might become a research target for translational medicine to treat chronic inflammatory diseases.

Macrophages are innate immune cells that differentiate from monocytes, which circulate in the bloodstream. Upon differentiation, they invade the surrounding tissue and become resident macrophages (1). Macrophages can be activated by cytokines or toll-like receptor agonists, *e.g.* lipopolysaccharide (LPS). In very general terms, macrophage activation can result in rather pro-inflammatory responses, serving as host defense mechanisms or in wound healing responses and aiding in tissue repair and remodeling. However, depending on the type of activation, very different subtypes of activation occur (2). Upon activation with LPS (M(LPS)) or the cytokine interferon-γ (M(INFγ)), macrophages undergo profound metabolic reprogramming, necessary to activate cellular defense mechanisms as well as to cope with different micro-environments in the inflamed tissue (3). A marker for pro-inflammatory activation is high expression of *Irg1* (4, 5). We recently showed that *Irg1* codes for the enzyme *cis*-aconitate decarboxylase (IRG1/CAD) that catalyzes the synthesis of the antimicrobial metabolite itaconate from *cis*-aconitate (6). Therefore, metabolic reprogramming due to these adaptations could affect the availability of substrate needed for the synthesis of itaconate during host defense.

The reprogramming during macrophage activation shows overlapping features with cancer cells; both have increased glycolytic rates and increased lactate release, known as aerobic glycolysis or the Warburg effect (7, 8). Increased glycolytic rates are observed in any cell type that exceeds the energy demand derived from oxidative phosphorylation (9). In macrophages, it has been revealed that this metabolic rewiring is mediated by stabilization of HIF1α (10). A well described HIF1 target is the gene encoding pyruvate dehydrogenase kinase 1 (PDK1), an inhibitor of Pyruvate dehydrogenase (PDH)[3] (11). When HIF1 is stabilized, the PDH flux can be inhibited by PDK1-mediated phosphorylation, resulting in decreased pyruvate-derived acetyl-CoA levels. In this case, reductive carboxylation of α-ketoglutarate (αKG) increases to provide sufficient acetyl-CoA for lipogenesis, needed for cell proliferation (12–15). Increased glycolytic rates, decreased PDH flux, and increased reductive carboxylation can also be induced in any cell type when oxygen tension is decreased or when oxidative phosphorylation is impaired. In this case, NADH oxidation is compromised, and citrate levels decrease. This decrease in citrate is linked to an increase in NADH, which thermodynamically promotes the metabolic adaptation to hypoxia by increasing reductive carboxylation of αKG (13, 16, 17). However, it is currently unclear

* This work was supported in part by the Fonds National de la Recherche Luxembourg Grant ATTRACT A10/03 (to K. H.) and AFR-Postdoc-3973022 (to J. M.). The authors declare that they have no conflicts of interest with the contents of this article.

[1] Recipient of financial support from the Helmholtz Virtual Institute of Complex Molecular Systems in Environmental Health.

[2] To whom correspondence should be addressed: Metabolomics Group, University of Luxembourg, Luxembourg Centre for Systems Biomedicine, 6 Avenue de Swing, L-4367 Belvaux, Luxembourg. Tel.: 352-46-66-44-6136; E-mail: karsten.hiller@uni.lu.

[3] The abbreviations used are: PDH, pyruvate dehydrogenase; αKG, α-ketoglutarate; MIDS, mass isotopomer distribution.

whether this full panel of metabolic consequences upon HIF1 stabilization is also true for pro-inflammatory macrophages. Although it has been demonstrated that HIF1α can be stabilized and activated by cytokines, *e.g.* TNFα and IL1β (18, 19), the detailed metabolic consequences are still uncertain.

HIF1 can bind to the promoter of the *Tlr4* gene, thereby acting through a positive feedback loop on the TLR4 defense axis (20). Reactive oxygen species were shown to inhibit proteasomal degradation of HIF1α (21), and recently, increased succinate levels in pro-inflammatory macrophages have also been described to stabilize HIF1α, by inhibiting prolyl hydroxylase-mediated hydroxylation of HIF1α (10).

In this study, we asked whether the stabilization of HIF1α in M(LPS) macrophages alters TCA cycle fluxes similarly to hypoxic cells. We show that LPS-activated macrophages exhibit a metabolic adaptation with overlapping features to hypoxic cells, but also distinct differences, resulting in a unique LPS-specific metabolic signature. The most striking difference to hypoxic cells with stabilized HIF1α is that there is no decrease in relative glucose flux through PDH and no increase in reductive carboxylation of αKG. The sustained PDH flux provides sufficient acetyl-CoA for citrate production, which keeps the rate of reductive carboxylation of αKG at a low level, as well as providing citrate that is needed for the synthesis of fatty acids and itaconate. Upon LPS stimulation, high PDH activity is maintained by a repression of *Pdk1*. As a result PDH phosphorylation on Ser-232 and Ser-293 remains at a low level. Finally, we demonstrate that the PDH flux is indeed important to sustain M(LPS) activation in macrophages.

Experimental Procedures

Chemicals—UK5099 (Sigma, PZ0160) was first diluted in DMSO and further diluted in medium to a working stock concentration of 10 mM and then added to the wells of the culture dish to a final concentration of 100 μM. The final concentration of DMSO did not exceed 1%; LPS (*Escherichia coli,* Sigma L6529) was prepared as a working stock of 1 μg/ml in glucose- and glutamine-free DMEM and added 1:100 into the wells of the culture dish for a final concentration of 10 ng/ml. Cells were stimulated for 6 h; interferon γ (mouse) (*E. coli*, Sigma I4777) was prepared as a working stock of 5 mg/ml in glucose- and glutamine-free DMEM and added 1:100 into the wells of the culture dish for a final concentration of 50 ng/ml. Cells were stimulated for 6 h.

Stable Isotope Tracing—^{13}C stable isotope tracers were obtained from Eurisotop as follows: glucose, CLM-1396; glutamine, CLM-1822-H. The tracer medium was prepared in DMEM without glucose and glutamine. [^{13}C]Glucose (final 25 mM) and [^{12}C]glutamine (final 4 mM) (or vice versa) was added to the medium; pH was set to 7.3; 10% FBS and 1% penicillin/streptomycin were added, and finally, the medium was sterile-filtered. Tracer medium was prepared in advance and incubated in the hypoxia chamber overnight to remove excessive oxygen from the medium (only for hypoxia conditions). The next morning, medium was replaced by tracer medium, and cells were incubated for 24 h with the tracer medium to reach isotopic steady state. LPS was added after 24 h and left on the cells for an additional 6 h prior to extraction. For further information regarding stable isotope-assisted metabolomics, see also Refs. 22, 23.

TABLE 1
Primer sequences used for quantitative PCR

Gene	5′ to 3′ sequence
*L27*_F	ACATTGACGATGGCACCTC
*L27*_R	GCTTGGCGATCTTCTTCTTG
*Irg1*_F	GCAACATGATGCTCAAGTCTG
*Irg1*_R	TGCTCCTCCGAATGATACCA
*Tnfa*_F	GGTTCTGTCCCTTTCACTCAC
*Tnfa*_R	TGCCTCTTCTGCCAGTTCC
*iNos*_F	AGCCCTCACCTACTTCCTG
*iNos*_R	CAATCTCTGCCTATCCGTCTC
*Pdk1*_F	TGCAAAGTTGGTATATCCAAAGCC
*Pdk1*_R	ACCCCGAAGCTCTCCTTGTA
*Il1b*_F	TGCCACCTTTTGACAGTGATG
*Il1b*_R	TGATGTGCTGCTGCGAGATT
*Cpt1*_F	TGGCAGTCGACTCACCTTTC
*Cpt1*_R	CAAACAGTTCCACCTGCTGC
*Hif1a*_F	TGACGGCGACATGGTTTACA
*Hif1a*_R	AATATGGCCCGTGCAGTGAA

Cell Culture—RAW 264.7 cells (ATCC® TIB-71™) were obtained from ATCC and were cultivated according to the manufacturer's instructions. Briefly, cells were kept in DMEM5796 with 10% FBS and 1% penicillin/streptomycin at 37 °C and 5% CO_2 under atmospheric oxygen concentrations. In the case of hypoxia, cells were cultivated in an incubator at 37 °C and 5% CO_2 located in a closed hypoxia chamber with an oxygen concentration of 2%. Cells were simultaneously seeded in the afternoon at a density of 150,000 cells per well in 12-well plates (Thermo Scientific, Nunc Multidish 12 Nunclon Delta Si) and then either incubated either at 21 or 2% O_2 overnight. The next day, medium was replaced. In the case of hypoxia, medium was already incubated in the hypoxia chamber overnight to remove excessive oxygen from the medium. For comparison reasons, medium for normoxic conditions was also prepared the day before and incubated in a similar way under atmospheric oxygen conditions. For LPS activation, LPS was added 18 h after medium replacement. 24 h after medium replacement cells were harvested.

Viability Assay—To assess cell viability, cells were transferred into tubes and analyzed using a Vi-Cell™ XR (Beckman Coulter) automated cell counter. To determine viability, cells were incubated with trypan blue and number of stained cells was determined.

cDNA Synthesis and Gene Expression Analysis—cDNA synthesis and quantitative PCR was performed as described previously (6). Briefly, RNA was isolated from the interphase after extraction of metabolites, using the Qiagen RNeasy mini kit. 0.5–1 μg of RNA was used for cDNA synthesis using SuperScript III (Invitrogen), following the manufacturer's instructions. Quantitative PCR was performed using iQ SYBR Green Supermix (Bio-Rad) as per the manufacturer's instructions. PCR was carried out on a Light Cycler 480 (Roche Applied Science). Data analysis was performed using the analysis software according to manufacturer's instructions (Roche Applied Science). Gene expression was normalized to the housekeeping gene *L27*. For primer sequences, see Table 1.

Extraction of Intracellular Metabolites—Extraction was according to Ref. 24. Briefly, cells were cultivated in 12-well plates and washed with 1 ml of 0.9% NaCl and quenched with

0.2 ml of −20 °C methanol. After adding an equal volume of 4 °C cold water, cells were collected with a cell scraper and transferred to tubes containing 0.2 ml −20 °C chloroform. The extracts were shaken at 1400 rpm for 20 min at 4 °C (Thermomixer Eppendorf) and centrifuged at 16,000 × *g* for 5 min at 4 °C. 0.2 ml of the upper aqueous phase was collected in specific glass vials with micro inserts and evaporated under vacuum at −4 °C using a refrigerated CentriVap Concentrator (Labconco).

Gas Chromatography-Mass Spectrometry—Metabolite derivatization was performed using a Gerstel MPS. Dried polar metabolites were dissolved in 15 μl of 2% methoxyamine hydrochloride in pyridine at 40 °C under shaking. After 60 min, an equal volume of MTBSTFA was added and held for 60 min at 40 °C. 1 μl of sample was injected into an SSL injector at 270 °C in splitless mode. GC/MS analysis was performed using an Agilent 7890A GC equipped with a 30-m DB-35MS + 5-m Duraguard capillary column. Helium was used as carrier gas at a flow rate of 1.0 ml/min. The GC oven temperature was held at 100 °C for 2 min and increased to 300 °C at 10 °C/min. After 3 min, the temperature was increased to 325 °C. The GC was connected to an Agilent 5975C inert XL MSD, operating under electron ionization at 70 eV. The MS source was held at 230 °C and the quadrupole at 150 °C. The MS was operated in selected ion monitoring. The total run time of one sample was 25.00 min. All GC/MS chromatograms were processed by using Metabolite Detector software (25). MIDs were determined and corrected for natural isotope abundance using Metabolite Detector software.

Measurement of glucose and lactate intensities was performed by derivatization with an equal volume of MSTFA (instead of MTBSTFA) and held for 30 min at 40 °C under continuous shaking. A 1-μl sample was injected into an SSL injector at 270 °C in split 10 mode. GC oven temperature was held at 90 °C for 1 min and increased to 300 °C at 15 °C/min for 8 min to 320 °C. The total run time of one sample was 24.3 min. For absolute quantification of glucose and lactate, a dilution series of a standard mix was included in the sequence and measured in triplicate. For normalization, we used [U-^{13}C]glucose and [U-^{13}C]lactate as internal standards (in this case, medium samples contained only [^{12}C]carbon sources).

Quantification of Amino Acids—Quantification of amino acids was performed on an Agilent 1100 HPLC system equipped with a Diode Array Detector. Separation was carried out on a ZORBAX amino acid analysis column (150 × 4.6 mm, 5 μm) with a preceding ZORBAX amino acid analysis guard cartridge (Agilent Technologies, Santa Clara, CA) at 40 °C in gradient mode (see Table 1). The eluents used were 40 mM Na_2HPO_4 (pH 7.8, eluent A) and a mixture of acetonitrile, methanol, and water (45:45:10, eluent B). 0.02% sodium azide was added to eluent A to prevent microbial growth. Primary amines were automatically derivatized with *ortho*-phthalaldehyde in borate buffer (0.4 N in water, pH 10.2) and diluted in eluent A prior to injection. The resulting *ortho*-phthalaldehyde derivatives were subsequently detected at 338 nm (10-nm bandwidth; reference wavelength, 390 nm; 20-nm bandwidth). All medium samples were diluted 1:1 with the internal standard L-2-aminobutyric acid (final concentration, 300 μM) to correct for deviations resulting from the derivatization process. External calibration standards as well as reference media with known concentrations were measured with every run to determine sample concentrations and ensure stability of the analysis. Gradient profile: 1.9 min, 0% eluent B; 18.1 min, 57% eluent B; 18.6 min, 100% eluent B; 22.3 min, 100% eluent B; 23.2 min,0% eluent B; 26 min, 0% eluent B.

Western Blot—For preparation of whole cell extract, 1 × 10^6 cells were harvested, washed with ice-cold 1× phosphate-buffered saline (PBS) (Invitrogen/Life Technologies, Inc., Europe BV Belgium), lysed in 1× M-PER®, mammalian protein extraction Reagent (Thermo Scientific, Belgium) completed with 1× protease inhibitor mixture (Complete®, Roche Applied Science, Luxembourg), and further processed according to the manufacturer's instructions. A nanodrop analyzer was used to measure the protein concentration. Proteins were separated by size using SDS-PAGE (12%) and transferred to an Immobilon-FL PVDF membrane (Merck Millipore) using the Mini-PROTEAN Tetra Cell and PowerPac Basic Power Supply (Bio-Rad, Belgium). The membrane was blocked in 5% nonfat milk powder in PBS/Tween for 1 h at room temperature or overnight at 4 °C. The antibodies used were as follows: anti-IRG1 (Sigma, hpa040143) 1:750 in PBS-T 5% nonfat milk powder for 1 h at room temperature; anti-PDK1 (rabbit) (Enzo catalog no. ADI-KAP-PK112) 1:3000 in TBST 5% BSA, overnight at 4 °C; anti-PDH-E1α (rabbit) (Ser(P)-232) (Millipore catalog no. AP1063) 1:1000 in TBST 5% BSA, overnight at 4 °C; anti-PDH-E1α (rabbit) (Ser(P)-300) (Millipore catalog no. ABS194) 1:1000 in TBST 5% BSA, overnight at 4 °C; anti-PDH-E1α (rabbit) (Ser(P)-293) (Millipore catalog no. ABS204) 1:10,000 in TBST 5% BSA, overnight at 4 °C; anti-α-tubulin (mouse) 1:5000 in TBST 5% BSA, overnight at 4 °C; anti-rabbit HRP 1:5000 in TBST 5% skim milk (Cell Signaling); anti-mouse HRP 1:5000 in TBST 5% skim milk (Cell Signaling). Visualization was done using the ECL Plus Western blotting detection system Kit (GE Healthcare, Netherlands). Signals were detected using the LI-COR system. Quantification of band intensities was done using the ImageStudioLight Software package.

Cell Imaging and Data Analysis—Phase contrast images were acquired using a ×10 objective on a Nikon Ti Eclipse inverted microscope with motorized stage (Nikon Corp., Tokyo, Japan) enclosed in a bench top incubator. Automatic microscope control, stage programming, and acquisition were done using the OptoMorph version of MetaMorph 7.8.10 (Cairn Research, Kent, UK). LPS-treated and untreated RAW 264.7 cells growing in 12-well Nunc plates (50,000 cells per well) were imaged in positive phase contrast. Nine adjacent but non-overlapping images were automatically acquired in a 3 × 3 grid around the center of each well. The entire imaging experiment was performed twice, resulting in 36 images acquired per condition. One out-of-focus image and five containing cell aggregates were excluded from further analysis. Surfaces of strongly attached cells were estimated by thresholding in ImageJ 2.0.0-rc-31/1.49v using the IJ_IsoData algorithm. Congruence of thresholding results with cell contours was verified by visual inspection. Cell sizes were calculated using the particle analysis tool, allowing for areas from 50 to 5000 pixels and excluding particles on the image edges. Average sizes were reported for

each image. Halo and contrast effects resulting from the phase-contrast imaging were analyzed to discriminate between strongly and weakly attached cells. Strongly attached cells appeared darker than background with a weak halo, although weakly attached cells appeared brighter than background with a strong halo. Histograms of pixel intensities of the entire field of view were analyzed using custom software written in MATLAB R2014b. First, the intensity peak corresponding to the background signal (cell-free surface) was identified and approximated by a Gaussian function. The approximated peak was subtracted from the original histogram, and the weighted sum of intensities below (dark) and above (bright) the background peak was calculated, respectively. The ratio of dark-to-bright values informs on the ratio of strongly-to-weakly attached cells. Renormalization of this ratio by values obtained for individual strongly and weakly attached cells yielded an adhesion index with values from 0 (no cells attached) to 1 (all cells attached).

Statistical Analyses—To analyze a significant difference between two groups, unpaired Welch's *t* test was applied. *p* values are indicated in each panel (*, $p < 0.01$; or as indicated) and was considered as significantly different with a *p* value <0.05. The number of independent replicates is indicated in the figure legends. Each experiment was at least performed three times with cells of a different passage. Each individual experiment consisted of three wells per condition.

Results

M(LPS) Macrophages Show a Distinct Metabolite Signature—The macrophage environment is likely to be hypoxic, as these cells infiltrate hypoxic tissues such as tumors, wounded regions, or sites of inflammation. At the site of inflammation, different oxygen tensions result from increased oxygen demand as well as swelling or vascular damage (26, 27). To physiologically meet these challenging conditions, macrophages are well adapted to hypoxia by their ability to adjust their gene expression profile and increase glycolytic activity (28). To study whether the activation of macrophages reprograms metabolism to a hypoxia-like phenotype, we cultivated the murine macrophage cell line RAW 264.7 under normoxia (21% oxygen) and hypoxia (2%) and activated it with LPS for 6 h. We selected this time point, because it reflects the highest expression level of *irg1/Cad*, the enzyme that catalyzes the synthesis of the antimicrobial metabolite itaconate (6).

We analyzed intracellular metabolite levels and revealed that LPS stimulation resulted in increased levels of itaconate, succinate, and lactate under normoxia (Fig. 1, *A–C*). These three metabolites are marker metabolites for M(LPS) activation, demonstrating a clear pro-inflammatory activation (6, 10, 29, 30). Moreover, we observed increased levels of the TCA cycle associated metabolites malate and glutamate, whereas aspartate and citrate levels remained unchanged (Fig. 1, *D–G*). The amino acids glycine, serine, and alanine were also elevated upon LPS stimulation (Fig. 1, *H–J*). Compared with normoxia, LPS treatment of hypoxic cells was unable to induce similar itaconate and succinate levels (Fig. 1, *A* and *B*). As expected, lactate levels further increased upon hypoxia as a result of reduced respiration and concomitant increased glycolysis, known as the Pasteur Effect. Non-activated hypoxic cells exhibited decreased levels of the TCA cycle associated metabolites malate, aspartate, glutamate, and citrate. However, LPS stimulation under hypoxia resulted in increased levels of malate, aspartate, and glutamate but not citrate (Fig. 1, *D–G*). The amino acids glycine and serine were unchanged between hypoxia and normoxia. Upon LPS activation of hypoxic cells, serine and alanine were increased (Fig. 1, *H–J*). Interestingly, we also observed a trend of increased levels of the branched chain amino acids isoleucine, leucine, and valine under hypoxia for both non-stimulated and LPS stimulated conditions (Fig. 1*K*; *p* value >0.05).

We concluded from these results that LPS affects the metabolite profile of macrophages independent of the oxygen supply and that this profile is clearly different from a pure hypoxic profile. Intriguingly, we observed decreased abundance of the antimicrobial metabolite itaconate under oxygen-limiting conditions, which could have direct effects on the immune response in tissues with low oxygen tension.

Decreased Itaconate Levels under Hypoxia Are Not the Result of Decreased Irg1 Expression or Lower IRG1/CAD Protein Abundance—To investigate whether the reduced levels of itaconate are caused by transcriptional repression, post-transcriptional regulation, or post-translational regulation, we analyzed gene expression and protein levels of the catalyzing enzyme IRG1/CAD. We found that hypoxia does not significantly reduce the gene expression level or the protein abundance of IRG1/CAD, indicating a regulation at the post-translational level or a result of decreased substrate concentrations (Fig. 2, *A* and *B*). To confirm LPS activation of macrophages, we analyzed gene expression of the pro-inflammatory marker genes *Tnfα, iNos,* and *Il1β* (Fig. 2, *C–E*). We found clear up-regulation under both oxygen conditions when the cells were treated with LPS. However, hypoxia resulted in a 20% reduction of *Tnfα* expression and ~3-fold higher expression of *Il1β* and *iNos*.

It has been reported in several recent publications that HIF1α gets stabilized in M(LPS) macrophages compared with resting macrophages (10, 21, 29, 31). Therefore, we also analyzed gene expression of *Hif1α*, and we observed increased expression of *Hif1α* in response to LPS treatment under hypoxia (Fig. 2*F*), indicating that HIF1α stabilization in hypoxic M(LPS) macrophages can be a combined effect of increased transcriptional expression and post-translational stabilization. Under normoxia, no difference in *Hif1α* expression was detected.

Based on these results, we conclude that the reduction of itaconate under hypoxia is mostly a result of post-translational effects such as altered metabolic fluxes, either due to an enzyme modification that regulates its activity or by changing substrate concentrations. To that end, we were interested to compare cellular flux changes with LPS activation between hypoxia and normoxia.

LPS Activation Promotes Pyruvate Oxidation via PDH by Preventing Pdk1 Expression—To monitor intracellular glucose-derived fluxes in M(LPS) macrophages, we incubated RAW 264 cells for 24 h in the presence of uniformly labeled [U-^{13}C]glucose to reach isotopic steady state conditions. During these 24 h, labeled glucose is metabolized within the cells and is incorporated in cellular metabolites downstream of glucose. To obtain the specific labeling patterns, intracellular metabolites

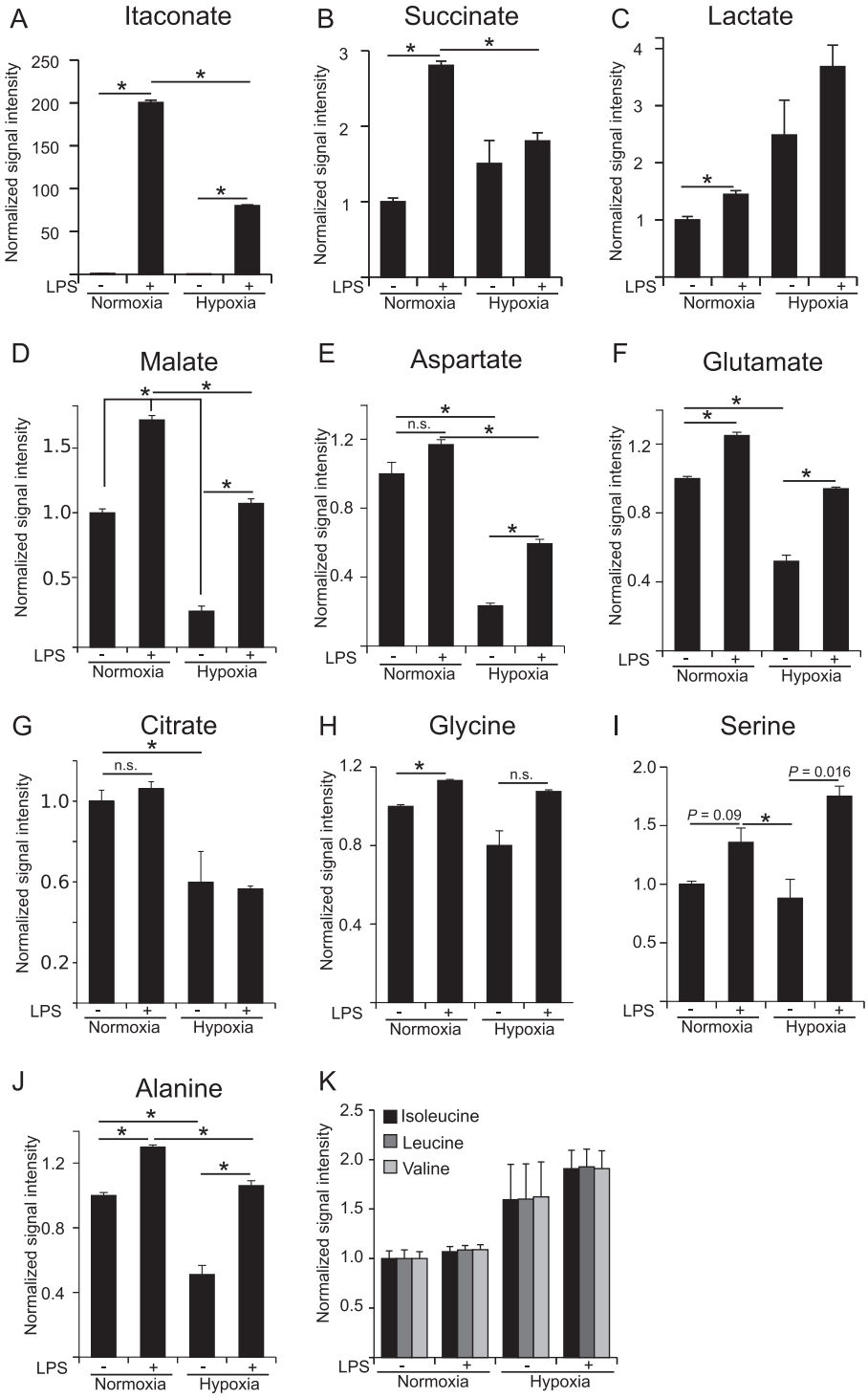

FIGURE 1. **Metabolome analysis of RAW 264 macrophages in the context of LPS activation and hypoxia.** Analysis of intracellular metabolite abundance in RAW 264 cells, cultivated under normoxia (21% O_2) and hypoxia (2% O_2), unstimulated or stimulated with LPS. Metabolites were extracted and analyzed by GC/MS. Signal intensities (peak area) are normalized to unstimulated cells under normoxia. Cells were treated with 10 ng/ml LPS for 6 h. *Error bars* indicate S.E. (Welsh's *t* test; *, $p < 0.01$, $n = 3$ wells). *n.s.*, not statistically significant. One representative experiment with three individual wells per condition is presented. The experiment was performed three times.

were extracted and analyzed with gas chromatography/mass spectrometry to determine MIDs (corrected for natural isotope abundance), which reflect relative metabolic fluxes (Fig. 3*A* for atom transitions) (22, 23).

As expected, stable isotope labeling revealed that hypoxia resulted in decreased pyruvate flux through PDH, illustrated by decreased M2 citrate isotopologues (Fig. 3*B*). Concomitant with decreasing citrate M2 isotopologues under hypoxia, we observed increased abundance of citrate M0 isotopologues, representing citrate molecules derived from carbon sources other than glucose (Fig. 3*B*). This decrease is a result of HIF1α stabilization and *Pdk1* induction, where the PDK1 protein

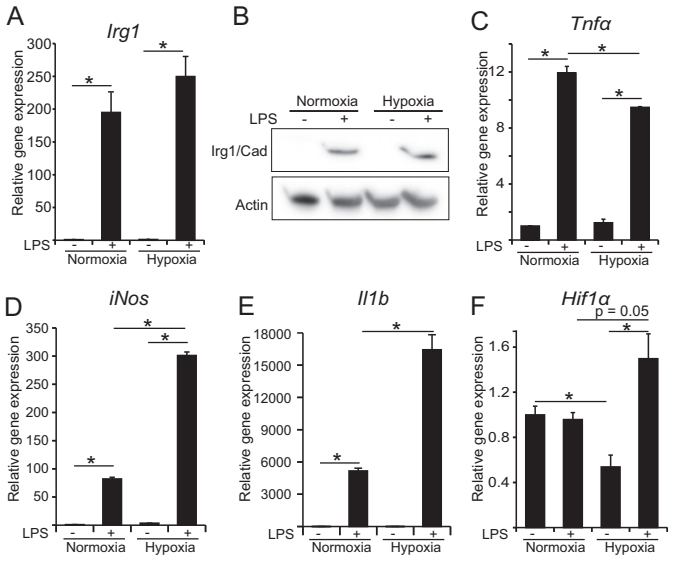

FIGURE 2. **Expression analysis of pro-inflammatory associated genes.** *A,* relative gene expression of *Irg1*. *B,* Western blot against IRG1/CAD, the protein that catalyzes the conversion of *cis*-aconitate to itaconate (no significant difference (data not shown)). *C–F,* relative gene expression of *Tnfα*, *iNos*, *Il1β*, and *Hif1α*, normalized to normoxia control (−*LPS*). *Error bars* indicate S.E. (Welsh's *t* test, *, $p < 0.01$, $n = 3$). Gene expression data represents the mean over three independent experiments.

inhibits PDH by phosphorylation (32, 33). Decreased pyruvate oxidation under hypoxia promotes decreasing downstream substrate levels, most probably resulting in the observed decreased itaconate levels (Fig. 1*A*). However, HIF1α has also been shown to be stabilized in M(LPS) macrophages under normoxic conditions (10, 29). Therefore, it is speculated that pyruvate oxidation through PDH is decreased in M(LPS) macrophages, a similar phenotype to cancer cells with stabilized HIF1α (3, 34). However, we did not observe decreased citrate M2 isotopologues in normoxic M(LPS) macrophages, raising the question whether PDH is inhibited under these conditions.

To analyze regulation of *Pdk1* in more detail, we investigated gene expression and protein abundance of PDK1 and phosphorylation status of PDH (Fig. 3, *C–H*). In line with current knowledge, hypoxia-mediated stabilization of HIF1α resulted in increased *Pdk1* expression (Fig. 3*C*), which complements our observation of hypoxia-dependent, decreased glucose flux to citrate (Fig. 3*B*). Intriguingly, we observed that LPS stimulation resulted in a drastic reduction of *Pdk1* expression at both normoxia and hypoxia, indicating that PDK1-mediated inhibition of PDH is reduced in M(LPS) macrophages (Fig. 3*C*). Moreover, analysis of PDK1 protein abundance revealed similar PDK1 levels in non-activated or M(LPS)-activated macrophages. Only in hypoxia did we observe a significant increase of PDK1 abundance (Fig. 3, *D* and *E*). To investigate whether the low levels of PDK1 have an effect on PDH, we analyzed phosphorylation of PDH on serine 232, 293, and 300 (Fig. 3, *D* and *F–H*). Phosphorylation of these residues has been reported to result in an inhibition of PDH activity (33). As expected, hypoxia resulted in increased phosphorylation of the three analyzed serine residues (not significant in case of Ser-300). However, and in line with low PDK1 levels in normoxic M(LPS) macrophages, LPS activation did not increase phosphorylation levels of Ser-232 and -293. Regarding Ser-300, we observed significantly increased phosphorylation upon LPS activation, although there was no further significantly increased phosphorylation due to hypoxia. Whether Ser-300 specifically has a unique function in the context of LPS activation in macrophages remains to be determined in future work. Our results from this part of the study reveal that HIF1-mediated induction of *Pdk1* can be attenuated by LPS stimulation, which is in line with increased citrate M2 isotopologues upon LPS activation (Fig. 3*B*).

In line with the results of PDK1 abundance and PDH phosphorylation status, our stable isotope analysis revealed that LPS stimulation did not result in a decreased relative pyruvate oxidation, both under hypoxia and normoxia (Fig. 3, *B* and *I*), indicating that HIF1 did not mediate PDH inhibition upon LPS stimulation. We observed increased citrate M2 isotopologue levels, reflecting even higher relative pyruvate flux through PDH (Fig. 3*B*). To normalize for upstream changes in glycolysis, we determined the ratio of M2 citrate/M3 pyruvate and observed an increase upon LPS stimulation, indicating increased pyruvate flux through PDH in M(LPS) macrophages (Fig. 3*I*). As a reduction of citrate M2 isotopologues was only observed under hypoxic conditions, HIF1-mediated inhibition of PDH depended only on the oxygen tension and not on the macrophage activation status. Indeed, LPS activation can even partially recover the HIF1- mediated PDH inhibition under hypoxia (Fig. 3, *B* and *I*).

The M2 abundance of αKG and malate was significantly lower than in citrate (Fig. 3, *J* and *K*), suggesting that large amounts of citrate, *cis*-aconitate, or isocitrate are either used for pathways other than the oxidative TCA cycle or that other carbon sources (*e.g.* glutamine) increase their contribution to αKG and malate. Stimulation with LPS as well as hypoxia further decreased glucose contribution to αKG and malate, as can be seen by a decreasing abundance of αKG and malate M2 isotopologues (Fig. 3, *J* and *K*).

Next, we analyzed glucose uptake from the medium and cellular lactate release, to evaluate whether M(LPS) macrophages increase their glycolytic rate. Under normoxia, LPS-stimulated macrophages increased glucose uptake and lactate release, and under hypoxia, glucose uptake and lactate release were exceeding the rate of M(LPS) macrophages under normoxia (Fig. 3*L*). This effect was further enhanced when hypoxic cells were additionally stimulated with LPS (Fig. 3*L*). Under normoxia, the lactate to glucose ratio was increased from 1.2 to 1.6 upon LPS stimulation, indicating increased activity of lactate dehydrogenase, which is in line with the Warburg-like phenotype of M(LPS) macrophages (3). However, 20% of the overall glucose carbon pool is still available for other metabolic pathways, indicating that M(LPS) macrophages still contain sufficient pyruvate to maintain oxidation through PDH.

It has been shown before that STAT3-specific signaling can inhibit PDH and thus block pyruvate oxidation through PDH in primary fibroblasts and cancer cell lines (35). Therefore, we investigated whether, and in contrast to LPS treatment, a STAT3-dependent activation with the cytokine INFγ might inhibit PDH. To this end, we treated the cells with INFγ or LPS and analyzed the isotope enrichment in citrate. We did not

PDH Flux Is Important for Activation of M(LPS) Macrophages

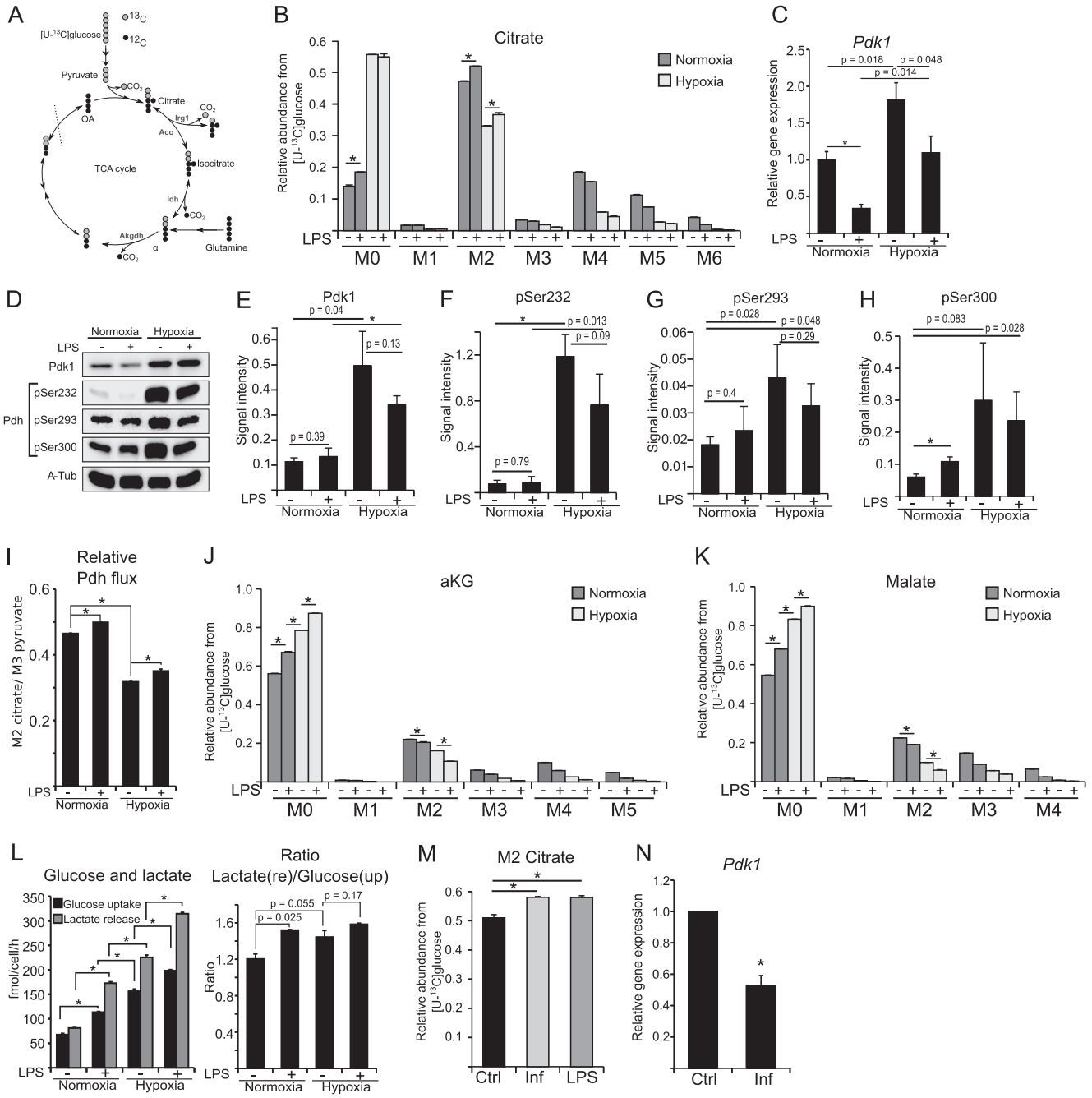

FIGURE 3. **PDH flux analysis in M(LPS) macrophages.** *A,* schematic of atom transitions in central metabolism using [U-^{13}C]glucose as a tracer for determination of MIDs to infer relative intracellular fluxes. ^{13}C-carbons are in *gray* and ^{12}C in *black*. The *dotted line* indicates end of one route. *Aco,* aconitase; *Idh,* isocitrate dehydrogenase; *Akgdh,* αKG dehydrogenase; *OA,* oxaloacetate. *B,* MID of citrate. *M0* to *M6* indicates the different mass isotopologues. *C,* gene expression analysis of *Pdk1*. *D–H,* Western blot analysis of PDK1 and PDH phosphorylation on Ser-232, -293, and -300. α-Tubulin serves as loading control. *D* shows one representative Western blot of three independent experiments. *α-Tub,* α-tubulin. *E–H* shows quantification of three independent experiments. *I,* ratio of M2 citrate/M3 pyruvate indicating relative pyruvate oxidation through PDH. *J* and *K,* MID of αKG and malate. *L,* absolute quantification of glucose uptake and lactate release, and ratio of lactate release/glucose uptake to infer fractional lactate formation per glucose. *M,* activation of RAW 264 cells with 10 ng/ml LPS or 50 ng/ml interferon-γ (*INF*) in medium with [U-^{13}C]glucose. Presented are citrate M2 isotopologues as a readout for relative glucose flux through PDH. *N,* relative gene expression of *Pdk1* normalized to normoxia control (*Ctrl*) (−*LPS*). *Error bars* indicate S.E. (Welsh's *t* test, *, $p < 0.01$, $n = 3$). One representative experiment with three individual wells per condition is presented. Each experiment was performed at least three times, except for *C*. Presented is the mean ± S.E. over three independent experiments. (Welsh's *t* test, *, $p < 0.01$, $n = 3$).

observe a difference between LPS and INFγ treatment (Fig. 3*M*). In both cases, M2 citrate was significantly increased compared with untreated controls. In line with LPS activation, we also observed decreased expression of *Pdk1* in M(INFγ) macrophages (Fig. 3*N*), indicating no inhibition of pyruvate oxidation in M(INFγ) macrophages. In conclusion, sustained pyruvate flux through PDH and its regulation by PDK1 seems to be independent of TLR4 signaling.

LPS Activation Increases Glutamine Uptake but Does Not Induce Reductive Carboxylation of αKG —It has been demonstrated that hypoxic cells metabolize increased amounts of glutamine via reverse IDH activity to generate citrate by reductive

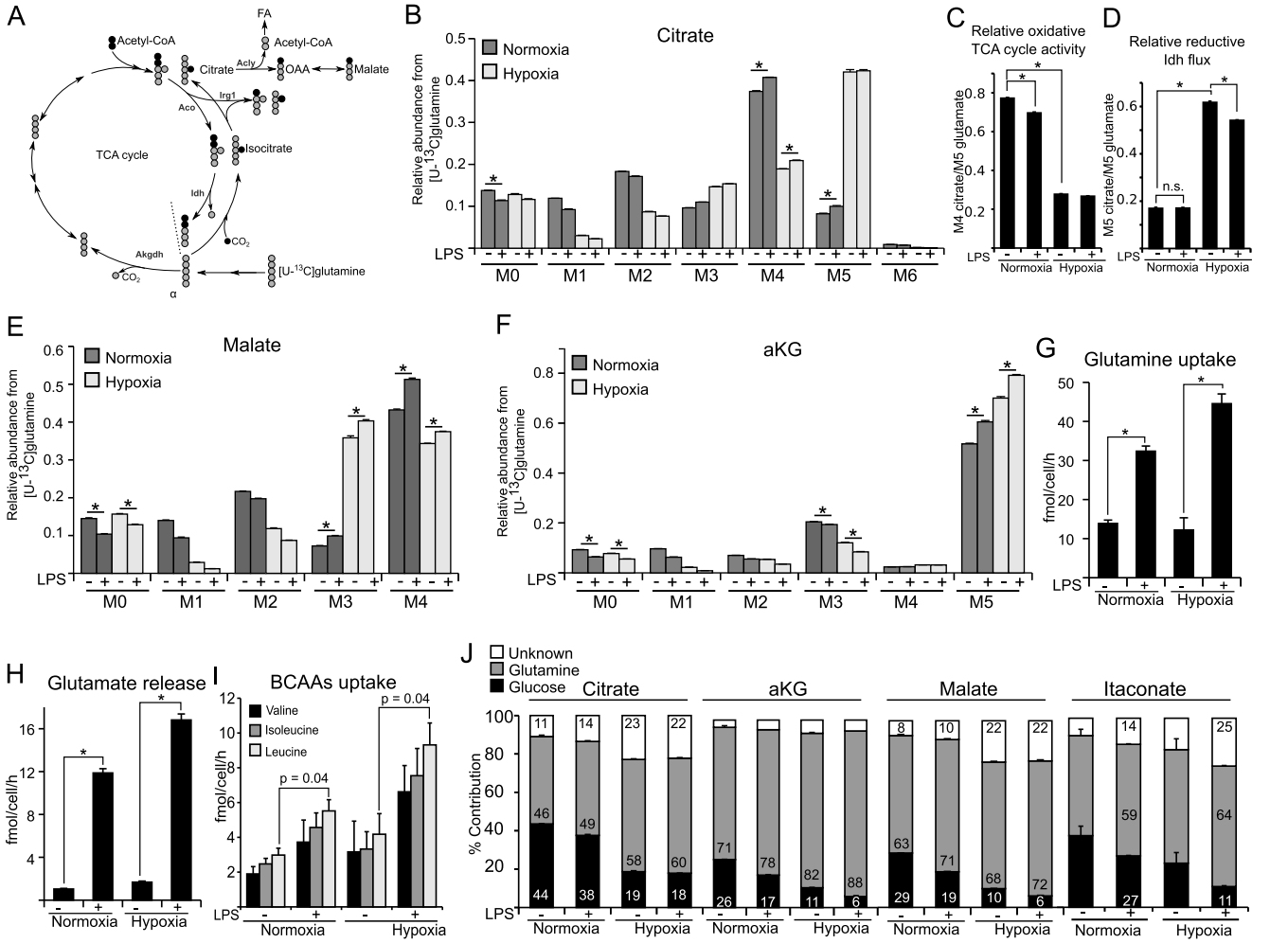

FIGURE 4. **Contribution of glutamine to central metabolism in M(LPS) macrophages.** *A,* schematic of atom transitions in central metabolism using [U-^{13}C]glutamine as a tracer. ^{13}C-carbons are in *gray*, ^{12}C in *black*. Citrate molecules derived from reductive carboxylation of αKG are M5 isotopologues, whereas citrate molecules from the oxidative route of the TCA cycle are M4 isotopologues. The *dotted line* indicates end of one route. *Aco,* aconitase; *Idh,* isocitrate dehydrogenase; *Akgdh,* αKG dehydrogenase; *Acly,* ATP-dependent citrate lyase; *FA,* fatty acid. *B,* MID of citrate. *M0* to *M6* indicates the different mass isotopologues. *C* and *D,* determination of oxidative TCA cycle activity: ratio of M4 citrate/M5 glutamate and ratio of M5 citrate/M5 glutamate indicating relative reductive Idh flux. *E* and *F,* MID of malate and αKG. *G–I,* absolute quantification of glutamine uptake, glutamate release, and uptake of the branched chain amino acids (valine, isoleucine, and leucine). *J,* carbon contribution (%) of glucose, glutamine, and other carbon sources to citrate, αKG, malate, and itaconate. Carbon contributions are based on MIDs from [U-^{13}C]glucose labeling (Fig. 3) and [U-^{13}C]glutamine labeling. Carbon contribution to itaconate under non-LPS conditions should not be considered because itaconate levels are negligibly low under these non-stimulated conditions (Fig. 1*A*). *Error bars* indicate S.E. (Welsh's *t* test, *, $p < 0.01$, $n = 3$). One representative experiment with three individual wells per condition is presented. Each experiment was performed at least three times.

carboxylation of αKG (12–15). This pathway fuels the citrate pool to provide sufficient acetyl-CoA for lipogenesis. Because M(LPS) activation also results in a stabilization of HIF1α (10, 19, 21, 29) and increased glycolytic flux (see Fig. 3, *I* and *L*), we investigated whether these cells exhibit increased reductive carboxylation of αKG. To that end, we applied a uniformly labeled [U-^{13}C]glutamine tracer and determined MIDs of TCA cycle metabolites (Fig. 4*A* for atom transitions).

As expected, under hypoxic conditions we observed a drop in oxidative TCA cycle activity and a strong induction of reductive carboxylation, inferred from decreased citrate M4 and increased citrate M5 isotopologues (Fig. 4, *B–D*). This pattern was also reflected by decreasing malate M4 (oxidative route) and increasing malate M3 (reductive route) isotopologues (Fig. 4*E*). However, when cells were stimulated with LPS at normoxic conditions, reductive carboxylation of αKG was not increased (Fig. 4*D*).

Using the glutamine tracer, we observed that the major carbon source of αKG was glutamine and that upon LPS stimulation and under hypoxia the abundance of M5 isotopologues increased, suggesting an increase in glutamine influx and a decreasing glucose contribution (Fig. 4*F*). Although hypoxia results in increased usage of αKG for reductive carboxylation and decreased αKG oxidation (14, 15), we did not find evidence that LPS stimulation under normoxia compromises the relative glutamine carbon flux through αKG dehydrogenase, indicated by a similar enrichment pattern of αKG and malate.

To analyze glutamine metabolism in more detail, we quantified glutamine uptake from the medium and glutamate release from the cells. Although hypoxia did not result in increased glutamine uptake, we observed a strong increase of glutamine uptake upon LPS stimulation under both oxygen levels (Fig. 4*G*). Because glutamate is produced from glutamine and can be

released from the cell, we quantified glutamate release to infer glutamine anaplerosis to the TCA cycle. Although we observed increased glutamate release upon LPS stimulation, the net uptake of glutamine in LPS-stimulated cells was still higher compared with untreated controls (control 12.84 *versus* LPS 20.5 fmol/cell/h) (Fig. 4, *G* and *H*). As indicated by the intracellular metabolite levels (Fig. 1*K*), we also observed a trend of increased consumption of branched chain amino acids from the medium upon LPS stimulation (Fig. 4*I*). However, these differences were only significant in the case of leucine. Nevertheless, we believe that the influence of branched chain amino acids on central metabolism is higher upon LPS activation.

To better understand the impact of the different carbon sources to the TCA cycle metabolites, we calculated the carbon contributions of glucose and glutamine to citrate, αKG, malate, and itaconate (Fig. 4*J*). We observed a small decrease in glucose contribution to citrate upon LPS activation. However, based on the [U-^{13}C]glucose-derived MIDs, this decrease mostly originated from decreased citrate cycling through the oxidative TCA cycle (compare M3, M4, and M5 isotopologues in Fig. 3*B*) or increased glutamine influx, rather than decreased pyruvate flux through PDH (M2 isotopologue). Hypoxia resulted in a stronger reduction of glucose contribution to citrate, which was a result of PDH inhibition. Along with the decrease in glucose contribution, the glutamine contribution to citrate was increased upon LPS, especially under hypoxia, where glutamine is the major carbon source of citrate. For αKG and malate, the glucose contribution was significantly lower compared with citrate, indicating that major parts of the citrate pool are not used for further oxidation through the oxidative TCA cycle, but for anabolic processes such as lipid synthesis or itaconate synthesis. In line with this observation, we observed higher glucose contribution to itaconate, compared with αKG and malate. Moreover, upon LPS stimulation, and especially with hypoxia, we observed an increase of other carbon sources than glucose or glutamine, which is in line with potentially increased uptake of branched chain amino acids (Figs. 1*K* and 4*I*).

In summary, we observed that glutamine is the major carbon source of the TCA cycle in M(LPS) macrophages and is the main substrate for TCA oxidation. Glucose carbon still enters the cycle at citrate; however, significant amounts of the citrate pool are not further oxidized through IDH but are distributed to other metabolic pathways. Glutamine serves to replenish this lack of carbon by increased uptake upon LPS stimulation.

LPS Causes an Increase in Lipogenesis in RAW 264 Cells—Besides transcriptional and metabolic adaptations to inflammation, it has been described that pro-inflammatory macrophages also undergo morphological changes from small and spherical to a larger and more attached form (Fig. 5*A*). To demonstrate the surface enlargement during LPS activation, we monitored cell size by using two orthogonal microscopy approaches (Fig. 5*B*), demonstrating an increase in cell surface and thus pointing to an increased demand on lipids needed for membrane formation. Furthermore, M(LPS) macrophages increase intracellular and extracellular vesicle formation during pathogen defense (36). Therefore, M(LPS) macrophages have an increased demand for lipids, needed for morphological changes and vesicle formation. To meet this demand, LPS-activated macrophages need to prioritize their metabolism toward lipogenesis and to repress lipid oxidation. In line with this necessary metabolic shift, we observed decreased expression of carnitine palmitoyltransferase 1 (*Cpt1*), the gene of the protein that imports palmitate into the mitochondrion for lipid oxidation and subsequent energy production (Fig. 5*C*). A reduction of β-oxidation is in line with reports of decreased oxidative metabolism in M(LPS) macrophages (37) and supports the observed increased demand for lipids. High activity of lipid degradation, simultaneously to their synthesis, would be a waste of energy.

To generate lipids from central metabolism, cells export mitochondrial citrate into the cytoplasm where it is hydrolyzed via ATP-dependent citrate lyase to provide acetyl-coA for lipogenesis. In this preferred case, citrate utilization is for anabolic processes rather than the TCA cycle. To analyze the contribution of glucose and glutamine to palmitate, an end point of fatty acid synthesis, we determined the MIDs of and the carbon contributions to palmitate after both the application of [U-^{13}C]glucose and [U-^{13}C]glutamine as tracers in independent experiments (Fig. 5, *D* and *E*). We observed that under normoxia, nearly 50% of the carbon in palmitate originated from glucose. Under hypoxic conditions, a shift in isotopologues indicated that the glucose contribution was reduced while glutamine contribution was increased, suggesting increased reductive carboxylation under hypoxia, but not as a result of LPS stimulation. Although dependent on the pool sizes of the metabolites, increased production of itaconate and palmitate from glucose-derived citrate in M(LPS) macrophages indicates reduced citrate oxidation through the TCA cycle in M(LPS) macrophages.

Pyruvate Flux to Citrate Is Important for LPS Activation in RAW 264 Cells—To investigate the importance of the PDH flux in M(LPS) macrophages, we used a pharmacological approach to impair pyruvate oxidation through PDH by inhibiting the pyruvate transporter with the specific inhibitor UK5099 (38). Using this inhibitor together with the [U-^{13}C]glucose tracer, we observed a significant decrease of citrate M2 isotopologues, indicating reduced relative pyruvate oxidation through PDH (Fig. 6*A*). Addition of LPS to UK509-treated cells could not restore the abundance of M2 citrate, because pyruvate supply is impaired by the inhibition of the transporter. Analysis of intracellular metabolite levels revealed that inhibition of pyruvate transport into the mitochondrion resulted in decreased amounts of citrate, originating from reduced substrate levels for citrate synthase (Fig. 6*B*). Intriguingly, we also observed decreased amounts of the inflammatory marker metabolites itaconate and succinate under pro-inflammatory conditions (Fig. 6, *C* and *D*). Decreased amounts of itaconate and succinate could either result from decreased glucose flux into the TCA cycle, similar to hypoxia, or from a metabolic alteration in M(LPS) macrophages. To analyze these hypotheses, we investigated the gene expression profiles of pro-inflammatory marker genes (Fig. 6, *E–H*). Although *Il1b* gene expression was not significantly decreased (Fig. 6*E*), we observed that UK5099 treatment of LPS-stimulated macrophages resulted in decreased expression levels of *iNos*, *Irg1*, and *Tnfα* (Fig. 6, *F–H*), indicating that in this case and in contrast to hypoxia, the observed decreased itaconate level roots back to decreased *Irg1*

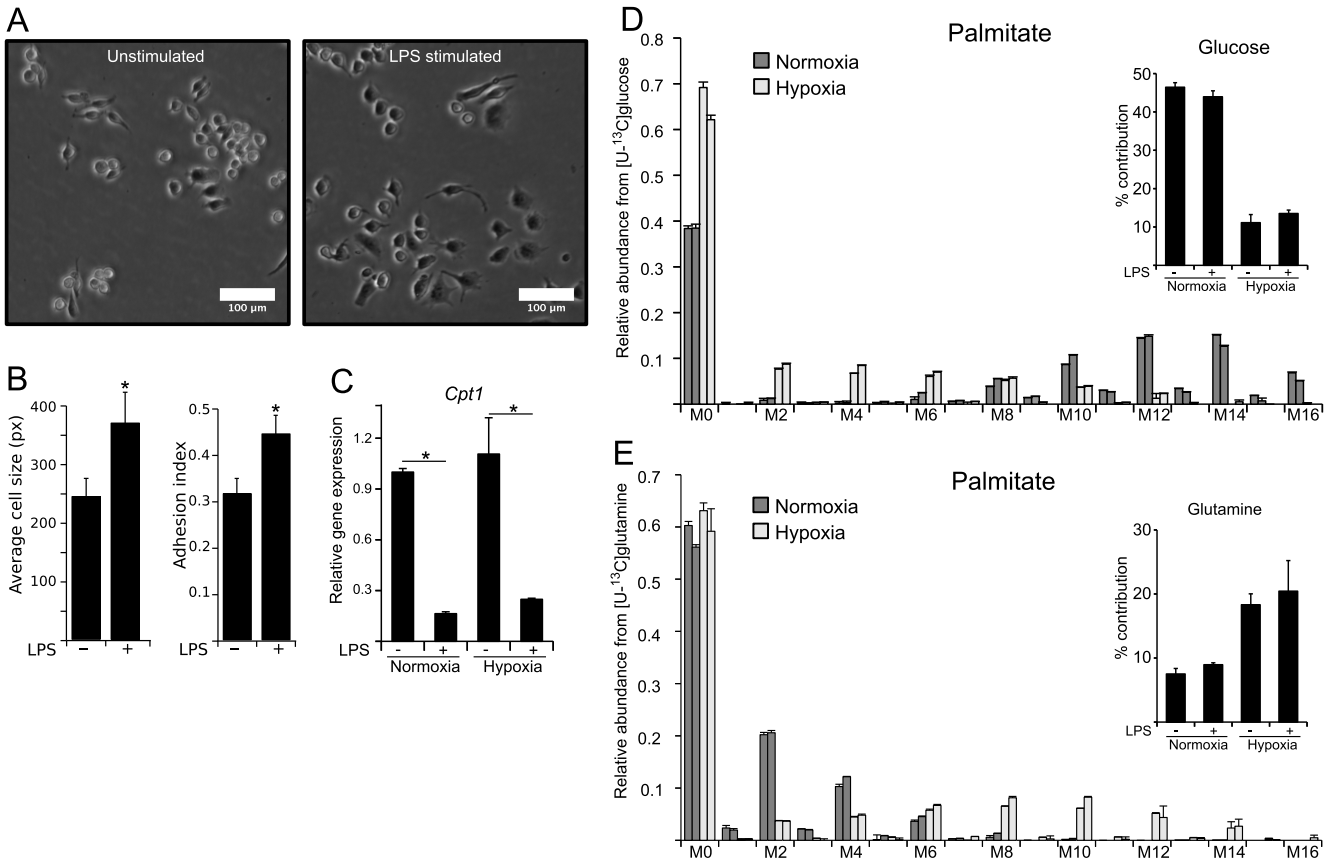

FIGURE 5. **Morphological changes upon LPS activation require sustained lipogenesis in macrophages.** *A,* microscopy (bright field image) of RAW macrophages unstimulated or stimulated with 10 ng/ml LPS for 6 h. *White bar* indicates 100 μm. *B,* mean average of cell size (pixels) (*left*) and analysis of adhesion index (*right*) of LPS-stimulated and -non-stimulated cells obtained from bright field microscopy. Analysis demonstrates morphological adaption of macrophages during LPS activation. For further details regarding the analysis approach, see under "Experimental Procedures." *C,* relative gene expression of carnitine palmitoyl transferase1 (*Cpt1*) normalized to normoxia control (*Ctrl*) (−*LPS*), indicating inhibition of β-oxidation upon LPS stimulation. *D* and *E,* MID of palmitate using [U-^{13}C]glucose (*D*) and [U-^{13}C]glutamine (*E*) as a tracer. Contribution of each carbon source is depicted in the *top right corner* of each panel. *Error bars* indicate S.E. (Welsh's *t* test, *, $p < 0.01$, $n \geq 3$). One representative experiment with three individual wells per condition is presented. Each experiment was performed at least three times, except for *C*. Presented is the mean ± S.E. over three independent experiments. (Welsh's *t* test, *, $p < 0.01$, $n = 3$).

levels. Moreover, application of UK5099 to LPS-stimulated cells resulted in increased *Cpt1* expression levels, similar to untreated controls, although *Pdk1* expression was still reduced, due to the fact that pyruvate import into the mitochondrion was inhibited and thus regulation of PDH not necessary (Fig. 6, *I* and *J*). To exclude a potential toxic effect of UK5099 on RAW 264 cells, we performed a viability assay and did not observe significant changes in viability (Fig. 6*K*). To further exclude the possibility of timing effects due to simultaneous addition of LPS and UK5099, we repeated the experiments with a modified experimental setup, where we first activated the cells with LPS for 3 h and then added UK5099 for an additional 6 h to investigate whether this intervention can repress the pro-inflammatory profile of M(LPS) macrophages (Fig. 6*L*). Following this approach, we also observed significantly decreased citrate, itaconate, and succinate levels (Fig. 6, *M–O*) and significantly decreased expression of *Tnfα, iNos*, *Irg1*, and *Il1b* (Fig. 6, *P–S*). These results indicate that inhibition of pyruvate import into the mitochondrion can indeed suppress pro-inflammatory responses in M(LPS) macrophages. Finally, we investigated the effect of carbon contribution to palmitate for these conditions, using [U-^{13}C]glucose as a tracer, in combination with UK5099. In line with decreased citrate, itaconate, and succinate levels upon UK5099 treatment, we also observed lower carbon contribution from glucose to palmitate (Fig. 6, *T* and *U*).

In summary, these data demonstrate that the pyruvate flux through PDH is important for LPS activation in macrophages. Apparently, altered metabolic fluxes or changes in metabolite concentrations enable a feedback mechanism to regulate cellular gene expression profiles. Hence, metabolic intervention can be used to attenuate activation of M(LPS) macrophages.

Discussion

M(LPS) macrophages require extensive reprogramming to enable host defense mechanisms. Although M(IL4) macrophages increase oxidative metabolism optimized for tissue repair (39), M(LPS) macrophages develop a Warburg-like phenotype by increasing glycolysis and lactate release (3). It has been demonstrated that pro-inflammatory activation results in the stabilization of HIF1α, HIF1 complex formation with monomeric or dimeric PKM2, along with an increased expression of M(LPS)-associated cytokines and bacterial defense mechanisms (29). While under hypoxia HIF1 not only increases the glycolytic activity but also represses PDH activity through PDK1, it was speculated that glucose flux

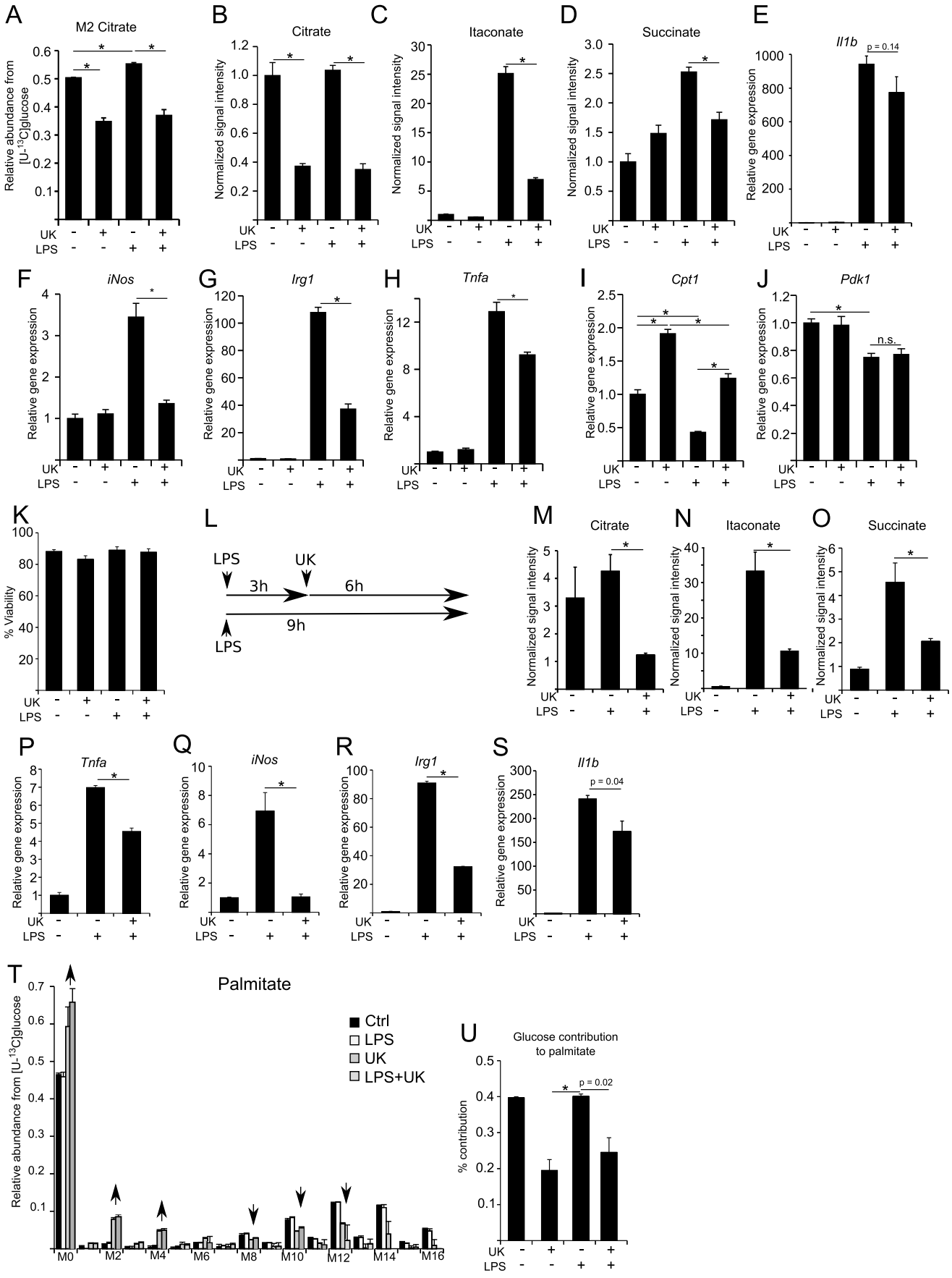

through PDH is also repressed in M(LPS) macrophages (3, 40). However, this would diminish the carbon supply necessary for lipogenesis and synthesis of the antimicrobial metabolite itaconate.

In this work, we demonstrate that the PDH flux plays an important role in maintaining full LPS-specific activation and that pharmacological intervention to prevent pyruvate oxidation represses pro-inflammatory activation. Although an active PDH flux has been speculated for early macrophage differentiation and for dendritic cells before (3, 41), our results demonstrate that pyruvate oxidation through PDH is fully active in mature M(LPS) macrophages and that this is even essential to sustain LPS activation. Moreover, we discovered that this process is facilitated by repressed *Pdk1* expression and no increase in PDK1 protein abundance, as well as significantly lower phosphorylation of PDH compared with hypoxic conditions, illustrating that M(LPS) macrophages sustain an active pyruvate flux through PDH.

Under hypoxia, HIF1 decreases pyruvate oxidation through PDH by inducing *Pdk1* (32). In contrast to hypoxia, we demonstrated that although glycolysis is increased and oxygen consumption is decreased (29) in M(LPS) macrophages, pyruvate oxidation through PDH is not inhibited, because PDK1 abundance is not increased. Active PDH facilitates a stable citrate pool, which in turn prevents increased reductive carboxylation of αKG by thermodynamic means (16). M(LPS) macrophages have been shown to increase their expression of the mitochondrial citrate carrier to transport citrate from the mitochondrion into the cytosol (42), and we have shown that M(LPS) macrophages have an increased lipid demand. Because we demonstrated that reductive carboxylation of αKG is not increased, the high demand of citrate has to be mostly supplied by glucose through PDH.

When PDH flux is repressed, citrate is increasingly generated by reductive carboxylation of αKG, which is mostly derived from glutamine (43). An increased demand on glutamine in M(LPS) macrophages has been reported before (44). Here, we describe in detail how this glutamine is utilized. In M(LPS) macrophages most glutamine is preferentially used for glutaminolysis rather than for reductive carboxylation of αKG. Besides ATP-dependent citrate lyase-derived oxaloacetate, increased glutaminolysis additionally provides oxaloacetate, which is needed as an acceptor for pyruvate-derived acetyl-CoA and the synthesis of citrate. It also replenishes the TCA cycle to compensate for increased lipogenesis and the loss of carbon that is used for the synthesis of itaconate.

It is known that LPS activation results in decreased oxygen consumption, which suggests that TCA cycle activity is decreased and would provide less NADH to be oxidized via the ETC (29, 45, 46). However, we found evidence that the oxidative TCA cycle is still running and is fueled by increased amounts of glutamine. TCA cycle-derived NADH can be used for alternative routes and would consequently not be oxidized via the ETC and thus would also result in reduced oxygen consumption rates. Mitochondrially derived NADH can alternatively be converted to NADPH by nicotinamide nucleotide transhydrogenase (17, 47), which is utilized by M(LPS) macrophages for ROS production via NADPH oxidase, needed for antibacterial activity (48), or transferred to the cytoplasm (49) where it is needed for lipogenesis. Therefore, it is possible that M(LPS) macrophages use increased amounts of TCA cycle-derived NADH for the generation of NADPH rather than oxidizing it via the ETC, which fits to the reported decreased oxygen consumption rates (6, 45, 46). Additionally, the ETC can be directly inhibited by nitrosylation (50, 51) promoted by increased expression of *iNos*, which we have shown to be increased upon LPS stimulation. Therefore, decreased oxygen consumption in M(LPS) macrophages due to decreased ETC activity is reasonable, but a decreased ETC activity does not necessarily have to result in decreased oxidative TCA cycle activity.

Although we could demonstrate that PDH activity is important in M(LPS) macrophages, the mechanism of how *Pdk1* repression is facilitated despite the presence of HIF1 needs additional research. One possibility would be a weaker stabilization because HIF1α is not as abundant as in hypoxic cells. However, in this case, we would still expect a similar mode of action and therefore a moderate induction of *Pdk1*. LPS activation exhibits distinct regulatory modules (2), and we conclude that these specific networks overlap with the classical HIF1 signature to mediate LPS-specific activation. Because we demonstrated that M(LPS) macrophages depend on the PDH flux to induce cytokine expression and synthesis of itaconate, it appears that a specific HIF1-induced upstream regulator exists which specifically prevents *Pdk1* expression. In this way, increased glucose uptake and lactate release can still be facilitated by HIF1, whereas PDK1 activity is prevented by an additional regulator. Overall, this points toward a context-dependent HIF1 response.

With the hypoxia model, we demonstrated that the decreased pyruvate flux through PDH results in decreased levels of the antimicrobial metabolite itaconate as well as decreased levels of succinate. However, gene expression of *Irg1* was unchanged. We conclude that, under hypoxia, decreased metabolite levels are a

FIGURE 6. **Inhibition of pyruvate transport into mitochondria suppresses pro-inflammatory responses in M(LPS) macrophages.** *A,* application of the specific pyruvate transport inhibitor UK5099 to inhibit flux through PDH. Cells were treated with 100 μM UK5099 for 6 h with or without 10 ng/ml LPS at normoxia. Prior to treatment start, cells were cultivated for 24 h in [U-^{13}C]glucose. Presented are citrate M2 isotopologues as a readout for relative glucose flux through PDH. *B–D,* intracellular metabolite levels of citrate, itaconate, and succinate upon LPS stimulation and after application of 100 μM UK5099. Metabolite levels were determined using GC/MS and normalized to cell number. *E–J,* relative gene expression of *Il1β, iNos, Irg1, Tnfα, Cpt1,* and *Pdk1* normalized to normoxia control (*Ctrl*) (−*LPS*), upon LPS stimulation and after application of 100 μM UK5099 for 6 h. *K,* viability assay to test a potential effect of UK5099 on cell viability. Assay was performed using trypan blue, dead and live cells were counted. *L,* to validate the effect of UK5099 a modified experimental setup has additionally been performed. Cells were first activated with 10 ng/ml LPS for 3 h and then UK5099 was added to the cells for additional 6 h. In total, LPS activation was 9 h in this case. Non-UK5099 treated and non-activated cells served as control. *M–O,* intracellular metabolite levels for citrate, itaconate, and succinate (analysis as in *B–D*). *P–S,* relative gene expression analysis of *Tnfα, iNos, Irg1,* and *Il1β*. *T* and *U,* MID of palmitate using [U-^{13}C]glucose as a tracer. Experimental setup as in *A*. *U,* glucose contribution to palmitate, determined from *T*. *Error bars* indicate S.E. (Welsh's *t* test, *, $p < 0.01$, $n = 3$). One representative experiment with three individual wells per condition is presented. Each experiment was performed at least three times.

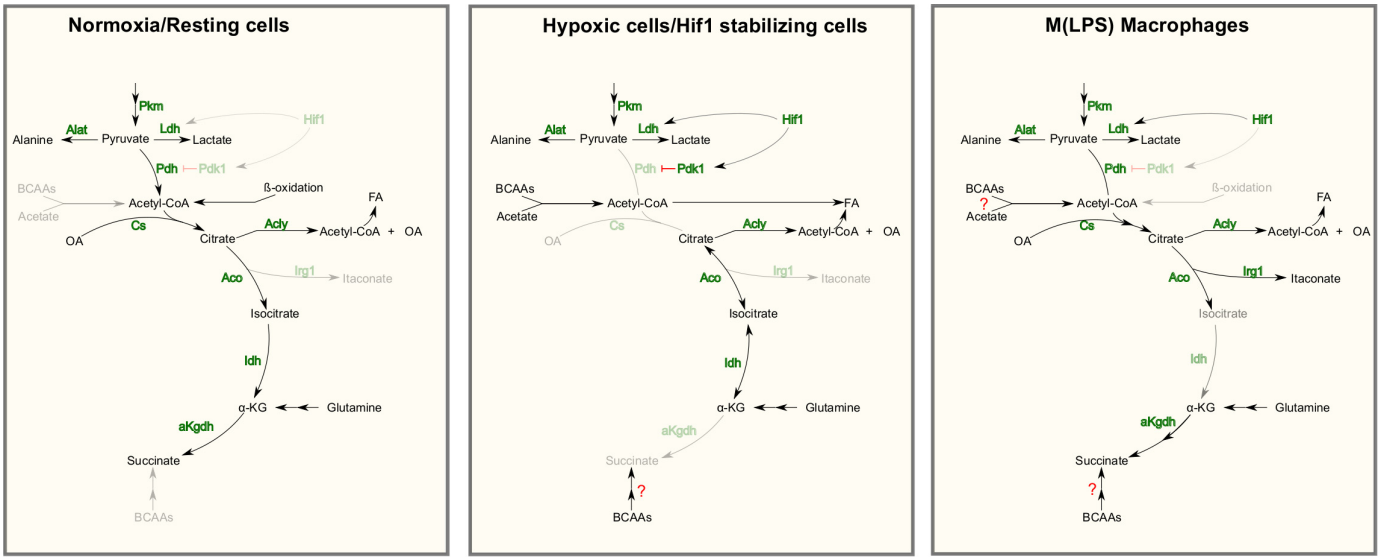

FIGURE 7. **Model summarizing the metabolic adaptations in M(LPS) macrophages.** Resting cells use glucose via PDH and TCA oxidation for energy production. Depending on the cell type, anabolic processes run in parallel. Hypoxic cells and cancer cells with stabilized HIF1α increase their glycolytic rate, inhibit PDH flux, and use glutamine-derived carbon for increased reductive carboxylation of αKG for subsequent lipogenesis. Highly proliferating cells promote anabolic processes to support proliferation. M(LPS) macrophages show stabilized HIF1α but do not decrease pyruvate oxidation through PDH. Under this condition, Hif1α does not increase PDK1 abundance. Compared with resting cells, less citrate is oxidized through the TCA cycle and is rerouted to serve as a precursor for itaconate and fatty acid synthesis. Glutamine serves to replenish the TCA cycle by increasing its carbon contribution to αKG and subsequent metabolites. BCAAs might also support carbon supply to the TCA cycle, but this needs additional research. Despite sustained pyruvate oxidation through PDH, oxygen consumption rates are lower than in resting cells.

passive effect of decreased pyruvate oxidation and decreased oxidative mitochondrial metabolism. This also illustrates that HIF1-mediated inhibition of PDH would be disadvantageous to M(LPS) macrophages and that parts of the TCA cycle are indeed important for M(LPS) macrophages, *e.g.* for the synthesis of lipids and itaconate.

By inhibiting the pyruvate import into the mitochondria of M(LPS) macrophages, we observed decreased metabolite levels of itaconate and succinate, similar to hypoxia. Intriguingly, in the case of transport inhibition, gene expressions of *Irg1, Tnfα*, and *iNos* were decreased as well. All of these genes are hallmarks of LPS activation, indicating a general impairment of activation in matured M(LPS) macrophages.

Based on our observations, we can now extend the existing metabolic model of M(LPS) macrophages (Fig. 7). 1) We confirmed the findings of increased glycolysis and increased lactate release. 2) Furthermore, reductive carboxylation of αKG is not increased in M(LPS) macrophages, but instead glutamine is still oxidized through αKG dehydrogenase. 3) Finally, pyruvate is still oxidized through PDH, which turned out to be essential for full LPS activation. Our work revealed an LPS-specific metabolic feature that is essential for activation and that might be approached by further studies in the light of translational medicine to develop novel therapies against inflammatory dysfunctions.

Author Contributions—J. M. designed the concept of this work, performed experiments, analyzed data, and wrote the manuscript. L. K. performed experiments and analyzed data. S. C. S. performed experiments, analyzed data, and revised the manuscript. N. B. and J. G. performed Western blots. A. F. and A. S. did the microscopy analysis. K. H. discussed experiments and revised the manuscript. All authors read and agreed to the content of this manuscript.

Acknowledgments—J. M. thanks Dr. Daniel Weindl and Dr. Andre Wegner from the Metabolomics Group for fruitful discussions. We thank Yannic Nonnenmacher from the Metabolomics Group for technical assistance with the HPLC. We thank Dr. Aidos Baumuratov from the Imaging Facility, Luxembourg Centre for Systems Biomedicine, for assistance and technical support with the microscopes.

References

1. Gordon, S., and Taylor, P. R. (2005) Monocyte and macrophage heterogeneity. *Nat. Rev. Immunol.* **5,** 953–964
2. Murray, P. J., Allen, J. E., Biswas, S. K., Fisher, E. A., Gilroy, D. W., Goerdt, S., Gordon, S., Hamilton, J. A., Ivashkiv, L. B., Lawrence, T., Locati, M., Mantovani, A., Martinez, F. O., Mege, J. L., Mosser, D. M., *et al.* (2014) Macrophage activation and polarization: nomenclature and experimental guidelines. *Immunity* **41,** 14
3. Kelly, B., and O'Neill, L. A. (2015) Metabolic reprogramming in macrophages and dendritic cells in innate immunity. *Cell Res.* **25,** 771–784
4. Basler, T., Jeckstadt, S., Valentin-Weigand, P., and Goethe, R. (2006) *Mycobacterium paratuberculosis, Mycobacterium smegmatis,* and lipopolysaccharide induce different transcriptional and post-transcriptional regulation of the IRG1 gene in murine macrophages. *J. Leukocyte Biol.* **79,** 628–638
5. Degrandi D., Hoffmann, R., Beuter-Gunia, C., and Pfeffer, K. (2009) The proinflammatory cytokine-induced IRG1 protein associates with mitochondria. *J. Interferon Cytokine Res.* **29,** 55–67
6. Michelucci, A., Cordes, T., Ghelfi, J., Pailot, A., Reiling, N., Goldmann, O., Binz, T., Wegner, A., Tallam, A., Rausell, A., Buttini, M., Linster, C. L., Medina, E., Balling, R., and Hiller, K. (2013) Immune-responsive gene 1 protein links metabolism to immunity by catalyzing itaconic acid production. *Proc Natl Acad Sci. U.S.A.* 110, 7820–7825
7. Warburg, O. (1924) Über den stoffwechsel der carcinomzelle. *Naturwissenschaften* **12,** 1131–1137
8. Warburg, O. (1956) On the origin of cancer cells. *Science* **123,** 309–314
9. Vazquez, A., Liu, J., Zhou, Y., Oltvai, Z. N. (2010) Catabolic efficiency of aerobic glycolysis: the Warburg effect revisited. *BMC Syst. Biol.* **4,** 58

10. Tannahill, G. M., Curtis, A. M., Adamik, J., Palsson-McDermott, E. M., McGettrick, A. F., Goel, G., Frezza, C., Bernard, N. J., Kelly, B., Foley, N. H., Zheng, L., Gardet, A., Tong, Z., Jany, S. S., Corr, S. C., *et al.* (2013) Succinate is an inflammatory signal that induces IL-1β through HIF-1α. *Nature* **496,** 238–242
11. Denko, N. C. (2008) Hypoxia, HIF1 and glucose metabolism in the solid tumour. *Nat. Rev. Cancer* **8,** 705–713
12. Filipp, F. V., Scott, D. A., Ronai, Z. A., Osterman, A. L., and Smith, J. W. (2012) Reverse TCA cycle flux through isocitrate dehydrogenases 1 and 2 is required for lipogenesis in hypoxic melanoma cells. *Pigment Cell Melanoma Res.* **25,** 375–383
13. Mullen, A. R., Wheaton, W. W., Jin, E. S., Chen, P.-H., Sullivan, L. B., Cheng, T., Yang, Y., Linehan, W. M., Chandel, N. S., and DeBerardinis, R. J. (2012) Reductive carboxylation supports growth in tumour cells with defective mitochondria. *Nature* **481,** 385–388
14. Wise, D. R., Ward, P. S., Shay, J. E., Cross, J. R., Gruber, J. J., Sachdeva, U. M., Platt, J. M., DeMatteo, R. G., Simon, M. C., and Thompson, C. B. (2011) Hypoxia promotes isocitrate dehydrogenase-dependent carboxylation of -ketoglutarate to citrate to support cell growth and viability. *Proc. Natl. Acad. Sci. U.S.A.* **108,** 19611–19616
15. Metallo, C. M., Gameiro, P. A., Bell, E. L., Mattaini, K. R., Yang, J., Hiller, K., Jewell, C. M., Johnson, Z. R., Irvine, D. J., Guarente, L., Kelleher, J. K., Vander Heiden, M. G., Iliopoulos, O., and Stephanopoulos, G. (2012) Reductive glutamine metabolism by IDH1 mediates lipogenesis under hypoxia. *Nature* **481,** 380–384
16. Fendt, S.-M., Bell, E. L., Keibler, M. A., Olenchock, B. A., Mayers, J. R., Wasylenko, T. M., Vokes, N. I., Guarente, L., Vander Heiden, M. G., and Stephanopoulos, G. (2013) Reductive glutamine metabolism is a function of the α-ketoglutarate to citrate ratio in cells. *Nat. Commun.* **4,** 2236
17. Mullen, A. R., Hu, Z., Shi, X., Jiang, L., Boroughs, L. K., Kovacs, Z., Boriack, R., Rakheja, D., Sullivan, L. B., Linehan, W. M., Chandel, N. S., and DeBerardinis, R. J. (2014) Oxidation of α-ketoglutarate is required for reductive carboxylation in cancer cells with mitochondrial defects. *Cell Rep.* 7, 1679–1690
18. Hellwig-Bürgel, T., Rutkowski, K., Metzen, E., Fandrey, J., and Jelkmann, W. (1999) Interleukin-1β and tumor necrosis factor-α stimulate DNA binding of hypoxia-inducible factor-1. *Blood* **94,** 1561–1567
19. Jung, Y., Isaacs, J. S., Lee, S., Trepel, J., Liu, Z. G., and Neckers, L. (2003) Hypoxia-inducible factor induction by tumour necrosis factor in normoxic cells requires receptor-interacting protein-dependent nuclear factor κB activation. *Biochem. J.* **370,** 1011–1017
20. Simon, M. C. (2010) *Diverse Effects of Hypoxia on Tumor Progression.* Springer, Berlin
21. Nishi, K., Oda, T., Takabuchi, S., Oda, S., Fukuda, K., Adachi, T., Semenza, G. L., Shingu, K., and Hirota, K. (2008) LPS induces hypoxia-inducible factor 1 activation in macrophage-differentiated cells in a reactive oxygen species-dependent manner. *Antioxid. Redox Signal.* **10,** 983–995
22. Walther, J. L., Metallo, C. M., Zhang, J., and Stephanopoulos, G. (2012) Optimization of 13C isotopic tracers for metabolic flux analysis in mammalian cells. *Metab. Eng.* **14,** 162–171
23. Metallo, C. M., Walther, J. L., Stephanopoulos, G. (2009) Evaluation of 13C isotopic tracers for metabolic flux analysis in mammalian cells. *J. Biotechnol.* **144,** 167–174
24. Sapcariu, S. C., Kanashova, T., Weindl, D., Ghelfi, J., Dittmar, G., and Hiller, K. (2014) Simultaneous extraction of proteins and metabolites from cells in culture. *MethodsX* **1,** 74–80
25. Hiller, K., Hangebrauk, J., Jäger, C., Spura, J., Schreiber, K., and Schomburg, D. (2009) Metabolite Detector: comprehensive analysis tool for targeted and nontargeted GC/MS based metabolome analysis. *Anal Chem.* **81,** 3429–3439
26. Leek, R. D., and Harris, A. L. (2002) Tumor-associated macrophages in breast cancer. *J. Mammary Gland Biol. Neoplasia* **7,** 177–189
27. Lewis, J. S., Lee, J. A., Underwood, J. C., Harris, A. L., and Lewis, C. E. (1999) Macrophage responses to hypoxia: relevance to disease mechanisms. *J. Leukocyte Biol.* **66,** 889–900
28. Murdoch, C. (2204) Mechanisms regulating the recruitment of macrophages into hypoxic areas of tumors and other ischemic tissues. *Blood* **104,** 2224–2234
29. Palsson-McDermott, E. M., Curtis, A. M., Goel, G., Lauterbach, M. A., Sheedy, F. J., Gleeson, L. E., van den Bosch, M. W., Quinn, S. R., Domingo-Fernandez, R., Johnston, D. G., Jiang, J. K., Jiang, J. K., Israelsen, W. J., Keane, J., Thomas, C., *et al.* (2015) Pyruvate kinase M2 regulates Hif-1α activity and IL-1β induction and is a critical determinant of the Warburg effect in LPS-activated macrophages. *Cell Metab.* **21,** 65–80
30. Strelko, C. L., Lu, W., Dufort, F. J., Seyfried, T. N., Chiles, T. C., Rabinowitz, J. D., and Roberts, M. F. (2011) Itaconic acid is a mammalian metabolite induced during macrophage activation. *J. Am. Chem. Soc.* **133,** 16386–16389
31. Blouin, C. C., Pagé, E. L., Soucy, G. M., and Richard, D. E. (2004) Hypoxic gene activation by lipopolysaccharide in macrophages: implication of hypoxia-inducible factor 1. *Blood* **103,** 1124–1130
32. Kim, J. W., Tchernyshyov, I., Semenza, G. L., Dang, C. V. (2006) HIF-1-mediated expression of pyruvate dehydrogenase kinase: a metabolic switch required for cellular adaptation to hypoxia. *Cell Metab.* **3,** 177–185
33. Patel, M. S., and Korotchkina, L. G. (2006) Regulation of the pyruvate dehydrogenase complex. *Biochem. Soc. Trans.* **34,** 217–222
34. King, A., Selak, M. A., and Gottlieb, E. (2006) Succinate dehydrogenase and fumarate hydratase: linking mitochondrial dysfunction and cancer. *Oncogene* **25,** 4675–4682
35. Demaria, M., Giorgi, C., Lebiedzinska, M., Esposito, G., D'Angeli, L., Bartoli, A., Gough, D. J., Turkson, J., Levy, D. E., Watson, C. J., Wieckowski, M. R., Provero, P., Pinton, P., and Poli, V. (2010) A STAT3-mediated metabolic switch is involved in tumour transformation and STAT3 addiction. *Aging* **2,** 823–842
36. Garzetti, L., Menon, R., Finardi, A., Bergami, A., Sica, A., Martino, G., *et al.* (2014) Activated macrophages release microvesicles containing polarized M1 or M2 mRNAs. *J. Leukocyte Biol.* **95,** 817–825
37. O'Neill, L. A., and Hardie, D. G. (2013) Metabolism of inflammation limited by AMPK and pseudo-starvation. *Nature* **493,** 346–355
38. Yang, C., Ko, B., Hensley, C. T., Jiang, L., Wasti, A. T., Kim, J., Sudderth, J., Calvaruso, M. A., Lumata, L., Mitsche, M., Rutter, J., Merritt, M. E., and DeBerardinis, R. J. (2014) Glutamine oxidation maintains the TCA cycle and cell survival during impaired mitochondrial pyruvate transport. *Mol. Cell* **56,** 414–424
39. Vats, D., Mukundan, L., Odegaard, J. I., Zhang, L., Smith, K. L., Morel, C. R., Wagner, R. A., Greaves, D. R., Murray, P. J., and Chawla, A. (2006) Oxidative metabolism and PGC-1β attenuate macrophage-mediated inflammation. *Cell Metab.* **4,** 13–24
40. Tan, Z., Xie, N., Cui, H., Moellering, D. R., Abraham, E., Thannickal, V. J., and Liu, G. (2015) Pyruvate dehydrogenase kinase 1 participates in macrophage polarization via regulating glucose metabolism. *J. Immunol.* **194,** 6082–6089
41. Everts, B., Amiel, E., Huang, S. C., Smith, A. M., Chang, C.-H., Lam, W. Y., Redmann, V., Freitas, T. C., Blagih, J., van der Windt, G. J., Artyomov, M. N., Jones, R. G., Pearce, E. L., and Pearce, E. J. (2014) TLR-driven early glycolytic reprogramming via the kinases TBK1-IKKϵ supports the anabolic demands of dendritic cell activation. *Nat. Immunol.* **15,** 323–332
42. Infantino, V., Convertini, P., Cucci, L., Panaro, M. A., Di Noia, M. A., Calvello, R., Palmieri, F., and Iacobazzi, V. (2011) The mitochondrial citrate carrier: a new player in inflammation. *Biochem. J.* **438,** 433–436
43. Wise, D. R., and Thompson, C. B. (2010) Glutamine addiction: a new therapeutic target in cancer. *Trends Biochem. Sci.* **35,** 427–433
44. Newsholme, P., Curi, R., Pithon Curi, T.C., Murphy, C. J., Garcia, C., and Pires de Melo, M. (1999) Glutamine metabolism by lymphocytes, macrophages, and neutrophils: its importance in health and disease. *J. Nutr. Biochem.* **10,** 316–324
45. Jha, A. K., Huang, S. C., Sergushichev, A., Lampropoulou, V., Ivanova, Y., Loginicheva, E., Chmielewski, K., Stewart, K. M., Ashall, J., Everts, B., Pearce, E. J., Driggers, E. M., and Artyomov, M. N. (2015) Network integration of parallel metabolic and transcriptional data reveals metabolic modules that regulate macrophage polarization. *Immunity* **42,** 419–430
46. Krawczyk, C. M., Holowka, T., Sun, J., Blagih, J., Amiel, E., DeBerardinis, R. J., Cross, J. R., Jung, E., Thompson, C. B., Jones, R. G., and Pearce, E. J. (2010) Toll-like receptor-induced changes in glycolytic metabolism regulate dendritic cell activation. *Blood* **115,** 4742–4749

47. Gameiro, P. A., Laviolette, L. A., Kelleher, J. K., Iliopoulos, O., and Stephanopoulos, G. (2013) Cofactor balance by nicotinamide nucleotide transhydrogenase (NNT) coordinates reductive carboxylation and glucose catabolism in the tricarboxylic acid (TCA) cycle. *J. Biol. Chem.* **288,** 12967–12977
48. West, A. P., Brodsky, I. E., Rahner, C., Woo, D. K., Erdjument-Bromage, H., Tempst, P., Walsh, M. C., Choi, Y., Shadel, G. S., and Ghosh, S. (2011) TLR signalling augments macrophage bactericidal activity through mitochondrial ROS. *Nature* **472,** 476–480
49. Houtkooper, R. H., Cantó, C., Wanders, R. J., and Auwerx, J. (2010) The secret life of NAD^+: an old metabolite controlling new metabolic signaling pathways. *Endocr. Rev.* **31,** 194–223
50. Clementi, E., Brown, G. C., Feelisch, M., and Moncada, S. (1998) Persistent inhibition of cell respiration by nitric oxide: crucial role of *S*-nitrosylation of mitochondrial complex I and protective action of glutathione. *Proc. Natl. Acad. Sci. U.S.A.* **95,** 7631–7636
51. Drapier, J. C., and Hibbs, J. B. (1988) Differentiation of murine macrophages to express nonspecific cytotoxicity for tumor cells results in L-arginine-dependent inhibition of mitochondrial iron-sulfur enzymes in the macrophage effector cells. *J. Immunol.* **140,** 2829–2838

IMMUNORESPONSIVE GENE 1 AND ITACONATE INHIBIT SUCCINATE DEHYDROGENASE TO MODULATE INTRACELLULAR SUCCINATE LEVELS

Cordes T, Wallace M, Michelucci A, Divakaruni AS, Sapcariu SC, Sousa C, Koseki H, Cabrales P, Murphy AN, Hiller K, Metallo CM. *Jounral of Biological Chemistry*. **2016**, 291(27), 14274-14284. *doi:10.1074/jbc.M115.685792*

My contributions to this article were the design, execution, and analysis of experiments related to *Irg1* knock out BMDMs. To support the findings that itaconic acid inhibit succinate dehydrogenase activity in order to increase intracellular succinate during the inflammatory response in macrophages, I stimulated *Irg1* KO BMDMs with LPS, and measured reduced intracellular levels of itaconic acid and succinic acid compared to wild type BMDMs. This data is seen in figure 6 in the manuscript.

THE JOURNAL OF BIOLOGICAL CHEMISTRY VOL. 291, NO. 27, pp. 14274–14284, July 1, 2016

Immunoresponsive Gene 1 and Itaconate Inhibit Succinate Dehydrogenase to Modulate Intracellular Succinate Levels*

Received for publication, August 14, 2015, and in revised form, April 28, 2016 Published, JBC Papers in Press, May 9, 2016, DOI 10.1074/jbc.M115.685792

Thekla Cordes[‡], Martina Wallace[‡], Alessandro Michelucci[§¶], Ajit S. Divakaruni[‖], Sean C. Sapcariu[¶], Carole Sousa[§¶], Haruhiko Koseki[**], Pedro Cabrales[‡], Anne N. Murphy[‖], Karsten Hiller[¶], and Christian M. Metallo[‡ ‡‡1]

*From the Departments of [‡]Bioengineering and [‖]Pharmacology and [‡‡]Institute of Engineering in Medicine, University of California, San Diego, La Jolla, California 92093, the [§]NORLUX Neuro-Oncology Laboratory, Department of Oncology, Luxembourg Institute of Health, 1526 Luxembourg, Luxembourg, the [¶]Luxembourg Centre for Systems Biomedicine, University of Luxembourg, 4362 Esch-Belval, Luxembourg, and the **RIKEN Center for Integrative Medical Sciences, Yokohama, Kanagawa 230-0045, Japan*

Metabolic reprogramming is emerging as a hallmark of the innate immune response, and the dynamic control of metabolites such as succinate serves to facilitate the execution of inflammatory responses in macrophages and other immune cells. Immunoresponsive gene 1 (*Irg1*) expression is induced by inflammatory stimuli, and its enzyme product *cis*-aconitate decarboxylase catalyzes the production of itaconate from the tricarboxylic acid cycle. Here we identify an immunometabolic regulatory pathway that links *Irg1* and itaconate production to the succinate accumulation that occurs in the context of innate immune responses. Itaconate levels and *Irg1* expression correlate strongly with succinate during LPS exposure in macrophages and non-immune cells. We demonstrate that itaconate acts as an endogenous succinate dehydrogenase inhibitor to cause succinate accumulation. Loss of itaconate production in activated macrophages from *Irg1*$^{-/-}$ mice decreases the accumulation of succinate in response to LPS exposure. This metabolic network links the innate immune response and tricarboxylic acid metabolism to function of the electron transport chain.

Immune cells must sense cues from the extracellular microenvironment and respond rapidly to protect against bacteria, viruses, or other pathogens (1). An emerging hallmark of inflammation and the innate immune system of cells is metabolic reprogramming (2). One of the most general metabolic changes that occurs under proinflammatory conditions is a biochemical switch from oxidative phosphorylation to aerobic glycolysis (3–5), which is mediated, in part, via stabilization of hypoxia-inducible factor 1α (HIF-1α)[2] after pathogen infection (6), LPS binding to toll-like receptors (7), or by cytokine exposure (8). Although it is known that macrophages undergo drastic metabolic reprogramming upon exposure to inflammatory stimuli, the underlying mechanisms driving this response are not completely understood.

Increased succinate levels in macrophages are important mediators of the inflammatory response, linking metabolism to innate immunity. In addition to its role in TCA metabolism, succinate acts as a regulatory signal enhancing *Il-1*β expression through stabilization of HIF-1α, which, in turn, influences the function of various other metabolic pathways (9). Succinate inhibits the hydroxylation of HIF-1α by *EGLN1*, resulting in pseudohypoxic HIF-1α stabilization under normoxic conditions (10–12). Various mechanisms have been proposed as the cause of succinate accumulation, including increased glutamine anaplerosis and oxidation in the TCA cycle or increased flux through the GABA shunt (9, 13), although glycolytic metabolism is a prerequisite (14). However, the specific driver(s) of this phenomenon has/have not yet been identified. Given the central role of succinate as a metabolic signal in inflammation, elucidation of the metabolic pathway(s) involved in succinate accumulation and its/their regulation may provide new avenues for controlling this process.

Metabolites are important functional triggers that can regulate the activity of enzymes via substrate/product inhibition, posttranslational modifications, or allosteric interactions (15). Beyond their direct roles as substrates and products, metabolites often serve as substrates for posttranslational modifications, as shown for succinate to succinylate proteins (9). On the other hand, fructose 1,6-bisphosphate (16), serine, and other amino acids can allosterically influence the activity of the enzyme pyruvate kinase isoform M2 (PKM2) (17, 18). Recently, synthesis of the antimicrobial metabolite itaconate was identified in mammalian immune cells as being selectively up-regulated under proinflammatory conditions (19). Itaconate exhibits an antibiotic function (20) via inhibition of isocitrate lyase, a key enzyme of the glyoxylate shunt needed by many bacteria to survive during infection (21–23). In mammals, itaconate is pro-

* This study was supported by National Institutes of Health Grants R01CA188652 (to C. M. M.) and P01DK054441 (to A. N. M.); California Institute of Regenerative Medicine (CIRM) Award RB5-07356 (to C. M. M.); a Searle scholar award (to C. M. M.); National Science Foundation CAREER Award 1454425 (to C. M. M.); NIAID, National Institutes of Health Grant R01AI082610 (to P. C.); NHLBI, National Institutes of Health Grants R53HL123015, P01HL110900, and R01HL052684 (to P. C.); Fonds National de la Recherche, Luxembourg Grant ATTRACT A10/03 (to K. H.); AFR Grant 6916713 (to C.S.); the HICE Virtual Institute (to S. C. S.); and Deutsche Forschungsgesellschaft (German Research Foundation) Grant CO1488/1-1 (to T. C.). The authors declare that they have no conflicts of interest with the contents of this article. The content is solely the responsibility of the authors and does not necessarily represent the official views of the National Institutes of Health.

[1] To whom correspondence should be addressed: Dept. of Bioengineering, University of California, San Diego, 9500 Gilman Dr., MC-0412 PFBH 204, La Jolla, CA 92093. Tel.: 858-534-8209; E-mail: cmetallo@ucsd.edu.

[2] The abbreviations used are: HIF, hypoxia-inducible factor; TCA, tricarboxylic acid; CAD, *cis*-aconitate decarboxylase; SDH, succinate dehydrogenase; BMDM, bone marrow-derived macrophage; MSTFA, 2,2,2-trifluoro-*N*-methyl-*N*-trimethylsilyl-acetamide; MTBSTFA, *N*-*tert*-butyldimethylsilyl-*N*-methyltrifluoroacetamide; OCR, oxygen consumption rate.

duced through the decarboxylation of the TCA cycle intermediate *cis*-aconitate, which is catalyzed by mammalian *cis*-aconitate decarboxylase (CAD, also known as immune-responsive gene 1 (IRG1) protein) encoded by immunoresponsive gene 1 (*IRG1*) (20). Itaconate production represents one of two characteristic TCA cycle "break points" discovered in classically activated immune cells (24, 25). The first break occurs at isocitrate dehydrogenase, leading to the accumulation of citrate, the precursor for itaconate, and the second break occurs at succinate dehydrogenase (SDH), which may allow for succinate accumulation. Although itaconate has been shown previously to inhibit SDH *ex vivo* (26–28), and LPS-activated murine macrophages produced up to 8 mM intracellular itaconate (20), a potential role of endogenously produced itaconate in succinate accumulation under inflammatory conditions has not yet been addressed and is unknown.

To elucidate the role of itaconate in reprogramming immune cell metabolism, we modulated intracellular itaconate levels in primary bone marrow-derived macrophages (BMDMs), a macrophage cell line, as well as a lung adenocarcinoma cell line. In all cell models we observed metabolic changes reminiscent of SDH inhibition, including succinate accumulation. By measuring substrate-specific mitochondrial respiration, we demonstrated the inhibition of SDH by itaconate in a dose-dependent manner. Furthermore, stimulated BMDMs from *Irg1* KO mice failed to produce itaconate and exhibited decreased succinate accumulation compared with BMDMs from WT mice. Based on these studies, we have elucidated an *Irg1*-induced immunomodulatory pathway in macrophages whereby its product, itaconate, acts as an endogenously produced metabolic regulator of mitochondrial metabolism.

Experimental Procedures

Cell Culture and Isotopic Labeling—RAW 264.7 macrophages (29) (ATCC, TIB-71) and A549 cells (30) (ATCC, CCL-185) were maintained in high-glucose DMEM (Life Technologies) supplemented with 10% (v/v) FBS, 100 units·ml^{-1} penicillin/streptomycin, 25 mM glucose, and 4 mM L-glutamine. Cell lines tested negative for mycoplasma contamination using the MycoAlert mycoplasma detection kit (Lonza) according to the instructions of the manufacturer. Purified *Escherichia coli* LPS was used for the activation of RAW 264.7 macrophages and BMDMs at a concentration of 10 ng·ml^{-1}. A549 and RAW 264.7 cells and BMDMs were exposed to increasing itaconate concentrations (5, 10, and 25 mM) for 6 h. For isotopic labeling experiments, RAW 264.7 macrophages were cultured in DMEM (Sigma) supplemented with 25 mM glucose, 4 mM [1-^{13}C]glutamine (Cambridge Isotopes Inc.) and 10% (v/v) dialyzed FBS for 24 h prior to addition of LPS for 6 h. For isotope tracing with exposure to unlabeled itaconate, RAW 264.7 cells were exposed to labeled [U-$^{13}C_6$]glucose and [U-$^{13}C_5$]glutamine tracers over a period of three subcultures and then exposed further for 6 and 24 h to 10 mM unlabeled itaconate.

BMDMs—BMDM collection was approved by the Institutional Animal Care and Use Committee and was conducted according to the Guide for the Care and Use of Laboratory Animals (US National Research Council, 2010). BMDMs were isolated from femora and tibiae of C57BL/6J mice (The Jackson Laboratory, Bar Harbor, ME). Bones were collected in ice-cold PBS, cleaned of muscle, and flushed with 5 ml BMDM growth medium (DMEM, Life Technologies) supplemented with 10% (v/v) FBS, 100 units·ml^{-1} penicillin/streptomycin, 25 mM glucose, 4 mM L-glutamine, 20 ng·ml^{-1} recombinant-macrophage colony-stimulating factor (eBioscience), and 3.4 μl·l^{-1} β-mercaptoethanol). Cells were seeded at 5×10^6 cells on Petri dishes in 10 ml of growth medium. 5 ml of fresh growth medium was added on day 3. On day 6, BMDMs were collected and replated into 6-well tissue culture plates at a density of 5×10^5 cells/well in growth medium containing 2 ng·ml^{-1} recombinant-macrophage colony-stimulating factor. Metabolites were extracted on day 7.

For *Irg1* KO *versus* WT BMDM experiments, all animal procedures, such as handling and euthanasia, were performed according to the Federation of European Laboratory Animal Science Associations guidelines for the use of animals in research. The *Irg1* KO mice were generated by Dr. Haruhiko Koseki at the RIKEN Institute using stem cells purchased from the Knockout Mouse Project Repository under strain ID Irg1$^{tm1a(KOMP)Wtsi}$. Mice were anesthetized by intraperitoneal injection of 50 mg·kg^{-1} of ketamine hydrochloride and 5 mg·kg^{-1} xylazine hydrochloride, and bone marrow was isolated and cultured as described previously (31). Briefly, bone marrow was flushed from femora and tibiae of *Irg1* KO and age-matched C57BL/6 WT mice, and the resultant cell suspension was passed through a 70-μm filter (Greiner Bio-One). After 10 min of centrifuging at 250 $\times$ *g*, the supernatant was discarded, and the pellet was resuspended in 2 ml of hypotonic solution (170 mM NH_4Cl) for 5 min to allow lysis of any remaining extracellular red blood cells. Bone marrow-derived cells were plated in 12-well plates (Greiner Bio-One) at 5×10^5 cells/well. Cells were cultured for 6 days at 37 °C in RPMI 1640 VLE (Very Low Endotoxin) (Biochrom FG 1415) supplemented with 10% FBS and 20% conditioned medium from macrophage colony-stimulating factor-secreting L929 fibroblasts. After 6 days in culture, the BMDMs were used for experiments.

Metabolite Quantification—Metabolite levels of itaconate and TCA cycle intermediates were quantified using external standard curves (three biological replicates). For metabolite standard curves, increasing standard solutions were extracted under the conditions of sample preparation. Using the depicted standard curve, the metabolite quantity in each cell extract was calculated, taking into account cellular diameter (d, micrometers) of detached cells and cell number. We assumed a spherical shape and calculated the intracellular metabolite concentration using the following equation: [metabolite] = metabolite quantity (moles)/(((4/3000) π (d/2)^3) cell number). Cell number and cell diameter were determined using a Countess automated cell counter (Invitrogen).

Cell Transfections—Irg1 gain-of function experiments in A549 cells were performed as described previously (20). Briefly, A549 cells were transfected with the pCMV6-*Irg1* (OriGene) overexpressing plasmid or empty plasmid using Lipofectamine 2000 (Invitrogen) and further incubated for 24 h.

RNA Isolation and RT-PCR—Total RNA was purified from cultured cells using the Qiagen RNeasy mini kit (Qiagen)

according to the instructions of the manufacturer. First-strand cDNA was synthesized from total RNA using SuperScript III (Invitrogen) with 1 μl (50 μM)/reaction oligo(dT)20 as primer according to the instructions of the manufacturer. Individual 20-μl SYBR Green real-time PCR reactions consisted of 2 μl of diluted cDNA, 10 μl of fast SYBR Green Master Mix (Applied Biosystems), and 0.5 μl of each 10 μM forward and reverse primers. For standardization of quantification, L27 was amplified simultaneously. PCR was carried out in 96-well plates on an Applied Biosystems Viia™ 7 real-time PCR system using the following program: 95 °C for 20 s, 40 cycles of 95 °C for 1 s, and 60 °C for 20 s (*Irg1*, GCAACATGATGCTCAAGTCTG (forward) and TGCTCCTCCGAATGATACCA (reverse); *L27*, ACATTGACGATGGCACCTC (forward) and GCTTGGCGATCTTCTTCTTG (reverse)).

Oxygen Consumption Measurements—Respiration was measured in adherent monolayers of RAW 264.7 macrophages or BMDMs using a Seahorse XF96 analyzer. RAW 264.7 macrophages were plated at 3×10^4 cells/well (for assays with permeabilized cells) and 4×10^4 cells/well (for assays with intact cells) and BMDMs at 5×10^4 cells/well 24 h before measurement. Intact cells were assayed in DMEM (Sigma, 5030) supplemented with 8 mM glucose, 3 mM glutamine, 3 mM pyruvate, and 2 mM HEPES. Cells were permeabilized with 3 nM perfringolysin O (commercially, XF PMP (XF Plasma Membrane Permeabilizer)) as described previously (32). Phosphorylating (state 3), succinate-driven respiration in permeabilized cells was measured in cells offered 4 mM ADP, 2 μM rotenone, two different succinate concentrations (2.5 and 10 mM), and increasing itaconate concentrations (0, 5, 10, and 25 mM). When measuring respiration on different respiratory substrates, permeabilized cells were offered succinate (10 mM)/rotenone (2 μM), glutamate/malate (each 10 mM), pyruvate/malate (each 10 mM), or ascorbate (10 mM) plus *N,N,N′,N′*-tetramethyl-*p*-phenylenediamine (TMPD) (100 μM) and antimycin A (1 μM). Maximal respiration was calculated as the difference between protonophore-stimulated respiration (600 nM carbonyl cyanide *p*-trifluoromethoxyphenylhydrazone) and nonmitochondrial respiration (measured after addition of 1 μM antimycin A). All data are mean ± S.E. of two or three repeated experiments (with a minimum of five biological replicates per experiment) as indicated in the text. For assays with BMDMs, cells were obtained from three different mice.

GC-MS Sample Preparation and Analysis—Polar metabolites were extracted using methanol/water/chloroform as described previously (20). For medium metabolites, medium was centrifuged at 4 °C for 5 min at 300 × *g*. 10 μl of supernatant was added to 80 μl of a −20 °C 8:1 methanol/water mixture, mixed for 10 min at 4 °C, and centrifuged at 16,000 × *g* for 10 min at 4 °C. 80 μl was collected and evaporated under a vacuum at −4 °C. Metabolite derivatization was performed using a Gerstel MPS. Dried polar metabolites were dissolved in 15 μl of 2% (w/v) methoxyamine hydrochloride (Thermo Scientific) in pyridine and incubated for 60 min at 45 °C. An equal volume of 2,2,2-trifluoro-*N*-methyl-*N*-trimethylsilyl-acetamide (MSTFA) or *N*-*tert*-butyldimethylsilyl-*N*-methyltrifluoroacetamide (MTBSTFA) with 1% *tert*-butyl dimethylchlorosilane (Regis Technologies) was added and incubated further for 30 min at 45 °C. After derivatization, MSTFA-derivatized samples were analyzed as described previously (20). Briefly, derivatized samples were analyzed by GC-MS using a DB-35MS column (30 × 0.25 mm inner diameter × 0.25 μm, Agilent J&W Scientific) installed in an Agilent 7890A gas chromatograph interfaced with an Agilent 5975C mass spectrometer. For MTBSTFA-derivatized samples, the GC oven was held at 100 °C for 1 min, increased to 255 °C at 3.5 °C min^{-1}, increased to 320 °C at 15 °C min^{-1}, and held at 320 °C for 3 min. The total run time for one sample was 54.62 min. For *Irg1* KO *versus* WT BMDM metabolite measurements, the GC oven was held at 100 °C for 2 min, increased to 300 °C at 10 °C min^{-1}, and held at 325 °C for 3 min. The total run time for one sample was 26 min.

MSTFA-derivatized metabolites were determined using the following quantification ions: itaconate (*m*/*z* 259) and succinate (*m*/*z* 247). Metabolite levels and mass isotopomer distributions of MTBSTFA-derivatized samples were analyzed by integrating metabolite fragment ions (itaconate, *m*/*z* 301–310; succinate, *m*/*z* 289–294; citrate, *m*/*z* 459–469; α-ketoglutarate, *m*/*z* 346–355; malate, *m*/*z* 419–428; and fumarate, *m*/*z* 287–292) and corrected for natural abundance using in-house algorithms.

Statistical Analysis—All results shown as averages of one to three repeated experiments with each at least two biological replicates as indicated in the text. A repeated experiment is defined as a separate experiment temporally. Biological replicates are defined as separate spatial replicates (*i.e.* wells of a tissue culture plate) within an experiment. In the case of BMDMs, repeated experiments are defined as cells from different mice. Error bars indicate mean ± S.E. The statistical tool R (33) was used to calculate the Pearson correlation coefficient. For comparison of means between two different treatments, the statistical analysis was done by two-tailed Student's *t* test. *, $p < 0.05$; **, $p < 0.01$; ***, $p < 0.001$.

Results

Succinate and Itaconate Accumulate in LPS-activated RAW 264.7 Macrophages—To better understand the relationship between *Irg1*-mediated itaconate production and the reprogramming of TCA metabolism under LPS-stimulated conditions, we quantified the dynamics of itaconate and TCA intermediate abundances in RAW 264.7 macrophages over time. To elicit an immune response, we exposed RAW 264.7 macrophages to 10 $ng \cdot ml^{-1}$ LPS for 6 h, conditions that induce high expression of *Irg1* encoding CAD, the enzyme catalyzing itaconate production from *cis*-aconitate (20). Intriguingly, the levels of itaconate and succinate exhibited similar trends upon activation, in contrast to the dynamics of citrate, α-ketoglutarate, fumarate, and malate (Fig. 1*a*), suggesting that itaconate and succinate (or the enzymes metabolizing them) are regulated in a coordinated manner. Notably, basal oxygen consumption rates (OCR) remained unchanged compared with resting macrophages (Fig. 1*b*).

Exogenous Itaconate Drives Succinate Accumulation—To determine whether itaconate directly contributes to succinate accumulation, we next supplemented the growth medium of resting and LPS-activated murine RAW 264.7 macrophages

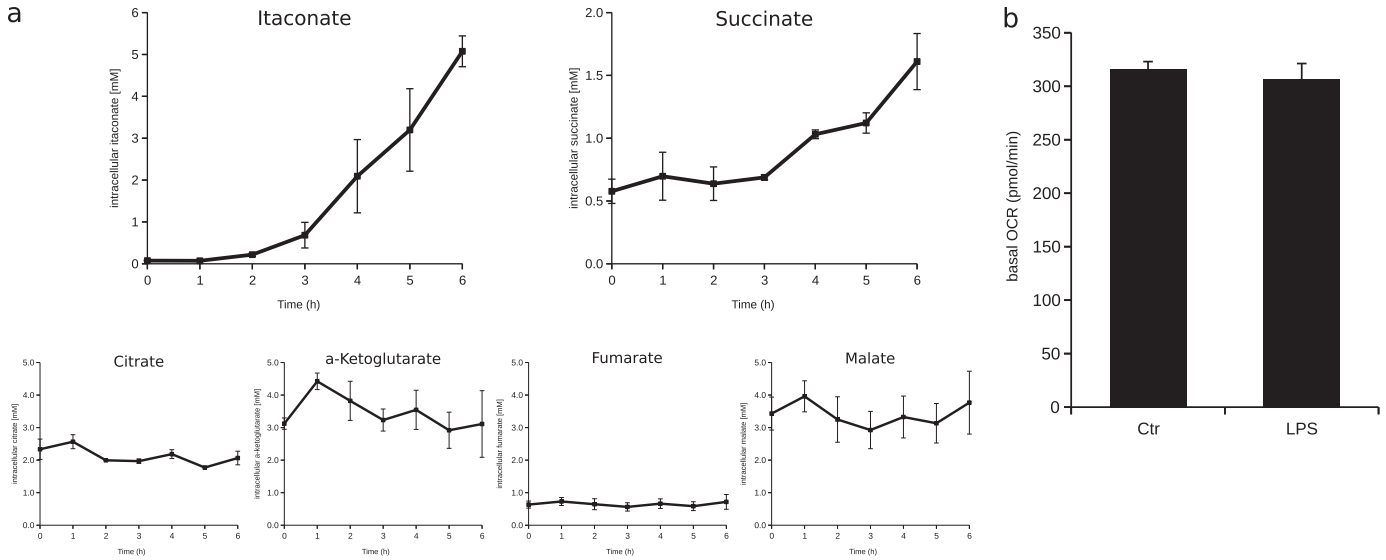

FIGURE 1. **Succinate and itaconate accumulate in LPS-activated murine RAW 264. 7 macrophages.** *a*, dynamics of itaconate, succinate, citrate, α-ketoglutarate, fumarate, and malate levels. Cells were exposed to 10 ng·ml^{-1} LPS, and metabolites were extracted every hour over a 6-h period. Graphs represent the mean ± S.E. of time-dependent, intracellular metabolite concentrations [mM] of two repeated experiments, each with three biological replicates. *b*, the basal OCR is unchanged in LPS-activated (*LPS*) macrophages compared with resting macrophages (*Ctr*). *Error bars* represent mean ± S.E. of two repeated experiments.

with increasing itaconate concentrations for 6 h and observed how intracellular itaconate levels correlated with those of various TCA cycle intermediates (Figs. 2, *a–f*). LPS-activated murine macrophages can produce up to 8 mM intracellular itaconate (20), but higher levels may accumulate in specific compartments (*e.g.* mitochondria). Therefore, we considered four different itaconate concentrations ranging from 0–25 mM. Exposure to exogenous itaconate resulted in increasing intracellular itaconate levels in a dose-dependent manner (Fig. 2*c*), indicating that cells have the capacity to take up itaconate from medium. However, medium itaconate levels were not appreciably affected (Fig. 2*g*). Interestingly, no mitochondrial or plasma membrane itaconate transporters have been described in mammalian cells to date.

We next calculated the Pearson correlation coefficient (r) between the intracellular abundance of itaconate and each TCA intermediate to gauge the relationship across each pair. Intriguingly, we observed that intracellular itaconate levels correlated strongly with succinate levels in resting ($r = 0.99$) as well as LPS-activated macrophages ($r = 0.99$) so that higher itaconate levels were associated with elevated succinate levels (Fig. 2*e*). Importantly, the levels of other TCA intermediates, including citrate, α-ketoglutarate, fumarate, and malate correlated poorly (or in some cases negatively) with intracellular itaconate levels (Fig. 2, *a*, *b*, *d*, and *f*). Because succinate accumulates after exposure to exogenous itaconate in RAW 264.7 macrophages (Fig. 2*e*) as well as BMDMs (Fig. 2*h*), these data suggest that LPS-induced itaconate production by mammalian CAD contributes to the elevated succinate levels observed in activated macrophages. Importantly, exposure to exogenous itaconate induces succinate accumulation in resting RAW 264.7 macrophages (Fig. 2*e*) as well as resting BMDMs (Fig. 2*h*), indicating that the mechanism through which itaconate acts is independent of other inflammatory signaling events.

Itaconate and Irg1-induced Succinate Accumulation Is Not Specific to Immune Cells—To further investigate whether itaconate reprograms TCA metabolism independent of inflammatory signals, we supplemented increasing itaconate concentrations (0, 5, 10, and 25 mM) to the growth medium of human A549 lung adenocarcinoma cells and quantified intracellular metabolite concentrations after 6 h. As before (Fig. 2*c*), uptake of extracellular itaconate from the medium was evidenced by increasing intracellular itaconate levels (Fig. 3*a*), whereas medium itaconate abundances did not change (Fig. 3*b*). Succinate levels increased linearly with itaconate levels and correlated strongly ($r = 0.99$), whereas other TCA cycle intermediates, including citrate, α-ketoglutarate, fumarate, and malate, did not accumulate (Fig. 3*a*). These results are consistent with our observations using RAW 264.7 macrophages (Fig. 2), and because A549 cells do not express *IRG1* (20) they suggest that itaconate-mediated succinate accumulation occurs even in the absence of an active inflammatory signaling cascade.

To determine whether CAD-mediated itaconate production can affect succinate levels in non-immune cells, we overexpressed *Irg1* in human A549 cells using a pCMV6-plasmid encoding murine *Irg1*. Itaconate was only produced at detectable levels in pCMV6 *Irg1*-overexpressing A549 cells (pm*Irg1*) compared with vector (pCMV6) controls (Fig. 3*c*). Notably, pm*Irg1* cells accumulated significantly higher amounts of succinate compared with pCMV6 controls (Fig. 3*d*), indicating that ectopic expression of CAD alone is sufficient to impact succinate levels. Collectively, these observations provide strong evidence that itaconate functions as metabolic trigger to modulate succinate levels.

Itaconate Is Not Metabolized to Succinate—One explanation for the above results could be that accumulated itaconate is metabolized to succinate directly or indirectly in macrophages. Indeed, *Pseudomonas* sp. can metabolize itaconate as a carbon

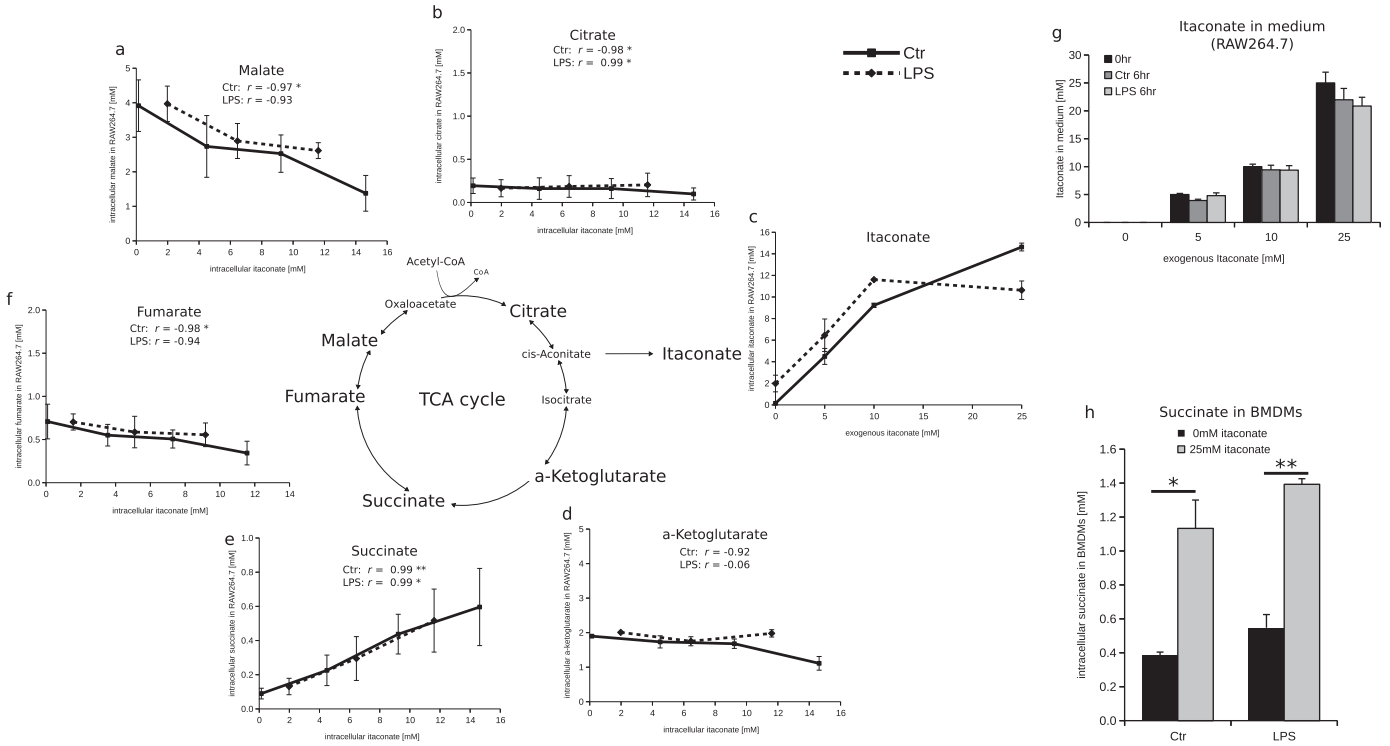

FIGURE 2. **Exogenous itaconate drives succinate accumulation.** Intracellular TCA cycle intermediate and itaconate quantification in resting (*Ctr*, *continuous line*) and LPS-activated (*LPS*, *dashed line*) RAW 264.7 macrophages after 6-h exposure to increasing extracellular itaconate concentrations (0, 5, 10, and 25 mM) (*a*, malate; *b*, citrate; *c*, itaconate; *d*, α-ketoglutarate; *e*, succinate; *f*, fumarate). Cells were exposed to 10 ng·ml^{-1} LPS for 6 h. Graphs represent the mean ± S.E. of intracellular metabolite concentrations [mM] of two repeated experiments, each with three biological replicates. Pearson correlation coefficient (*r*) represents correlation between intracellular itaconate and TCA cycle intermediate concentrations. *g*, medium itaconate levels of resting and LPS-activated RAW 264.7 macrophages (10 ng·ml^{-1} LPS) at 0 h (*black*) and after 6 h (*gray*). Data represent the mean ± S.E. of metabolite levels [mM] of three biological replicates. *h*, intracellular succinate quantification in resting and LPS-activated BMDMs after 6-h exposure to 0 mM (*black*) or 25 mM (*gray*) extracellular itaconate. Cells were exposed to 10 ng·ml^{-1} LPS for 6 h. Graphs represent the mean ± S.E. of succinate concentration [mM] obtained from two different mice, each with three biological replicates. *, $p < 0.05$; **, $p < 0.01$.

source through cleavage into pyruvate and acetyl-CoA (34), and a similar itaconate degradation pathway has been observed in isolated liver mitochondria (35). To exclude the possibility that degradation of itaconate to succinate occurs, we applied a [1-^{13}C]glutamine tracer to LPS-activated RAW 264.7 macrophages. During oxidative glutamine metabolism, decarboxylation of M1 α-ketoglutarate derived from this tracer results in M0 succinate. In contrast to the oxidative pathway, M1 α-ketoglutarate is converted to M1 isocitrate and citrate via reductive carboxylation (36), subsequently leading to M1 itaconate labeling. Thus, if itaconate is appreciably metabolized to succinate through the aforementioned degradation pathways, then we would detect significant labeling on succinate from this tracer (Fig. 4*a*). Although we observed high fractions of M1 itaconate isotopologues (~65%) because of itaconate production via reductive glutamine metabolism, no labeling was detected on succinate (Fig. 4*b*).

To further demonstrate that itaconate is not metabolized to succinate, we cultured ^{13}C-labeled resting and LPS-activated RAW 264.7 macrophages in the presence of 10 mM unlabeled itaconate and quantified succinate labeling. We exposed cells to labeled [U-$^{13}C_6$]glucose and [U-$^{13}C_5$] glutamine tracers over a period of three subcultures to obtain adequate isotope enrichment in succinate pools (Fig. 4*c*). Because labeling of succinate after exposure to exogenous, unlabeled itaconate was unchanged (even in the physiological concentration used here) (Fig. 4*d*), these data therefore confirm that itaconate is not metabolized to succinate in these mammalian cells.

Itaconate Inhibits SDH—Although enhanced flux through succinate-producing pathways from glutamine or glucose is likely contributing to its accumulation in inflammatory cells, our results suggest that itaconate degradation does not occur. An alternative mechanism through which endogenous itaconate could influence succinate levels is through inhibition of SDH/complex II. Indeed, *in vitro* enzyme activity assays using isolated SDH and respiratory studies have indicated that itaconate can reduce the activity of SDH (27, 28, 37). Mammalian CAD is localized to mitochondria in murine macrophages (38); therefore, itaconate production within or near this compartment could modulate SDH activity and, subsequently, succinate levels. To investigate the potential for itaconate to act as an SDH inhibitor, we measured mitochondrial respiration in permeabilized murine RAW 264.7 macrophages and BMDMs. First, we exposed permeabilized macrophages to increasing itaconate concentrations (0–25 mM) in the presence of two different succinate concentrations (2.5 and 10 mM) with 2 μM rotenone. Succinate is the substrate for complex II (SDH) of the mitochondrial respiratory chain, whereas rotenone was used to inhibit complex I and to prevent accumulation of the SDH inhibitor oxaloacetate (39), enabling us to directly measure maximal SDH-driven respiration. We observed a dose depen-

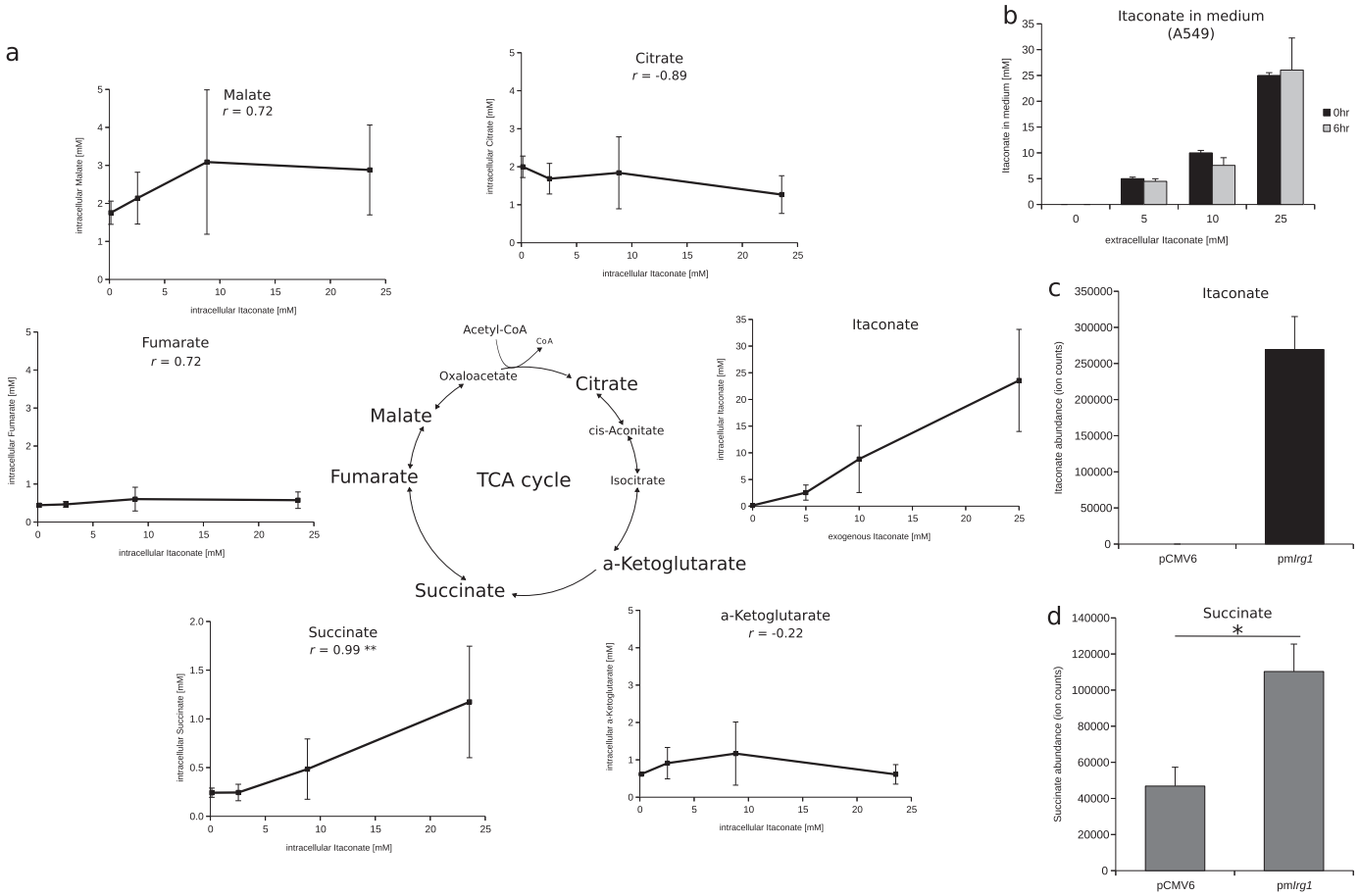

FIGURE 3. **Itaconate- and *Irg1*-induced succinate accumulation is not specific to immune cells.** *a*, intracellular itaconate and succinate levels increase in A549 lung adenocarcinoma cells after exposure to increasing exogenous itaconate concentrations (0, 5, 10, and 25 mM). Data represent the mean ± S.E. of metabolite levels [mM] of two repeated experiments with each three biological replicates. *b*, itaconate levels in medium after 6 h (*gray*) are not significantly affected compared with 0 h (*black*). Data represent the mean ± S.E. of metabolite levels of two repeated experiments with three biological replicates each. *c* and *d*, intracellular levels of itaconate (*c*, *black*) and succinate (*d*, *gray*) increased in *Irg1* overexpression A549 cells after transient transfection with murine pCMV6-*Irg1* overexpression (*pmIrg1*) plasmid compared with empty pCMV6-Entry (*pCMV6*) control plasmid. *Error bars* represent the intracellular metabolite levels (ion counts) 24 h after transfection of three biological replicates (mean ± S.E.). *, $p < 0.05$; **, $p < 0.01$.

dent inhibition of OCRs by itaconate in RAW 264.7 macrophages (Fig. 5*a*) and BMDMs (Fig. 5*b*), suggesting a regulatory role of itaconate for SDH activity. When the succinate concentration was lowered to 2.5 mM, itaconate had a greater proportional inhibitory effect. Considering the structural similarity of succinate to itaconate (also known as methylene succinate), our data suggest that itaconate acts as a competitive SDH inhibitor in immune cells, similar to the mechanisms described previously for the inhibition of purified SDH (27) and purified isocitrate lyase (22).

Next, to confirm that itaconate specifically inhibits SDH rather than other mitochondrial pathways, we offered permeabilized RAW 264.7 macrophages various oxidizable substrates and compared the maximal uncoupler-stimulated OCR in the presence of 0 and 10 mM itaconate (Fig. 5*c*). As expected, itaconate supplementation significantly reduced respiration (>75%) in the presence of succinate (SDH substrate) and rotenone (complex I inhibitor). On the other hand, oxygen consumption rates in permeabilized cells in the presence of either pyruvate with malate or glutamate with malate, substrates that drive respiration via complex I activity, were not affected by itaconate supplementation. Additionally, ascorbate and TMPD were used to supply electrons for complex IV activity in the presence of antimycin A, an inhibitor of complex III. Itaconate also failed to impact this complex IV-mediated respiration. Together, these data provide evidence that itaconate contributes to succinate accumulation in macrophages by acting as an endogenous SDH inhibitor.

Loss of Irg1 Influences Succinate Levels in BMDMs—To determine how succinate levels are affected in the absence of endogenously produced itaconate, we analyzed BMDMs derived from *Irg1* KO mice. We confirmed that *Irg1* mRNA was not expressed in LPS-stimulated KO-derived BMDMs (Fig. 6*a*). Consistent with this result, LPS-stimulated BMDMs from *Irg1* KO mice failed to produce significant levels of itaconate (Fig. 6*b*). Notably, succinate concentrations in stimulated BMDMs from *Irg1* KO mice were significantly lower than those quantified in BMDMs from WT mice, suggesting that CAD-derived itaconate influences succinate accumulation in LPS-induced macrophages (Fig. 6*c*).

These results provide evidence that *Irg1*-mediated itaconate production plays a role in succinate accumulation within immune cells. Taken together, our data highlight a mechanistic function of itaconate whereby this metabolite acts as a SDH

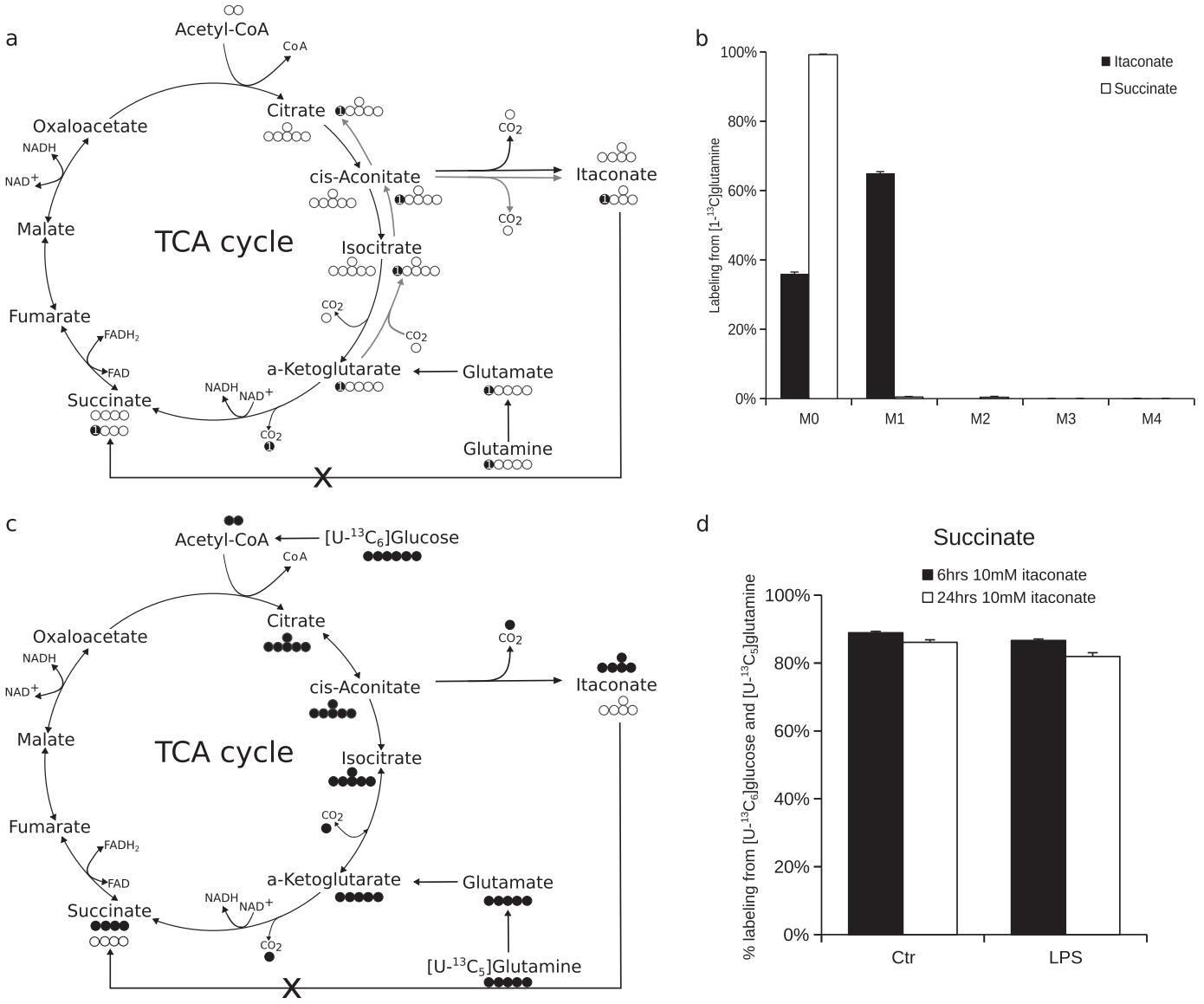

FIGURE 4. **Itaconate is not metabolized to succinate in RAW 264. 7 macrophages.** *a*, carbon labeling indicating oxidative (*black lines*) and reductive (*gray lines*) glutamine metabolism using [1-^{13}C]glutamine. Labeled itaconate (M1) is only synthesized through reductive glutamine metabolism (*gray*), and if it is metabolized to succinate, then it would result in succinate containing one labeled carbon (M1). *b*, mass isotopomer distribution of itaconate (*black*) and succinate (*white*) of LPS-activated RAW 264.7 macrophages after 24-h exposure to [1-^{13}C]glutamine tracer and 6-h exposure to 10 ng·ml^{-1} LPS. The major fraction of labeled itaconate contains one labeled carbon, whereas no labeling was found on succinate. *Error bars* represent the mean ± S.E. of mass isotopomer levels of three biological replicates. *c*, carbon labeling of TCA cycle intermediates using [U-$^{13}C_6$]glucose and [U-$^{13}C_5$]glutamine tracers. If exogenous, unlabeled itaconate is metabolized to succinate, then labeling would decrease but does not here. *d*, mass isotopomer distribution of succinate in resting and LPS-activated RAW 264.7 macrophages after 6-h (*black*) and 24-h (*gray*) exposure to exogenous, unlabeled itaconate remains ~90%, indicating that itaconate is not metabolized to succinate. Cells were prelabeled with [U-$^{13}C_6$]glucose and [U-$^{13}C_5$]glutamine over a period of three subcultures. *Error bars* represent the mean ± S.E. of mass isotopomer levels of three biological replicates.

inhibitor to influence TCA cycle metabolism by driving succinate accumulation (Fig. 7).

Discussion

Here we have demonstrated an important function of itaconate; it acts as a key regulatory metabolite to modulate TCA metabolism and succinate levels. In the cells studied, exogenous and endogenous, CAD-produced itaconate strongly correlated with succinate accumulation. Substrate-specific respirometry studies in permeabilized cells confirmed that itaconate acts as an SDH inhibitor. Finally, modulation of endogenous itaconate production in LPS-activated primary macrophages from *Irg1* KO mice reduces succinate levels. Thus, itaconate alters mitochondrial metabolism to influence succinate accumulation in macrophages (Fig. 7).

Numerous metabolic pathways have been implicated in the metabolic reprogramming of immune cells, in particular those that regulate succinate levels, which, in turn, can influence HIF signaling or other pathways (13, 25, 40, 41). Glutamine serves as a major carbon source for succinate production in LPS-activated macrophages via α-ketoglutarate or, alternatively, through the GABA shunt (9). A recent systems-based analysis of macrophages under proinflammatory conditions described key break points in TCA metabolism at isocitrate dehydroge-

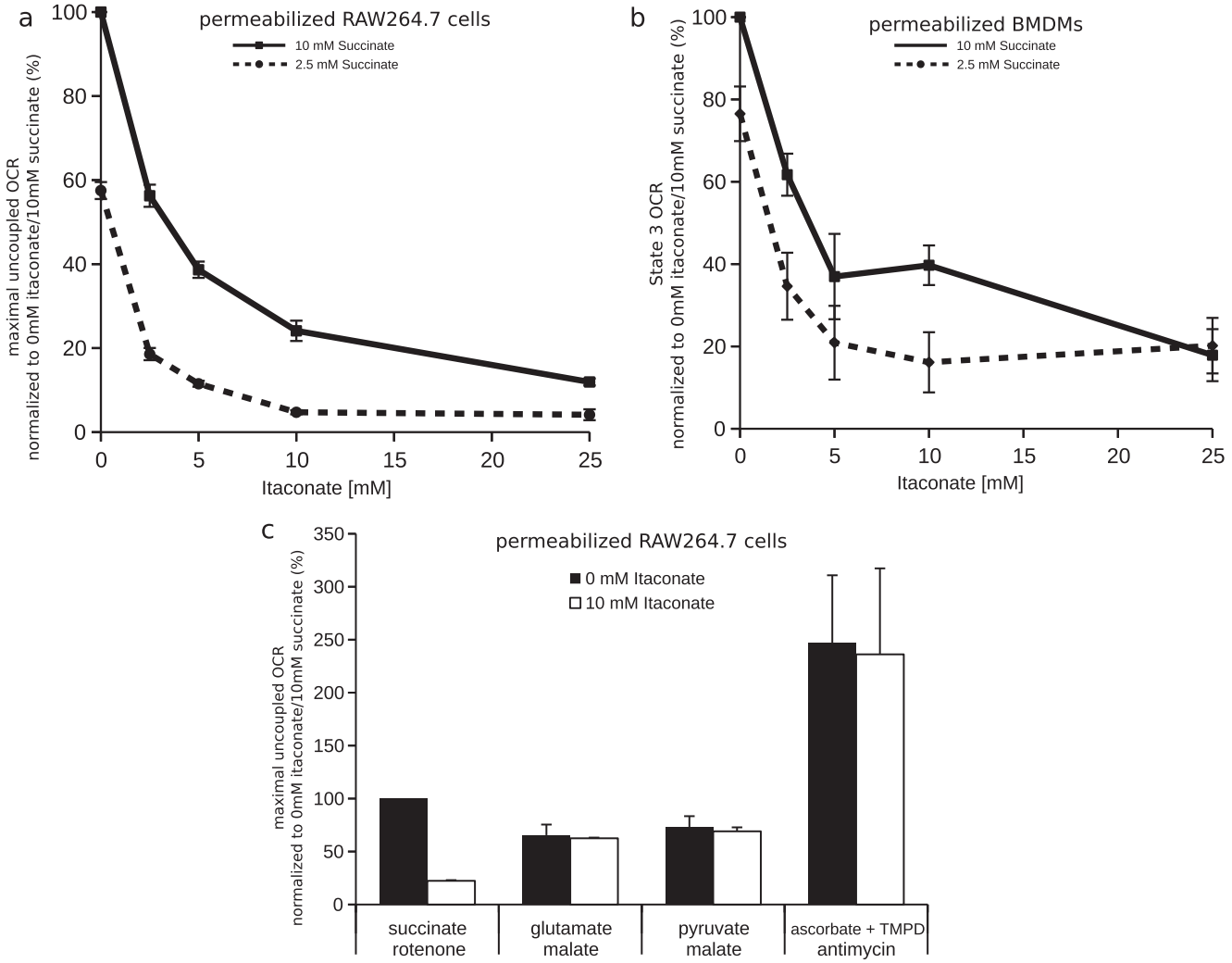

FIGURE 5. **Itaconate inhibits SDH.** *a* and *b*, itaconate inhibits the OCR in (*a*) RAW 264. 7 macrophages and (*b*) BMDMs in a dose-dependent manner. Shown are normalized OCRs of resting permeabilized cells exposed to increasing itaconate concentrations (0, 2.5, 5, 10, and 25 mM) with either 10 mM (*continuous line*) or 2.5 mM (*dashed line*) succinate. Data represent the mean ± S.E. of three repeated experiments. *c*, itaconate inhibits SDH of the respiratory chain. Shown is the normalized maximal uncoupled OCR of permeabilized resting RAW 264.7 macrophages exposed to various substrates in the presence of 0 mM (*black*) or 10 mM (*white*) itaconate. Data represent the mean ± S.E. of three repeated experiments normalized to conditions with 0 mM itaconate and 10 mM succinate.

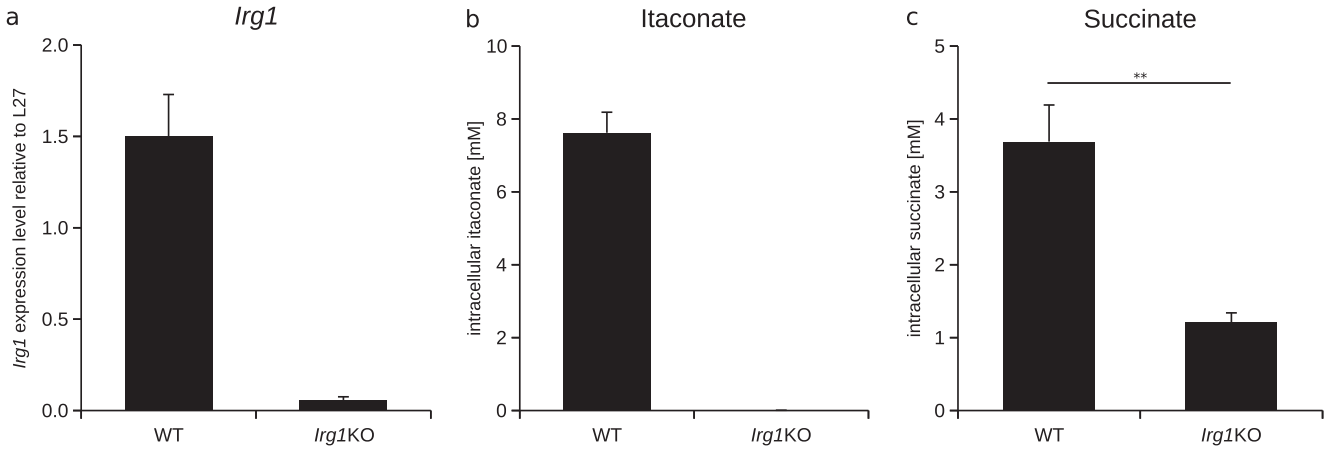

FIGURE 6. **Loss of *Irg1* decreases itaconate and succinate levels in *Irg1* KO BMDMs.** *a*, *Irg1* expression levels in LPS-activated (24 h, 10 ng·ml^{-1} LPS) BMDMs obtained from *Irg1* KO and WT mice. *Error bars* represent expression levels obtained from two independent mice (mean ± S.E.) relative to L27. *b* and *c*, itaconate and succinate levels in BMDMs obtained from *Irg1* KO and WT mice. Cells were activated for 6 h with 10 ng·ml^{-1} LPS. *Error bars* represent mean ± S.E. of metabolite levels [mM] of six biological replicates obtained from two independent mice.

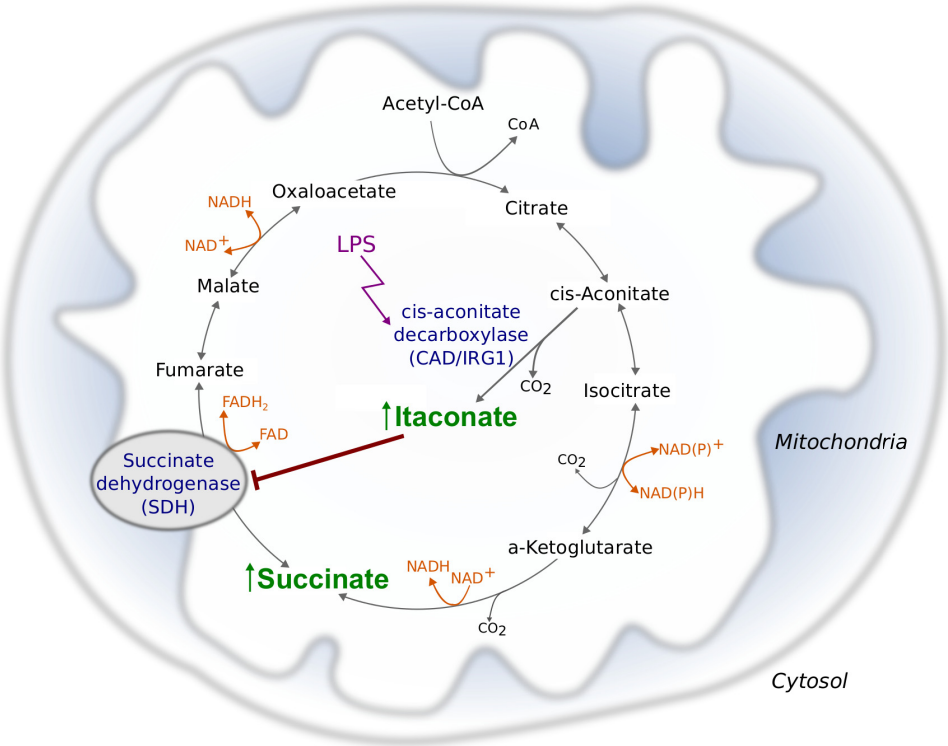

FIGURE 7. **Mechanism of LPS-induced succinate accumulation.** Under inflammatory conditions, such as LPS stimulation, mammalian CAD catalyzes the decarboxylation of the TCA cycle intermediate *cis*-aconitate to produce itaconate. This metabolite contributes to succinate accumulation in macrophages by acting as an endogenous SDH inhibitor.

nase and SDH (25). We have now identified a functional link between these nodes of the TCA cycle, where itaconate produced by mammalian CAD at the first break-point regulates SDH activity at the second break point. Within our analyses, we did observe variability in succinate accumulation upon LPS stimulation when comparing RAW 264.7 macrophages and BMDMs. This variance is in the range of succinate accumulation levels reported by others and is likely a function of cell, medium formulation, and LPS variability (9). However, we consistently observed increased succinate downstream of itaconate production or administration in a variety of cell types.

Succinate accumulation plays important roles during inflammation so that it contributes to the induction of *Il-1β* expression via HIF-1α stabilization (9). Our results suggest that *Irg1*-mediated itaconate production may influence downstream inflammatory responses in macrophages (*e.g.* expression of *Il-1β* or associated inflammatory genes). At present, it is not known whether this inflammatory response is accomplished directly by succinate or itaconate or mediated through other mechanisms. Succinate inhibits HIF-1α signaling through inhibition of PHD2 but can also impact the activity of numerous α-ketoglutarate-dependent dioxygenases (42, 43). As such, itaconate may have pleiotropic effects on cells depending on the expression, K_i, and compartment-specific impacts on succinate concentrations. However, the physiological role of itaconate and *Irg1* require further investigations, particularly in the context of macrophage development and differentiation. As noted above, various other pathways (*e.g.* GABA shunt, glutaminolysis) contribute to succinate synthesis in macrophages and could allow compensation (9, 13, 14). Intracellular signaling pathways also play key roles in macrophage polarization and likely sustain inflammation to some degree in the absence of *Irg1* (44).

Given the diverse effects of inflammation in human disease, the mechanistic interplay between itaconate and succinate is of clinical interest. Itaconate was only recently identified as an endogenous mammalian biochemical (19), and subsequent studies demonstrated that this molecule was produced by mammalian CAD activity on *cis*-aconitate (20). Itaconate reprograms the metabolism of pathogens, such as *Mycobacterium tuberculosis*, by inhibition of isocitrate lyase, a key enzyme in the glyoxylate shunt (45); thus, macrophages produce the antimicrobial metabolite itaconate to combat against invading pathogens (20). Following these discoveries, it has recently been speculated that itaconate might contribute to the function of innate immune cells (2, 46). Importantly, *IRG1* is induced by various non-bacterial stimuli, including influenza A viral infection (47), Marek disease infection (48), during embryonic implantation (49), neurotropic viral infections of neurons (50), and in murine epidermal cells (51). Given the regulatory role of itaconate in succinate accumulation described here, *IRG1*-mediated itaconate production may act as a signaling molecule in other inflammatory situations or cellular states. Indeed, succinate can inhibit various other α-ketoglutarate-dependent dioxygenases to impact diverse cellular processes (42, 43). On the other hand, the mechanism outlined here for SDH inhibition could be used to mitigate pathogenic inflammation under certain circumstances (*e.g.* via CAD inhibition). For example, high levels of succinate have also been reported to occur under ischemic conditions because of reverse SDH activity (40, 41). The accumulated succinate is rapidly oxidized after reperfu-

sion, resulting in increased mitochondrial reactive oxygen species production and damage. A similar mechanism has been speculated to occur during sepsis (52). Notably, SDH inhibition protected against brain injury after ischemia/reperfusion (40, 41), suggesting that inhibition of SDH by endogenously produced itaconate may buffer against potential oxidative damage that can occur under such conditions.

Our findings provide critical new insights into the regulatory machinery governing TCA cycle function, with mammalian CAD-produced itaconate serving as a metabolic inhibitor to cause succinate accumulation. Ultimately, these results may be clinically important when drugs that target such metabolic inflammatory signals are identified. The emerging role of itaconate as a regulatory molecule to reprogram immune cell metabolism provides an intriguing link between innate immunity, metabolism, and disease pathogenesis.

Author Contributions—T. C., M. W., K. H., and C. M. M. designed the research. A. S. D. and A. N. M. designed the oxygen consumption assays. T. C. performed the experiments and analyzed the data. T. C., M. W., and P. C. isolated primary BMDMs. H. K. derived the *Irg1* KO mice. A. M., C. S., and S. C. S. performed the experiments with Irg1 KO BMDMs. T. C. and C. M. M. wrote the manuscript.

Acknowledgments—We thank Gregory Fonseca and Rudi Balling for helpful discussions.

References

1. Akira, S., Uematsu, S., and Takeuchi, O. (2006) Pathogen recognition and innate immunity. *Cell* **124,** 783–801
2. Kelly, B., and O'Neill, L. A. (2015) Metabolic reprogramming in macrophages and dendritic cells in innate immunity. *Cell Res.* **25,** 771–784
3. Krawczyk, C. M., Holowka, T., Sun, J., Blagih, J., Amiel, E., DeBerardinis, R. J., Cross, J. R., Jung, E., Thompson, C. B., Jones, R. G., and Pearce, E. J. (2010) Toll-like receptor-induced changes in glycolytic metabolism regulate dendritic cell activation. *Blood.* **115,** 4742–4749
4. Pearce, E. L., and Pearce, E. J. (2013) Metabolic pathways in immune cell activation and quiescence. *Immunity* **38,** 633–643
5. Rodríguez-Prados, J.-C., Través, P. G., Cuenca, J., Rico, D., Aragonés, J., Martín-Sanz, P., Cascante, M., and Boscá, L. (2010) Substrate fate in activated macrophages: a comparison between innate, classic, and alternative activation. *J. Immunol.* **185,** 605–614
6. Kempf, V. A., Lebiedziejewski, M., Alitalo, K., Wälzlein, J.-H., Ehehalt, U., Fiebig, J., Huber, S., Schütt, B., Sander, C. A., Müller, S., Grassl, G., Yazdi, A. S., Brehm, B., and Autenrieth, I. B. (2005) Activation of hypoxia-inducible factor-1 in bacillary angiomatosis: evidence for a role of hypoxia-inducible factor-1 in bacterial infections. *Circulation* **111,** 1054–1062
7. Blouin, C. C., Pagé, E. L., Soucy, G. M., and Richard, D. E. (2004) Hypoxic gene activation by lipopolysaccharide in macrophages: implication of hypoxia-inducible factor 1α. *Blood* **103,** 1124–1130
8. Hellwig-Bürgel, T., Rutkowski, K., Metzen, E., Fandrey, J., and Jelkmann, W. (1999) Interleukin-1β and tumor necrosis factor-α stimulate DNA binding of hypoxia-inducible factor-1. *Blood* **94,** 1561–1567
9. Tannahill, G. M., Curtis, A. M., Adamik, J., Palsson-McDermott, E. M., McGettrick, A. F., Goel, G., Frezza, C., Bernard, N. J., Kelly, B., Foley, N. H., Zheng, L., Gardet, A., Tong, Z., Jany, S. S., Corr, S. C., *et al.* (2013) Succinate is an inflammatory signal that induces IL-1β through HIF-1α. *Nature* **496,** 238–242
10. Selak, M. A., Armour, S. M., MacKenzie, E. D., Boulahbel, H., Watson, D. G., Mansfield, K. D., Pan, Y., Simon, M. C., Thompson, C. B., and Gottlieb, E. (2005) Succinate links TCA cycle dysfunction to oncogenesis by inhibiting HIF-alpha prolyl hydroxylase. *Cancer Cell* **7,** 77–85
11. Epstein, A. C., Gleadle, J. M., McNeill, L. A., Hewitson, K. S., O'Rourke, J., Mole, D. R., Mukherji, M., Metzen, E., Wilson, M. I., Dhanda, A., Tian, Y. M., Masson, N., Hamilton, D. L., Jaakkola, P., Barstead, R., Hodgkin, J., Maxwell, P. H., Pugh, C. W., Schofield, C. J., and Ratcliffe, P. J. (2001) C. elegans EGL-9 and mammalian homologs define a family of dioxygenases that regulate HIF by prolyl hydroxylation. *Cell* **107,** 43–54
12. Losman, J.-A., and Kaelin, W. G., Jr. (2013) What a difference a hydroxyl makes: mutant IDH, (R)-2-hydroxyglutarate, and cancer. *Genes Dev.* **27,** 836–852
13. Mills, E., and O'Neill, L. A. (2014) Succinate: a metabolic signal in inflammation. *Trends Cell Biol.* **24,** 313–320
14. Palsson-McDermott, E. M., Curtis, A. M., Goel, G., Lauterbach, M. A., Sheedy, F. J., Gleeson, L. E., van den Bosch, M. W., Quinn, S. R., Domingo-Fernandez, R., Johnson, D. G., Jiang, J. K., Israelsen, W. J., Keane, J., Thomas, C., Clish, C., *et al.* (2015) Pyruvate kinase M2 regulates Hif-1α activity and IL-1β induction and is a critical determinant of the Warburg effect in LPS-activated macrophages. *Cell Metab.* **21,** 65–80
15. Wegner, A., Meiser, J., Weindl, D., and Hiller, K. (2015) How metabolites modulate metabolic flux. *Curr. Opin. Biotechnol.* **34,** 16–22
16. Bailey, E., Stirpe, F., and Taylor, C. B. (1968) Regulation of rat liver pyruvate kinase. The effect of preincubation, pH, copper ions, fructose 1,6-diphosphate and dietary changes on enzyme activity. *Biochem. J.* **108,** 427–436
17. Chaneton, B., Hillmann, P., Zheng, L., Martin, A. C., Maddocks, O. D., Chokkathukalam, A., Coyle, J. E., Jankevics, A., Holding, F. P., Vousden, K. H., Frezza, C., O'Reilly, M., and Gottlieb, E. (2012) Serine is a natural ligand and allosteric activator of pyruvate kinase M2. *Nature* **491,** 458–462
18. Chaneton, B., and Gottlieb, E. (2012) Rocking cell metabolism: revised functions of the key glycolytic regulator PKM2 in cancer. *Trends Biochem. Sci.* **37,** 309–316
19. Strelko, C. L., Lu, W., Dufort, F. J., Seyfried, T. N., Chiles, T. C., Rabinowitz, J. D., and Roberts, M. F. (2011) Itaconic acid is a mammalian metabolite induced during macrophage activation. *J. Am. Chem. Soc.* **133,** 16386–16389
20. Michelucci, A., Cordes, T., Ghelfi, J., Pailot, A., Reiling, N., Goldmann, O., Binz, T., Wegner, A., Tallam, A., Rausell, A., Buttini, M., Linster, C. L., Medina, E., Balling, R., and Hiller, K. (2013) Immune-responsive gene 1 protein links metabolism to immunity by catalyzing itaconic acid production. *Proc. Natl. Acad. Sci. U.S.A.* **110,** 7820–7825
21. Patel, T. R., and McFadden, B. A. (1978) *Caenorhabditis elegans* and *Ascaris suum*: inhibition of isocitrate lyase by itaconate. *Exp. Parasitol.* **44,** 262–268
22. Williams, J. O., Roche, T. E., and McFadden, B. A. (1971) Mechanism of action of isocitrate lyase from *Pseudomonas indigofera*. *Biochemistry* **10,** 1384–1390
23. McFadden, B. A., and Purohit, S. (1977) Itaconate, an isocitrate lyase-directed inhibitor in *Pseudomonas indigofera*. *J. Bacteriol.* **131,** 136–144
24. O'Neill, L. A. (2015) A broken Krebs cycle in macrophages. *Immunity* **42,** 393–394
25. Jha, A. K., Huang, S. C., Sergushichev, A., Lampropoulou, V., Ivanova, Y., Loginicheva, E., Chmielewski, K., Stewart, K. M., Ashall, J., Everts, B., Pearce, E. J., Driggers, E. M., and Artyomov, M. N. (2015) Network integration of parallel metabolic and transcriptional data reveals metabolic modules that regulate macrophage polarization. *Immunity* **42,** 419–430
26. Booth, A. N., Taylor, J., Wilson, R. H., and Deeds, F. (1952) The inhibitory effects of itaconic acid *in vitro* and *in vivo*. *J. Biol. Chem.* **195,** 697–702
27. Ackermann, W. W., and Potter, V. R. (1949) Enzyme inhibition in relation to chemotherapy. *Proc. Soc. Exp. Biol. Med.* **72,** 1–9
28. Dervartanian, D. V., and Veeger, C. (1964) Studies on succinate dehydrogenase: I: spectral properties of the purified enzyme and formation of enzyme-competitive inhibitor complexes. *Biochim. Biophys. Acta.* **92,** 233–247
29. Raschke, W. C., Baird, S., Ralph, P., and Nakoinz, I. (1978) Functional macrophage cell lines transformed by Abelson leukemia virus. *Cell* **15,** 261–267
30. Giard, D. J., Aaronson, S. A., Todaro, G. J., Arnstein, P., Kersey, J. H., Dosik, H., and Parks, W. P. (1973) *In vitro* cultivation of human tumors: estab-

lishment of cell lines derived from a series of solid tumors. *J. Natl. Cancer Inst.* **51,** 1417–1423
31. Zhang, X., Goncalves, R., and Mosser, D. M. (2008) The isolation and characterization of murine macrophages. *Curr. Protoc. Immunol.* Chapter 14, Unit 14.1
32. Divakaruni, A. S., Rogers, G. W., and Murphy, A. N. (2014) Measuring mitochondrial function in permeabilized cells using the Seahorse XF analyzer or a Clark-type oxygen electrode. *Curr. Protoc. Toxicol.* **60,** 25.2.1–25.2.16
33. R Core Team (2013). *R: A language and environment for statistical computing*, R Foundation for Statistical Computing, Vienna, Austria
34. Cooper, R. A., and Kornberg, H. L. (1964) The utilization of itaconate by *Pseudomonas* sp. *Biochem. J.* **91,** 82–91
35. Adler, J., Wang, S.-F., and Lardy, H. A. (1957) The metabolism of itaconic acid by liver mitochondria. *J. Biol. Chem.* **229,** 865–879
36. Metallo, C. M., Gameiro, P. A., Bell, E. L., Mattaini, K. R., Yang, J., Hiller, K., Jewell, C. M., Johnson, Z. R., Irvine, D. J., Guarente, L., Kelleher, J. K., Vander Heiden, M. G., Iliopoulos, O., and Stephanopoulos, G. (2012) Reductive glutamine metabolism by IDH1 mediates lipogenesis under hypoxia. *Nature* **481,** 380–384
37. Németh, B., Doczi, J., Csete, D., Kacso, G., Ravasz, D., Adams, D., Kiss, G., Nagy, A. M., Horvath, G., Tretter, L., Mócsai, A., Csépányi-Kömi, R., Iordanov, I., Adam-Vizi, V., and Chinopoulos, C. (2015) Abolition of mitochondrial substrate-level phosphorylation by itaconic acid produced by LPS-induced Irg1 expression in cells of murine macrophage lineage. *FASEB J.* 10.1096/fj.15–279398
38. Degrandi, D., Hoffmann, R., Beuter-Gunia, C., and Pfeffer, K. (2009) The proinflammatory cytokine-induced IRG1 protein associates with mitochondria. *J. Interferon Cytokine Res.* **29,** 55–67
39. Wojtczak, L., Wojtczak, A. B., and Ernster, L. (1969) The inhibition of succinate dehydrogenase by oxaloacetate. *Biochim. Biophys. Acta* **191,** 10–21
40. Chouchani, E. T., Pell, V. R., James, A. M., Work, L. M., Saeb-Parsy, K., Frezza, C., Krieg, T., and Murphy, M. P. (2016) A unifying mechanism for mitochondrial superoxide production during ischemia-reperfusion injury. *Cell Metab.* **23,** 254–263
41. Chouchani, E. T., Pell, V. R., Gaude, E., Aksentijević, D., Sundier, S. Y., Robb, E. L., Logan, A., Nadtochiy, S. M., Ord, E. N. J., Smith, A. C., Eyassu, F., Shirley, R., Hu, C.-H., Dare, A. J., James, A. M., *et al.* (2014) Ischaemic accumulation of succinate controls reperfusion injury through mitochondrial ROS. *Nature* **515,** 431–435
42. Xiao, M., Yang, H., Xu, W., Ma, S., Lin, H., Zhu, H., Liu, L., Liu, Y., Yang, C., Xu, Y., Zhao, S., Ye, D., Xiong, Y., and Guan, K.-L. (2012) Inhibition of α-KG-dependent histone and DNA demethylases by fumarate and succinate that are accumulated in mutations of FH and SDH tumor suppressors. *Genes Dev.* **26,** 1326–1338
43. Metallo, C. M., and Vander Heiden, M. G. (2013) Understanding metabolic regulation and its influence on cell physiology. *Mol. Cell* **49,** 388–398
44. Sica, A., and Mantovani, A. (2012) Macrophage plasticity and polarization: *in vivo veritas*. *J. Clin. Invest.* **122,** 787–795
45. Eoh, H., and Rhee, K. Y. (2014) Methylcitrate cycle defines the bactericidal essentiality of isocitrate lyase for survival of *Mycobacterium tuberculosis* on fatty acids. *Proc. Natl. Acad. Sci. U.S.A.* **111,** 4976–4981
46. Cordes, T., Michelucci, A., and Hiller, K. (2015) Itaconic acid: the surprising role of an industrial compound as a mammalian antimicrobial metabolite. *Annu. Rev. Nutr.* **35,** 451–473
47. Preusse, M., Tantawy, M. A., Klawonn, F., Schughart, K., and Pessler, F. (2013) Infection- and procedure-dependent effects on pulmonary gene expression in the early phase of influenza A virus infection in mice. *BMC Microbiol.* **13,** 293
48. Smith, J., Sadeyen, J.-R., Paton, I. R., Hocking, P. M., Salmon, N., Fife, M., Nair, V., Burt, D. W., and Kaiser, P. (2011) Systems analysis of immune responses in Marek's disease virus-infected chickens identifies a gene involved in susceptibility and highlights a possible novel pathogenicity mechanism. *J. Virol.* **85,** 11146–11158
49. Cheon, Y.-P., Xu, X., Bagchi, M. K., and Bagchi, I. C. (2003) Immune-responsive gene 1 is a novel target of progesterone receptor and plays a critical role during implantation in the mouse. *Endocrinology.* **144,** 5623–5630
50. Cho, H., Proll, S. C., Szretter, K. J., Katze, M. G., Gale, M., Jr., and Diamond, M. S. (2013) Differential innate immune response programs in neuronal subtypes determine susceptibility to infection in the brain by positive-stranded RNA viruses. *Nat. Med.* **19,** 458–464
51. Hall, C. J., Boyle, R. H., Sun, X., Wicker, S. M., Misa, J. P., Krissansen, G. W., Print, C. G., Crosier, K. E., and Crosier, P. S. (2014) Epidermal cells help coordinate leukocyte migration during inflammation through fatty acid-fuelled matrix metalloproteinase production. *Nat. Commun.* **5,** 3880
52. Bar-Or, D., Carrick, M. M., Mains, C. W., Rael, L. T., Slone, D., and Brody, E. N. (2015) Sepsis, oxidative stress, and hypoxia: are there clues to better treatment? *Redox Rep.* **20,** 193–197

COMPARING AND CONTRASTING METABOLISM AND CYTOKINE EXPRESSION DURING THE EARLY STAGES OF INFLAMMATION IN CELL LINES AND PRIMARY MACROPHAGES

Sapcariu SC, Wolf C, Delcambre S, Krämer L, Dong X, Schneider J, Hiller, K *To Be Submitted*. **2016**.

This study compares and contrasts cell lines and primary mouse macrophages, in order to better understand their utility and limitations for scientific studies into inflammatory processes. Metabolic and transcriptional changes were looked at over the initial stage of an common inflammatory stimulus. It was found that while both cell types are somewhat comparable in terms of cytokine regulation and antimicrobial activity, basal metabolism is changed in the transformed cell line, and this should be taken into account when looking at metabolic changes based on inflammation in macrophage cell lines.

For this study, I conceived the idea and performed all experiments (with the assistance of the other co-authors), as well as performed all data analysis and wrote the manuscript.

Comparing and contrasting metabolism and cytokine expression during the early stages of inflammation in cell lines and primary macrophages

Sean C. Sapcariu Cristina Wolf Sylvie Delcambre
Lisa Krämer Xiangyi Dong Jochen Schneider
Karsten Hiller

Abstract

Inflammation is a cellular process designed to rid the body of pathogens and repair damaged tissue, and requires a time-resolved set of steps in order to facilitate this activity. One of the main cell types involved in the inflammatory process are macrophages, and these cells are widely studied in laboratory settings using a variety of cell lines as well as primary cells from both mice and humans. Macrophage research has uncovered a wealth of important information about regulation of this process from mRNA levels and metabolic changes. In this study, we compared one of the most common mouse macrophage cell lines, RAW 264.7, with bone marrow derived macrophages, using a series of time course experiments to determine transcriptional and metabolic changes of these cells when stimulated to a pro-inflammatory phenotype. While both cell types had active pro-inflammatory pathways leading to cytokine expression and bacterial clearance, changes in the metabolic program (most likely due to *HIF-1α* expression) could only be observed in the differentiated primary macrophages. The results of this study illuminate two important factors of macrophage research: 1) the appropriate cell type to use for a study depends on the scientific question asked, and 2) there is a time-dependent cascade of early-stage inflammation in macrophages, and this should be taken into account when trying to understand the process.

1 Abstract

Introduction

The innate immune response in mammals acts as the first line of defense against external pathogens, utilizing processes such as the inflammatory response in order to remove infectious threats before they cause significant damage to the host. Inflammation is a tightly controlled process that follows a time-resolved set of actions in order to destroy pathogens and repair damaged tissue in an effective and quick manner (Medzhitov, 2008). Improper regulation of the inflammatory process has been implicated in a variety of diseases, including diabetes,

neurodegenerative diseases, and cancer (Eizirik et al., 2009; Amor et al., 2010; Coussens and Werb, 2002). One of the main cell types responsible for regulating the inflammatory response are macrophages, a type of mononuclear cell that is derived from bone marrow, but can both circulate through the body and natively reside in all non-brain tissues (Murray and Wynn, 2011). During infection, macrophages are recruited to the site of the inflammatory response to assist with phagocytosis and bacterial removal, maintain homeostasis through the cleanup of internal antigens, and act as the interface between the innate and adaptive immune responses (Murray and Wynn, 2011). Macrophages recognize pathogen-associated molecular patterns (PAMPs) and damage-associated molecular patterns (DAMPs) through transmembrane Toll-like receptors (TLRs) (Seong and Matzinger, 2004), activating signaling cascades that initiate the inflammatory response and subsequent reprogramming of the cell (Zhang and Mosser, 2008).

In laboratory settings, the bacterial PAMP lipopolysaccharide (LPS) is often used to stimulate macrophages to a pro-inflammatory state. LPS is a component of the Gram-negative bacterial surface membrane and is recognized by macrophage TLR4 and CD14 surface receptors, inducing a cascade that results in the expression of cytokines (such as *Il-1β*, *Tnfα*, and *Il-6*) and a transformation into a pro-inflammatory phenotype (often called the M1 or M(LPS) state) (Mosser and Edwards, 2008). Pro-inflammatory macrophages have increased bactericidal activity and endocytosis, and it is these characteristics which aggressively remove pathogens through processes that can also create tissue damage, while anti-inflammatory macrophages (often called the M2 state) are involved in wound healing and regulatory processes (Mosser and Edwards, 2008). The process of inflammation is commonly thought to have different stages with regards to macrophage activity, which would suggest that the activation and phenotype of pro-inflammatory macrophages changes as inflammation proceeds. While there has been a good deal of study about the transcriptional regulation of inflammation in macrophages (see review in Medzhitov and Horng (2009)), we could find no study that looked at time-dependent regulation of inflammatory cytokines.

Traditionally, pro-inflammatory macrophages are classified through their activity and cytokine release profiles. However, it has recently been shown that there are metabolic changes that occur in a pro-inflammatory macrophage which are just as important to their activity, and are interconnected with cytokine production. Succinic acid, a metabolite in the TCA cycle, is increased under LPS stimulation, and has been shown to stabilize hypoxia-inducible factor 1-alpha (HIF-1α), an important transcription factor and regulator of metabolic activity and cytokine production, to enhance *Il-1β* production (Tannahill et al., 2013). Another important metabolite which is produced in macrophages only when stimulated to a pro-inflammatory state is itaconic acid. This metabolite is produced in the mitochondria through the activity of cis-aconitate decarboxylase (CAD, encoded by immunoresponsive gene 1 - *Irg1*) using cis-aconitate as a substrate, and acts as a bacteriostatic antimicrobial by inhibiting isocitrate lyase (Michelucci et al., 2013). Through the combined use of network analysis and stable isotope labeling experiments, Jha *et al* identified two metabolic breakpoints in the TCA cycle of pro-inflammatory macrophages, which lead to the accumulation of succinic acid and itaconic acid (Jha et al., 2015). Furthermore, itaconic acid was shown to inhibit succinate dehydrogenase activity, leading to the buildup of succinic acid in LPS-stimulated macrophages. Indeed,

metabolism is more than an endpoint of transcriptional changes arising from macrophage activation, it instead is interwoven in the regulating of inflammatory activity while at the same time producing the means to defend against microbial invasion.

The study of pro-inflammatory macrophage activity in laboratory settings requires access to macrophage cells that can be manipulated and experimented upon. As in most areas of cellular biology, there exist both primary cells and immortalized cell lines for this purpose. RAW 264.7 cells are a Abelson Leukaemia Virus transformed mouse macrophage-like cell line which is widely used for *in vitro* studies of macrophage response under inflammatory conditions (Tannahill et al., 2013; Michelucci et al., 2013; Meiser et al., 2015). They have the advantage of being easy to cultivate and handle in a laboratory setting, and are seen as consistent and comparable between experiments and laboratories. Much of the knowledge about pro-inflammatory macrophage activation has been obtained using this cell line, and has proven to be transferable to *in vivo* systems. It is important to note that these cells have been transformed to be continuously proliferative, and this must be taken into account when making conclusions about cellular processes for macrophages in general.

Bone marrow derived macrophages (BMDMs) are differentiated macrophages obtained through the culture of mammalian bone marrow, typically from *Mus musculus*. Cells from bone marrow are differentiated using either pure granulocyte macrophage colony-stimulating factor (GM-CSF), or supernatant from the culture of the L929 mouse fibroblast cell line, which also produces GM-CSF in combination with other factors which promote macrophage differentiation Francke et al. (2011); Boltz-Nitulescu et al. (1987). As this cell model comes directly from an individual animal without any transformations, it is considered to be a more applicable model for translating experimental results to what is actually occurring in nature. However, primary cells such as BMDMs can be highly variable between animals, and are much more costly to obtain and work with. It is thus important to understand both the similarities between the cell line and the primary cell as well as the limitations of substituting one for the other. Previous studies have compared RAW cells to BMDMs with regard to cytokine expression, cell surface markers, and culture ability on different biomaterial surfaces, determining that cell lines respond differently to LPS than BMDMs, with different cytokine response profiles and surface marker populations (Berghaus et al., 2010; Chamberlain et al., 2009). In addition, there has been research into how cellular energy sources are taken up and metabolic products secreted over time in activated RAW cells and BMDMs, suggesting that activated macrophages are glycolitic cells, with RAW cells utilizing glycolysis to a greater extent than the BMDMs (Rodríguez-Prados et al., 2010). However, there have not been any studies directly comparing RAW cells and BMDMs with regards to the timing of cytokine production or intracellular metabolic changes.

This work presents a targeted integration of metabolomics, stable isotope labeled analysis, and RNA expression in order to profile metabolism in the short-term response after LPS stimulation (as a model pro-inflammatory stimulus). Concurrently, we want to highlight the benefits and weaknesses of using RAW cells as a substitute model for primary mouse macrophages in the study of inflammation. A clearly regulated short-term response to a pro-inflammatory stimulation in terms of classical inflammatory transcriptional and metabolic markers can be seen on in both RAW cells and BMDMs, and while the pat-

terns of regulation are similar, the scale differs between the cell types. At the same time, there are metabolic differences between primary cells and cell line macrophages, as the transcriptional changes allowing RAW cells to act as an immortalized cell line mask the metabolic changes that occur during the initial inflammatory response in primary macrophages.

Materials and Methods

Cell culture and reagents

The mouse macrophage RAW 264.7 cell line was obtained from ATCC (ATCC TIB-71, Manassas, VA, USA). Cells were cultured in Dulbecco's Modified Eagle's Medium (DMEM) 5796 (Sigma Aldrich) with 10% Fetal Bovine Serum (PAA or Invitrogen) and 1% penicillin/streptomycine (Gibco, Invitrogen), and stored in an incubator with humidified atmosphere at 37°C with 5% CO_2. Cells were grown and cultured in cell culture flasks (Thermo Fisher Scientific), and split through scraping three times a week.

Bone marrow was extracted from femur and tibia of 8-weeks old C57BL/6 mice, and cultured for 7 days in the same conditions as above, using Roswell Park Memorial Institute medium (RPMI) 1640 VLE (Merck Millipore) supplemented with 10% Fetal Bovine Serum and 20% L929 cell culture supernatant. Cells were detached by scraping, and cell seeding and experiments were performed using RPMI as defined without added L929 supernatant.

Escherichia coli purified LPS (Sigma Aldrich) was used to stimulate macrophages into a pro-inflammatory state, using 10 ng/mL and 100 ng/mL for RAW cells and BMDMs respectively. Concentrations for experiments follow commonly used concentrations in the literature.

Stable isotope labeling experiments

For stable isotope labeling experiments, cells were cultured as above, but were seeded in a labeled medium 24 hours before treatment.

RAW cells were seeded in Dulbecco's Modified Eagle's Medium (D5030, Sigma Aldrich), supplemented with 3.7 g/L of sodium bicarbonate and 10% dialyzed fetal bovine serum. 25 mmol/L glucose and 5 mmol/L glutamine were also supplemented in the medium. For labeled glucose experiments, [U-$^{13}C_6$]-Glucose (Cambridge Isotope Laboratories) was substituted, and for labeled glutamine experiments, [U-$^{13}C_5$]-Glutamine (Campro Scientific) was substituted. The pH of the finished medium was adjusted to 7.4, sterile filtered through a 0.22 µm Steriflip filter unit (Merck Millipore), and stored at 4°C until use.

For BMDMs, RPMI 1640 was used, which contained either no glucose or no glutamine. For labeled glucse experiments, 11 mmol/L of [U-$^{13}C_6$]-Glucose (Cambridge Isotope Laboratories) was used, and for labeled glutamine experiments, 2 mmol/L of [U-$^{13}C_5$]-Glutamine (Campro Scientific) was used. The medium was pH adjusted and sterile filtered in the same manner as above.

Metabolite extraction protocol

The extraction protocol was performed as per Sapcariu et al. (2014). Briefly, cells were washed with 0.9% NaCl, and immediately quenched with 200 µL

Chromasolv® Methanol (Sigma) at -20°C and 200 µL Millipore H_2O on ice. Cell extracts were scraped and added to Eppendorf reaction tubes containing 200 µL Chromasolv® chloroform at -20°C. Tubes with extract were then vortexed in a 4°C Thermomixer Eppendorf shaker at 1400 rpm for 20 minutes and centrifuged at 4°C for 5 minutes at 20,000 g. 200 µL of the polar phase was transfered to a glass vial specific for GC-MS analysis (Chromatographie Zubehor Trott), dried in a rotary vacuum evaporator (Labconco) at -4°C overnight, and stored at -80°C until analysis. The interphase was stored at -80°C until RNA extraction. As an internal standard, pentanedioic-d_6 acid was added to the extraction water at a concentration of 1 µg/mL.

GC-MS Analysis

Derivitization was performed with an Gerstel autosampler directly before measurement on a gas chromotography-mass spectrometry instrument (GC-MS). Dried metabolites were dissolved in 15 µL of 2% methoxyamine hydrochloride in pyridine at a temperature of 40°C for 90 minutes. 15 µL of 2,2,2-trifluoro-N-methyl-N-trimethylsilyl-acetamide + 1% chloro-trimethyl-silane was added and incubated at 55°C for 60 minutes.

The metabolite extracts were measured on an Agilent 7890A GC containing with a 30 m DB-35MS capillary column. The GC was connected to an Agilent 5975C MS operating in electron ionization (EI) at 70 eV.

1 µL of derivatized sample was hot injected into a split/splitless inlet at 270°C in splitless mode. Helium was used as the carrier gas at a flow rate of 1 mL/min. The GC oven temperature was kept constant at 100°C for 2 minutes and then increased to 300°C at 10°C/min, where it was held for 4 minutes. The total GC-MS run time of one sample was 26 minutes. For relative quantification of metabolite levels, an alkane mix was run with the sequence in order to provide retention index calibration for the experimental samples.

The MS source was kept at a constant temperature of 230°C and the quadrupole at 150°C. For relative quantification of metabolite levels, the detector was operated in scan mode with an m/z range of 70 to 800. For analysis of stable isotope labeling, the detector was operated in SIM mode with specific ions selected for all compounds of interest.

mRNA extraction and Quantitative Real-Time PCR

Washed interphases were dried in a rotary vacuum evaporator (Labconco) at 4°C until all liquid phase was evaporated, and then brought to room temperature. RNA was extracted from the interphase of the samples using the Qiagen RNeasy minikit following manufacturer's instructions, and RNA purity was checked on a Thermo Scientific NanoDrop 2000C spectrophotometer. RNA was reverse transcribed into cDNA using Invitrogen SuperScript™ III reverse transcriptase following manufacturer's instructions, and stored at -20°C until qPCR analysis. All treatments were performed in experimental triplicates and technical duplicates on the 96-well plate for statistical robustness.

Analysis of cDNA was performed on a Roche LightCycler 480 II, with iQ™ SYBR® green supermix including the fluorescent pigment and the polymerase required for the reactions. The program for the qPCR was as follows: activation of the polymerase for 3 minutes at 95°C, 40 amplification cycles (30 seconds

denaturation at 95°C, 30 seconds annealing at 60°C, 30 seconds elongation at 72°C), melting curve analysis, and a cooling step at 40°C. Comparative quantification (using the ΔΔCt method) was performed using LibreOffice Calc. The primers used in qPCR analysis are shown in 1.

Table 1: Primers used for qPCR Analysis

Il-1b forward	5'-GCTTCAGGCAGGCAGTATC-3'
Il-1b reverse	5'-AGGATGGGCTCTTCTTCAAAG-3'
Tnfα forward	5'-GGTTCTGTCCCTTTCACTCAC-3'
Tnfα reverse	5'-TGCCTCTTCTGCCAGTTCC-3'
Il6 forward	5'-CGGCCTTCCCTACTTCACAA-3'
Il6 reverse	5'-TCTGCAAGTGCATCATCGTT-3'
Irg1 forward	5'-GCAACATGATGCTCAAGTCTG-3'
Irg1 reverse	5'-TGCTCCTCCGAATGATACCA-3'
Hif-1 forward	5'-TGACGGCGACATGGTTTACA-3'
Hif-1 reverse	5'-AATATGGCCCGTGCAGTGAA-3'
Pdk1 forward	5'-TGCAAAGTTGGTATATCCAAAGCC-3'
Pdk1 reverse	5'-ACCCCGAAGCTCTCCTTGTA-3'
Idh1 forward	5'-AAGGTTATGGCTCCCTTGGC-3'
Idh1 reverse	5'-TAGTGACGTGTGACAGTGCC-3'
Idh2 forward	5'-TTCCAAACCGTGACCAGACC-3'
Idh2 reverse	5'-GGATCGTTCCGTTAGGGCTC-3'
Idh3 forward	5'-GAGTACGCTCGGAACAACCA-3'
Idh3 reverse	5'-AGTTCTCCGCAACTTCCCTG-3'
L27 forward	5'-ACATTGACGATGGCACCTC-3'
L27 reverse	5'-GCTTGGCGATCTTCTTCTTG-3'

Metabolomics Data Analysis

Analysis of the raw peak data for both relative metabolite quantification and mass isotopomer distribution (MID) analysis was performed using MetaboliteDetector (Hiller et al., 2009). This software provided chromatogram alignment, peak matching, and automated compound identification (using an in-house library). Raw data was exported from MetaboliteDetector and processed using either R statistical software (R Core Team, 2016) or LibreOffice Calc.

All metabolites identified with MetaboliteDetector were verified through manual chromatogram analysis of characteristic fragment peaks.

Normalization of the metabolite raw data was performed using the following methods: First, all metabolites were normalized to the internal standard added to the extraction water in order to control for variations in extraction amount and GC-MS measurements. Where applicable, normalized metabolite signal intensity was further normalized to cell count as well as to the control (or t=0) treatment, in order to provide a standard basis for comparison across experiments.

MIDs were determined from samples cultured with labeled tracers using SIM measurements. The data was corrected for natural isotope abundances using MetaboliteDetector software.

Weighted carbon contribution for labeled compounds was calculated using the following formula:

$\frac{1}{n} * \sum_{i=1}^{n} M_i \times i$

where n is the number of carbons in the compound of interest, and M_i is the i^{th} mass isotopomer. Glucose and Glutamine contribution was calculated with samples from the same experimental replicate, and contribution from other sources was calculated by:

$1 - (C_{Glc} + C_{Gln})$

where C_{Glc} and C_{Gln} are the weighted carbon contributions from glucose and glutamine, respectively.

Statistical Methodology

Experiments were performed in biological triplicates, either with different cell passages (in the case of the RAW 264.7 cell line) or different mice (in the case of the BMDMs). Within each experiment, each condition was repeated three times in separate wells.

Statistically significant differences of metabolites or transcript level were determined between specific treatments using an unpaired two-tailed Student's t-test. Error bars represent the standard error of the mean of the samples.

2 Results

2.1 Transcriptional regulation under short-term LPS stimulation

2.1.1 Cytokine regulation

The two classical cytokines associated with pro-inflammatory macrophages, IL-1β, and TNF-α were seen to be increased with LPS stimulation in both RAW cells and BMDMs, as is known (Medzhitov and Horng, 2009). Interestingly, the expression of these cytokines peaked at an early phase after stimulation, and then behaved differently during the following phase (fig. 1). In both primary cells and the cell line, levels of *Tnf-α* seem to be the first which increased, followed by *Il-1β* expression. Then, levels of *Tnf-α* decreased back to almost basal levels by 8 hours in both cell types, and this behavior was consistent with *Il-1β* expression in RAW cells, while in BMDMs this decrease did not occur. In addition, expression level increases for both cytokines appear to be much higher in BMDMs compared to RAW cells.

The cytokine *Il-6* plays a role in macrophages stimulated to a pro-inflammatory state, but there is increasing evidence that it acts as well as an anti-inflammatory cytokine (Xing et al., 1998). *Il-6* expression followed the same trend as seen with *Tnf-α*, having increased to a local maximum around 3 hours and then having decreased steadily to the 8 hour timepoint (fig. 1). The transcriptional regulation pattern of this cytokine was similar in both RAW cells and BMDMs, but again at a higher expression level in BMDMs than in RAW cells.

Hif-1α plays an important role in pro-inflammatory macrophages, influencing the transcriptional regulation of many metabolic genes and cytokines (reviewed in Imtiyaz and Simon (2010)), and is known to be increased and stabilized on a transcriptional and protein level, respectively (Nishi et al., 2008) in

order to affect macrophage polarization (Galván-Peña and O'Neill, 2015). In RAW cells, *Hif-1α* showed no significant change with LPS stimulation, but expression levels steadily increased over the 8 hour stimulation period in BMDMs (fig. 2).

2.1.2 Regulation of metabolic enzymes

Immunoresponsive gene 1 (*Irg1*), like the cytokines described above, showed a transcriptional increase in both the RAW cells and the BMDMs from almost no expression to a relative peak around the 3 hour timepoint (fig. 2). In both cell types, this was followed by a decrease in expression to the 8 hour timepoint, with expression levels higher in BMDMs compared to RAW cells. The primary known function of *Irg1*/CAD is the enzymatic function of cis-aconitate decarboxylase (CAD), which catalyzes the production of itaconic acid from cis-aconitate, an antimicrobial compound associated with pro-inflammatory macrophages (Michelucci et al., 2013).

In pro-inflammatory macrophages, it was thought that HIF-1α blocks pyruvate flux into the TCA cycle through transcription of pyruvate dehydrogenase kinase 1 (*Pdk1*), which inhibits pyruvate dehydrogenase (PDH) activity (Kim et al., 2006). Recently, we found that pyruvate oxidation into the TCA cycle is maintained in pro-inflammatory macrophages; *Pdk1* was seen to have reduced transcript levels after 6 hours of LPS stimulation, and PDH was shown to be active in transporting pyruvate into the TCA cycle (Meiser et al., 2015). In the present work, expression levels of *Pdk1* were found to decrease and stay low under LPS stimulation in RAW cells, reaching a local minimum within 2-3 hours. In BMDMs, *Pdk1* expression was increased at later time-points over the 8 hour stimulation, showing the opposite effect as in RAW cells (fig. 2).

The different isoforms of isocitrate dehydrogenase (IDH) catalyze the reversible conversion of isocitric acid to α-ketoglutaric acid, with IDH2 and IDH3 acting in the mitochondria, and IDH1 present in the cytosol. As these enzymes require either NADP(H) (in the case of IDH1 and IDH2) or NAD(H) (for IDH3) as cofactors, they have a strong influence in the energy state of the cell as well as dealing with reactive oxygen species (Maeng et al., 2004). In addition, the IDH reaction was found to be a metabolic breakpoint in pro-inflammatory macrophages (Jha et al., 2015). For *Idh1* and *Idh2*, a gradual decrease in expression was seen over the 8 hour time period in both RAW cells and BMDMs, reaching a local minimum only at around 6 hours (fig. 2). This decrease was also seen with *Idh3* in RAW cells, but expression increased in BMDMs, with the upregulation of the *Idh* isoform seen beginning around 6 hours (fig. 2). Expression levels of *Idh1* were higher in BMDMs, while the other two isoforms had higher expression in RAW cells over the time period studied.

2.2 Changes in pro-inflammatory associated metabolite pools under short-term LPS stimulation

Itaconic acid, an antimicrobial metabolite found in pro-inflammatory macrophages (Michelucci et al., 2013), was present at a very low baseline in non-stimulated cells, but production increased relatively quickly upon LPS stimulation (fig. 3a). Following the same pattern as with *Irg1* regulation (fig. 2), with an observed delay most likely corresponding to the process of transcription and translation),

a strong increase in itaconic acid started around 3 hours in both RAW cells and BMDMs, and did not plateau for the entire period of time studied (fig. 3a). Intracellular metabolite pools of itaconic acid were much higher in RAW cells compared to BMDMs, but in both cell types increased to almost 100 times the basal level.

The relative amount of succinic acid was increased under LPS stimulation, and has been shown to be linked to increased *Il-1β* expression through HIF-1α stabilization (Tannahill et al., 2013). This increase could be seen already occurring as early as 3-4 hours, similar to the production of itaconic acid (fig. 3b).

2.3 Relative carbon contribution from glucose and glutamine in central carbon metabolism

Through the replacement of normal carbon sources of cellular metabolism (glucose and glutamine) with those having stable-isotope labeled carbons, it is possible to measure the relative carbon contribution of glucose and glutamine to metabolites in central metabolism from the overall labeling patterns of the metabolites. This methodology complements normal measurement of metabolite levels by adding information on how much of the overall metabolite pool comes from which carbon source, and how this can change under different conditions (such as LPS stimulation). To obtain a more comprehensive view of how macrophage metabolism is affected under LPS stimulation, we applied this technique to both RAW cells and BMDMs under the same conditions as the above analyses. Glucose contribution was measured using [U-$^{13}C_6$]-Glucose, and glutamine contribution was measured using [U-$^{13}C_5$]-Glutamine.

In RAW cells, the relative carbon contribution of glucose and glutamine to most metabolites showed a short-term effect of perturbation, with a rapid return to a stable contribution from both carbon sources. Between 5 and 15 minutes, a small reduction of carbon contribution from glucose could be observed in pyruvic acid and citric acid (figs. 4 and 4), while an corresponding increase could be seen in itaconic acid (fig. 4); afterwards relative carbon contribution returned to a stable level, albeit with itaconic acid taking more time to stabilize. The only metabolite that we measured which did not follow this pattern is succinic acid, showing increasing relative glutamine contribution with a longer stimulation time, while carbon contribution from glucose remains stable over the 8 hours (fig. 4).

BMDMs showed different patterns of time-dependent change in glucose and glutamine carbon contribution to metabolites. Relative carbon contribution from one or both of the measured carbon sources were seen to increase for many metabolites after the LPS perturbation. A gradual increase accounting for a 20% change in carbon going from glucose to pyruvic acid could be seen over the 8 hours, with almost no supplementation from glutamine (fig. 4). Citric acid carbon showed the same trend, with perturbation leading to a decrease and gradual recovery of glutamine carbon (fig. 4). Carbon contribution to itaconic acid remained relatively stable over the 8 hours of LPS stimulation in both RAW cells and BMDMs, even as the metabolite pool increased rapidly; in BMDMs, there was an increase of glucose carbon with longer stimulation, but only around 6% over 8 hours (fig. 4). An increasing relative carbon contribution from both glutamine and glucose could be observed in succinic acid over the 8 hours, with an increase of over 20% from glucose carbon (fig. 4).

Other metabolites from both glycolysis and the TCA cycle which were measured (alanine, lactic acid, fumaric acid, and malic acid) show similar changes as described above: RAW cells showed stable carbon contributions after an initial change due to the LPS challenge, while BMDMs had a general increase of carbon contribution from one or both of the carbon sources measured (fig. 6). To validate that glucose carbon entering the TCA cycle was done so through PDH activity, the M2 isotopologue of certain TCA cycle metabolites were measured. We found that PDH was indeed active in pro-inflammatory macrophages, as a significant percentage of labeled TCA cycle metabolites came from glucose carbon metabolized through PDH (fig. 7)

3 Discussion

The results of this study point to practical similarities as well as integral differences between the RAW 264.7 macrophage cell line and BMDMs on both a transcriptional level and a metabolic level. Interestingly, all cytokines measured in this study show a similar trend of time-dependent regulation in both the cell line and the primary cells, only differing in scale, as well as long term activity (in the case of *Il-1β* - fig. 1. Cytokine expression is drastically increased in primary cells compared to the cell line macrophages, an effect highlighting a possible saturation effect or reduced sensitivity in RAW macrophages, which could arise from the transformational process. In both cell types, expression of *Tnf-α* reached a peak first, then followed by *Il-1β* around an hour later. These data suggest that for the study of cytokine transciptional regulation in pro-inflammatory macrophages, the RAW 264.7 cell line works as a comparable substitute for primary mouse macrophages, as long as quantification of cytokine expression is not being compared. The increased sensitivity to LPS of primary cells compared to cell lines has also been observed in microglia, where differing concentrations of LPS were used to achieve equivalent activation levels between primary microglia and the MMGT12 cell line (Michelucci et al., 2009).

Although not a cytokine, *Irg1*/CAD has been shown to be important for the anti-bacterial activity of macrophages through the production of itaconic acid (Michelucci et al., 2013). Indeed, *Irg1* expression was seen to increase over time, but decreases after an early peak in RAW cells (fig. 2). The data from this work expands this previous study with more detailed short term regulatory information. However, as the previous study did not look at BMDMs, it is interesting to note that the scale and timing of regulation is different in the primary cells compared to the cell line, similar to the cytokines described above. *Irg1* expression is higher in primary cells, again underlining the differences in mRNA levels of pro-inflammatory related genes between BMDMs and RAW cells.

In addition, itaconic acid production in both cell types continues to increase even after expression of *Irg1* has been reduced (fig. 3a). Michelucci et al. (2013) show that in RAW cells, itaconic acid levels drop a few hours after *Irg1* expression has been decreased (from 10 to 16 hours), and most likely the timepoints we measured did not reach this point in either cell type. These results suggest that the production of itaconic acid is an important part of the early-phase macrophage response to inflammation, and is less important as part of the long-term response. Michelucci et al. (2013) found a much lower increase of itaconic

in primary human macrophages compared to the RAW cell line, and this trend is the same in BMDMs. Itaconic acid levels therefore do not need to be very high for cellular activities in primary cells, and the discordance in metabolite levels can be attributed to metabolic differences in the TCA cycle between immortalized cell lines and primary cells. Interestingly, much higher levels of *Irg1* are required in BMDMs in order to produce lower levels of itaconic acid, and there could be other regulatory steps which control the production of this antimicrobial metabolite, such as post-translational modification to CAD, the enzyme catalyzing the reaction.

Previous work has shown that *Irg1* has been seen to suppress production of *Il-1β* and *Tnf-α* in LPS-tolerized macrophage (Li et al., 2013). Our data from both RAW cells and BMDMs show *Irg1* expression increase lagging behind the expression increase of *Tnf-α* while peaking around the same time as *Il-1β* in both cell types. The expression pattern of *Irg1*, with a delayed peak and less pronounced decrease, represents a pattern that supports the concept of *Irg1*-mediated suppression of cytokine expression. Itaconic acid production then follows after the peak of *Irg1* expression is reached, illustrating the impact of different time scales that connect transcriptional and metabolic regulation.

Expression changes of *Hif-1α* are not comparable between the different cell types, which raises questions about connections between transciptional and metabolic activity (fig. 2). HIF-1α is known to be a positive regulator of glycolysis in macrophages (through inducing transcription of genes encoding the glucose transporter, GLUT1, and PDK, which inhibits oxidation of pyruvate into acetyl-CoA), as well as implicated in an increased NAD^+/NADH ratio in monocytes (Cramer et al., 2003; Cheng et al., 2014). In addition, expression of *Hif-1α* is known to be controlled by growth factors (DeBerardinis et al., 2008), and stimulation of macrophages with LPS induces a cascade leading to *Hif-1α* expression (Frede et al., 2006). Most likely, the metabolic differences between the two cell types comes from the fact that RAW cells are virus transformed to be immortalized, which makes significant changes to the transcriptional machinery in order to allow the cells to continuously proliferate. This process of proliferation requires a specific metabolic function, geared towards macromolecule biosynthesis and energy production, which is not present in post-mitotic primary macrophages. The differences seen in metabolite levels is in alignment with this hypothesis fig. 3, and point to a specialized regulation of central carbon metabolism, including under pro-inflammatory conditions in macrophages.

Consistent with how *Hif-1α* expression (and most likely the connected transcriptional program) in RAW cells stays consistent with LPS stimulation while increasing in BMDMs (fig. 2), the carbon contribution data shows strong differences between the cell line and primary cells, as almost every metabolite measured in RAW cells showed unchanging levels of relative carbon contribution from glucose and glutamine, in contrast to a mostly increasing utilization of glucose and glutamine carbon for metabolites in pro-inflammatory BMDMs. It has been shown previously that for both macrophages cell types, glucose and glutamine consumption as well as glutamine and lactate secretion are increased over time with LPS stimulation (Rodríguez-Prados et al., 2010), so a static carbon contribution to intracellular metabolites in RAW cells most likely suggests that metabolic fluxes are not changing with stimulation, and simply handle the increased carbon influx with normal proliferative activity. For future macrophage cell line scientific studies, it should be noted that metabolism of

RAW cells (and the modified associated transcriptional regulation) does not react to pro-inflammatory perturbation in the same way as primary cells, and are therefore not an adequate model for studies into normal metabolic machinery under pro-inflammatory conditions.

As mentioned above, expression of *Pdk1* is regulated by HIF-1α, and our results confirm the link between them over the initial stage of macrophage response to inflammation. In RAW cells, the expression level decrease seen in *Pdk1* (fig. 2), occurs while *Hif-1α* levels remain unchanged (fig. 2); this data in combination with carbon contribution data from TCA cycle metabolites (fig. 4) is consistent with our previous findings of PDH activity in LPS-stimulated RAW cells (Meiser et al., 2015), and lends evidence to the idea that glucose carbon is needed to fuel the TCA cycle of RAW macrophages at the beginning phase of an inflammatory response. However, *Pdk1* expression shows an overall increase over the 8 hour stimulation in BMDMs (fig. 2), which parallels the increase of *Hif-1α* expression in these primary cells (fig. 2),and reinforces the hypothesis of metabolism being significantly different in RAW cells when compared to BMDMs. Interestingly, there was increased glucose carbon entering the TCA cycle through PDH, as evidenced by M2 isotopologues of TCA cycle metabolites measured in cells cultured with uniformly labeled glucose (fig. 7), meaning that PDH activity must be present in pro-inflammatory BMDMs. as regulation of PDH by PDK happens on a protein level, it can not be confirmed by our data whether the regulation of glucose carbon flux into the TCA cycle is governed by this reaction.

As metabolites associated with the pro-inflammatory state of macrophages, intracellular levels of both succinic acid and itaconic acid in macrophages are increased upon LPS stimulation, regardless of the cell type (fig. 3). Succinic acid is a key metabolite linked to signaling in pro-inflammatory macrophages, which has been shown to be metabolized from glutamine and is thought to be exported from the mitochondria to stabilize HIF-1α (Tannahill et al., 2013), and thus propagate further inflammatory processes (Cramer et al., 2003). The data found in this study support this key role for this key pro-inflammatory metabolite. The importance of itaconic acid in pro-inflammatory macrophage activity is only beginning to be understood, but it is seen as such an important part of macrophage anti-bacterial defense, the normal TCA cycle activity is restructured just to produce this metabolite (Michelucci et al., 2013; Jha et al., 2015). Recently, it has been shown that itaconic acid can act to inhibit succinate dehydrogenase activity, thus leading to an accumulation of intracellular succinic acid (Cordes et al., 2016). The alignment of timing patterns between the two metabolites adds evidence to this postulation, and this can be seen independently of the differences in the metabolite levels between primary cells and cell lines.

The increased relative carbon contribution from both glucose and glutamine to succinic acid over the 8 hour stimulation time highlights the importance of this metabolite in pro-inflammatory macrophages, showing increased utilization of cellular carbon sources for its production (fig. 4). Even in RAW cells, an increase in utilization of glutamine-derived carbon can be seen in succinic acid (fig. 4), the only metabolite differing from the pattern of stable contribution levels. The accumulation of itaconic acid and succinic acid, as well as the carbon contribution data, all support the growing body of evidence that these are two key metabolites for pro-inflammatory macrophage activity, and all car-

bon sources are utilized to rapidly synthesize them during the initial phase of inflammatory stimulation in macrophages.

Jha et al. (2015) explained this phenomenon by uncovering that the biochemical reactions catalyzed by IDH and SDH are the two reactions which are classified as "metabolic breakpoints" in LPS-stimulated macrophages. These breakpoints cause increased production of itaconic acid and succinate, respectively, as major metabolic features of pro-inflammatory macrophage polarization. Our data supports and extends this idea on both an transcriptional and metabolic level. In addition to the metabolite accumulation and labeling data, expression levels of the three different *Idh* isoforms elucidate the timing of one of these breakpoints, as well as differences between RAW cells and BMDMs.

Expression level changes in *Idh* isoforms show metabolic differences between RAW cells and BMDMs at a transcriptional level. *Idh1* and *Idh2* show gradual decreased expression over the 8 hour stimulation in both cell types, with a stronger effect in BMDMs for *Idh2* while having a lower expression level compared to RAW cells fig. 2. The decreased expression levels of these *Idh* isoforms suggest reduced enzyme production, and therefore less activity of this reaction, with carbon being diverted to itaconic acid as described above. For *Idh3*, expression was seen to be decreased in RAW cells, while increased in BMDMs fig. 2. For the cytosolic isoform, *Idh1*, expression was higher in BMDMs, while the mitochondrial isoforms show increased expression levels in RAW cells, increasing the metabolic differences between primary cells and cell lines. For each isoform of *Idh*, expression level changes begin after *TNF*α, in the second phase of the initial response (together with *Il-1*β and *Irg1*. IDH3 is a mitochondrial isoform of the IDH protein, and requires NAD(H) as a cofactor, in contrast to IDH1 and IDH2, which require NADP(H). For both cofactors, the forward reaction creates the reduced form, which can be used in other cellular processes. NADPH is mostly required for ROS generation and detoxification, while NADH is used in redox regulation and cellular energy production through the electron transport chain, and its oxidized form is required for the activity of sirtuins, a class of deacetylases which are known to have multiple targets in the mitochondria (reviewed in Ying (2008)).

It is important to note that the changes shown in this data are only important in the initial phase of macrophage-mediated inflammation. Time-dependent regulation of most intracellular metabolites has not been clearly studied, only itaconic acid levels over time have been shown to decrease at later timepoints (Michelucci et al., 2013), and the change in succinic acid levels has not been studied. Future work should go in the direction of how time-dependent expression level changes of cytokines and metabolic genes during inflammation are connected to metabolite pool and metabolic flux changes, and how this regulates the pro-inflammatory macrophage phenotype and inflammatory response.

4 Outlook

Through the comparison of the RAW 264.7 macrophage cell line to primary mouse bone marrow derived macrophages, it can be seen that in the case of macrophages, the validity of using a cell line model to make conclusions about cellular activity in primary cells is dependent on the scope of the question. Much of the transcriptional regulation patterns under inflammation was com-

parable between RAW cells and BMDMs, including cytokine regulation and pro-inflammatory phenotypic activity, which allows for valid comparisons and is utilized to create useful insights into inflammatory regulation of macrophages (Michelucci et al., 2013), however, the scale of response must be taken into account, as there exist strong differences between primary macrophage mRNA expression response and the corresponding changes in cell lines. In contrast, metabolic changes are not consistent between the cell types, most likely due to the proliferative nature of the RAW 264.7 cell line compared to the post-differentiation phenotype of the BMDMs. However, metabolites which can be linked to a pro-inflammatory phenotype (including itaconic acid and succinic acid) act independently of these transcriptional differences, and can be studied. The results of this study back up and complement previous work (Berghaus et al., 2010; Chamberlain et al., 2009; Rodríguez-Prados et al., 2010) showing that while there are important differences between RAW 264.7 cells and primary BMDMs in terms of cytokine regulation and carbon metabolism, focused questions in areas where there is known overlap between the responses of the different cell types allow researchers to substitute cell lines for primary cells without fear of inappropriate results.

On a transcriptional level in both cell line and primary macrophages, a phase response of cytokine regulation in macrophages to LPS stimulation has been shown. This is important to emphasize, as most studies choose one time point for looking at the impact of inflammation on macrophage processes, and the activity of the cell will be different depending on the time point chosen. Therefore, it is necessary for studies on pro-inflammatory macrophages to determine which phase of stimulation most directly is impacted by the question asked, as results can be misleading.

A previous study has found that LPS stimulation leads to increase of cytokine production, but too much LPS reduces cytokine expression, attributed to the cytokine regulation by IRG1 and A20 (Li et al., 2013). Our results have shown possible correlation between regulation of different cytokines (as well as other genes implicated in pro-inflammatory macrophages). A tight regulation of *TNFα*, *Il-1β*, and *Irg1* is necessary to balance levels of different mediators and activity of signaling pathways over time, as macrophages change roles during the response to inflammation. More research is needed to determine what factors and processes are orchestrating this regulation, and what role metabolism plays in these changes.

The timing patterns of the genes and metabolites studied in this work infer that there is a cascading effect of regulation tying transcriptional and metabolic regulation. Our hypothesis of the initial pro-inflammatory macrophage timeline can be seen in fig. 5. LPS stimulation starts a two pronged cascade: cytokines and *Irg1* are activated to aid in the initial inflammatory signaling and bacterial clearance through itaconic acid production, while *Hif-1α* is induced in order to prepare the transciptional and metabolic machinery necessary for a pro-inflammatory macrophage phenotype. Succinic acid, which is accumulated in part through itaconic acid activity, can stabilize HIF-1α to provide a positive feedback loop for maintaining the macrophage in this state. However, our findings show that the *Hif-1α* side of regulation in RAW 264.7 macrophages is not consistent with primary BMDMs, suggesting that for studying this aspect of pro-inflammatory macrophages, a primary cell model is necessary.

Future studies in this field should investigate the different regulatory phases

of inflammation in macrophages, and response to pro-inflammatory stimulation should be framed in terms of these phases as well as the current metabolic and transcriptional state of the macrophage. Macrophages are a constantly shifting regulator of the inflammatory process, and will most likely have different regulatory control points depending on the current phenotypic phase of the cell. Thinking about macrophages in this way can open up new ways of looking at phenotypic switching, and help to find these control points in both time and regulatory pathways which will allow for novel therapies and treatments for diseases where macrophage regulation plays a role.

5 Bibliography

References

Sandra Amor, Fabiola Puentes, David Baker, and Paul Van Der Valk. Inflammation in neurodegenerative diseases. *Immunology*, 129(2):154–169, 2010.

Londa J Berghaus, James N Moore, David J Hurley, Michel L Vandenplas, Barbara P Fortes, Margreet A Wolfert, and Geert-Jan Boons. Innate immune responses of primary murine macrophage-lineage cells and raw 264.7 cells to ligands of toll-like receptors 2, 3, and 4. *Comparative immunology, microbiology and infectious diseases*, 33(5):443–454, 2010.

George Boltz-Nitulescu, Christoph Wiltschke, Christoph Holzinger, Alois Fellinger, Otto Scheiner, Alois Gessl, and Othmar Förster. Differentiation of rat bone marrow cells into macrophages under the influence of mouse l929 cell supernatant. *Journal of leukocyte biology*, 41(1):83–91, 1987.

Lisa M Chamberlain, Marisha L Godek, Mercedes Gonzalez-Juarrero, and David W Grainger. Phenotypic non-equivalence of murine (monocyte-) macrophage cells in biomaterial and inflammatory models. *Journal of Biomedical Materials Research Part A*, 88(4):858–871, 2009.

Shih-Chin Cheng, Jessica Quintin, Robert A Cramer, Kelly M Shepardson, Sadia Saeed, Vinod Kumar, Evangelos J Giamarellos-Bourboulis, Joost HA Martens, Nagesha Appukudige Rao, Ali Aghajanirefah, et al. mtor-and hif-1α–mediated aerobic glycolysis as metabolic basis for trained immunity. *Science*, 345(6204):1250684, 2014.

Thekla Cordes, Martina Wallace, Alessandro Michelucci, Ajit S Divakaruni, Sean C Sapcariu, Carole Sousa, Haruhiko Koseki, Pedro Cabrales, Anne N Murphy, Karsten Hiller, et al. Immunoresponsive gene 1 and itaconate inhibit succinate dehydrogenase to modulate intracellular succinate levels. *Journal of Biological Chemistry*, pages jbc–M115, 2016.

Lisa M Coussens and Zena Werb. Inflammation and cancer. *Nature*, 420(6917): 860–867, 2002.

Thorsten Cramer, Yuji Yamanishi, Björn E Clausen, Irmgard Förster, Rafal Pawlinski, Nigel Mackman, Volker H Haase, Rudolf Jaenisch, Maripat Corr, Victor Nizet, et al. Hif-1α is essential for myeloid cell-mediated inflammation. *Cell*, 112(5):645–657, 2003.

Ralph J DeBerardinis, Julian J Lum, Georgia Hatzivassiliou, and Craig B Thompson. The biology of cancer: metabolic reprogramming fuels cell growth and proliferation. *Cell metabolism*, 7(1):11–20, 2008.

Décio L Eizirik, Maikel L Colli, and Fernanda Ortis. The role of inflammation in insulitis and β-cell loss in type 1 diabetes. *Nature Reviews Endocrinology*, 5(4):219–226, 2009.

Alexander Francke, Joerg Herold, Soenke Weinert, Ruth H Strasser, and Ruediger C Braun-Dullaeus. Generation of mature murine monocytes from heterogeneous bone marrow and description of their properties. *Journal of Histochemistry & Cytochemistry*, 59(9):813–825, 2011.

Stilla Frede, Christian Stockmann, Patricia Freitag, and Joachim Fandrey. Bacterial lipopolysaccharide induces hif-1 activation in human monocytes via p44/42 mapk and nf-κb. *Biochemical Journal*, 396(3):517–527, 2006.

Silvia Galván-Peña and Luke AJ O'Neill. Metabolic reprograming in macrophage polarization. *M1/M2 Macrophages: The Arginine Fork in the Road to Health and Disease*, 5(420):275, 2015.

Karsten Hiller, Jasper Hangebrauk, Christian Jäger, Jana Spura, Kerstin Schreiber, and Dietmar Schomburg. MetaboliteDetector: comprehensive analysis tool for targeted and nontargeted GC/MS based metabolome analysis. *Analytical chemistry*, 81(9):3429–39, May 2009.

Hongxia Z Imtiyaz and M Celeste Simon. Hypoxia-inducible factors as essential regulators of inflammation. In *Diverse Effects of Hypoxia on Tumor Progression*, pages 105–120. Springer, 2010.

Abhishek K Jha, Stanley Ching-Cheng Huang, Alexey Sergushichev, Vicky Lampropoulou, Yulia Ivanova, Ekaterina Loginicheva, Karina Chmielewski, Kelly M Stewart, Juliet Ashall, Bart Everts, et al. Network integration of parallel metabolic and transcriptional data reveals metabolic modules that regulate macrophage polarization. *Immunity*, 42(3):419–430, 2015.

Jung-whan Kim, Irina Tchernyshyov, Gregg L Semenza, and Chi V Dang. Hif-1-mediated expression of pyruvate dehydrogenase kinase: a metabolic switch required for cellular adaptation to hypoxia. *Cell metabolism*, 3(3):177–185, 2006.

Yingke Li, Peng Zhang, Chengcai Wang, Chaofeng Han, Jun Meng, Xingguang Liu, Sheng Xu, Nan Li, Qingqing Wang, Xueyin Shi, et al. Immune responsive gene 1 (irg1) promotes endotoxin tolerance by increasing a20 expression in macrophages through reactive oxygen species. *Journal of Biological Chemistry*, 288(23):16225–16234, 2013.

Oky Maeng, Yong Chan Kim, Han-Jae Shin, Jie-Oh Lee, Tae-Lin Huh, Kwang-il Kang, Young Sang Kim, Sang-Gi Paik, and Hayyoung Lee. Cytosolic nadp+-dependent isocitrate dehydrogenase protects macrophages from lps-induced nitric oxide and reactive oxygen species. *Biochemical and biophysical research communications*, 317(2):558–564, 2004.

Ruslan Medzhitov. Origin and physiological roles of inflammation. *Nature*, 454 (7203):428–435, 2008.

Ruslan Medzhitov and Tiffany Horng. Transcriptional control of the inflammatory response. *Nature Reviews Immunology*, 9(10):692–703, 2009.

Johannes Meiser, Lisa Krämer, Sean C Sapcariu, Nadia Battello, Jenny Ghelfi, Aymeric Fouquier D'Herouel, Alexander Skupin, and Karsten Hiller. Pro-inflammatory macrophages sustain pyruvate oxidation through pyruvate dehydrogenase for the synthesis of itaconate and to enable cytokine expression. *Journal of Biological Chemistry*, pages jbc–M115, 2015.

Alessandro Michelucci, Tony Heurtaux, Luc Grandbarbe, Eleonora Morga, and Paul Heuschling. Characterization of the microglial phenotype under specific pro-inflammatory and anti-inflammatory conditions: effects of oligomeric and fibrillar amyloid-β. *Journal of neuroimmunology*, 210(1):3–12, 2009.

Alessandro Michelucci, Thekla Cordes, Jenny Ghelfi, Arnaud Pailot, Norbert Reiling, Oliver Goldmann, Tina Binz, André Wegner, Aravind Tallam, Antonio Rausell, et al. Immune-responsive gene 1 protein links metabolism to immunity by catalyzing itaconic acid production. *Proceedings of the National Academy of Sciences*, 110(19):7820–7825, 2013.

David M Mosser and Justin P Edwards. Exploring the full spectrum of macrophage activation. *Nature reviews immunology*, 8(12):958–969, 2008.

Peter J Murray and Thomas A Wynn. Protective and pathogenic functions of macrophage subsets. *Nature reviews immunology*, 11(11):723–737, 2011.

Kenichiro Nishi, Tomoyuki Oda, Satoshi Takabuchi, Seiko Oda, Kazuhiko Fukuda, Takehiko Adachi, Gregg L Semenza, Koh Shingu, and Kiichi Hirota. Lps induces hypoxia-inducible factor 1 activation in macrophage-differentiated cells in a reactive oxygen species-dependent manner. *Antioxidants & redox signaling*, 10(5):983–996, 2008.

R Core Team. *R: A Language and Environment for Statistical Computing*. R Foundation for Statistical Computing, Vienna, Austria, 2016. URL `https://www.R-project.org/`.

Juan-Carlos Rodríguez-Prados, Paqui G Través, Jimena Cuenca, Daniel Rico, Julián Aragonés, Paloma Martín-Sanz, Marta Cascante, and Lisardo Boscá. Substrate fate in activated macrophages: a comparison between innate, classic, and alternative activation. *The Journal of Immunology*, 185(1):605–614, 2010.

Sean C Sapcariu, Tamara Kanashova, Daniel Weindl, Jenny Ghelfi, Gunnar Dittmar, and Karsten Hiller. Simultaneous extraction of proteins and metabolites from cells in culture. *MethodsX*, 1:74–80, 2014.

Seung-Yong Seong and Polly Matzinger. Hydrophobicity: an ancient damage-associated molecular pattern that initiates innate immune responses. *Nature Reviews Immunology*, 4(6):469–478, 2004.

GM Tannahill, AM Curtis, J Adamik, EM Palsson-McDermott, AF McGettrick, G Goel, C Frezza, NJ Bernard, B Kelly, NH Foley, et al. Succinate is an inflammatory signal that induces il-1 [bgr] through hif-1 [agr]. *Nature*, 496 (7444):238–242, 2013.

Zhou Xing, Jack Gauldie, Gerard Cox, Heinz Baumann, Manel Jordana, Xue-Feng Lei, and Michelle K Achong. Il-6 is an antiinflammatory cytokine required for controlling local or systemic acute inflammatory responses. *Journal of Clinical Investigation*, 101(2):311, 1998.

Weihai Ying. Nad+/nadh and nadp+/nadph in cellular functions and cell death: regulation and biological consequences. *Antioxidants & redox signaling*, 10(2): 179–206, 2008.

X Zhang and DM Mosser. Macrophage activation by endogenous danger signals. *The Journal of pathology*, 214(2):161–178, 2008.

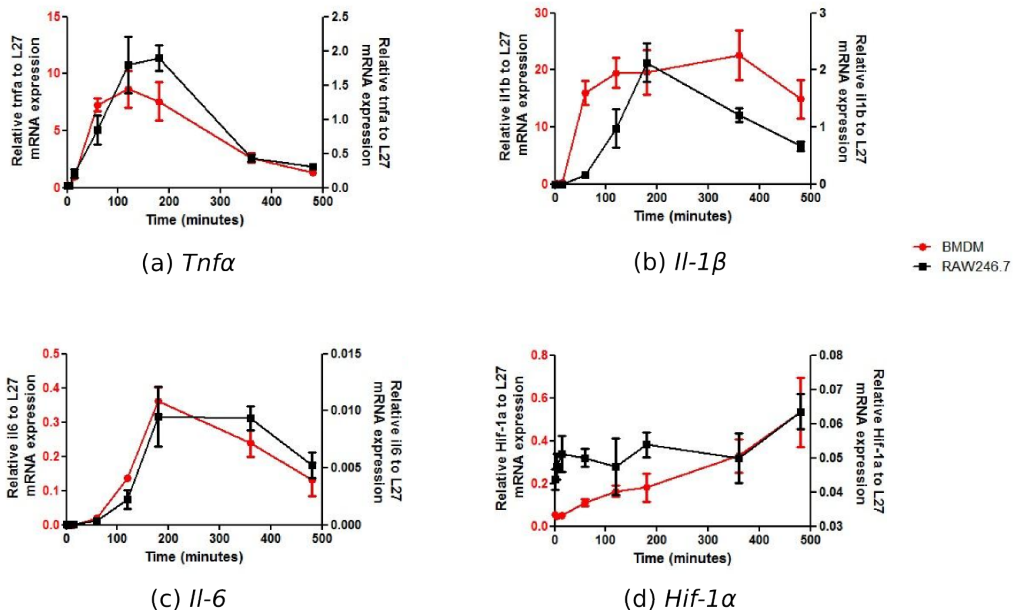

Figure 1: **Relative transcript levels of selected cytokines in LPS stimulated macrophages unnormalized:** (a) *Tnf-α* (b) *Il-1β* (c) *Il-6* (d) *Hif-1α*

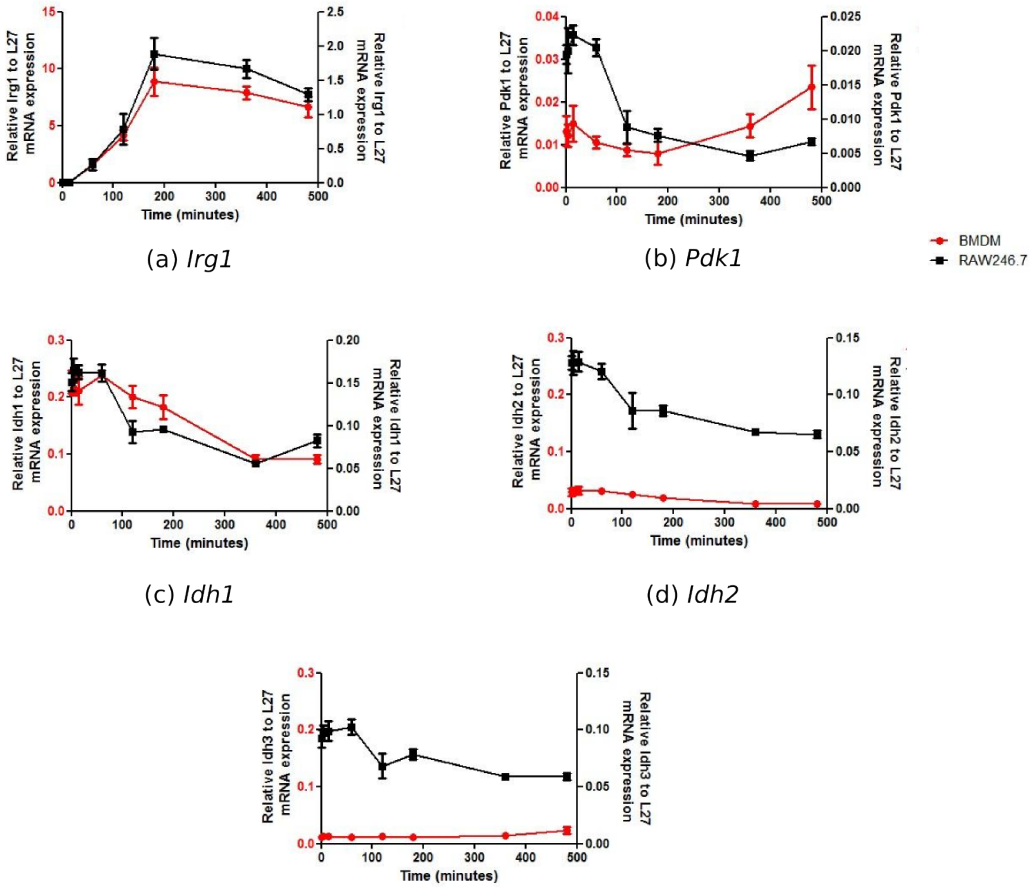

Figure 2: **Relative transcript levels of selected metabolic genes in LPS stimulated macrophages unnormalized:** (a) *Irg1* (b) *Pdk1* (c) *Idh1* (d) *Idh2* (e) *Idh3*

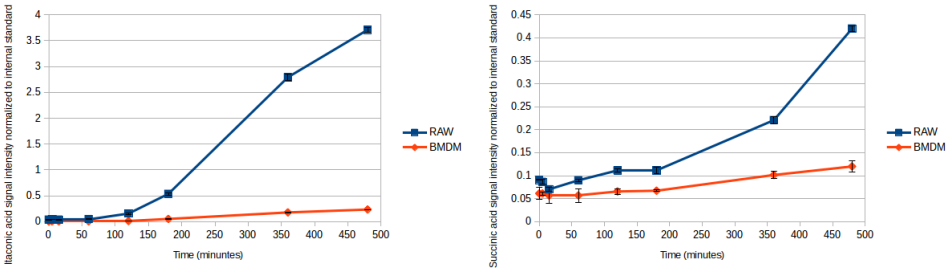

Figure 3: **Relative levels of pro-inflammatory associated metabolites in LPS stimulated macrophages:** (a) Itaconic Acid (b) Succinic Acid

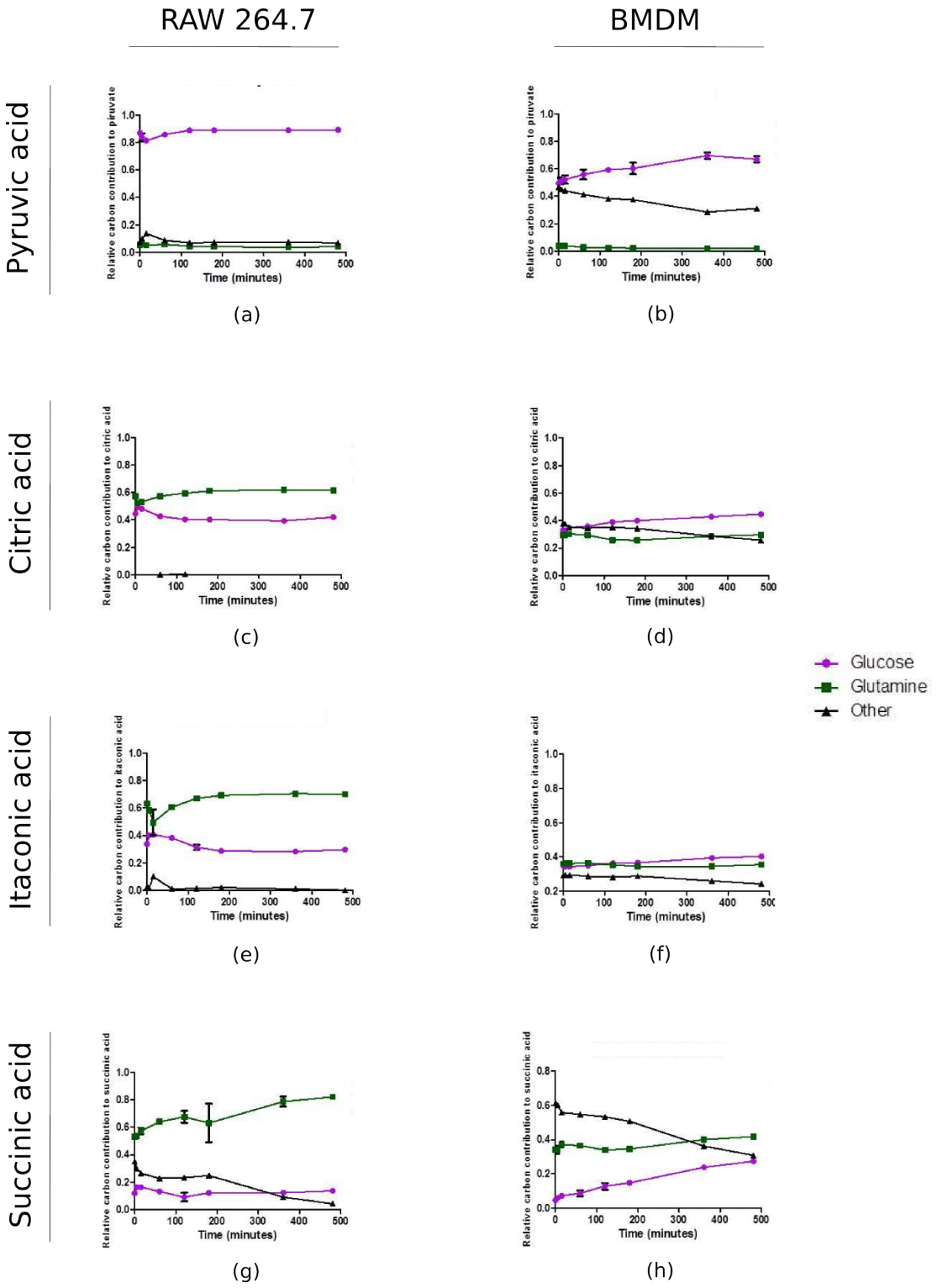

Figure 4: **Relative carbon contribution from glucose and glutamine to selected metabolites in LPS stimulated macrophages:** (a) RAW cells and (b) BMDMs Pyruvic acid carbon contribution (c) RAW cells and (d) BMDMs Citric acid carbon contribution (e) RAW cells and (f) BMDMs Itaconic acid carbon contribution (g) RAW cells and (h) BMDMs Succinic acid carbon contribution

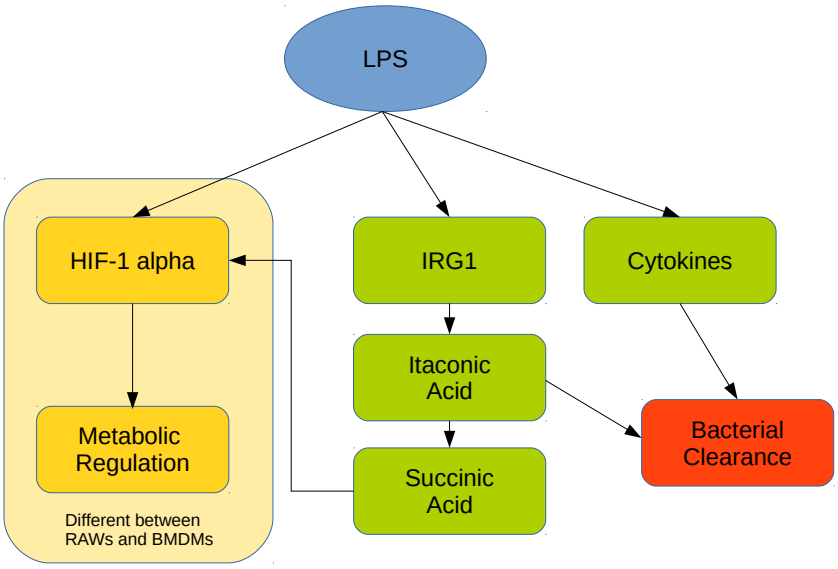

Figure 5: **Summary Figure - Cascading Response to LPS** LPS stimulation in macrophages leads to cytokine and *Irg1* expression, both of which aid the macrophage in bacterial clearance processes (through the use of antimicrobial compounds such as itaconic acid). Itaconic acid increases accumulation of succinic acid, which stabilizes HIF-1α, modifying metabolic machinery. *Hif-1α* expression is also increased through LPS stimulation (leading to the same metabolic response), but this regulation under pro-inflammatory conditions cannot be seen in a constituently proliferating cell line

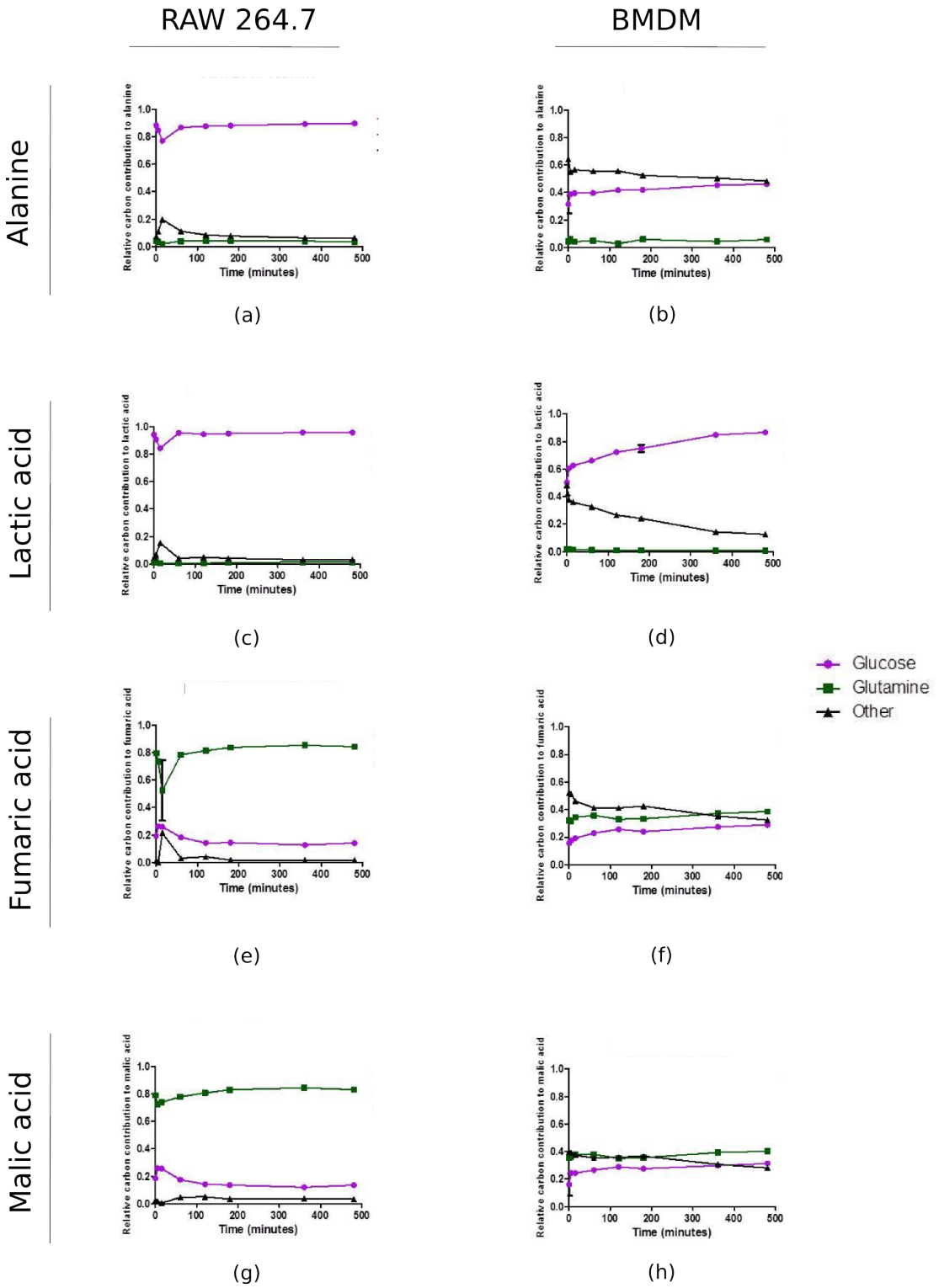

Figure 6: **Supplemental Figure: Relative carbon contribution from glucose and glutamine to selected metabolites in LPS stimulated macrophages:** (a) RAW cells and (b) BMDMs Alanine carbon contribution (c) RAW cells and (d) BMDMs Lactic acid carbon contribution (e) RAW cells and (f) BMDMs Fumaric acid carbon contribution (g) RAW cells and (h) BMDMs Malic acid carbon contribution

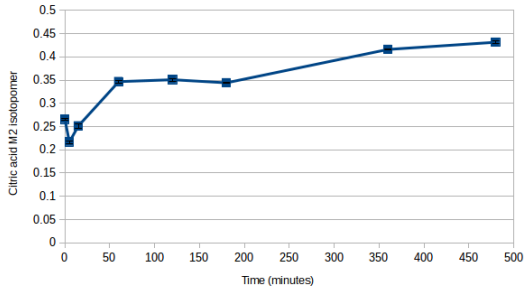

(a) BMDM - Citric Acid M2

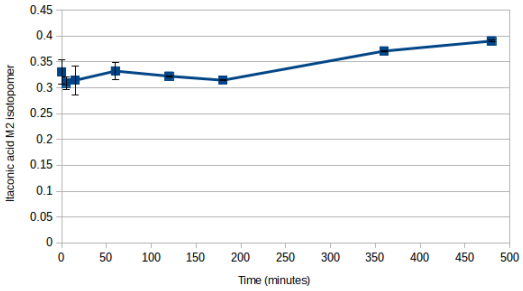

(b) BMDM - Itaconic Acid M2

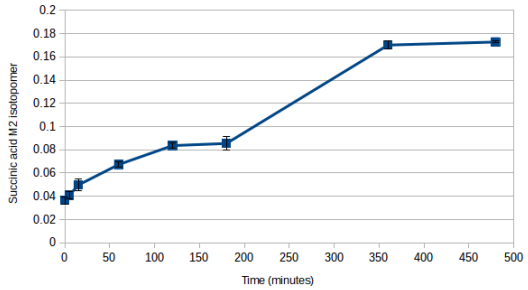

(c) BMDM - Succinic Acid M2

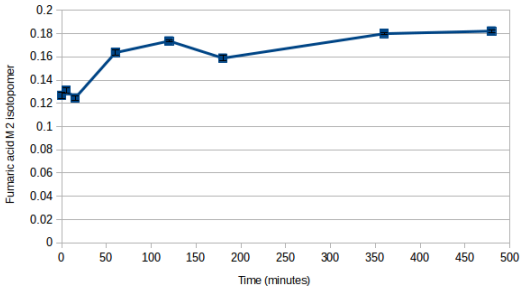

(d) BMDM - Fumaric Acid M2

Figure 7: **Supplemental Figure: Mass isotopomer distributions from glucose labeling in selected metabolites in LPS stimulated BMDMs:** (a) Citric acid M2 (b) Itaconic acid M2 (c) Succinic acid M2 (d) Fumaric acid M2

SIRT3 DECREASE IN PRO-INFLAMMATORY MACROPHAGES REGULATES POLARIZATION TO AN ANTIMICROBIAL PHENOTYPE

Sapcariu SC*, Gutiérrez S*, Wolf C, Dong X, Delcambre S, Schneider J, Robinson N, Hiller K. *To Be Submitted*. **2016**.
* These authors contributed equally to this work

This manuscript comprises a series of experiments with the aim of elucidating the effect of *Sirt3* expression reduction in macrophages stimulated to a pro-inflammatory state. By a combination of metabolomics and other complementary analyses, we determine that SIRT3 reduction in macrophages aids in the pro-inflammatory and antimicrobial phenotype, regulating cytokine secretion, inflammatory pathway regulation, as well as bacterial clearance through what is most likely an itaconic acid-dependent mechanism.

In this work, I conceived the idea of the study, performed metabolomics experiments and assisted with qPCRs. In addition, I drafted the manuscript and made figures relating to metabolomics and gene expression analysis.

SIRT3 decrease in pro inflammatory macrophages helps with polarization to a antimicrobial phenotype

Saray Gutiérrez* Sean Sapcariu* Cristina Wolf
Xiangyi Dong Sylvie Delcambre Jochen Schneider
Karsten Hiller Nirmal Robinson

* These authors contributed equally to this work

1 Introduction

The sirtuin family was discovered as a conserved family of class III NAD^+-dependent histone lysine deacetylases, active in the regulation of proteins through post-translational modification. (Michan and Sinclair, 2007). After years of study, sirtuins are still known to be NAD^+ dependent, but have been observed to act on non-histone cellular proteins in multiple cellular compartments (He et al., 2012), and to perform a wider variety of post-translational modifications including demalonylation and desuccinylation (Du et al., 2011; Peng et al., 2011).

Most sirtuin targets that have been discovered control cellular metabolism, and three sirtuin family members which are known to be active in the mitochondria, SIRT3, SIRT4, and SIRT5. These mitochondrial sirtuins affect important metabolic and regulatory pathways (including the TCA cycle, urea cycle, fatty acid oxidation, ROS metabolism, and oxidative phosphorylation), with over 20 confirmed targets (He et al., 2012). SIRT3, a lysine deacetylase, is the most studied mitochondrial sirtuin, with over 933 acetylation sites discovered in the mitochondria, affecting oxidative phosphorylation, fatty acid metabolism, and the TCA cycle (Sol et al., 2012). SIRT3 is the main sirtuin family member responsible for mitochondrial protein deacetylation, since knockout of SIRT4 and SIRT5 were shown to produce no changes in the mitochondrial acetylome (Lombard et al., 2007).

SIRT3 deacetylation activity in the mitochondria can target critical junctions of energy metabolism and inflammatory response. Two subunits of the succinate dehydrogenase (SDH) complex were found to be SIRT3 targets, showing deacetylation affects TCA cycle metabolism and oxidative phosphorylation (Cimen et al., 2009; Finley et al., 2011b). Isocitrate dehydrogenase 2 (IDH2), which regulates levels of NADPH and glutathione, protecting against ROS-mediated damage, has also been identifed as a SIRT3 target (Yu et al., 2012). Activity of mitochondrial antioxidant manganese superoxide dismutase (Mn-SOD) is directly regulated by SIRT3, impacting reactive oxygen species (ROS) in the mitochondria (Tao et al., 2010).

Macrophages are a phagocytic innate immune system cell, known to aid in the coordination of inflammatory processes for the purpose of fighting off infections (Murray and Wynn, 2011). Through inflammatory cytokine production (Duque and Descoteaux, 2015) as well as direct destruction of pathogenic bacteria (Jayaraman et al., 2013), macrophages are extremely important in tissue defense. Cytokines expressed in pro-inflammatory macrophages include IL-1β, IL-6, and TNFα, and production is triggered by cellular signaling cascades, including nuclear factor kappa B (NF-kB) and mitogen-activated protein kinase (MAPK) (Barton, 2008; Shi et al., 2009).

Salmonella enterica serovar Typhimimurium (*S.* Typhimuirum) is a gram-negative facultative anaerobic bacterium characterized by strongly inducing the secretion of pro-inflammatory cytokines in mouse models (Zhang et al., 2003). Simultaneously, *S.* Typhimurium utilizes its virulence effector proteins to modulate host cell metabolism and induce pro-inflammatory cell death (Robinson et al., 2012). Host cell defense mechanisms against *S.* Typhimurium infection involve phagolysosomal degradation, ROS production (West et al., 2011) and itaconic acid production (Cordes et al., 2015).

On a metabolic level, pro-inflammatory macrophages exhibit increased glycolytic activity and reduced oxidative phosphorylation (Galván-Peña and O'Neill, 2015) Succinic acid, a metabolite in the TCA cycle, has been found to be increased in pro-inflammatory macrophages through the metabolism of glutamine, leading to increased IL-1β activity and increased glycolytic activity through succinic acid-dependent increased HIF-1α stabilization (Tannahill et al., 2013). Also, LPS stimulation leads to increased expression of *Irg1* in macrophages, which leads to the production of the antimicrobial metabolite itaconic acid, metabolized from cis-aconitate (a TCA cycle intermediate) through CAD (Michelucci et al., 2013). Glucose oxidized into the TCA cycle through PDH is one source of carbon for itaconic acid, as HIF-1α-mediated inhibition of PDH activity through transcription of *Pdk1* is not active in LPS-activated macrophages (Meiser et al., 2015).

These two metabolites have recently been found to be connected, with itaconic acid inhibiting succiniate dehydrogenase (SDH) in order to promote the accumulation of succinic acid in LPS-stimulated macrophages (Cordes et al., 2016). This regulation fits perfectly into the "metabolic breakpoints" found in the TCA cycle by Jha et al. (2015), where network analysis shows the accumulation of these two metabolites to be the main feature of pro-inflammatory macrophage polarization.

While not yet directly implicated with metabolic changes, SIRT3 has been seen to have an play a role in pro-inflammatory macrophage activity. IDH2 and mnSOD have been shown to be a deacetylation target of SIRT3 in macrophages for the purpose of mediating ROS regulation under inflammatory conditions (Tao et al., 2010; Sheng et al., 2015). In LPS treated primary human macrophages, SIRT1 and SIRT3 mRNA and protein expression is decreased (Storka et al., 2013). Knockdown of *Sirt3* also affects inflammatory cytokine expression, increasing levels of iNOS and TNFα in RAW 264.7 macrophages (Xu et al., 2016). These findings suggest a role for SIRT3 at the interface of metabolism and inflammation, able to regulate both processes in order to drive cellular processes important for pro-inflammatory macrohpage activity.

However, previous studies have only used pathogen associated molecular patterns, and the role of SIRT3 in the innate immune defense against invading

pathogens is currently unknown. To expand upon these results, we further investigated the role of SIRT3 decrease in macrophages, and how SIRT3 regulates the macrophage response to bacterial infection. Using primary macrophages, we determined that a decrease in SIRT3 expression serves to regulate macrophage pro-inflammatory and antimicrobial activity under both LPS stimulation and bacterial infection. This regulation is mediated through the *Irg1*-itaconic-acid-SDH pathway, resulting in an increase of both itaconic acid for bacterial clearance as well as succinate for pro-inflammatory cytokine stimulation.

2 Materials and Methods

2.1 BMDM differentiation

Bone marrow was extracted from femur and tibia of 8-weeks old WT and SIRT3 KO C57BL/6 mice, and cultured for 7 days in Roswell Park Memorial Institute medium (RPMI) 1640 VLE (Merck Millipore) supplemented with 10% Fetal Bovine Serum and 20% L929 cell culture supernatant. Cells were detached by scraping, and all cell seeding and experiments were performed using RPMI as defined without L929 supernatant.

2.2 Infection and stimulation

Infection with *Salmonella* enterica serovar Typhimurium SL1344 was performed at a M.O.I. of 10 for all experiments. After addition of bacteria cells were incubated for 10 min at RT and then for 30 min at 37°C. Cells were then washed with medium containing gentamycin 50 µg/mL and left in this same medium. After two hours in medium with gentamycin 50 µg/mL, the concentration of gentamycin was reduced to 10 µg/mL.

Escherichia coli and *Salmonella enterica* serovar Typhimimurium purified LPS (Sigma Aldrich) was used, at a concentration of 100 ng/mL for all indicated experiments. Cell medium was changed directly before stimulation.

2.3 Stable isotope labeling experiments

For stable isotope labeling experiments, cells were cultured as above, but were seeded in a labeled medium 24 hours before treatment. RPMI 1640 was used which contained either no glucose or no glutamine (Thermo Fisher). For labeled glucse experiments, 11 mmol/L of U-$^{13}C_6$-Glucose (Cambridge Isotope Laboratories) was added to the medium, and for labeled glutamine experiments, 2 mmol/L of U-$^{13}C_5$-Glutamine (Campro Scientific) was added. The pH of the finished medium was adjusted to 7.4, sterile filtered through a 0.22 µm Steriflip filter unit (Merck Millipore), and stored at 4°C until use.

2.4 Metabolite and mRNA extraction protocol

The extraction protocol was performed as per Sapcariu et al. (2014). Briefly, cells were washed with 0.9% NaCl, and immediately quenched with 200 µL Chromasolv® Methanol (Sigma) at -20°C and 200 µL Millipore H_2O on ice. Cell extracts were scraped and added to eppendorf tubes containing 200 µL Chromasolv® chloroform at -20°C. Tubes with extract were then vortexed in

a 4°C shaker at 1400 rpm for 20 minutes and centrifuged at 4°C for 5 minutes at 20,000 g. 200 µL of the polar phase was transfered to a glass vial specific for GC-MS analysis (Chromatographie Zubehor Trott), dried in a rotary vacuum evaporator (Labconco) at -4°C overnight, and stored at -80°C until analysis. The interphase was stored at -80°C until RNA extraction. As an internal standard, pentanedioic-d_6 acid was added to the extraction water at a concentration of 1 µg/mL.

2.5 GC-MS Analysis

Derivitization was performed with an Gerstel autosampler directly before measurement on the GC-MS. Dried metabolites were dissolved in 15 µL of 2% methoxyamine hydrochloride in pyridine at a temperature of 40°C for 60 minutes. Then, 15 µL of 2,2,2-trifluoro-N-methyl-N-trimethylsilyl-acetamide + 1% chloro-trimethyl-silane was added and incubated at 40°C for 30 minutes.

The metabolite extracts were measured on an Agilent 7890A GC containing with a 30 m DB-35MS capillary column. The GC was connected to an Agilent 5975C MS operating in electron ionization (EI) at 70 eV.

1 µL of derivatized sample was hot injected at 270°C in splitless mode. Helium was used as the carrier gas at a flow rate of 1 mL/min. The GC oven temperature was kept constant at 100°C for 2 minutes and then increased to 300°C at 10°C/min, where it was held for 4 minutes. The total GC-MS run time of one sample was 26 minutes. For relative quantification of metabolite levels, an alkane mix was run with the experimental sequence in order to provide retention index calibration for the experimental samples.

The MS source was kept at a constant temperature of 230°C and the quadrupole at 150°C. For relative quantification of metabolite levels, the detector was operated in scan mode with an m/z range of 70 to 800. For analysis of stable isotope labeling, the detector was operated in SIM mode with specific ions selected for all compounds of interest.

2.6 mRNA extraction and Quantitative Real-Time PCR

Washed interphases were dried in a rotary vacuum evaporator (Labconco) at 4°C until all liquid phase was evaporated, and then brought to room temperature. RNA was extracted from the interphase of the samples using the Qiagen RNeasy minikit, and RNA purity was checked on a Thermo Scientific NanoDrop 2000C spectrophotometer. RNA was reverse transcribed into cDNA using Invitrogen SuperScript™ III reverse transcriptase, and stored at -20°C until qPCR analysis. All treatments were performed in technical triplicates on the 96-well plate for statistical robustness.

Analysis of cDNA was performed on a Roche LightCycler 480 II, with iq™ SYBR® green supermix including the fluorescent pigment and the polymerase required for the reactions. The program for the qPCR was as follows: activation of the polymerase for 3 minutes at 95°C, 40 amplification cycles (30 seconds denaturation at 95°C, 30 seconds annealing at 60°C, 30 seconds elongation at 72°C), melting curve analysis, and a cooling step at 40°C. Comparative quantification (using the ΔΔCt method) was performed using LibreOffice Calc. The primers used in qPCR analysis are shown in 1.

Il-1b forward	5'-GCTTCAGGCAGGCAGTATC-3'
Il-1b reverse	5'-AGGATGGGCTCTTCTTCAAAG-3'
Tnfα forward	5'-GGTTCTGTCCCTTTCACTCAC-3'
Tnfα reverse	5'-TGCCTCTTCTGCCAGTTCC-3'
Sirt3 forward	5'-TCACAACCCCAAGCCCTTTT-3'
Sirt3 reverse	5'-GTGGGCTTCAACCAGCTTTG-3'
Sirt4 forward	5'-TGAAAGAGGCGGACTCCCTA-3'
Sirt4 reverse	5'-CAACTCTCCACAGCGGGAAT-3'
Sirt5 forward	5'-CCTGGATCCTGCCATTCTGG-3'
Sirt5 reverse	5'-GGGTCCGGGAAAATGAAACC-3'
Il6 forward	5'-CGGCCTTCCCTACTTCACAA-3'
Il6 reverse	5'-TCTGCAAGTGCATCATCGTT-3'
Il10 forward	5'-GCTGCCTGCTCTTACTGACT-3'
Il10 reverse	5'-CCTGGGGCATCACTTCTACC-3'
Irg1 forward	5'-GCAACATGATGCTCAAGTCTG-3'
Irg1 reverse	5'-TGCTCCTCCGAATGATACCA-3'
Casp3 forward	5'-TCATCTCGCTCTGGTACGGA-3'
Casp3 reverse	5'-ACACACACAAAGCTGCTCCT-3'
L27 forward	5'-ACATTGACGATGGCACCTC-3'
L27 reverse	5'-GCTTGGCGATCTTCTTCTTG-3'

Table 1: Primers used for qPCR Analysis

2.7 Bacterial CFU quantification

BMDMs were infected with *S.* Typhimurium as above described. For the quantification of colony forming units (CFU) cells were washed with cold PBS and lysed with 1% Triton-X, 0.01% SDS in PBS. Several dilutions of the lysate were plated in BHI plates and incubated over night at 37°C. Next day, *S.* Typhimurium CFU were counted.

2.8 Cytokine secretion quantification (ELISA)

Supernatants from *S.* Typhimurium (MOI 10) or LPS-treated BMDMs were collected at 6h and 24h post-treatment. Analysis of secreted IL-6, TNFα, IL-1β and IL-10 in the supernatants was performed using ELISA commercial kits according to manufacturer instructions (R&D).

2.9 Cell viability assay

Cell viability of LPS-treated or *S.* Typhimurium-infected (MOI 10) BMDMs was assessed using the commercial kit RealTime-Glo (Promega) according to manufacturer instructions.

2.10 ROS measurement

The production of ROS in BMDMs upon LPS stimulation (100 ng/mL) or ST infection (MOI 10) was assessed using a commercial kit (CellROX Green, Life Technologies) according to manufacturer instructions.

2.11 Metabolomics Data Analysis

Analysis of the raw peak data for both relative metabolite quantification and MID analysis was performed using MetaboliteDetector (Hiller et al., 2009). This software provided chromatogram alignment, peak matching, and automated compound identification (using an in-house library). Raw data was exported from MetaboliteDetector and processed using either R statistical software (R Core Team, 2016) or LibreOffice Calc.

All metabolites identified with MetaboliteDetector were verified through manual chromatogram analysis of characteristic fragement peaks.

Normalization of the metabolite raw data was performed using the following methods: First, all metabolites were normalized to the internal standard added to the extraction water in order to control for variations in extraction amount and GC-MS measurements. Where applicable, normalized metabolite signal intensity was further normalized to cell count as well as to the control (or t=0) treatment, in order to provide a standard basis for comparison across experiments.

MIDs were determined from samples cultured with labeled tracers using SIM measurements. The data was corrected for natural isotope abundances using MetaboliteDetector software.

2.12 Statistical Methodology

Experiments were performed in biological triplicates with different pairs of WT and KO mice; within each experiment, each condition was repeated three times in separate wells.

Statistically significant differences of metabolites or transcript level were determined between specific treatments using an unpaired two-tailed Student's t-test. For explanation of significance in the figures, * denotes $p < 0.05$, ** denotes $p < 0.01$, and *** denotes $p < 0.001$. Error bars represent the standard deviation of the samples.

3 Results

3.1 SIRT3 mRNA expression is decreased in LPS-stimulated macrophages

In order to confirm the knowledge that *Sirt3* expression is reduced in pro-inflammatory macrophages, as well as to profile the expression changes in other mitochondrial sirtuins, we looked at a time-dependent regulation of sirtuins expression with LPS stimulation. *Sirt3* expression was reduced very quickly, reaching a local minimum after 3 hours, and stayed reduced until expression levels start to increase at the 8 hour time point (fig. 1a). Levels of *Sirt4* show no drastic change in expression aside from a short increase within an hour of LPS stimulation (fig. 1b). Expression of *Sirt5* follows the pattern of *Sirt3*, with a strong decrease by 3 hours; however, *Sirt5* levels increase more rapidly than *Sirt3*, already changing by 6 hours (fig. 1c).

SIRT3 has been seen to co-localize with SIRT5, suggesting a functional connection (Nakamura et al., 2008), and both enzymes have been found to have the same targets (Nakagawa and Guarente, 2014; Zhang et al., 2015). Thus, a

similar expression pattern shows evidence for both enzymes working together to control pro-inflammatory macrophage activity.

3.2 Knockout of *Sirt3* leads to increased inflammatory response with LPS stimulation

Using BMDMs from *Sirt3* KO mice, we investigated the effects of LPS treatment when SIRT3 was not present. SIRT3 mRNA and protein levels were measured in the *Sirt3* KO BMDMs in order to confirm that the knockout was present in the BMDMs used (fig. 2).

Knockout of *Sirt3* increased cell viability of BMDMs with LPS treatment (fig. 3), suggesting SIRT3 contributes to the metabolic fitness of macrophages upon pro-inflammatory insults. As this response is regulated in part by the macrophage inflammatory process, we treated WT and *Sirt3* KO BMDMs with LPS and monitored changes in the secretion profile of inflammatory cytokines, to study whether SIRT3 may play a role in the regulation of inflammation. We found that in the *Sirt3* KO BMDMs, the secretion of the inflammatory cytokines IL-6, IL-1β and IL-10 were significantly enhanced upon LPS stimulation (fig. 4). However, there was no change in the secretion levels of TNFα.

To look at central signaling pathways in inflammatory processes, protein expression and phosphorylation of p65, a major component of the NF-κB signaling pathway, was analyzed by western blot, showing increased activation with *Sirt3* knockout (fig. 5a). In addition, there was also an increase in the complementary MAPK pathway, as evidenced through amplified phosphorylation of p38 protein in *Sirt3* KO BMDMs (fig. 5b).

3.3 Increased inflammatory response due to a combination of ROS production and metabolite regulation

In order to determine whether this increase in inflammatory activity was a result of increased ROS production, we measured ROS levels through a fluorescense assay, and found no significant reduction in ROS in *Sirt3* KO compared to WT BMDMs treated with LPS (fig. 6). However, differences in abundances of known pro-inflammatory metabolites under LPS stimulation were found, with both itaconic acid and succinic acid increased with knockout of *Sirt3* (figs. 7a and 7b), suggesting that metabolic changes were regulating inflammatory processes when *Sirt3* was knocked out.

As it is known that SIRT3 targets multiple enzymes in the mitochondria, we investigated the effect of a knockout on intracellular metabolism. Using classical metablolomics to measure the metabolite pool sizes, as well as stable isotope assisted metabolomics techniques to determine relative carbon flux changes and the relative carbon contribution of glucose and glutamine to different metabolites.

Through incubating the macrophages with stable isotope labeled glucose and glutamine, we were able to determine the utilization of these carbon sources in LPS-stimulated macrophages, and how this changed when *Sirt3* was knocked out. While there was no significant difference between the carbon contribution from glucose to itaconic acid between WT and *Sirt3* KO BMDMs, there was a slight decrease in the carbon contribution from glutamine when SIRT3 was not active (fig. 8b). For succinic acid, there was a strong decrease in the contribution

of carbon from both glucose and glutamine in the *Sirt3* KO BMDMs (fig. 8c), signifying a dilution of these carbons from other sources. It should be noted that glutamine contribution to succinic acid continued to increase with *Sirt3* KO compared to the WT, suggesting that the inactivty of SIRT3 stops the control of glutamine metabolized to succinic acid, which could influence the increased succinic acid buildup (fig. 7b) and subsequent IL-1β secretion (fig. 4).

The labeled carbon sources also allowed us to determine how relative carbon flux to these two metabolites changed between WT and *Sirt3* knockout BMDMs stimulated with LPS. U-$^{13}C_6$-Glucose is metabolized to M1 isotopologues of itaconic acid and M2 isotopologues of succinic acid. U-$^{13}C_5$-Glutamine is metabolized to M4 isotopologues of succinic acid.

While relative glucose flux to the M1 isotopologues of itaconic acid did not change after 6 hours of LPS stimulation (fig. 9c), succinic acid M2 isotopologues increased over time with LPS stimulation (fig. 9d). Similarly to the carbon contribution from glutamine, *Sirt3* KO BMDMs show a more rapid increase of M2 labeling than the WT cells, adding evidence to the hypothesis that SIRT3 activity helps control glutamine flux to succinic acid. Relative glutamine flux was reduced to both M4 itaconic acid and M4 succinic acid in *Sirt3* knockout BMDMs for the first 6 hours of stimulation, compared to WT cells (fig. 10a), with a stronger effect in succinic acid.

These results point to a role for SIRT3 in the regulation of succinic and itaconic acid production under pro-inflammatory conditions, mostly through affecting glutamine anaplerosis. As SIRT3 is known to target and activate glutamate dehydrogenase (GDH) (Schlicker et al., 2008), knockout of the gene would lead to a reduction of glutamate entering the TCA cycle through GDH.

3.4 Metabolic implications of *Sirt3* knockout

To further investigate metabolic changes due to *Sirt3* reduction in pro-inflammatory macrophages, we looked at how SIRT3 activity could affect glycolysis. Previously, knockout of *Sirt3* was seen in fibroblasts to reduce glycolytic activity (Finley et al., 2011a), so we looked at how this pathway is regulated in inflammed macrophages. Two endpoints of glycolysis, pyruvic acid and lactic acid, show an increase in pool size in *Sirt3* KO BMDMs with LPS stimulation (fig. 11). Previous studies have found that a reduction of SIRT3 activity slows pyruvate dehydrogenase activity (Jing et al., 2013; Ozden et al., 2014), which reduces the amount of pyruvic acid which is metabolized into the TCA cycle. This, in turn, would lead to a buildup of the intracellular pyruvic acid pool. Interestingly, knock out of SIRT3 activity resulted in an increase of pyruvate dehydrogenase kinase (PDHK) protein in *S.* Typhimurium infected macrophages (fig. 17). PDHK inhibits pyruvate dehydrogenase activity, which causes the buildup of pyruvic acid as well as the funneling of this metabolite to lactic acid production.

Through glycolysis, U-$^{13}C_6$-Glucose metabolizes into M3 isotopologues of both pyruvic acid and lactic acid, and these results are shown in fig. 9. *Sirt3* knockout reduces the amount of M3 isotopologues of both metabolites, with a stronger effect in pyruvic acid. With active SIRT3, labeling of pyruvic acid reaches a plateau after 1 hour and remains stable, while an absence of SIRT3 causes a constant increase of relative glucose flux to pyruvate, suggesting a more active glycolysis (fig. 9a). This effect is present in lactic acid as well, but

to a lesser extent (fig. 9b). This hypothesis is reinforced through analysis of the relative carbon contribution from glucose and glutamine to pyruvic acid (fig. 8a), which shows the same trend as the M3 isotopologue from glucose (fig. 9a). The similarity between the two illustrate how a large majority of the labeled carbon from glucose is metabolized into an M3 lactate, with no other isotopologues being formed.

3.5 Knockout of *Sirt3* protects macrophages against *Salmonella* Typhimurium infection

We then wanted to determine how SIRT3 affects pro-inflammatory macrophage activity under an infection scenario, using *Salmonella enterica* serovar Typhimimurium as our model bacteria. First, sirtuin mRNA expression levels in infected WT BMDMs were measured in order to validate that the reduction seen in LPS-stimulated macrophages is also occurring under infection conditions. All sirtuin family members except for *Sirt1* showed reduced expression levels with *S.* Typhimurium infection (fig. 12).

To measure pro-inflammatory activity of WT and *Sirt3* KO BMDMs infected with *S.* Typhimurium, secretion profiles of cytokines were measured. Levels of secreted IL-6, IL-1β and IL-10 were enhanced in the *Sirt3* KO BMDMs upon infection (fig. 14). In contrast, levels of TNFα secretion were reduced. In addition, activity of the NF-κB and MAPK pathways were analyzed as with the LPS-stimulated BMDMs, with knockout of *Sirt3* leading to increased p65 phosphorylation (fig. 15a) and no change in p38 phosphorylation (fig. 15b).

To gain further insight into the effect of SIRT3 in the innate immune defense against bacterial infection we quantified the colony forming units (CFU) in WT and *Sirt3* KO BMDMs after 24h of infection with *S.* Typhimurium. We found a decreased number of CFU in the *Sirt3* KO BMDMs compared to WT, indicating that the absence of SIRT3 enhances the clearance of intracellular pathogens (fig. 13). Increased bacterial clearance correlated with decreased cell death in the *Sirt3* KO BMDMs (fig. 3), a similar result to LPS-stimulated macrophages.

The increased antimicrobial activity can be attributed to two known sources, increased itaconic acid (Michelucci et al., 2013) and increased ROS (Tao et al., 2010). Infection with *S.* Typhimurium increased ROS and itaconic acid production in macrophages (fig. 6), showing a regulatory role for SIRT3 in antimicrobial macrophage activities. SIRT3 has been shown to target IDH2 (Yu et al., 2012), which is a proposed "metabolic breakpoint" leading to the buildup of itaconic acid (Jha et al., 2015). We observed that knock out of SIRT3 activity causes hyperacetylation of IDH2 (fig. 17), which in turn decreases its activity. This reduction of IDH2 activity causes a shunting of carbon towards itaconic acid production.

3.6 CAD is a potential target for SIRT3 deacetylation activity

In order to understand how SIRT3 is able to regulate the metabolic activity of itaconic acid, we investigated a possible link between SIRT3 and *Irg1*/CAD. Using both *Sirt3* KO and *Irg1* KO BMDMs, we measured the expression level of the other gene, and found no dependence of mRNA level between the two genes (fig. 16). In addition, the protein levels of IRG1/CAD were measured in *S.*

Typhimurium infected cells, with no discernible difference between the wild type and the knockout (fig. 17). Fluroescence microscopy showed that SIRT3 and CAD proteins co-localize outside of the nucleus after 6 hours of LPS stimulation (fig. 18).

CAD acetylation results are in process. If CAD is acetylated, there is a strong possibility that it is a SIRT3 target, thus regulating itaconic acid.

4 Discussion

While decreased expression of *Sirt3* has been seen before in LPS-stimulated macrophages, no further research has been performed to uncover the effects of this downregulation. In this study, we investigated how a reduction of SIRT3 activity in macrophages can affect inflammatory cytokine and metabolic regulation. Our results uncover that the reduction of *Sirt3* expression in pro-inflammatory macrophages serves to increase the production of itaconic acid and pro-inflammatory cytokines, therefore aiding in bacterial clearance and improving the viability of macrophages under a pro-inflammatory challenge.

Both stimulation with LPS and infection with *Salmonella* Typhimurium in *Sirt3* knockout BMDMs induced an increase in pro-inflammatory cytokines, an upregulation of NF-kB and MAPK signaling pathways, as well as an increase in the pro-inflammatory metabolites itaconic and succinic acid. As a reduction of SIRT3 activity would concurrently reduce the activity of IDH2, PDH, and GDH, the amount of carbon from glucose and glutamine present in the production of itaconic acid and succinic acid should decrease. Glutamine contribution to succinic acid continued to increase with *Sirt3* KO compared to the WT (fig. 8c), suggesting that the inactivty of SIRT3 stops the control of glutamine metabolized to succinic acid, which could influence the increased succinic acid buildup (fig. 7b) and subsequent IL-1β secretion (fig. 4). There was no significant decrease in contribution from either glucose or glutamine to itaconic acid (fig. 8b). This highlights the metabolic importance of these two metabolites under pro-inflammatory conditions, as the cell attempts to maximize production of both metabolites when challenged.

Absence of *Sirt3* in *S.* Typhimurium infected BMDMs led to increased clearance of the bacteria and improved viability of the macrophages, most likely due to the induction of the pro-inflammatory phenotype. However, this was not due to SIRT3 induction of ROS in the cell (Tao et al., 2010), and is instead due to an increase in itaconic acid production, a known antimicrobial (Michelucci et al., 2013). The increase of itaconic acid through a reduction of *Sirt3* could be due to SIRT3 activity on CAD, the enzyme catalyzing the production of itaconic acid. However, the link between SIRT3 and CAD is not yet confirmed, and this should be followed up with further studies investigating direct interactions between the two proteins.

Recently, it was found that itaconic acid can inhibit succinate dehydrogenase, leading to a buildup of succinic acid in the cell (Cordes et al., 2016). This, in turn, will lead to increased expression of IL-1β (Tannahill et al., 2013), a result found in our study. Upregulation of *Irg1* has been found to inhibit production of pro-inflammatory cytokines in LPS-tolerized macrophages (Li et al., 2013), and *Irg1*-mediated production of itaconic acid has been recently shown to reduce both pro-inflammatory cytokine production as well as oxygen consump-

tion in LPS-activated macrophages (Lampropoulou et al., 2016). The results of our study point to SIRT3 activity being integrated into this process, partly mediating the production of pro-inflammatory metabolites and the reduction in pro-inflammatory cytokines (fig. 19).

It is known that SIRT3 can co-localize with SIRT5 (Nakamura et al., 2008), and both sirtuin family members have been observed to have the same targets in the mitochondria(Nakagawa and Guarente, 2014; Zhang et al., 2015). Our results show the expression levels of both *Sirt3* and *Sirt5* decrease similarity, which could lead to a combined regulation of the metabolic processes leading to increased itaconic and succinic acid. Further research on the role of SIRT5 in pro-inflammatory macrophages would be necessary to elucidate the role of this enzyme.

Interestingly, reduction of SIRT3 activity leads to a buildup of pyruvic and lactic acid (fig. 11), and possibly a more active glycolysis. These results mimic those found previously in fibroblasts (Finley et al., 2011a), but as SIRT3 is mainly located in the mitochondria, it is currently unclear as to why there would be an effect on a cytosolic pathway. While SIRT3 is not known to be active in the cytosol, there are other sirtuins which regulate activity there. This could be an interesting point of study to understand currently unknown areas of sirtuin research, such as how sirtuins act interact with each other, and any possible signaling that may take place between them.

This study uncovers a new role for SIRT3 in the macrophage response to bacterial invasion, through a regulatory network combining SIRT3 with *Irg1*/CAD and SDH, as well as itaconic and succinic acid production. Our results add SIRT3 as well to a list of targets that can be utilized as control points for combating diseases where macrophage dysregulation and activity

5 Bibliography

References

Gregory M Barton. A calculated response: control of inflammation by the innate immune system. *The Journal of clinical investigation*, 118(2):413–20, February 2008. doi: 10.1172/JCI34431.

Huseyin Cimen, Min-Joon Han, Yongjie Yang, Qiang Tong, Hasan Koc, and Emine C Koc. Regulation of succinate dehydrogenase activity by sirt3 in mammalian mitochondria. *Biochemistry*, 49(2):304–311, 2009.

Thekla Cordes, Alessandro Michelucci, and Karsten Hiller. Itaconic acid: the surprising role of an industrial compound as a mammalian antimicrobial metabolite. *Annual review of nutrition*, 35:451–473, 2015.

Thekla Cordes, Martina Wallace, Alessandro Michelucci, Ajit S Divakaruni, Sean C Sapcariu, Carole Sousa, Haruhiko Koseki, Pedro Cabrales, Anne N Murphy, Karsten Hiller, et al. Immunoresponsive gene 1 and itaconate inhibit succinate dehydrogenase to modulate intracellular succinate levels. *Journal of Biological Chemistry*, pages jbc–M115, 2016.

Jintang Du, Yeyun Zhou, Xiaoyang Su, Jiu Jiu Yu, Saba Khan, Hong Jiang, Jungwoo Kim, Jimin Woo, Jun Huyn Kim, Brian Hyun Choi, et al. Sirt5 is

a nad-dependent protein lysine demalonylase and desuccinylase. *Science*, 334 (6057):806–809, 2011.

Guillermo Arango Duque and Albert Descoteaux. Macrophage cytokines: involvement in immunity and infectious diseases. *Secretion of Cytokines and Chemokines by Innate Immune Cells*, page 6, 2015.

Lydia WS Finley, Arkaitz Carracedo, Jaewon Lee, Amanda Souza, Ainara Egia, Jiangwen Zhang, Julie Teruya-Feldstein, Paula I Moreira, Sandra M Cardoso, Clary B Clish, et al. Sirt3 opposes reprogramming of cancer cell metabolism through hif1α destabilization. *Cancer cell*, 19(3):416–428, 2011a.

Lydia WS Finley, Wilhelm Haas, Valérie Desquiret-Dumas, Douglas C Wallace, Vincent Procaccio, Steven P Gygi, and Marcia C Haigis. Succinate dehydrogenase is a direct target of sirtuin 3 deacetylase activity. *PloS one*, 6(8): e23295, 2011b.

Silvia Galván-Peña and Luke AJ O'Neill. Metabolic reprograming in macrophage polarization. *M1/M2 Macrophages: The Arginine Fork in the Road to Health and Disease*, 5(420):275, 2015.

Wenjuan He, John C Newman, Margaret Z Wang, Linh Ho, and Eric Verdin. Mitochondrial sirtuins: regulators of protein acylation and metabolism. *Trends in Endocrinology & Metabolism*, 23(9):467–476, 2012.

Karsten Hiller, Jasper Hangebrauk, Christian Jäger, Jana Spura, Kerstin Schreiber, and Dietmar Schomburg. MetaboliteDetector: comprehensive analysis tool for targeted and nontargeted GC/MS based metabolome analysis. *Analytical chemistry*, 81(9):3429–39, May 2009.

Pushpa Jayaraman, Isabel Sada-Ovalle, Tomoyasu Nishimura, Ana C Anderson, Vijay K Kuchroo, Heinz G Remold, and Samuel M Behar. Il-1β promotes antimicrobial immunity in macrophages by regulating tnfr signaling and caspase-3 activation. *The Journal of Immunology*, 190(8):4196–4204, 2013.

Abhishek K Jha, Stanley Ching-Cheng Huang, Alexey Sergushichev, Vicky Lampropoulou, Yulia Ivanova, Ekaterina Loginicheva, Karina Chmielewski, Kelly M Stewart, Juliet Ashall, Bart Everts, et al. Network integration of parallel metabolic and transcriptional data reveals metabolic modules that regulate macrophage polarization. *Immunity*, 42(3):419–430, 2015.

Enxuan Jing, Brian T O'Neill, Matthew J Rardin, André Kleinridders, Olga R Ilkeyeva, Siegfried Ussar, James R Bain, Kevin Y Lee, Eric M Verdin, Christopher B Newgard, et al. Sirt3 regulates metabolic flexibility of skeletal muscle through reversible enzymatic deacetylation. *Diabetes*, 62(10):3404–3417, 2013.

Vicky Lampropoulou, Alexey Sergushichev, Monika Bambouskova, Sharmila Nair, Emma E Vincent, Ekaterina Loginicheva, Luisa Cervantes-Barragan, Xiucui Ma, Stanley Ching-Cheng Huang, Takla Griss, et al. Itaconate links inhibition of succinate dehydrogenase with macrophage metabolic remodeling and regulation of inflammation. *Cell Metabolism*, 24(1):158–166, 2016.

Yingke Li, Peng Zhang, Chengcai Wang, Chaofeng Han, Jun Meng, Xingguang Liu, Sheng Xu, Nan Li, Qingqing Wang, Xueyin Shi, et al. Immune responsive gene 1 (irg1) promotes endotoxin tolerance by increasing a20 expression in macrophages through reactive oxygen species. *Journal of Biological Chemistry*, 288(23):16225–16234, 2013.

David B Lombard, Frederick W Alt, Hwei-Ling Cheng, Jakob Bunkenborg, Ryan S Streeper, Raul Mostoslavsky, Jennifer Kim, George Yancopoulos, David Valenzuela, Andrew Murphy, et al. Mammalian sir2 homolog sirt3 regulates global mitochondrial lysine acetylation. *Molecular and cellular biology*, 27(24):8807–8814, 2007.

Johannes Meiser, Lisa Krämer, Sean C Sapcariu, Nadia Battello, Jenny Ghelfi, Aymeric Fouquier D'Herouel, Alexander Skupin, and Karsten Hiller. Pro-inflammatory macrophages sustain pyruvate oxidation through pyruvate dehydrogenase for the synthesis of itaconate and to enable cytokine expression. *Journal of Biological Chemistry*, pages jbc–M115, 2015.

Shaday Michan and David Sinclair. Sirtuins in mammals: insights into their biological function. *Biochemical Journal*, 404(1):1–13, 2007.

Alessandro Michelucci, Thekla Cordes, Jenny Ghelfi, Arnaud Pailot, Norbert Reiling, Oliver Goldmann, Tina Binz, André Wegner, Aravind Tallam, Antonio Rausell, et al. Immune-responsive gene 1 protein links metabolism to immunity by catalyzing itaconic acid production. *Proceedings of the National Academy of Sciences*, 110(19):7820–7825, 2013.

Peter J Murray and Thomas a Wynn. Protective and pathogenic functions of macrophage subsets. *Nature reviews. Immunology*, 11(11):723–37, November 2011. doi: 10.1038/nri3073.

Takashi Nakagawa and Leonard Guarente. Snapshot: sirtuins, nad, and aging. *Cell metabolism*, 20(1):192–192, 2014.

Yasuhiko Nakamura, Masahito Ogura, Daisuke Tanaka, and Nobuya Inagaki. Localization of mouse mitochondrial sirt proteins: shift of sirt3 to nucleus by co-expression with sirt5. *Biochemical and biophysical research communications*, 366(1):174–179, 2008.

Ozkan Ozden, Seong-Hoon Park, Brett A Wagner, Ha Yong Song, Yueming Zhu, Athanassios Vassilopoulos, Barbara Jung, Garry R Buettner, and David Gius. Sirt3 deacetylates and increases pyruvate dehydrogenase activity in cancer cells. *Free Radical Biology and Medicine*, 76:163–172, 2014.

Chao Peng, Zhike Lu, Zhongyu Xie, Zhongyi Cheng, Yue Chen, Minjia Tan, Hao Luo, Yi Zhang, Wendy He, Ke Yang, et al. The first identification of lysine malonylation substrates and its regulatory enzyme. *Molecular & Cellular Proteomics*, 10(12):M111–012658, 2011.

R Core Team. *R: A Language and Environment for Statistical Computing*. R Foundation for Statistical Computing, Vienna, Austria, 2016. URL `https://www.R-project.org/`.

Nirmal Robinson, Scott McComb, Rebecca Mulligan, Renu Dudani, Lakshmi Krishnan, and Subash Sad. Type i interferon induces necroptosis in macrophages during infection with salmonella enterica serovar typhimurium. *Nature immunology*, 13(10):954–962, 2012.

Sean C Sapcariu, Tamara Kanashova, Daniel Weindl, Jenny Ghelfi, Gunnar Dittmar, and Karsten Hiller. Simultaneous extraction of proteins and metabolites from cells in culture. *MethodsX*, 1:74–80, 2014.

Christine Schlicker, Melanie Gertz, Panagiotis Papatheodorou, Barbara Kachholz, Christian FW Becker, and Clemens Steegborn. Substrates and regulation mechanisms for the human mitochondrial sirtuins sirt3 and sirt5. *Journal of molecular biology*, 382(3):790–801, 2008.

Shangchun Sheng, Yi Kang, Yongchan Guo, Qinli Pu, Miao Cai, and Zhiguang Tu. Overexpression of sirt3 inhibits lipid accumulation in macrophages through mitochondrial idh2 deacetylation. *International journal of clinical and experimental pathology*, 8(8):9196, 2015.

Liang Shi, Saiful M Chowdhury, Heather S Smallwood, Hyunjin Yoon, Heather M Mottaz-Brewer, Angela D Norbeck, Jason E McDermott, Therese R W Clauss, Fred Heffron, Richard D Smith, and Joshua N Adkins. Proteomic investigation of the time course responses of RAW 264.7 macrophages to infection with Salmonella enterica. *Infection and immunity*, 77(8):3227–33, August 2009. doi: 10.1128/IAI.00063-09.

Eri Maria Sol, Sebastian A Wagner, Brian T Weinert, Amit Kumar, Hyun-Seok Kim, Chu-Xia Deng, and Chunaram Choudhary. Proteomic investigations of lysine acetylation identify diverse substrates of mitochondrial deacetylase sirt3. *PloS one*, 7(12):e50545, 2012.

Angela Storka, Gerhard Führlinger, Martin Seper, Lisa Wang, Michael Jew, Asha Leisser, and Michael Wolzt. E. coli endotoxin modulates the expression of sirtuin proteins in pbmc in humans. *Mediators of inflammation*, 2013, 2013.

GM Tannahill, AM Curtis, J Adamik, EM Palsson-McDermott, AF McGettrick, G Goel, C Frezza, NJ Bernard, B Kelly, NH Foley, et al. Succinate is an inflammatory signal that induces il-1 [bgr] through hif-1 [agr]. *Nature*, 496 (7444):238–242, 2013.

Randa Tao, Mitchell C Coleman, J Daniel Pennington, Ozkan Ozden, Seong-Hoon Park, Haiyan Jiang, Hyun-Seok Kim, Charles Robb Flynn, Salisha Hill, W Hayes McDonald, et al. Sirt3-mediated deacetylation of evolutionarily conserved lysine 122 regulates mnsod activity in response to stress. *Molecular cell*, 40(6):893–904, 2010.

A Phillip West, Igor E Brodsky, Christoph Rahner, Dong Kyun Woo, Hediye Erdjument-Bromage, Paul Tempst, Matthew C Walsh, Yongwon Choi, Gerald S Shadel, and Sankar Ghosh. Tlr signalling augments macrophage bactericidal activity through mitochondrial ros. *Nature*, 472(7344):476–480, 2011.

Hongliang Xu, Ann V Hertzel, Kaylee A Steen, and David A Bernlohr. Loss of fatty acid binding protein 4/ap2 reduces macrophage inflammation through activation of sirt3. *Molecular Endocrinology*, pages me–2015, 2016.

Wei Yu, Kristin E Dittenhafer-Reed, and John M Denu. Sirt3 protein deacetylates isocitrate dehydrogenase 2 (idh2) and regulates mitochondrial redox status. *Journal of Biological Chemistry*, 287(17):14078–14086, 2012.

Shuping Zhang, Robert A Kingsley, Renato L Santos, Helene Andrews-Polymenis, Manuela Raffatellu, Josely Figueiredo, Jairo Nunes, Renee M Tsolis, L Garry Adams, and Andreas J Bäumler. Molecular pathogenesis of salmonella enterica serotype typhimurium-induced diarrhea. *Infection and immunity*, 71(1):1–12, 2003.

Yuxun Zhang, Sivakama S Bharathi, Matthew J Rardin, Radha Uppala, Eric Verdin, Bradford W Gibson, and Eric S Goetzman. Sirt3 and sirt5 regulate the enzyme activity and cardiolipin binding of very long-chain acyl-coa dehydrogenase. *PloS one*, 10(3):e0122297, 2015.

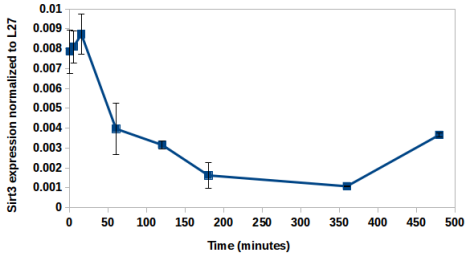

(a) Sirt3

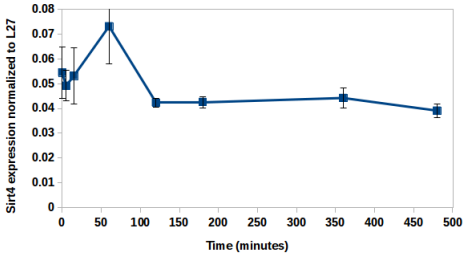

(b) Sirt4

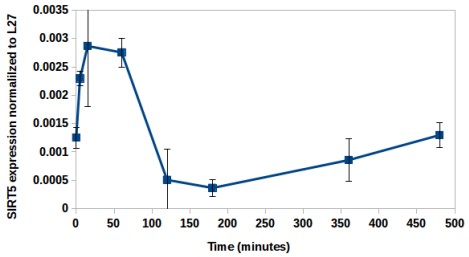

(c) Sirt5

Figure 1: **mRNA expression of (a) Sirt3 (b) Sirt4 and (c) Sirt5 in LPS treated macrophages**

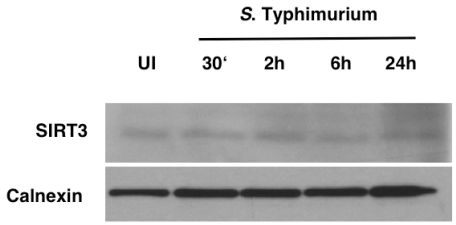

Figure 2: **Protein expression of SIRT3 in ST infected *Sirt3* WT and KO macrophages**

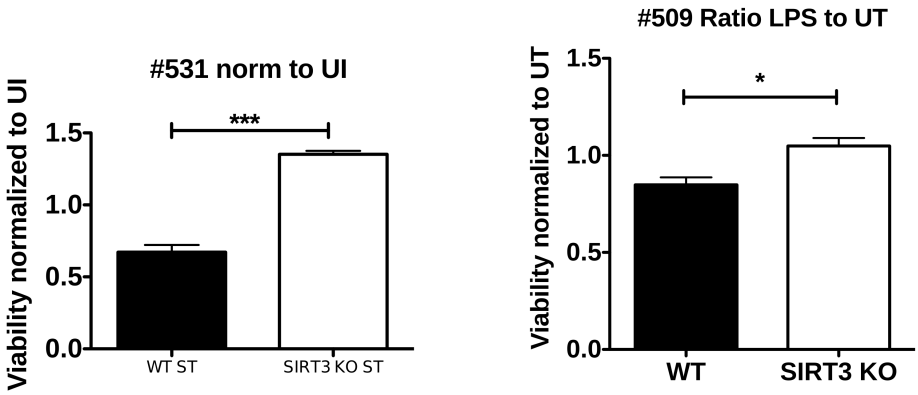

Figure 3: **Cell viability in LPS treated and ST infected *Sirt3* WT and KO macrophages**

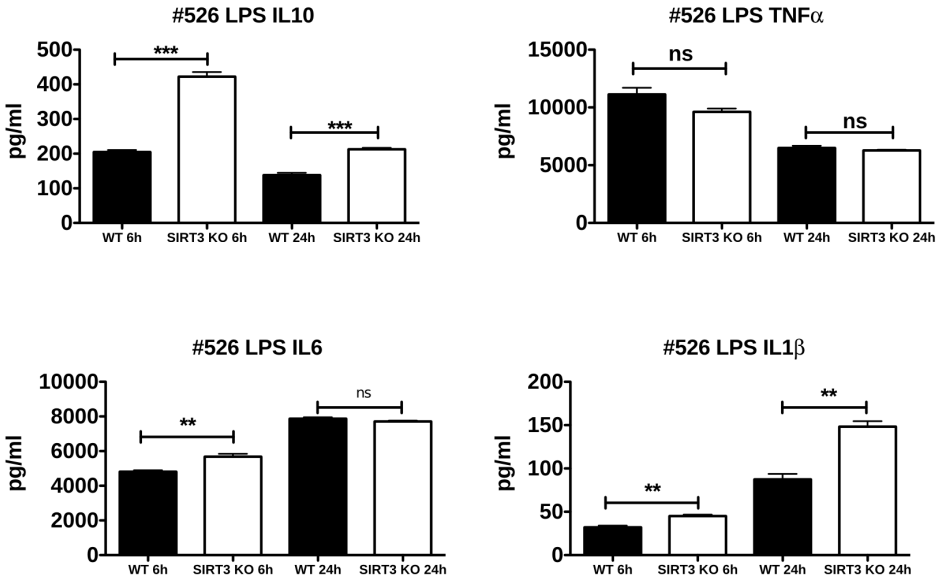

Figure 4: **ELISA analysis of protein activity in LPS treated *Sirt3* WT and KO macrophages**

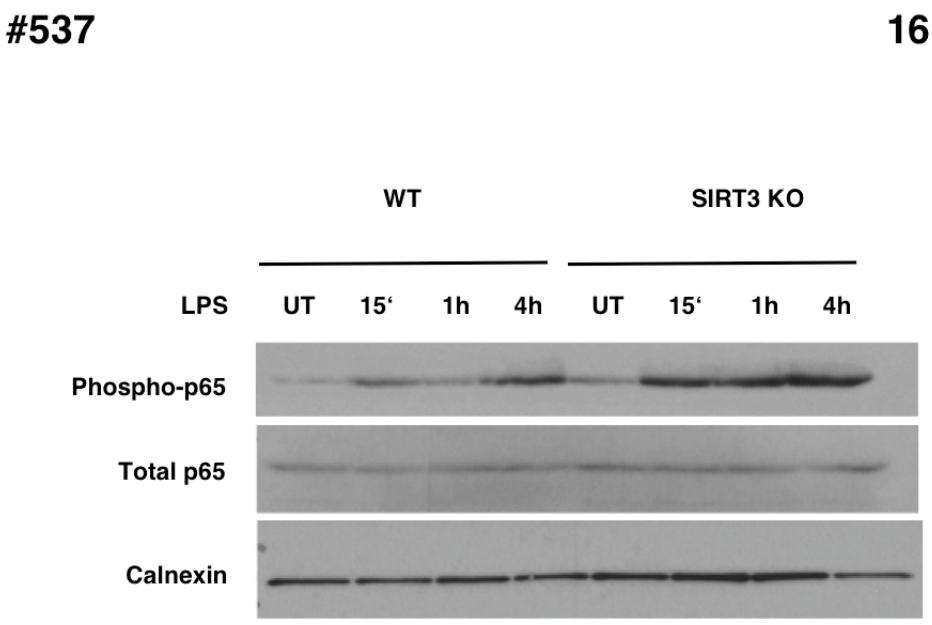

(a) p65 - NFkB signaling

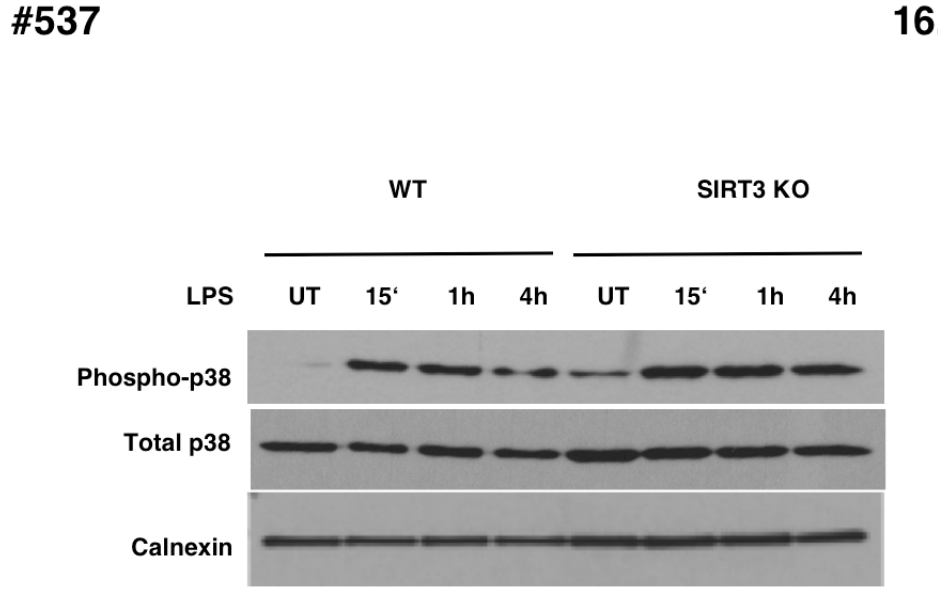

(b) p38 - MAPK signaling

Figure 5: **Protein expression of (a) p65 and (b) p38 in LPS treated *Sirt3* WT and KO macrophages**

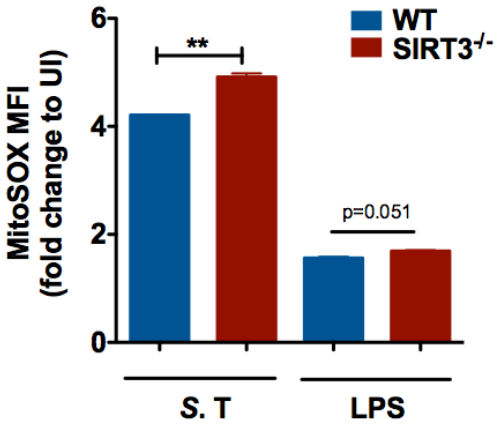

Figure 6: **ROS levels in LPS treated and ST infected *Sirt3* WT and KO macrophages**

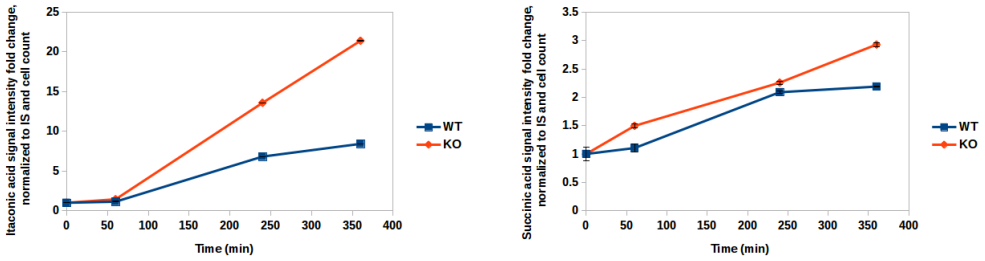

(a) Itaconic Acid

(b) Succinic Acid

Figure 7: **Metabolite levels in LPS treated *Sirt3* WT and KO macrophages** (a) Itaconic acid (b) Succinic acid

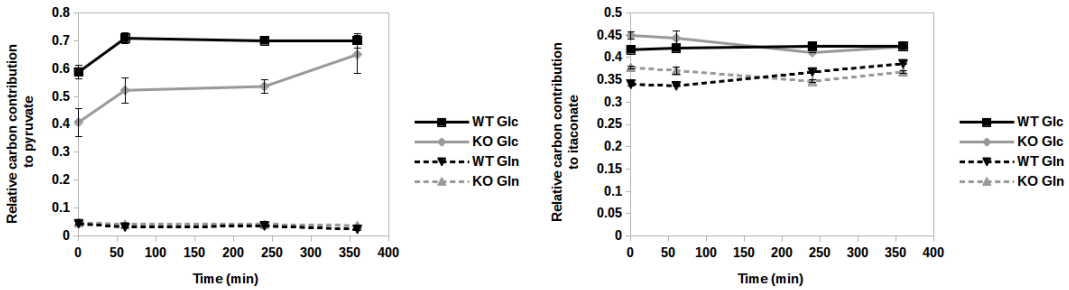

(a) Pyruvate

(b) Itaconic acid

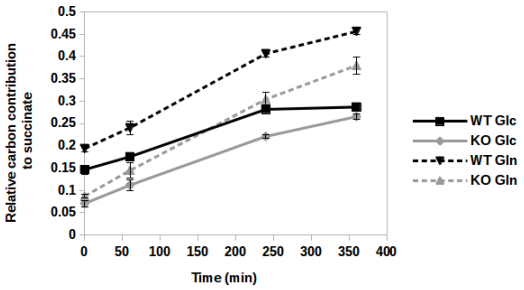

(c) Succinic acid

Figure 8: **Relative carbon contribution for selected metabolites:** (a) Pyruvate (b) Itaconic acid (c) Succinic acid

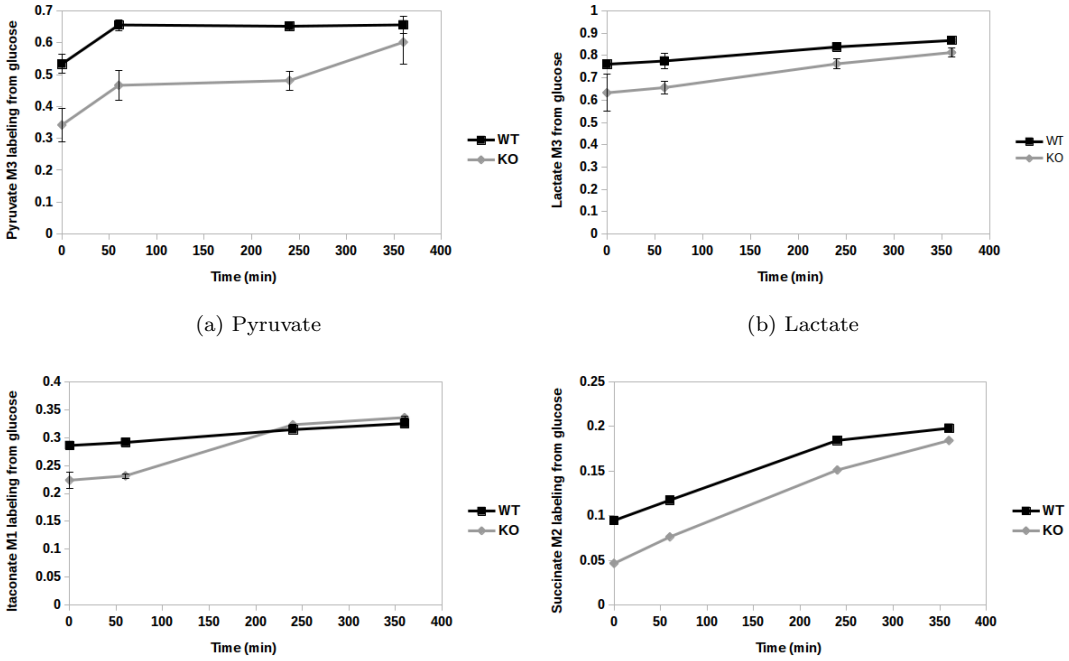

(a) Pyruvate

(b) Lactate

(c) Itaconic acid

(d) Succinic acid

Figure 9: **Glucose derived MIDs for selected metabolites:** (a) Pyruvate (b) Lactate (c) Itaconic acid (d) Succinic acid

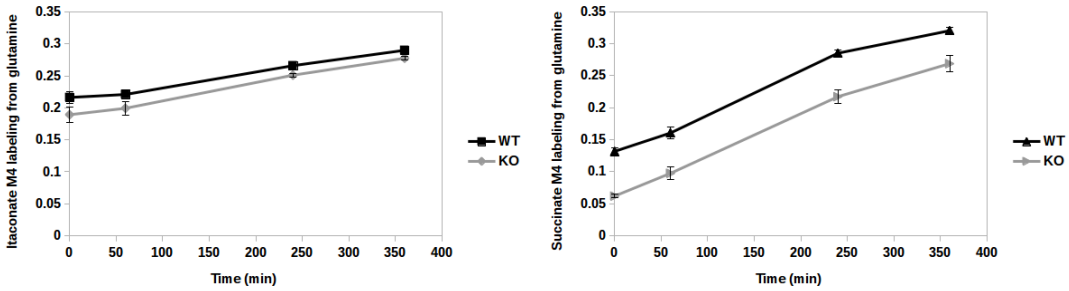

(a) Itaconic acid

(b) Succinic acid

Figure 10: **Glutamine derived MIDs for selected metabolites:** (a) Itaconic acid (b) Succinic acid

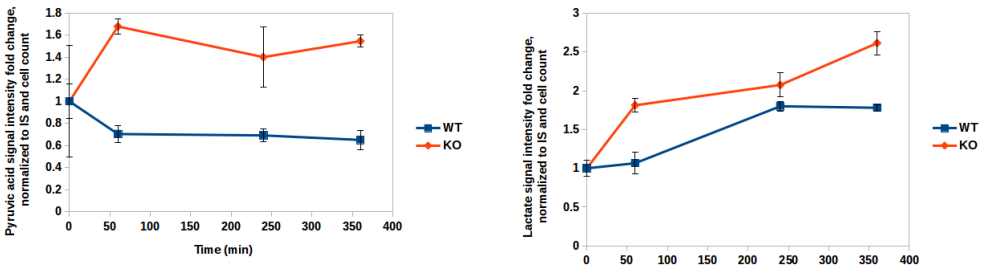

(a) Pyruvic acid (b) Lactic acid

Figure 11: **Selected metabolite levels in LPS treated WT and *Sirt3* KO BMDMs (a) Pyruvic acid and (b) Lactic acid**

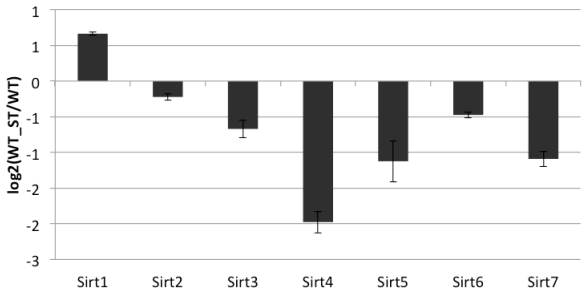

Figure 12: Expression levels of sirtuin mRNA in ST infected BMDMs

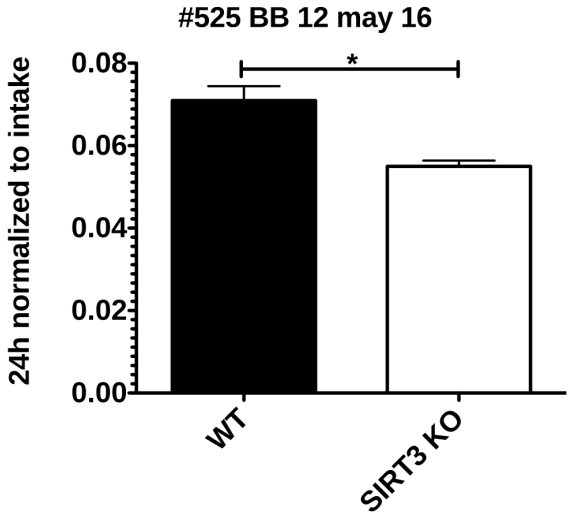

Figure 13: **Bactrerial clearance in ST infected *Sirt3* WT and KO macrophages**

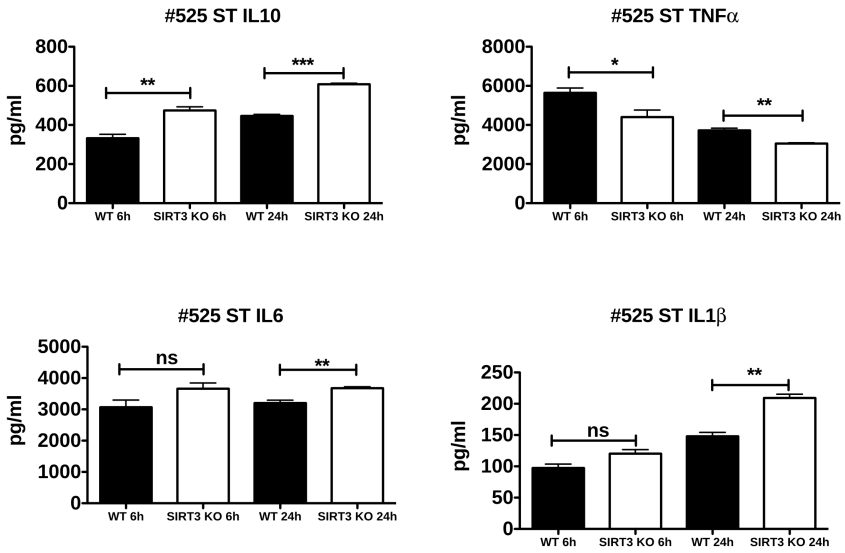

Figure 14: **ELISA analysis of protein activity in ST infected *Sirt3* WT and KO macrophages**

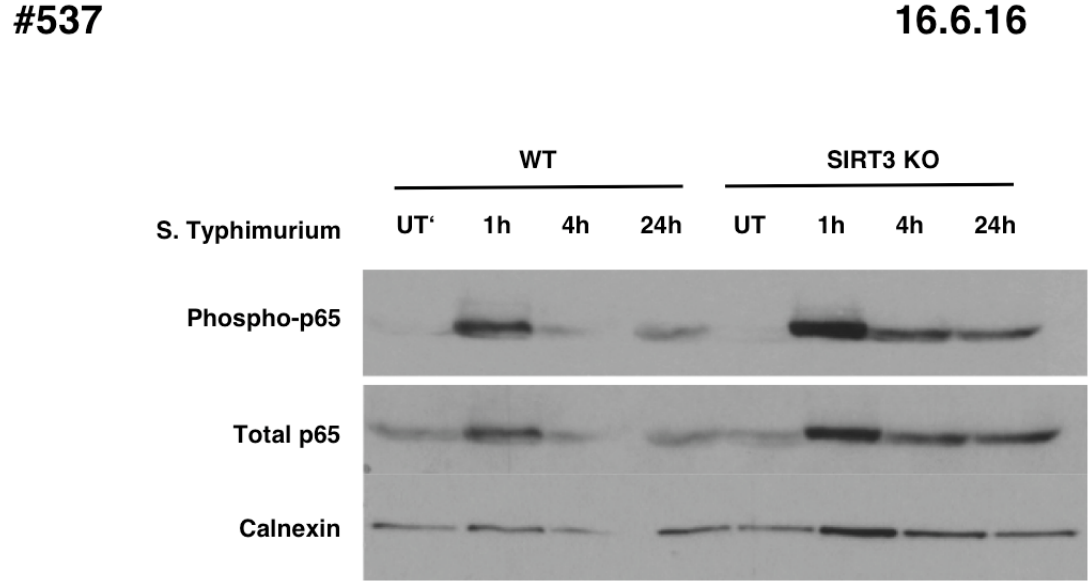

(a) p65 - NFkB signaling

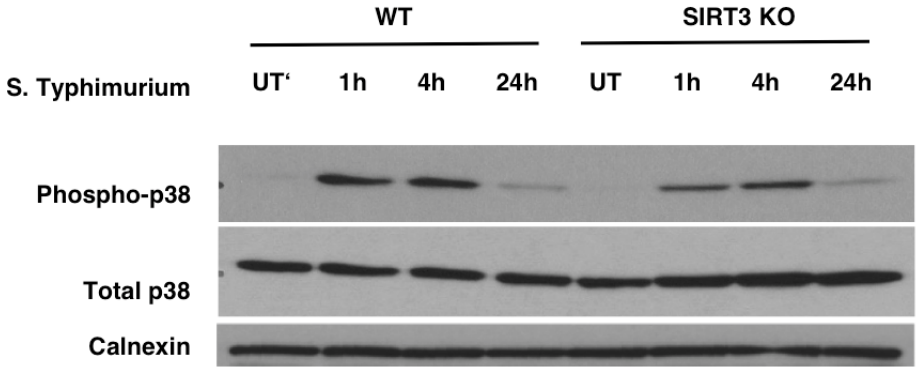

(b) p38 - MAPK signaling

Figure 15: **Protein expression of (a) p65 and (b) p38 in ST infected *Sirt3* WT and KO macrophages**

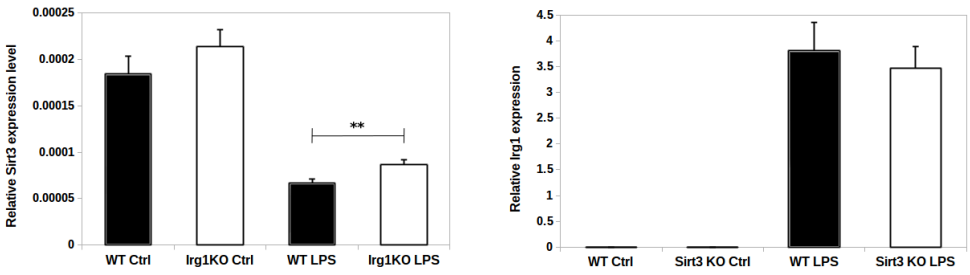

(a) *Sirt3* expression in *Irg1* KO BMDMs (b) *Irg1* expression in *Sirt3* KO BMDMs

Figure 16: **mRNA expression levels of (a) *Sirt3* in *Irg1* KO BMDMs and (b) *Irg1* in *Sirt3* KO BMDMs**

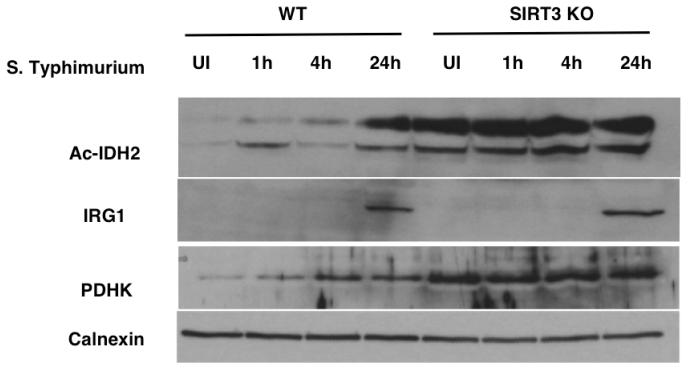

Figure 17: **Protein expression of acetylated IDH2, IRG1, and PDHK in LPS treated and ST infected *Sirt3* WT and KO macrophages**

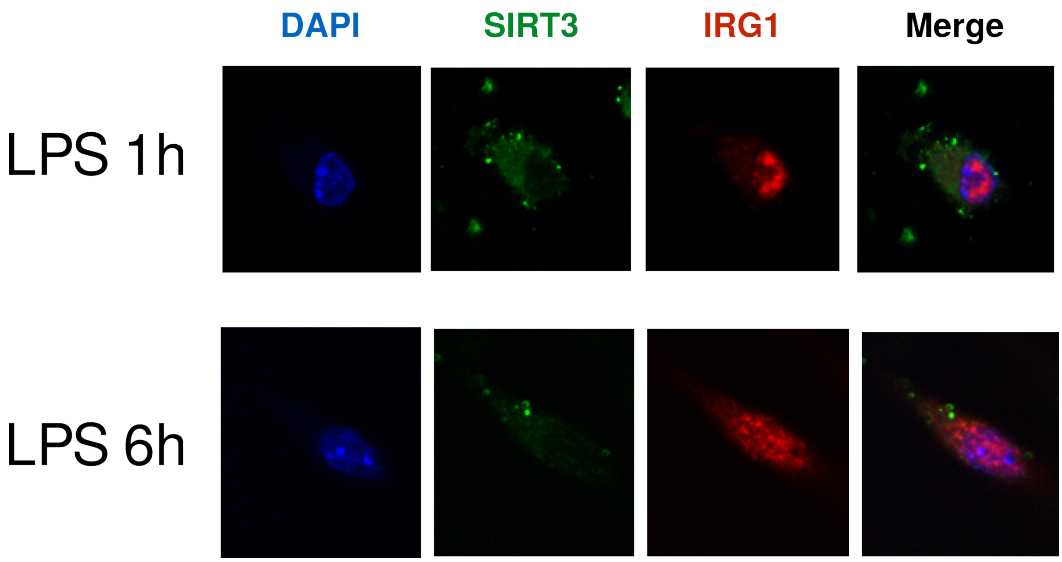

Figure 18: **Fluorescence imagery of IRG1 and SIRT3 localization in LPS stimulated WT macrophages**

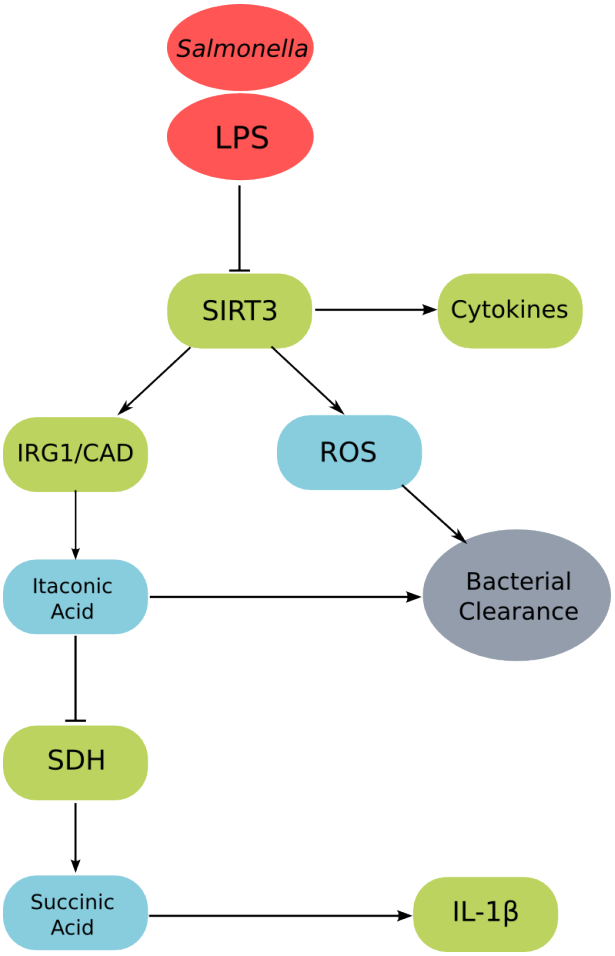

Figure 19: **Summary figure** - Challenge with LPS or bacterial infection causes a decrease in SIRT3, which promotes IRG1/CAD activity. This causes an increase in the production of itaconic acid, which in turn inhibits succinate dehydrogenase, leading to a buildup of succinic acid. This increases the secretion of IL-1β. Simultaneously, SIRT3 reduction causes an increase in other cytokine production. The increase in cytokines along with the production of an antimicrobial metabolite itaconic acid lead to increased bacterial clearance in the macrophage.

4

DISCUSSION AND PERSPECTIVES

Through multiple studies utilizing the combination of metabolomics experiments with complementary analyses on other levels of cellular regulation, the work in this thesis aimed to extend current knowledge about macrophage metabolism under inflammatory conditions. Digging deeper into the metabolic regulation of pro-inflammatory macrophages, a series of studies were performed in order to understand more about TCA cycle metabolism, and how this is affected under inflammatory conditions. The main scientific questions all corresponded to both itaconic acid production and how cellular central carbon metabolism is reorganized during the inflammatory process in macrophages, as well as the role that the mitochondrial deacetylase SIRT3 plays in the regulation of these changes.

It must be noted that for all of these studies, the joint omics extraction method utilized by our lab was extremely important for obtaining experimental data (Sapcariu *et al.*, 2014) (see Chapter 3). This method allows the maximal amount of data to be derived from individual samples, increasing experimental efficiency, and minimizing variance through the reduction of experiments required. Normally, a protocol is given in a materials and methods section of an article. These descriptions are not always fully detailed, and important steps may be omitted. Thus, it was very important to share this specific protocol with the greater scientific community, to make sure that as many laboratories as possible are able to utilize this technique for their own studies. A standardized methodology can only improve data interpretation between experiments, and is a good step towards more reproducible results from metabolomics studies.

4.1 PRO-INFLAMMATORY EFFECTS OF AEROSOLS ON MULTIPLE LEVELS OF CELLULAR REGULATION

Inflammatory effects are known to result from exhaust particle exposure in lung cells (Schwarze *et al.*, 2013), but there have been no studies looking at omics level regulation of cells using an air-liquid interface exposure system. Through studies carried out as a part of the HICE consortium, we used an ALI system to conduct a multi-omics analysis of lung epithelial cells exposed to diesel fuel and heavy fuel oil aerosols, two common fuels used in transport shipping (Oeder *et al.*, 2015) (see Chapter 3). Heavy fuel oil is a sulfur containing shipping fuel used for long distance high energy engine use, while diesel fuel is considered to be cleaner, and used more in harbor regions in order to reduce sulfur emissions near populated areas.

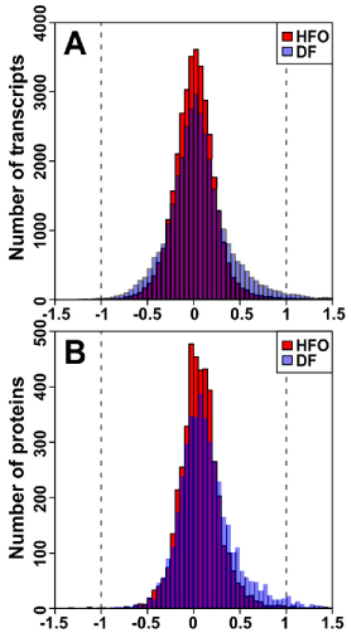

Figure 9: Particle effects on lung cells. (A) Histogram of regulated components in the transcriptome, (B) Histogram of regulated components in the proteome. On both levels of cellular regulation, heavy fuel oil shows a narrower range of regulation than diesel fuel oil. HFO - heavy marine fuel oil, DF - diesel fuel. From Oeder *et al.* (2015), figure created by J. Passig

Unlike submerged experiments, which use particles dissolved in cell culture medium, ALI experiments mimic the composition of lung tissue in an experimental setup, leading to an exposure model which is a much more biologically relevant model of how aerosols are entering the lung. While heavy fuel oil particle exposure led to mRNA upregulation of classical inflammatory pathways, diesel fuel showed a significantly larger amount of regulation on the transcriptomic and proteomic level compared to HFO, a surprising result for a "cleaner" fuel type (Figure 9).

In order to validate and extend these results, macrophages were exposed to the same conditions in order to investigate a cell type directly implicated in the inflammatory response, and we found striking differences between effects of the particle phase and the gas phase (Sapcariu *et al.*, 2016) (See Chapter 3). While particles in the aerosols elicited a higher cytotoxic effect on the macrophages, the gas phase changed the metabolic profile of the macrophages, and proteomic changes occurred under heavy fuel oil aerosol exposure pointing to an activation of the immune response (Figure 10). The importance of the gas phase in aerosol exposure experiments are beginning to be acknowledged (Dilger *et al.*, 2016), and future studies should shift away from using submerged experiments. In this way, gas phase effects can be measured, as well as how the interaction between particle and gas phase modifies the impact of the individual aerosol components.

One of the metabolic changes discovered in this study was that itaconic acid is produced in macrophages exposed to heavy fuel oil. Itaconic acid was discovered in 2011 to be produced in macrophages under classical pro-inflammatory conditions (Strelko *et al.*, 2011), but we have found the first evidence of this metabolite being produced due to anthropogenic pollutants.

Together, these two studies (Oeder *et al.*, 2015; Sapcariu *et al.*, 2016) validate the idea that stricter regulations need to be in place for shipping-based aerosol emissions, and further research needs to be done in order to understand health effects of anthropogenic aerosols. In this way, we can further our understanding of how pollution affects us, and environ-

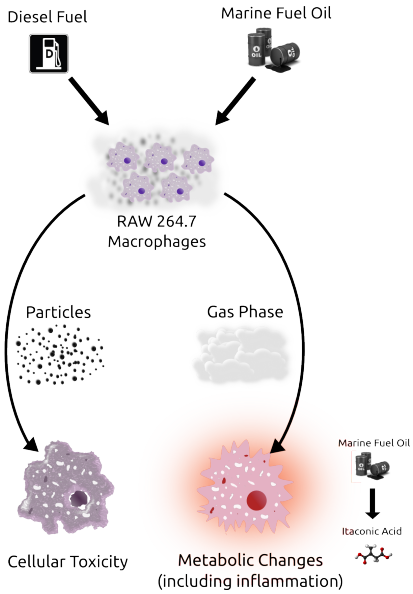

Figure 10: Aerosol effects on RAW 264.7 macrophages. For both heavy marine fuel oil and diesel fuel, particles causes increased toxicity in macrophages, while the gas phase was implicated in metabolic changes. For heavy marine fuel oil, itaconic acid was found to be produced by exposed macrophages. From Sapcariu *et al.* (2016)

mental policy can be built around data and evidence-based argumentation.

4.2 GLUCOSE FLUX INTO THE TCA CYCLE IS VITAL FOR THE INFLAMMATORY RESPONSE

Studies on macrophage metabolism under inflammatory conditions show decreased cellular oxygen consumption (Tannahill *et al.*, 2013), which suggest that there is less TCA cycle activity as oxidative phosphorylation is decreased, and this process is mainly driven by TCA cycle-derived NADH. One of the reasons for this is the cascade initiated through LPS-induced HIF-1α stabilization, suggesting a transcriptional activation of PDK and thus a reduction of pyruvate dehydrogenase (PDH) complex activity, catalyzing the oxidation of pyruvate into the TCA cycle. However, we discovered that PDH activity is constitutively active in

LPS-stimulated macrophages, and is necessary for pro-inflammatory cytokine expression (Meiser *et al.*, 2015) (see Chapter 3).

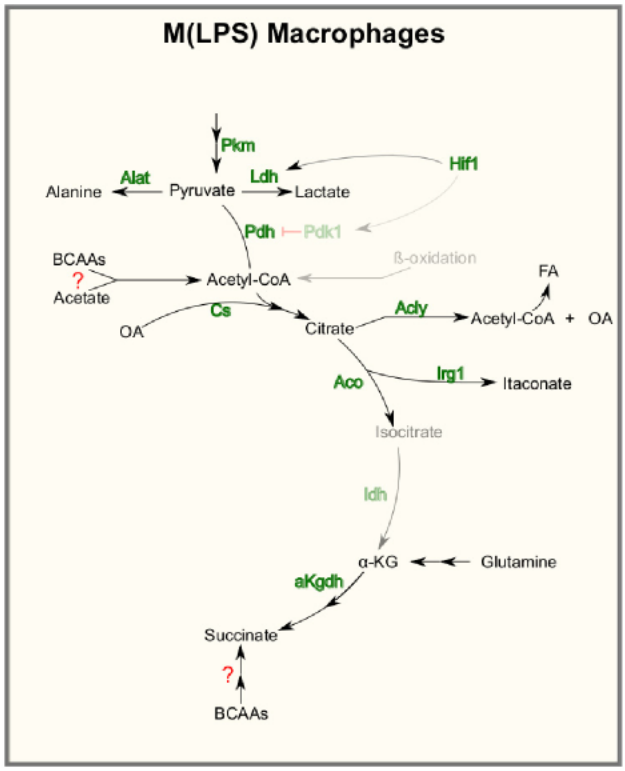

Figure 11: Metabolic network of pro-inflammatory macrophages. Glucose is utilized macrophages for glycolysis as well as the TCA cycle, through the oxidation of pyruvate through pyruvate dehydrogenase. This carbon is then used to produce itaconic acid and acetyl-CoA (for fatty acid synthesis). Glutamine anaplerosis is used to replenish the TCA cycle. Pkm - pyruvate kinase, Alat - alanine transanimase, Ldh - lactate dehydrogenase, Hif1 - hypoxia-inducible factor 1, Pdh - pyruvate dehydrogenase, Cs - citrate synthase, Acly - ATP citrate lyase, Irg1 - immunoresponsive gene 1, Aco - aconitase, Idh - isocitrate dehydrogenase, aKgdh - alpha-ketoglutarate dehydrogenase. From Meiser *et al.* (2015), figure created by J. Meiser

Glucose oxidation into the TCA cycle is necessary to supply carbon for the production of itaconic acid and other TCA cycle metabolites, as well as fatty acids for morphological changes resulting from LPS stimulation (Figure 11). Expression levels of *Pdk1* were reduced, while PDK1 protein levels and their phosphorylation did not change, showing that PDH-inhibiting activity was not increased with LPS stimulation. Trac-

ing of [U-$^{13}C_6$]glucose to citric acid showed a basal level of 50% labeling and increased with LPS, showing not only that PDH activity was active in resting macrophages, but that it was an important part of the pro-inflammatory macrophage phenotype. In addition, macrophage metabolic activity under hypoxia was investigated, and itaconic acid was seen to be strongly decreased when macrophages were stimulated with LPS in hypoxic conditions.

The results of this study refute the assumption long held in the macrophage research community that since oxidative phosphorylation is reduced, the TCA cycle is less active in pro-inflammatory macrophages. Instead, this study adds to a growing body of evidence that the TCA cycle is vital to macrophage metabolism throughout the inflammatory process. In addition, it is interesting to note how the central carbon metabolic network dissociates during a pro-inflammatory challenge, with rerouting of metabolic pathways in order to focus on the production of necessary biomolecules for bacterial clearance. This theory has been suggested for the TCA cycle specifically by Jha *et al.* (2015), and future studies should attempt to understand how the concept of "metabolic breakpoints" could be related to different cell types in disease states to determine important regulatory points of disease metabolism.

4.3 INCREASES IN ITACONIC AND SUCCINIC ACID ARE LINKED

The antimicrobial activity of itaconic acid (Michelucci *et al.*, 2013) and the pro-inflammatory signaling properties of succinic acid (Tannahill *et al.*, 2013) have established these two metabolites as vital for the macrophage response to infections and other inflammatory stimuli. While downstream succinic acid metabolism is known, what happens to itaconic acid (aside from shutting down bacterial metabolism) is still being researched. We found a link between the two metabolites, and were able to show that itaconic acid is able to inhibit SDH activity to induce an accumulation of succinic acid (Cordes *et al.*, 2016) (see Chapter 3).

This regulation was shown to be present in both macrophages and *Irg1*-overexpressing transformed lung cells, and to be attenuated with

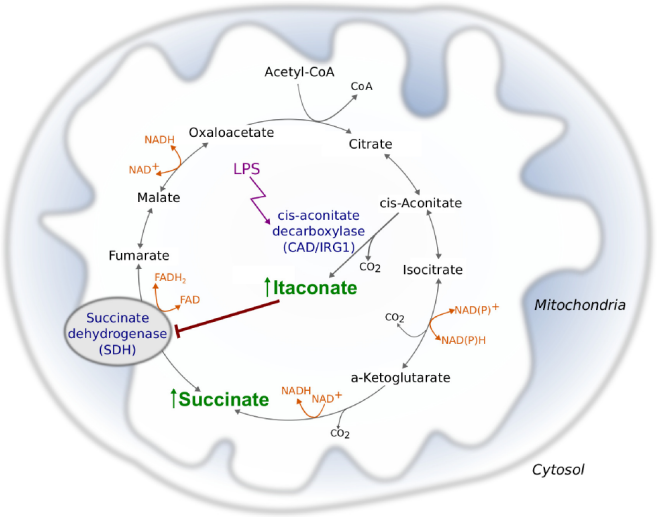

Figure 12: Itaconic acid inhibits succinate dehydrogenase. In pro-inflammatory macrophages, the buildup of itaconic acid causes inhibition of succinate dehydrogenase, leading to a buildup of succinate in the mitochondria. From Cordes *et al.* (2016), figure created by T. Cordes

knockout of *Irg1* gene expression in BMDMs. While itaconic acid acts on SDH, it is not metabolized into succinic acid, and downstream products of its metabolism in macrophages still remain unidentified (Figure 12). The results of this study point to a coordinated inflammatory response on a metabolic level, one that plays a role in the regulation of both cytokine activity and microbial defense. There has been some work on determining how this process is regulated, with interferon regulatory factor 1 (IRF1) identified as a transcription factor for *Irg1* (Tallam *et al.*, 2016). However, as metabolism is able to react quickly to perturbations, there might be more regulatory steps at non-transcriptional levels contributing to the production of itaconic acid.

4.4 METABOLIC PROPERTIES OF CELL LINES DIFFER FROM PRIMARY MACROPHAGES

Cell lines are constantly used as biological models for a wide variety of studies, in order to provide a cheaper and more readily accessible experimental tool compared to primary cells. While it can be assumed that

there are differences between primary cells and cell lines, we wanted to judge how representative a cell line is of a primary cell model for the study of the macrophage inflammatory process. This comparison was performed through the identification of similarities and differences in pro-inflammatory cytokine expression and metabolic changes. By comparing RAW 264.7 cells and BMDMs over the first 8 hours of the inflammatory response, we were able to determine that there are important differences that need to be taken into account when substituting a cell line for primary cells on both mRNA expression and metabolic levels (see Chapter 3).

Pro-inflammatory cytokine expression is consistently higher in BMDMs, even though the pattern of regulation is similar, showing that primary cells have a stronger response to LPS stimulation (Figure 13). This is also true for pro-inflammatory associated genes not typically classified as cytokines, such as *Irg1* or *iNos*.

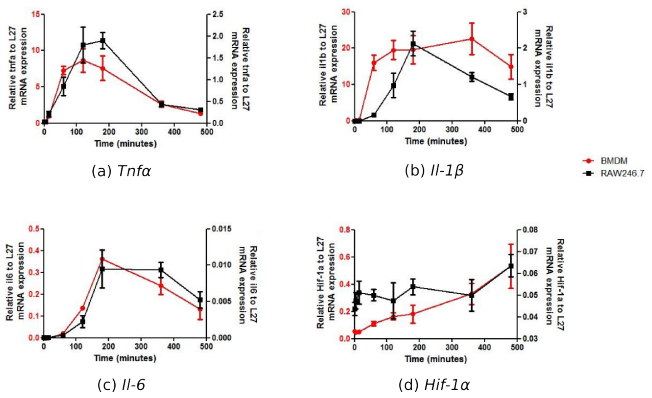

(a) *Tnfα* (b) *Il-1β* (c) *Il-6* (d) *Hif-1α*

Figure 13: Comparison of cytokines in early-stage macrophage LPS response. (a) *Tnf-α* (b) *Il-1β* (c) *Il-6* (d) *Hif-1α*

Metabolic changes due to pro-inflammatory stimulation are not comparable between the cell types, most likely because of transcriptional changes necessary to have a proliferating cell line. This can immediately be seen in *Hif-1α* expression (Figure 13), which is constant in RAW cells while increasing over time in BMDMs. *Pdk1* expression also has different expression patterns in primary cells, showing an increase in expression similar to *Hif-1α*, possibly due to the transcriptional link between the two (Figure 14). Expression of all three *Idh* isoforms decreased in

RAW cells, while only *Idh1* and *Idh2* decreased in BMDMs (Figure 14), reinforcing the idea of IDH as a metabolic breakpoint put forth by Jha *et al.* (2015).

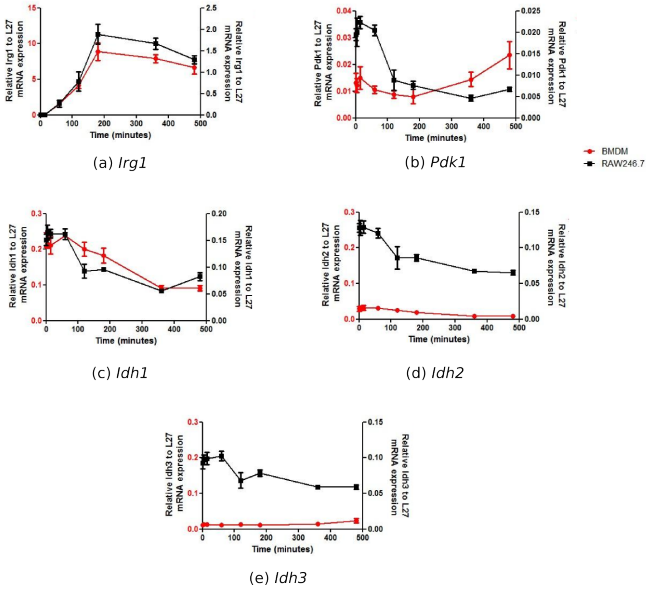

Figure 14: Comparison of metabolic genes in early-stage macrophage LPS response. (a) *Irg1* (b) *Pdk1* (c) *Idh1* (d) *Idh2* (e) *Idh3*

Metabolic changes show a similar difference between the cell types as with metabolic gene expression. Through the tracing of stable isotope labeled glucose and glutamine in central carbon metabolism, we found that over time, RAW cell carbon use from glucose and glutamine is not significantly affected by a pro-inflammatory stimulus, while BMDMs show increased use of glucose and glutamine for the production of metabolites (Figure 15). In addition, relative metabolic flux of glucose to metabolites in the TCA cycle (such as citric acid, fumaric acid, and succinic acid) are not significantly affected by LPS in RAW cells, while in BMDMs this flux increases over time. Metabolite pools of succinic and itaconic acid, the two metabolites implicated in pro-inflammatory macrophages, increased with the same trend in both cell types. Even though the trends are similar, pool size of both metabolites were higher in RAW 264.7 cells than BMDMs. In addition, the carbon use from glucose and glutamine for these pro-inflammatory metabolites increases in both RAW cells and BMDMs.

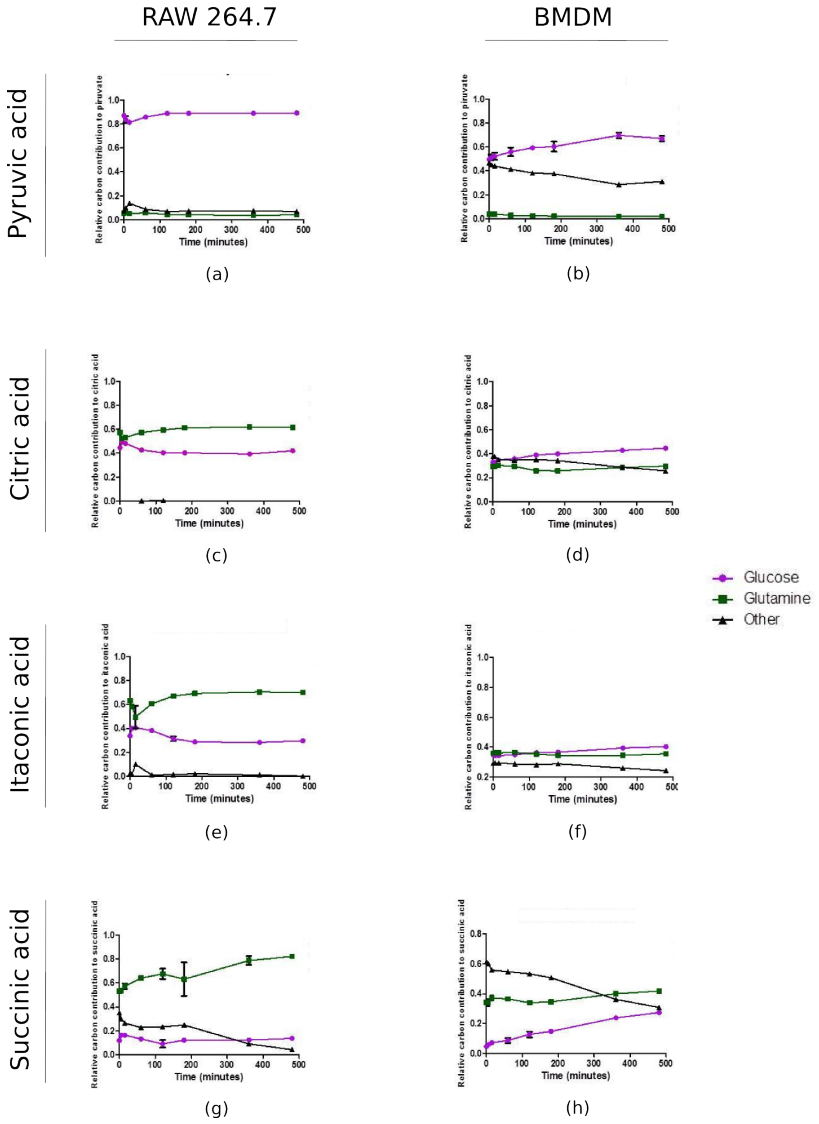

Figure 15: Comparison of carbon contribution from glucose and glutamine in early-stage macrophage LPS response. (a) RAW cells and (b) BMDMs - Pyruvic acid, (c) RAW cells and (d) BMDMs - Citric acid, (e) RAW cells and (f) BMDMs - Itaconic acid, (g) RAW cells and (h) BMDMs - Succinic acid.

LPS stimulation in macrophages thus leads to metabolic changes and pro-inflammatory cascades, which have a specific order in the early stage of the inflammatory response. Cytokine expression (as well as *Irg1*) are increased early, followed by *Hif-1α* increase and decreases in metabolic genes. This leads to an increase in the pro-inflammatory metabolites itaconic acid and succinic acid, which lead to an antimicrobial response from the macrophage.

The results of this paper show important similarities and differences between the RAW 264.7 macrophage cell line and primary BMDMs with regard to pro-inflammatory cytokine expression and relative metabolic flux changes. For the study of pro-inflammatory cytokines and metabolites, RAW cells are a good substitute for primary BMDMs, since the timing of these effects after LPS stimulation is directly comparable. However, the fact that RAW cells have been transformed to be proliferative and immortalized cause drastic changes to the metabolic machinery of the cell, including *Hif-1α* expression. This means that for the study of metabolic changes as a result of a pro-inflammatory stimulus, the results from RAW cells do not represent the metabolic activity in primary BMDMs. In future studies, care should be taken to choose a correct experimental model during the design of a study in order to make sure the model accurately can respond to the scientific question asked.

4.5 SIRT3 REGULATION PROMOTES ANTI-BACTERIAL ACTIVITY IN PRO-INFLAMMATORY MACROPHAGES

After uncovering the flux of glucose complementary to that of glutamine as a carbon source for itaconic acid production, and then determining a link between itaconic acid and succinic acid, the next step was to understand how these metabolic changes are regulated in order to identify regulatory points for possible drug targets. As it is known that the mitochondrial sirtuin SIRT3 has reduced expression in LPS-treated macrophages (Figure 16), we investigated how a reduction of SIRT3 in macrophages can affect inflammatory cytokine and metabolic regulation. In doing so, we uncovered that SIRT3 reduction serves to regulate

the pro-inflammatory and anti-microbial phenotype in macrophages by increasing production of itaconic acid and pro-inflammatory cytokines (Manuscript in preparation - see Chapter 3).

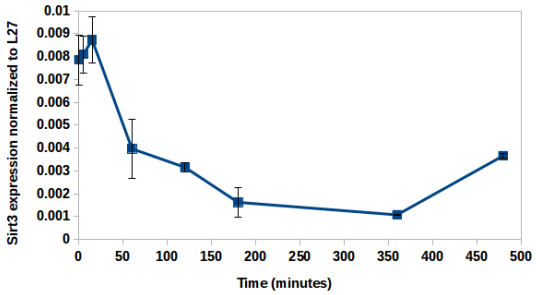

Figure 16: *Sirt3* expression decreases in LPS-treated BMDMs.

In *Sirt3* knockout BMDMs, both stimulation with LPS and infection with *Salmonella* typhimurium induced an increase in pro-inflammatory cytokines, upregulation of NF-κB and MAPK signaling pathways, and increased clearance of the bacterial infection, all of which led to improved macrophage viability. This was not due to SIRT3 induction of ROS in the cell, but instead from increased itaconic and succinic acid levels in the *Sirt3* knockout macrophages (Figure 18), possibly from SIRT3 deacetylation of CAD, the enzyme catalyzing the production of itaconic acid. However, the link between SIRT3 and CAD could not be confirmed, and this should be followed up with further studies investigating direct interactions between the two proteins.

Irg1 upregulation has been found to reduce pro-inflammatory cytokine production in LPS-tolerized macrophages (Li *et al.*, 2013), and a paper published very recently suggests that *Irg1*-mediated production of itaconic acid can reduce both pro-inflammatory cytokine production as well as oxygen consumption in LPS-activated macrophages (Lampropoulou *et al.*, 2016). Our results show that this reduction could be partly mediated by SIRT3 activity. Thus, in the macrophage response to pathogens, the activity of SIRT3 can be implicated in the regulatory network of *Irg1*/CAD, itaconic acid, SDH, and succinic acid determined through these studies.

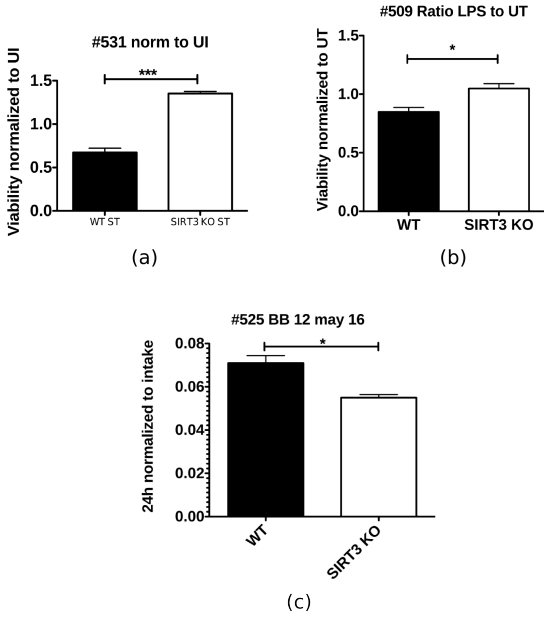

Figure 17: Cell viability and bacterial clearance of *Sirt3* KO BMDMs. (a) Cell viability of WT and *Sirt3* KO macrophages infected with *S.* Typhimuirum, (b) Cell viability of WT and *Sirt3* KO macrophages stimulated with LPS, (c) Bacterial clearance of WT and *Sirt3* KO macrophages infected with *S.* Typhimuirum Figure by S. Gutiérrez

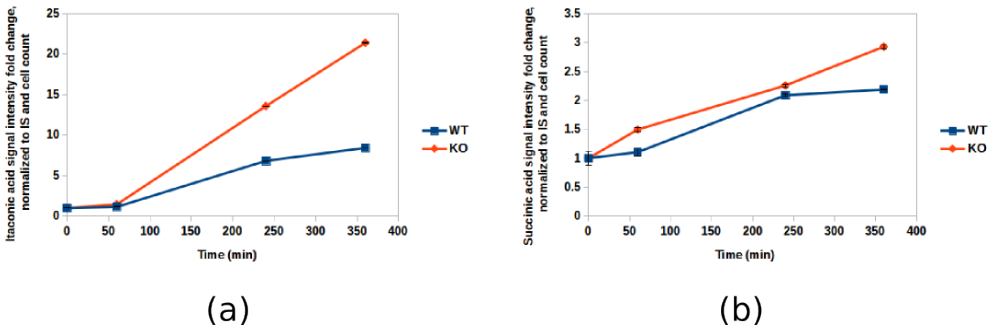

Figure 18: Metabolite levels in LPS treated WT *Sirt3* and KO BMDMs. (a) Itaconic acid (b) Succinic acid

4.6 OUTLOOK

Throughout this work, I have looked at pro-inflammatory macrophages stimulated with different cellular agonists, including ship engine exhaust aerosols, LPS, and *Salmonella* typhimurium. Interestingly, while the sources of inflammation can be varied, the production of itaconic acid by macrophages seems to be conserved with most pro-inflammatory stimulations, suggesting that itaconic acid accumulation is important to the general macrophage inflammatory response.

In addition, glucose and glutamine both supply carbons into the TCA cycle, where they are funneled towards production of itaconic and succinic acid in pro-inflammatory macrophages. The combination of constant PDH activity independent of HIF-1α stabilization and repression of SDH allow for glucose and glutamine influx to increase metabolite levels of itaconic and succinic acid, consistent with the hypothesized "metabolic breakpoints" put forth by Jha *et al.* (2015).

The role of itaconic acid as an antimicrobial is known, but to discover other roles of this metabolite is vital for determining human health applications (as well as implications of its use). Itaconic acid's ability to inhibit SDH and promote the buildup of succinic acid shows that this antimicrobial metabolite can also affect TCA cycle activity. As SDH is also complex II of the ETC, there is also the possibility that inhibition due to itaconic acid is linked to the reduction in oxidative phosphorylation and the redox state of the cell. Further research should be performed on itaconic acid to determine other possible biochemical reactions it can affect, in order to understand the potential of this metabolite with regards to artificially regulating metabolic activity in diseases where metabolic dysregulation plays a role.

Just as itaconic acid has been found to have multiple roles in the cell, the same is likely for *Irg1*, the gene implicated in its production. Studies link *Irg1* with ROS production and cytokine secretion (Li *et al.*, 2013; Ren *et al.*, 2016), and it is starting to look like *Irg1* is a main regulator of inflammatory processes in macrophages. Understanding the transcriptional regulation of *Irg1* is the next step, and recently it was discovered

that *Irf1* serves to affect mRNA and protein expression of *Irg1*/CAD (Tallam *et al.*, 2016).

In addition to transcriptional regulation of itaconic acid production, we have uncovered additional regulation of this process through the SIRT3 deacetylase, which most likely affects CAD activity and thus regulates itaconic acid production. In addition, SIRT3 activity regulates pro-inflammatory cytokine production as well as the NF-κB and MAPK signaling pathways. This regulation helps to promote a pro-inflammatory macrophage phenotype as well as aiding in clearance of pathogenic bacteria and thus cellular survival under infections.

As SIRT3 is implicated (and decreased to serve cellular needs) in classical inflammation, this protein (as well as other sirtuin family members) could be exploited as therapeutic targets, in order to modulate uncontrolled inflammation in diseases with a metabolic aspect. One further avenue of research is probing whether CAD is a target of SIRT3, and how this regulation affects itaconic acid levels. The results in this thesis suggest that CAD is acetylated, and deacetylation activity of SIRT3 could regulate the production of itaconic acid levels, but this must be confirmed. The consequence of SIRT3 involvement in macrophage inflammation is that metabolic regulation plays an important role in inflammatory processes, as well as confirming SIRT3 as a promising drug target in metabolically linked diseases.

The combined results of the study point to a tightly linked network of pro-inflammatory metabolic regulation for the purpose of promoting antimicrobial and increased cytokine activity through the interplay of SIRT3, *Irg1*, succinic acid (as well as SDH), and itaconic acid. In addition, the work in this thesis adds evidence to the idea that the TCA cycle is extremely important for both pro-inflammatory metabolite production as well as regulation of cytokine expression in active macrophages, separating its role from that of glycolysis and showing a decoupling of central carbon metabolism under inflammatory conditions.

BIBLIOGRAPHY

Bong-Hyun Ahn, Hyun-Seok Kim, Shiwei Song, In Hye Lee, Jie Liu, Athanassios Vassilopoulos, Chu-Xia Deng, and Toren Finkel. A role for the mitochondrial deacetylase sirt3 in regulating energy homeostasis. *Proceedings of the National Academy of Sciences*, 105(38):14447–14452, 2008.

Shizuo Akira and Hiroaki Hemmi. Recognition of pathogen-associated molecular patterns by tlr family. *Immunology letters*, 85(2):85–95, 2003.

Kristin A Anderson, Michelle F Green, Frank K Huynh, Gregory R Wagner, and Matthew D Hirschey. Snapshot: mammalian sirtuins. *Cell*, 159(4):956–956, 2014.

Evangelos Andreakos, Sandra M Sacre, Clive Smith, Anna Lundberg, Serafim Kiriakidis, Tim Stonehouse, Claudia Monaco, Marc Feldmann, and Brian M Foxwell. Distinct pathways of lps-induced nf-κb activation and cytokine production in human myeloid and non-myeloid cells defined by selective utilization of myd88 and mal/tirap. *Blood*, 103(6):2229–2237, 2004.

Gregory M Barton. A calculated response: control of inflammation by the innate immune system. *The Journal of clinical investigation*, 118(2): 413–420, 2008.

EL Bell, BM Emerling, SJH Ricoult, and L Guarente. Sirt3 suppresses hypoxia inducible factor 1α and tumor growth by inhibiting mitochondrial ros production. *Oncogene*, 30(26):2986–2996, 2011.

Londa J Berghaus, James N Moore, David J Hurley, Michel L Vandenplas, Barbara P Fortes, Margreet A Wolfert, and Geert-Jan Boons. Innate immune responses of primary murine macrophage-lineage cells and raw 264.7 cells to ligands of toll-like receptors 2, 3, and 4. *Com-*

parative immunology, microbiology and infectious diseases, 33(5):443–454, 2010.

Laya Bhavaraju, Jonathan Shannahan, Aaron William, Robert McCormick, John McGee, Urmila Kodavanti, and Michael Madden. Diesel and biodiesel exhaust particle effects on rat alveolar macrophages with in vitro exposure. *Chemosphere*, 104:126–133, 2014.

Johannes G Bode, Christian Ehlting, and Dieter Häussinger. The macrophage response towards lps and its control through the p38 mapk–stat3 axis. *Cellular signalling*, 24(6):1185–1194, 2012.

George Boltz-Nitulescu, Christoph Wiltschke, Christoph Holzinger, Alois Fellinger, Otto Scheiner, Alois Gessl, and Othmar Förster. Differentiation of rat bone marrow cells into macrophages under the influence of mouse l929 cell supernatant. *Journal of leukocyte biology*, 41 (1):83–91, 1987.

Aarash Bordbar, Monica L Mo, Ernesto S Nakayasu, Alexandra C Schrimpe-Rutledge, Young-Mo Kim, Thomas O Metz, Marcus B Jones, Bryan C Frank, Richard D Smith, Scott N Peterson, *et al.* Model-driven multi-omic data analysis elucidates metabolic immunomodulators of macrophage activation. *Molecular systems biology*, 8(1):558, 2012.

Joerg M Buescher, Maciek R Antoniewicz, Laszlo G Boros, Shawn C Burgess, Henri Brunengraber, Clary B Clish, Ralph J DeBerardinis, Olivier Feron, Christian Frezza, Bart Ghesquiere, *et al.* A roadmap for interpreting 13 c metabolite labeling patterns from cells. *Current opinion in biotechnology*, 34:189–201, 2015.

Angeliki Chalkiadaki and Leonard Guarente. High-fat diet triggers inflammation-induced cleavage of sirt1 in adipose tissue to promote metabolic dysfunction. *Cell metabolism*, 16(2):180–188, 2012.

Angeliki Chalkiadaki and Leonard Guarente. The multifaceted functions of sirtuins in cancer. *Nature Reviews Cancer*, 2015.

Lisa M Chamberlain, Marisha L Godek, Mercedes Gonzalez-Juarrero, and David W Grainger. Phenotypic non-equivalence of murine

(monocyte-) macrophage cells in biomaterial and inflammatory models. *Journal of Biomedical Materials Research Part A*, 88(4):858–871, 2009.

Nazia Chaudhuri, Hannah Jary, Simon Lea, Naimat Khan, Katie C Piddock, David H Dockrell, Ken Donaldson, Rodger Duffin, Dave Singh, Lisa C Parker, *et al.* Diesel exhaust particle exposure in vitro alters monocyte differentiation and function. *PloS one*, 7(12):e51107, 2012.

Ajay Chawla, Khoa D Nguyen, and YP Sharon Goh. Macrophage-mediated inflammation in metabolic disease. *Nature Reviews Immunology*, 11(11):738–749, 2011.

Grace Y Chen and Gabriel Nuñez. Sterile inflammation: sensing and reacting to damage. *Nature Reviews Immunology*, 10(12):826–837, 2010.

Edward T Chouchani, Victoria R Pell, Edoardo Gaude, Dunja Aksentijević, Stephanie Y Sundier, Ellen L Robb, Angela Logan, Sergiy M Nadtochiy, Emily NJ Ord, Anthony C Smith, *et al.* Ischaemic accumulation of succinate controls reperfusion injury through mitochondrial ros. *Nature*, 515(7527):431–435, 2014.

Huseyin Cimen, Min-Joon Han, Yongjie Yang, Qiang Tong, Hasan Koc, and Emine C Koc. Regulation of succinate dehydrogenase activity by sirt3 in mammalian mitochondria. *Biochemistry*, 49(2):304–311, 2009.

Andreas Comouth, Harald Saathoff, Karl-Heinz Naumann, Sonja Muelhopt, Hanns-Rudolf Paur, and Thomas Leisner. Modelling and measurement of particle deposition for cell exposure at the air–liquid interface. *Journal of Aerosol Science*, 63:103–114, 2013.

Thekla Cordes, Alessandro Michelucci, and Karsten Hiller. Itaconic acid: the surprising role of an industrial compound as a mammalian antimicrobial metabolite. *Annual review of nutrition*, 35:451–473, 2015.

Thekla Cordes, Martina Wallace, Alessandro Michelucci, Ajit S Divakaruni, Sean C Sapcariu, Carole Sousa, Haruhiko Koseki, Pedro Cabrales, Anne N Murphy, Karsten Hiller, *et al.* Immunoresponsive gene 1 and itaconate inhibit succinate dehydrogenase to modulate

intracellular succinate levels. *Journal of Biological Chemistry*, 291(27): 14274–14284, 2016.

Thorsten Cramer, Yuji Yamanishi, Björn E Clausen, Irmgard Förster, Rafal Pawlinski, Nigel Mackman, Volker H Haase, Rudolf Jaenisch, Maripat Corr, Victor Nizet, *et al.* Hif-1α is essential for myeloid cell-mediated inflammation. *Cell*, 112(5):645–657, 2003.

Alfred Csibi, Sarah-Maria Fendt, Chenggang Li, George Poulogiannis, Andrew Y Choo, Douglas J Chapski, Seung Min Jeong, Jamie M Dempsey, Andrey Parkhitko, Tasha Morrison, *et al.* The mtorc1 pathway stimulates glutamine metabolism and cell proliferation by repressing sirt4. *Cell*, 153(4):840–854, 2013.

David C Dale, Laurence Boxer, and W Conrad Liles. The phagocytes: neutrophils and monocytes. *Blood*, 112(4):935–945, 2008.

G D'Amato, G Liccardi, M D'Amato, and S Holgate. Environmental risk factors and allergic bronchial asthma. *Clinical & Experimental Allergy*, 35(9):1113–1124, 2005.

Silvia Diabaté, Sonja Muelhopt, Hanns-Rudolf Paur, and Harald F Krug. The response of a co-culture lung model to fine and ultrafine particles of incinerator fly ash at the air-liquid interface. *Alternatives to laboratory animals: ATLA*, 36(3):285–298, 2008.

Marco Dilger, Jürgen Orasche, Ralf Zimmermann, Hanns-Rudolf Paur, Silvia Diabaté, and Carsten Weiss. Toxicity of wood smoke particles in human a549 lung epithelial cells: the role of pahs, soot and zinc. *Archives of toxicology*, pages 1–16, 2016.

Peter Droste, Stephan Miebach, Sebastian Niedenführ, Wolfgang Wiechert, and Katharina Nöh. Visualizing multi-omics data in metabolic networks with the software omixâa case study. *Biosystems*, 105(2):154–161, 2011.

Jintang Du, Yeyun Zhou, Xiaoyang Su, Jiu Jiu Yu, Saba Khan, Hong Jiang, Jungwoo Kim, Jimin Woo, Jun Huyn Kim, Brian Hyun Choi,

et al. Sirt5 is a nad-dependent protein lysine demalonylase and desuccinylase. *Science*, 334(6057):806–809, 2011.

Guillermo Arango Duque and Albert Descoteaux. Macrophage cytokines: involvement in immunity and infectious diseases. *Secretion of Cytokines and Chemokines by Innate Immune Cells*, page 6, 2015.

Jennifer Christina Ewald, SteÌphanie Heux, and Nicola Zamboni. High-throughput quantitative metabolomics: workflow for cultivation, quenching, and analysis of yeast in a multiwell format. *Analytical chemistry*, 81(9):3623–3629, 2009.

Sarah-Maria Fendt, Eric L Bell, Mark A Keibler, Benjamin A Olenchock, Jared R Mayers, Thomas M Wasylenko, Natalie I Vokes, Leonard Guarente, Matthew G Vander Heiden, and Gregory Stephanopoulos. Reductive glutamine metabolism is a function of the α-ketoglutarate to citrate ratio in cells. *Nature communications*, 4, 2013.

Lydia WS Finley, Arkaitz Carracedo, Jaewon Lee, Amanda Souza, Ainara Egia, Jiangwen Zhang, Julie Teruya-Feldstein, Paula I Moreira, Sandra M Cardoso, Clary B Clish, *et al.* Sirt3 opposes reprogramming of cancer cell metabolism through hif1α destabilization. *Cancer cell*, 19(3):416–428, 2011a.

Lydia WS Finley, Wilhelm Haas, Valérie Desquiret-Dumas, Douglas C Wallace, Vincent Procaccio, Steven P Gygi, and Marcia C Haigis. Succinate dehydrogenase is a direct target of sirtuin 3 deacetylase activity. *PloS one*, 6(8):e23295, 2011b.

Alexander Francke, Joerg Herold, Soenke Weinert, Ruth H Strasser, and Ruediger C Braun-Dullaeus. Generation of mature murine monocytes from heterogeneous bone marrow and description of their properties. *Journal of Histochemistry & Cytochemistry*, 59(9):813–825, 2011.

Masakuni Fukuzumi, Hiroto Shinomiya, Yasutake Shimizu, Kazuhito Ohishi, and Sayaka Utsumi. Endotoxin-induced enhancement of glucose influx into murine peritoneal macrophages via glut1. *Infection and immunity*, 64(1):108–112, 1996.

Bart Ghesquière, Brian W Wong, Anna Kuchnio, and Peter Carmeliet. Metabolism of stromal and immune cells in health and disease. *Nature*, 511(7508):167–176, 2014.

Siamon Gordon and Fernando O Martinez. Alternative activation of macrophages: mechanism and functions. *Immunity*, 32(5):593–604, 2010.

Siamon Gordon and Philip R Taylor. Monocyte and macrophage heterogeneity. *Nature Reviews Immunology*, 5(12):953–964, 2005.

Sergei I Grivennikov, Florian R Greten, and Michael Karin. Immunity, inflammation, and cancer. *Cell*, 140(6):883–899, 2010.

Arvand Haschemi, Paul Kosma, Lars Gille, Charles R Evans, Charles F Burant, Philipp Starkl, Bernhard Knapp, Robert Haas, Johannes A Schmid, Christoph Jandl, *et al.* The sedoheptulose kinase carkl directs macrophage polarization through control of glucose metabolism. *Cell metabolism*, 15(6):813–826, 2012.

Wenjuan He, John C Newman, Margaret Z Wang, Linh Ho, and Eric Verdin. Mitochondrial sirtuins: regulators of protein acylation and metabolism. *Trends in Endocrinology & Metabolism*, 23(9):467–476, 2012.

Karsten Hiller and Christian M Metallo. Profiling metabolic networks to study cancer metabolism. *Current opinion in biotechnology*, 24(1):60–68, 2013.

Karsten Hiller, Jasper Hangebrauk, Christian Jäger, Jana Spura, Kerstin Schreiber, and Dietmar Schomburg. MetaboliteDetector: comprehensive analysis tool for targeted and nontargeted GC/MS based metabolome analysis. *Analytical chemistry*, 81(9):3429–39, 2009.

Karsten Hiller, Christian Metallo, and Gregory Stephanopoulos. Elucidation of cellular metabolism via metabolomics and stable-isotope assisted metabolomics. *Current pharmaceutical biotechnology*, 12(7):1075–1086, 2011.

Matthew Hirschfeld, Janis J Weis, Vladimir Toshchakov, Cindy A Salkowski, M Joshua Cody, Dawn C Ward, Nilofer Qureshi,

Suzanne M Michalek, and Stefanie N Vogel. Signaling by toll-like receptor 2 and 4 agonists results in differential gene expression in murine macrophages. *Infection and immunity*, 69(3):1477–1482, 2001.

Gökhan S Hotamisligil. Inflammation and metabolic disorders. *Nature*, 444(7121):860–867, 2006.

Riekelt H Houtkooper, Eija Pirinen, and Johan Auwerx. Sirtuins as regulators of metabolism and healthspan. *Nature reviews Molecular cell biology*, 13(4):225–238, 2012.

Konrad T Howitz, Kevin J Bitterman, Haim Y Cohen, Dudley W Lamming, Siva Lavu, Jason G Wood, Robert E Zipkin, Phuong Chung, Anne Kisielewski, Li-Li Zhang, *et al.* Small molecule activators of sirtuins extend saccharomyces cerevisiae lifespan. *Nature*, 425(6954): 191–196, 2003.

Vittoria Infantino, Paolo Convertini, Liana Cucci, Maria Antonietta Panaro, Maria Antonietta Di Noia, Rosa Calvello, Ferdinando Palmieri, and Vito Iacobazzi. The mitochondrial citrate carrier: a new player in inflammation. *Biochemical Journal*, 438(3):433–436, 2011.

Pushpa Jayaraman, Isabel Sada-Ovalle, Tomoyasu Nishimura, Ana C Anderson, Vijay K Kuchroo, Heinz G Remold, and Samuel M Behar. Il-1β promotes antimicrobial immunity in macrophages by regulating tnfr signaling and caspase-3 activation. *The Journal of Immunology*, 190 (8):4196–4204, 2013.

Abhishek K Jha, Stanley Ching-Cheng Huang, Alexey Sergushichev, Vicky Lampropoulou, Yulia Ivanova, Ekaterina Loginicheva, Karina Chmielewski, Kelly M Stewart, Juliet Ashall, Bart Everts, *et al.* Network integration of parallel metabolic and transcriptional data reveals metabolic modules that regulate macrophage polarization. *Immunity*, 42(3):419–430, 2015.

Yariv Kanfi, Shoshana Naiman, Gail Amir, Victoria Peshti, Guy Zinman, Liat Nahum, Ziv Bar-Joseph, and Haim Y Cohen. The sirtuin sirt6 regulates lifespan in male mice. *Nature*, 483(7388):218–221, 2012.

Anu Kauppinen, Tiina Suuronen, Johanna Ojala, Kai Kaarniranta, and Antero Salminen. Antagonistic crosstalk between nf-κb and sirt1 in the regulation of inflammation and metabolic disorders. *Cellular signalling*, 25(10):1939–1948, 2013.

Jung-whan Kim, Irina Tchernyshyov, Gregg L Semenza, and Chi V Dang. Hif-1-mediated expression of pyruvate dehydrogenase kinase: a metabolic switch required for cellular adaptation to hypoxia. *Cell metabolism*, 3(3):177–185, 2006.

JW Knebel, D Ritter, and M Aufderheide. Exposure of human lung cells to native diesel motor exhaustâdevelopment of an optimized in vitro test strategy. *Toxicology in vitro*, 16(2):185–192, 2002.

Vicky Lampropoulou, Alexey Sergushichev, Monika Bambouskova, Sharmila Nair, Emma E Vincent, Ekaterina Loginicheva, Luisa Cervantes-Barragan, Xiucui Ma, Stanley Ching-Cheng Huang, Takla Griss, *et al.* Itaconate links inhibition of succinate dehydrogenase with macrophage metabolic remodeling and regulation of inflammation. *Cell Metabolism*, 24(1):158–166, 2016.

Ae Sin Lee, Yu Jin Jung, Dal Kim, Tung Nguyen-Thanh, Kyung Pyo Kang, Sik Lee, Sung Kwang Park, and Won Kim. Sirt2 ameliorates lipopolysaccharide-induced inflammation in macrophages. *Biochemical and biophysical research communications*, 450(4):1363–1369, 2014.

Yingke Li, Peng Zhang, Chengcai Wang, Chaofeng Han, Jun Meng, Xingguang Liu, Sheng Xu, Nan Li, Qingqing Wang, Xueyin Shi, *et al.* Immune responsive gene 1 (irg1) promotes endotoxin tolerance by increasing a20 expression in macrophages through reactive oxygen species. *Journal of Biological Chemistry*, 288(23):16225–16234, 2013.

Ching Yu Lin, Huifeng Wu, Ronald S Tjeerdema, and Mark R Viant. Evaluation of metabolite extraction strategies from tissue samples using nmr metabolomics. *Metabolomics*, 3(1):55–67, 2007.

Tie Fu Liu, Vidula T Vachharajani, Barbara K Yoza, and Charles E McCall. Nad+-dependent sirtuin 1 and 6 proteins coordinate a switch

from glucose to fatty acid oxidation during the acute inflammatory response. *Journal of Biological Chemistry*, 287(31):25758–25769, 2012.

Yuanbin Liu, Gary Fiskum, and David Schubert. Generation of reactive oxygen species by the mitochondrial electron transport chain. *Journal of neurochemistry*, 80(5):780–787, 2002.

Alberto Mantovani, Antonio Sica, Silvano Sozzani, Paola Allavena, Annunciata Vecchi, and Massimo Locati. The chemokine system in diverse forms of macrophage activation and polarization. *Trends in immunology*, 25(12):677–686, 2004.

BA McFadden and S Purohit. Itaconate, an isocitrate lyase-directed inhibitor in pseudomonas indigofera. *Journal of bacteriology*, 131(1):136–144, 1977.

Patrick L McGeer and Edith G Mcgeer. Inflammation and the degenerative diseases of aging. *Annals of the New York Academy of Sciences*, 1035 (1):104–116, 2004.

Ruslan Medzhitov. Recognition of microorganisms and activation of the immune response. *Nature*, 449(7164):819–826, 2007.

Ruslan Medzhitov. Inflammation 2010: new adventures of an old flame. *Cell*, 140(6):771–776, 2010.

Johannes Meiser, Lisa Krämer, Sean C Sapcariu, Nadia Battello, Jenny Ghelfi, Aymeric Fouquier D'Herouel, Alexander Skupin, and Karsten Hiller. Pro-inflammatory macrophages sustain pyruvate oxidation through pyruvate dehydrogenase for the synthesis of itaconate and to enable cytokine expression. *Journal of Biological Chemistry*, pages jbc–M115, 2015.

Christian M Metallo, Paulo A Gameiro, Eric L Bell, Katherine R Mattaini, Juanjuan Yang, Karsten Hiller, Christopher M Jewell, Zachary R Johnson, Darrell J Irvine, Leonard Guarente, *et al.* Reductive glutamine metabolism by idh1 mediates lipogenesis under hypoxia. *Nature*, 481 (7381):380–384, 2012.

Shaday Michan and David Sinclair. Sirtuins in mammals: insights into their biological function. *Biochemical Journal*, 404(1):1–13, 2007.

Alessandro Michelucci, Thekla Cordes, Jenny Ghelfi, Arnaud Pailot, Norbert Reiling, Oliver Goldmann, Tina Binz, André Wegner, Aravind Tallam, Antonio Rausell, *et al.* Immune-responsive gene 1 protein links metabolism to immunity by catalyzing itaconic acid production. *Proceedings of the National Academy of Sciences*, 110(19):7820–7825, 2013.

Diana Moreira, Vasco Rodrigues, Maria Abengozar, Luis Rivas, Eduardo Rial, Mireille Laforge, Xiaoling Li, Marc Foretz, Benoit Viollet, Jérôme Estaquier, *et al.* Leishmania infantum modulates host macrophage mitochondrial metabolism by hijacking the sirt1-ampk axis. *PLoS Pathog*, 11(3):e1004684, 2015.

David M Mosser and Justin P Edwards. Exploring the full spectrum of macrophage activation. *Nature reviews immunology*, 8(12):958–969, 2008.

Sonja Mülhopt, Hanns-Rudolf Paur, Silvia Diabaté, and Harald F Krug. In vitro testing of inhalable fly ash at the air liquid interface. In *Advanced Environmental Monitoring*, pages 402–414. Springer, 2008.

Sonja Mülhopt, Marco Dilger, Silvia Diabaté, Christoph Schlager, Tobias Krebs, Ralf Zimmermann, Jeroen Buters, Sebastian Oeder, Thomas Wäscher, Carsten Weiss, *et al.* Toxicity testing of combustion aerosols at the air–liquid interface with a self-contained and easy-to-use exposure system. *Journal of Aerosol Science*, 96:38–55, 2016.

Peter J Murray and Thomas A Wynn. Protective and pathogenic functions of macrophage subsets. *Nature reviews immunology*, 11(11):723–737, 2011.

Nargis Nasrin, Xiaoping Wu, Eric Fortier, Yajun Feng, Olivia Claire Bare, Sumiao Chen, Xianglin Ren, Zhidan Wu, Ryan S Streeper, and Laura Bordone. Sirt4 regulates fatty acid oxidation and mitochondrial gene expression in liver and muscle cells. *Journal of Biological Chemistry*, 285 (42):31995–32002, 2010.

Philip Newsholme, Joaquim Procopio, Manuela Maria Ramos Lima, Tania Cristina Pithon-Curi, and Rui Curi. Glutamine and glutamateâtheir central role in cell metabolism and function. *Cell biochemistry and function*, 21(1):1–9, 2003.

Sebastian Oeder, Tamara Kanashova, Olli Sippula, Sean C Sapcariu, Thorsten Streibel, Jose Manuel Arteaga-Salas, Johannes Passig, Marco Dilger, Hanns-Rudolf Paur, Christoph Schlager, *et al.* Particulate matter from both heavy fuel oil and diesel fuel shipping emissions show strong biological effects on human lung cells at realistic and comparable in vitro exposure conditions. *PloS one*, 10(6):e0126536, 2015.

Luke AJ O'Neill and D Grahame Hardie. Metabolism of inflammation limited by ampk and pseudo-starvation. *Nature*, 493(7432):346–355, 2013.

Erika M Palmieri, Iolanda Spera, Alessio Menga, Vittoria Infantino, Vito Porcelli, Vito Iacobazzi, Ciro L Pierri, Douglas C Hooper, Ferdinando Palmieri, and Alessandra Castegna. Acetylation of human mitochondrial citrate carrier modulates mitochondrial citrate/malate exchange activity to sustain nadph production during macrophage activation. *Biochimica et Biophysica Acta (BBA)-Bioenergetics*, 1847(8):729–738, 2015.

Jeongsoon Park, Yue Chen, Daniel X Tishkoff, Chao Peng, Minjia Tan, Lunzhai Dai, Zhongyu Xie, Yi Zhang, Bernadette MM Zwaans, Mary E Skinner, *et al.* Sirt5-mediated lysine desuccinylation impacts diverse metabolic pathways. *Molecular cell*, 50(6):919–930, 2013.

Thakor R Patel and Bruce A McFadden. Caenorhabditis elegans and ascaris suum: inhibition of isocitrate lyase by itaconate. *Experimental parasitology*, 44(2):262–268, 1978.

Hanns-Rudolf Paur, Flemming R Cassee, Justin Teeguarden, Heinz Fissan, Silvia Diabate, Michaela Aufderheide, Wolfgang G Kreyling, Otto Hänninen, Gerhard Kasper, Michael Riediker, *et al.* In-vitro cell exposure studies for the assessment of nanoparticle toxicity in the lungâa dialog between aerosol science and biology. *Journal of Aerosol Science*, 42(10):668–692, 2011.

Chao Peng, Zhike Lu, Zhongyu Xie, Zhongyi Cheng, Yue Chen, Minjia Tan, Hao Luo, Yi Zhang, Wendy He, Ke Yang, *et al.* The first identification of lysine malonylation substrates and its regulatory enzyme. *Molecular & Cellular Proteomics*, 10(12):M111–012658, 2011.

Sharen Provoost, Tania Maes, Monique AM Willart, Guy F Joos, Bart N Lambrecht, and Kurt G Tournoy. Diesel exhaust particles stimulate adaptive immunity by acting on pulmonary dendritic cells. *The journal of immunology*, 184(1):426–432, 2010.

Aparna Purushotham, Thaddeus T Schug, Qing Xu, Sailesh Surapureddi, Xiumei Guo, and Xiaoling Li. Hepatocyte-specific deletion of sirt1 alters fatty acid metabolism and results in hepatic steatosis and inflammation. *Cell metabolism*, 9(4):327–338, 2009.

R Core Team. *R: A Language and Environment for Statistical Computing*. R Foundation for Statistical Computing, Vienna, Austria, 2013. URL http://www.R-project.org.

Ahmed A Reda, J Schnelle-Kreis, J Orasche, G Abbaszade, J Lintelmann, JM Arteaga-Salas, B Stengel, R Rabe, H Harndorf, O Sippula, *et al.* Gas phase carbonyl compounds in ship emissions: Differences between diesel fuel and heavy fuel oil operation. *Atmospheric Environment*, 112: 370–380, 2015.

Anna C Reisetter, Larissa V Stebounova, Jonas Baltrusaitis, Linda Powers, Amit Gupta, Vicki H Grassian, and Martha M Monick. Induction of inflammasome-dependent pyroptosis by carbon black nanoparticles. *Journal of Biological Chemistry*, 286(24):21844–21852, 2011.

Ke Ren, Yuanzi Lv, Yujie Zhuo, Changmai Chen, Hengfei Shi, Lin Guo, Guang Yang, Yayi Hou, Ren Xiang Tan, and Erguang Li. Suppression of irg-1 improves immune lung injury after rsv infection by reducing ros production. *Journal of virology*, pages JVI–00563, 2016.

Nirmal Robinson, Scott McComb, Rebecca Mulligan, Renu Dudani, Lakshmi Krishnan, and Subash Sad. Type i interferon induces necroptosis in macrophages during infection with salmonella enterica serovar typhimurium. *Nature immunology*, 13(10):954–962, 2012.

Juan-Carlos Rodríguez-Prados, Paqui G Través, Jimena Cuenca, Daniel Rico, Julián Aragonés, Paloma Martín-Sanz, Marta Cascante, and Lisardo Boscá. Substrate fate in activated macrophages: a comparison between innate, classic, and alternative activation. *The Journal of Immunology*, 185(1):605–614, 2010.

Tina Rubic, Günther Lametschwandtner, Sandra Jost, Sonja Hinteregger, Julia Kund, Nicole Carballido-Perrig, Christoph Schwärzler, Tobias Junt, Hans Voshol, Josef G Meingassner, *et al.* Triggering the succinate receptor gpr91 on dendritic cells enhances immunity. *Nature immunology*, 9(11):1261–1269, 2008.

Sushabhan Sadhukhan, Xiaojing Liu, Dongryeol Ryu, Ornella D Nelson, John A Stupinski, Zhi Li, Wei Chen, Sheng Zhang, Robert S Weiss, Jason W Locasale, *et al.* Metabolomics-assisted proteomics identifies succinylation and sirt5 as important regulators of cardiac function. *Proceedings of the National Academy of Sciences*, 113(16):4320–4325, 2016.

Sean C Sapcariu, Tamara Kanashova, Daniel Weindl, Jenny Ghelfi, Gunnar Dittmar, and Karsten Hiller. Simultaneous extraction of proteins and metabolites from cells in culture. *MethodsX*, 1:74–80, 2014.

Sean C Sapcariu, Tamara Kanashova, Marco Dilger, Silvia Diabaté, Sebastian Oeder, Johannes Passig, Christian Radischat, Jeroen Buters, Olli Sippula, Thorsten Streibel, *et al.* Metabolic profiling as well as stable isotope assisted metabolic and proteomic analysis of raw 264.7 macrophages exposed to ship engine aerosol emissions: Different effects of heavy fuel oil and refined diesel fuel. *PloS one*, 11(6):e0157964, 2016.

Per E Schwarze, Annike Irene Totlandsdal, Marit Låg, Magne Refsnes, Jørn Andreas Holme, and Johan Øvrevik. Inflammation-related effects of diesel engine exhaust particles: studies on lung cells in vitro. *BioMed research international*, 2013, 2013.

JeanClare Seagrave, Sandy Dunaway, Jacob D McDonald, Joe L Mauderly, Patrick Hayden, and Christine Stidley. Responses of differentiated primary human lung epithelial cells to exposure to diesel ex-

haust at an air-liquid interface. *Experimental lung research*, 33(1):27–51, 2007.

Christopher A Sellick, Rasmus Hansen, Arfa R Maqsood, Warwick B Dunn, Gillian M Stephens, Royston Goodacre, and Alan J Dickson. Effective quenching processes for physiologically valid metabolite profiling of suspension cultured mammalian cells. *Analytical chemistry*, 81(1):174–183, 2008.

Gregg L Semenza. Hif-1 mediates the warburg effect in clear cell renal carcinoma. *Journal of bioenergetics and biomembranes*, 39(3):231–234, 2007.

Seung-Yong Seong and Polly Matzinger. Hydrophobicity: an ancient damage-associated molecular pattern that initiates innate immune responses. *Nature Reviews Immunology*, 4(6):469–478, 2004.

Catherine A Shaw, Sarah Robertson, Mark R Miller, Rodger Duffin, Caroline M Tabor, Ken Donaldson, David E Newby, and Patrick WF Hadoke. Diesel exhaust particulate–exposed macrophages cause marked endothelial cell activation. *American journal of respiratory cell and molecular biology*, 44(6):840–851, 2011.

Shangchun Sheng, Yi Kang, Yongchan Guo, Qinli Pu, Miao Cai, and Zhiguang Tu. Overexpression of sirt3 inhibits lipid accumulation in macrophages through mitochondrial idh2 deacetylation. *International journal of clinical and experimental pathology*, 8(8):9196, 2015.

Chao Shi and Eric G Pamer. Monocyte recruitment during infection and inflammation. *Nature Reviews Immunology*, 11(11):762–774, 2011.

Liang Shi, Saiful M Chowdhury, Heather S Smallwood, Hyunjin Yoon, Heather M Mottaz-Brewer, Angela D Norbeck, Jason E McDermott, Therese RW Clauss, Fred Heffron, Richard D Smith, *et al.* Proteomic investigation of the time course responses of raw 264.7 macrophages to infection with salmonella enterica. *Infection and immunity*, 77(8): 3227–3233, 2009.

Eri Maria Sol, Sebastian A Wagner, Brian T Weinert, Amit Kumar, Hyun-Seok Kim, Chu-Xia Deng, and Chunaram Choudhary. Proteomic investigations of lysine acetylation identify diverse substrates of mitochondrial deacetylase sirt3. *PloS one*, 7(12):e50545, 2012.

Sandro Steiner, Jan Czerwinski, Pierre Comte, Loretta L Müller, Norbert V Heeb, Andreas Mayer, Alke Petri-Fink, and Barbara Rothen-Rutishauser. Reduction in (pro-) inflammatory responses of lung cells exposed in vitro to diesel exhaust treated with a non-catalyzed diesel particle filter. *Atmospheric Environment*, 81:117–124, 2013.

Angela Storka, Gerhard Führlinger, Martin Seper, Lisa Wang, Michael Jew, Asha Leisser, and Michael Wolzt. E. coli endotoxin modulates the expression of sirtuin proteins in pbmc in humans. *Mediators of inflammation*, 2013, 2013.

Cheryl L Strelko, Wenyun Lu, Fay J Dufort, Thomas N Seyfried, Thomas C Chiles, Joshua D Rabinowitz, and Mary F Roberts. Itaconic acid is a mammalian metabolite induced during macrophage activation. *Journal of the American Chemical Society*, 133(41):16386–16389, 2011.

A Sydbom, Anders Blomberg, S Parnia, Nikolai Stenfors, Thomas Sandström, and SE Dahlen. Health effects of diesel exhaust emissions. *European Respiratory Journal*, 17(4):733–746, 2001.

Aravind Tallam, Thaneer M Perumal, Paul M Antony, Christian Jäger, Joëlle V Fritz, Laurent Vallar, Rudi Balling, Antonio Del Sol, and Alessandro Michelucci. Gene regulatory network inference of immunoresponsive gene 1 (irg1) identifies interferon regulatory factor 1 (irf1) as its transcriptional regulator in mammalian macrophages. *PloS one*, 11(2):e0149050, 2016.

GM Tannahill, AM Curtis, J Adamik, EM Palsson-McDermott, AF McGettrick, G Goel, C Frezza, NJ Bernard, B Kelly, NH Foley, *et al.* Succinate is an inflammatory signal that induces il-1β through hif-1α. *Nature*, 496(7444):238–242, 2013.

Randa Tao, Mitchell C Coleman, J Daniel Pennington, Ozkan Ozden, Seong-Hoon Park, Haiyan Jiang, Hyun-Seok Kim, Charles Robb Flynn, Salisha Hill, W Hayes McDonald, *et al.* Sirt3-mediated deacetylation of evolutionarily conserved lysine 122 regulates mnsod activity in response to stress. *Molecular cell*, 40(6):893–904, 2010.

Philip R Taylor, Luisa Martinez-Pomares, Martin Stacey, Hsi-Hsen Lin, Gordon D Brown, and Siamon Gordon. Macrophage receptors and immune recognition. *Annu. Rev. Immunol.*, 23:901–944, 2005.

Divya Vats, Lata Mukundan, Justin I Odegaard, Lina Zhang, Kristi L Smith, Christine R Morel, David R Greaves, Peter J Murray, and Ajay Chawla. Oxidative metabolism and pgc-1β attenuate macrophage-mediated inflammation. *Cell metabolism*, 4(1):13–24, 2006.

Manish Verma, Nataly Shulga, and John G Pastorino. Sirtuin-4 modulates sensitivity to induction of the mitochondrial permeability transition pore. *Biochimica et Biophysica Acta (BBA)-Bioenergetics*, 1827(1): 38–49, 2013.

Jing Wang and Paul Kubes. A reservoir of mature cavity macrophages that can rapidly invade visceral organs to affect tissue repair. *Cell*, 165 (3):668–678, 2016.

Otto Warburg, Franz Wind, and Erwin Negelein. The metabolism of tumors in the body. *The Journal of general physiology*, 8(6):519–530, 1927.

January Weiner 3rd, Shreemanta K Parida, Jeroen Maertzdorf, Gillian F Black, Dirk Repsilber, Anna Telaar, Robert P Mohney, Cordelia Arndt-Sullivan, Christian A Ganoza, Kellen C Faé, *et al.* Biomarkers of inflammation, immunosuppression and stress with active disease are revealed by metabolomic profiling of tuberculosis patients. *PloS one*, 7(7):e40221, 2012.

Haitao Wen, Jenny PY Ting, and Luke AJ O'Neill. A role for the nlrp3 inflammasome in metabolic diseases [mdash] did warburg miss inflammation [quest]. *Nature immunology*, 13(4):352–357, 2012.

A Phillip West, Igor E Brodsky, Christoph Rahner, Dong Kyun Woo, Hediye Erdjument-Bromage, Paul Tempst, Matthew C Walsh, Yongwon Choi, Gerald S Shadel, and Sankar Ghosh. Tlr signalling augments macrophage bactericidal activity through mitochondrial ros. *Nature*, 472(7344):476–480, 2011.

H-E Wichmann. Diesel exhaust particles. *Inhalation toxicology*, 19(sup1): 241–244, 2007.

Thomas A Wynn, Ajay Chawla, and Jeffrey W Pollard. Macrophage biology in development, homeostasis and disease. *Nature*, 496(7446): 445–455, 2013.

Hongliang Xu, Ann V Hertzel, Kaylee A Steen, and David A Bernlohr. Loss of fatty acid binding protein 4/ap2 reduces macrophage inflammation through activation of sirt3. *Molecular Endocrinology*, pages me–2015, 2016.

Fan Yeung, Jamie E Hoberg, Catherine S Ramsey, Michael D Keller, David R Jones, Roy A Frye, and Marty W Mayo. Modulation of nf-κb-dependent transcription and cell survival by the sirt1 deacetylase. *The EMBO journal*, 23(12):2369–2380, 2004.

Wei Yu, Kristin E Dittenhafer-Reed, and John M Denu. Sirt3 protein deacetylates isocitrate dehydrogenase 2 (idh2) and regulates mitochondrial redox status. *Journal of Biological Chemistry*, 287(17):14078–14086, 2012.

Shuping Zhang, Robert A Kingsley, Renato L Santos, Helene Andrews-Polymenis, Manuela Raffatellu, Josely Figueiredo, Jairo Nunes, Renee M Tsolis, L Garry Adams, and Andreas J Bäumler. Molecular pathogenesis of salmonella enterica serotype typhimurium-induced diarrhea. *Infection and immunity*, 71(1):1–12, 2003.

Lisha Zhou, Fang Wang, Renqiang Sun, Xiufei Chen, Mengli Zhang, Qi Xu, Yi Wang, Shiwen Wang, Yue Xiong, Kun-Liang Guan, *et al.* Sirt5 promotes idh2 desuccinylation and g6pd deglutarylation to enhance cellular antioxidant defense. *EMBO reports*, page e201541643, 2016.